UTS UNIVERSITY OF TECHNOLOGY SYDNEY

Optimized Pixelated Antenna Design for Multistandard Wireless Applications

by Md. Amanath Ullah

Thesis submitted in fulfilment of the requirements for the degree of

Doctor of Philosophy

under the supervision of Dr. Negin Shariati, Dr. Rasool Keshavarz, A/Prof. Justin Lipman and Prof. Mehran Abolhasan

University of Technology Sydney
Faculty of Engineering and Information Technology

October 2023

CERTIFICATE OF ORIGINAL AUTHORSHIP

I, Md. Amanath Ullah, declare that this thesis, is submitted in fulfilment of the requirements for the award of Doctoral Degree, in the School of Electrical and Data Engineering, Faculty of Engineering and Information Technology at the University of Technology Sydney.

This thesis is wholly my own work unless otherwise referenced or acknowledged. In addition, I certify that all information sources and literature used are indicated in the thesis.

This document has not previously been submitted for qualifications to any other academic institution.

This research is supported by the Australian Government Research Training Program.

Production Note:
Signature removed prior to publication.

Md. Amanath Ullah

October 09, 2023

ABSTRACT

Over the past decade, there has been a significant increase in the need for multi-functional antenna designs, driven by stringent design prerequisites in wireless systems. Simultaneously, different challenges arise because of the requirements for the antenna module in limited design space. Electromagnetic simulation of parametric changes in traditional patch antennas generally result in sub-optimal designs due to topological complexity.

In this thesis, novel systematic approaches to design pixelated antennas to support multistandard wireless application have been presented. Firstly, a low-profile dual-band pixelated defected ground antenna has been proposed. The design introduces the idea of utilizing pixelated defected ground for efficient antenna design without depending on geometric optimization of design parameters of defected ground area, unlike conventional defected ground antenna. Compact antenna design can be achieved by making the best use of designated design space on the defected ground plane.

Secondly, a systematic approach to achieve optimal design of a Pixelated Stacked Antenna has been presented. The antenna design uses pixelization on the two radiating patches to enable simultaneous optimization of multiple layers, resulting in improved optimization balance. The design methodology utilizes a combination of triangular and square pixel shapes where triangular-shaped pixels are used to form the principal radiating patch, and square-shaped pixels are implemented on the stacked parasitic patch.

Thirdly, a pixelated cubic antenna with enhanced isolation and diverse radiation pattern has been presented. The issue of mutual coupling comes into effect when multiple antenna elements are closely placed together. The presented antenna system with four patches has been pixelated and optimized simultaneously to achieve desired performance and high isolation without using any additional resonators or elements.

Finally, a novel approach to increasing bandwidth in log periodic antennas has been investigated. This research involves novel design of Pixelated Log Periodic Antenna (PLPA), which demonstrates remarkable improvements in bandwidth compared to conventional printed log periodic antennas of similar size. The study showcases the potential of PLPAs to achieve significant enhancements in fractional bandwidth. In the first design case, PLPAs achieved a

substantial 13% increase in fractional bandwidth. Notably, in the second design case, the antenna reached an even more impressive 22.2% improvement in fractional bandwidth.

It is anticipated that the presented pixelated antennas and the illustrated design methodologies in this thesis will find wide applications in present and future wireless systems to support the trend towards multistandard wireless systems to enable fast, secure, and reliable communications.

ACKNOWLEDGEMENTS

I would like to express my sincere gratitude and indebtedness to my supervisor Dr. Negin Shaiati for all the support and guideline throughout my PhD study. Dr. Negin Shariati has provided me with an excellent research environment. My sincere thanks goes to my co-supervisors Dr. Rasool Keshavarz, Professor Mehran Abolhasan and A/Professor Justin Lipman for their excellent ideas, invaluable guidance, and constant support in making this research possible over the years. I would like to thank my supervisors for their endless inspiration, kindness, friendly availability in spite of their busy schedule and allocation of their precious time for advising me during my research.

I am grateful to the School of Electrical and Data Engineering for providing the facilities and working enviornment. I am thankful to my fellow labmates for the stimulating discussions, and for all the fun we have had in the last four years. My sincere thanks goes to the staffs of RFCT Lab at University of Technology Sydney. I would like to thank Kevin Sharp and Brett Lowder for their technical support whenever needed. My special thanks goes to Majid for all the support and insightful discussion during the journey.

I would like to express my heartfelt thanks to all my friends, especially Badhon and Prerna, for their unwavering support and encouragement. I also want to thank everyone, both directly and indirectly, who has contributed to this journey.

I extend my deepest gratitude to my wonderful wife Sania Mahrin for her constant love and encouragement. Her patience, understanding, and belief in me have been my pillars of strength throughout this journey.

Last, but not least, I owe special gratitude to my family for all the love, constant support, and encouragement throughout my life. I dedicate this thesis to my mother, Shamsun Nahar, and my father, Ahmed Hussain.

LIST OF PUBLICATIONS

Peer-reviewed Journal Articles:

- **M. A. Ullah,** R. Keshavarz, M. Abolhasan, J. Lipman, K. P. Esselle, and N. Shariati. "A Review on Antenna Technologies for Ambient RF Energy Harvesting And Wireless Power Transfer: Designs, Challenges And Applications." IEEE Access, 2022 (IF: 3.476).

- **M. A. Ullah,** R. Keshavarz, M. Abolhasan, J. Lipman, and N. Shariati. "Low-Profile Dual-band Pixelated Defected Ground Antenna for Multistandard IoT Devices." Scientific Reports 12, 2022 (IF 4.997).

- **M. A. Ullah,** R. Keshavarz, M. Abolhasan, J. Lipman and N. Shariati, "Multi-Service Compact Pixelated Stacked Antenna with Different Pixel Shapes for IoT Applications, IEEE Internet of Things Journal, 2023, doi: 10.1109/JIOT.2023.3281816**.**, (IF: 10.238).

- **M. A. Ullah**, R. Keshavarz, M. Abolhasan, J. Lipman, and N. Shariati, "Multidirectional Pixelated Cubic Antenna with Enhanced Isolation for Vehicular Applications," IEEE Transactions on Antennas and Propagation, 2023, (Under review).

- R. Keshavarz, **M. A. Ullah**, J. Jafaryahya, and N. Shariati, "Pixelated Log Periodic Antenna Array for Wireless Applications," IEEE Transactions on Antennas and Propagation, 2023, (Drafted and awaiting submission).

CONTENTS

LIST OF FIGURES

LIST OF TABLES

LIST OF ABBREVIATIONS

ABS	Acrylonitrile Butadiene Styrene
AM	Amplitude Modulation
AUT	Antenna Under Test
BW	Bandwidth
BPSO	Binary Particle Swarm Optimization
CF	Cost Function
CP	Circular Polarization
DC	Direct Current
DE	Differential Algorithm
DG	Defected Ground
DGA	Defected Ground Antenna
DGS	Defected Ground Structure
DTV	Digital Television
EA	Evolutionary Algorithms
EH	Energy Harvesting
EBG	Electromagnetic Band Gap
EIRP	Effective Isotropic Radiated Power
EM	Electromagnetic
ESA	Electrically Small Antenna
FCC	Federal Communications Commissions
FF	Fitness Function
FM	Frequency Modulation
FSS	Frequency Selective Surfaces
FSPL	Free Space Path Loss
GA	Genetic Algorithm
GPS	Global Positioning System
GSM	Global System for Mobile
HPBW	Half Power Beamwidth
IoT	Internet of Things
ISM	Industrial Scientific and Medical
LP	Linear Polarization

LPA	Log Periodic Antenna
LPDA	Log Periodic Dipole Array
LTE	Long Term Evolution
MICS	Medical Implant Communication System
MIMO	Multiple Input Multiple Output
MPA	Microstrip Patch Antenna
PCB	Printed Circuit Board
PCE	Power Conversion Efficiency
PDG	Pixelated Defected Ground
PDGA	Pixelated Defected Ground Antenna
PEC	Perfect Electric Conductor
PIFA	Planar Inverted-F Antenna
PLPA	Pixelated Log Periodic Antenna
PSA	Pixelated Stacked Antenna
PSO	Particle Swarm Optimization
RFEH	Radio Frequency Energy Harvesting
RFID	Radio Frequency Identification
SWIPT	Simultaneous Wireless Information and Power Transfer
UAV	Unmanned Aerial Vehicle
UWB	Ultra-Wideband
VBPSO	V-shaped Binary Particle Swarm Optimization
WBN	Wireless Body Area Network
WiFi	Wireless Fidelity
WIT	Wireless Information Transfer
WLAN	Wireless Local Area Network
WPT	Wireless Power Transfer
WSN	Wireless Sensor Network
3D	Three-dimensional

LIST OF SYMBOLS

G	Gain
$\mathcal{E}_R$	Radiation efficiency
D	Directivity
°	Degree
c	Speed of Light
f	Frequency
f_r	Resonance Frequency
δ	Delta
ε	Epsilon
ε_r	Permittivity of the Substrate
θ	Theta
λ	Wavelength
μ	Mu
σ	Sigma
Q	Quality factor
η	Efficiency
Γ	Reflection Coefficient
Ω	Ohm

Chapter 1

Introduction

1.1 Introduction

The emergence of rapidly growing Internet-of-Things (IoT) has introduced numerous interconnected electronic devices and sensors through the Internet [1, 2]. The number of connected devices will expand to be 30.9 billion by 2025 [3]. Antennas serve a crucial role in both wireless communication and wireless power transmission, as they send and receive electromagnetic (EM) waves that convey energy or data wirelessly.

Antennas are used in wireless communication to send and receive electromagnetic waves that transport information between devices. The sending antenna generates electromagnetic waves that convey the data, while the receiving antenna receives the waves and turns them back into electrical signals. Antennas are utilized in a number of wireless communication technologies, including Wi-Fi, Bluetooth, cellular networks, and satellite communication. Dipole antennas, patch antennas, Yagi antennas, and helical antennas are examples of antennas utilized in wireless communication. Antennas are used in wireless power transfer to generate and receive electromagnetic fields that carry electrical energy from a transmitter to a receiver. The transmitter antenna generates an electromagnetic field that induces a current in the receiving antenna, so facilitating the transmission of energy. Coil antennas, resonant antennas, and patch antennas are some examples of antennas used for wireless power transfer. Antennas are also utilized in numerous applications that require both wireless power transfer and wireless communication, such as mobile device wireless charging systems. These systems use antennas to both deliver power wirelessly and communicate wirelessly between the charging pad and the device being charged.

Autonomous operation of low-power sensors and electronic devices require sustainable power supply rather than just relying on the stored energy in batteries. A sensor node's operational duration is determined by its battery capacity or available energy resources. Historically, batteries have been the most reliable source of energy for sensor nodes and portable electronic gadgets. Periodic battery replacement is required to extend the life of a sensor network [4]. However, there are scenarios where wireless sensor networks (WSNs) are deployed in remote areas or inaccessible locations such as the deep sea, underground, chemical plants, areas of environmental disasters and agricultural farmland monitoring, where it is difficult to replace batteries [5-8]. Moreover, sensor nodes may be left unchecked for weeks, months or years. The task of replacing or charging of batteries for a large number of wireless sensor nodes is impractical. Replacement of batteries after a finite time is also troublesome in context of maintenance cost and self-sustainability of devices [9-11], not to mention the environmental impacts.

Researchers have been studying various energy harvesting approaches to reduce maintenance costs and enable self-sustainability for remotely deployed low-power sensors [12, 13] and devices. Ambient energy from the environment could be used to energize wireless sensor devices, prolonging operational time [14-16]. Solar, heat, wind, electric field, magnetic field, vibration, and RF are the most common sources of ambient energy; an overview of these common sources of ambient energy is depicted in Figure 1.1 and Table 1.1 [4, 8, 17-28]. The exponential growth of RF and wireless sources including AM/FM radio, cellular networks, Wi-Fi signals, and digital/analogue TV makes RF energy an excellent ambient energy source. An advantage of RF energy harvesting is the ability to convert ambient signals to useful DC power throughout day and night, both indoor and outdoor. Penetration of RF signals into obstacles such as opaque walls or enclosed spaces, makes it a good candidate for indoor applications. In addition, the small

physical size and lightweight of RF energy harvesting systems enable portable and wearable applications [9, 29-31]. Other ambient energy harvesting technologies, including solar cells, can be paired with various antennas to enable hybrid energy harvesting solutions [32, 33].

Notably, RF power density is low in rural areas. Wireless sensor networks (WSNs) or IoT devices in remote places can be powered via dedicated RF sources [17, 34, 35]. Automatically transmitting power to the device in need of charge or power can be a viable option to provide a cordless experience using WPT [36, 37]. WPT technologies can be categorized according to the method of coupling, i.e. inductive coupling, EM radiation and magnetic resonance coupling [38]. Most of the WPT research have been on inductive coupling and magnetic resonance coupling. Numerous studies have been documented on magnetic coupled or inductive coupled WPT schemes. These schemes operate in the evanescent or near-field region [39]. However, inductive coupling and magnetic resonance coupling are appropriate for short-range applications in which the transmitter and receiver are within a few meters of each other and the distance is strictly related to the loop's dimension and frequency [36, 38]. The research scope of WPT based on microwave power transmission (MPT) has been expanding as it can facilitate long-distance operation. Unidirectional and omnidirectional antennas can be used to sustain the power link for interaction in far-field radiative WPT. Radiated power in propagating electromagnetic waves is received using antennas in the far-field region [38, 40]. However, the efficiency of this method is lower than magnetic resonance and inductive coupling [41] at present and researchers have been investigating different techniques to improve the system efficiency. General frequencies of interest for radiative WPT are 900 MHz, 2.4 GHz and 5.8 GHz [41]. Nevertheless, research on radiative WPT schemes are still in its infancy, and have numerous future applications [42, 43].

Receiving side of RF energy harvesting and radiative WPT systems generally include receiving antenna, matching network, rectification circuit and power management unit. The receiving antenna and the rectifier when combined, are defined as a rectenna. Performance of RFEH or WPT significantly depends on the radiation performance of the receiving antenna. The antenna is the key element of a rectenna that determines the performance of RFEH or WPT, as the antenna is required to capture RF signals. However, impedance matching between the rectifier circuit and the antenna also impacts the optimal efficiency [17, 44]. Design of an appropriate antenna is of paramount importance. Design of the antenna depends on application specific conditions and antenna properties. For example, operating frequency, impedance bandwidth, gain, efficiency, radiation pattern and polarization have significant impact on the received power. Many antenna topologies have been proposed in the literature for ambient RF energy harvesting (RFEH) and wireless power transfer (WPT) applications, focusing on performance enhancement of antennas. Since the advancement of electronic circuits requires low-profile antennas, it becomes a challenge to meet all the strict design requirements. Table 1.2 illustrates some key challenges of receiving antennas in RFEH and WPT systems.

Table 1.1 Overview of Ambient Energy Sources

	Solar [8, 18, 19]	Heat/ Thermal [8, 19-21]	Wind [4, 22]	Piezoelectric[23, 24]	Ambient RF [8, 17, 19, 25, 26]
Source	Sun	Sun, system losses, body	Wind flow	Difference in pressure, Vibrations,	Radio/TV stations, Mobile phone & base stations, wireless networks, radar, wireless routers
Availability	During daylight (4-8 Hours)	Continuous based on the activity or operation of the system	Depends on weather	Dependent on activity	Always
Harvesting mechanism	Solar/photovoltaic cell	Thermoelectricity, Seebeck effect	Turbine, DC motor, aero-elastic, Anemometer [4]	Piezoelectric devices interfaced with power	Rectenna

				electronic equipment	
Power density [19, 27, 28]	100 μW/cm^2	60 μW/cm^2	177 μW/cm^2 [22]	250 μW/cm^3	40 μW/cm^2
Efficiency [17, 18, 20, 21]	11.7% to 26.7% depending on different classification [18]	5-15% [20, 21]	---	~5-30%	0.4% to over 50% at -40 to -5 dBm input power[17, 25] (Can be increased with more input power)
Advantages [45]	Large amount of energy, low-profile harvester, commercially available, well developed technology	Available commercially, compact harvester	Harvesting can be possible even in low wind	Simple and fast power conversion, Output voltage high High durability,	Certainty [26] of available power, commercially available, low-profile harvester circuitry
Disadvantages [45]	Severely dependent on climatic condition, large area requirement, incident light orientation issue	Thermal matching issue, low power, large area requirement	Availability is not steady, harvesting system can be bulky	Material properties linked with coupling coefficient, Expensive material, Dependent on material property	Dependent on distance and availability of wireless signal power, propagation medium (e.g., multipath effects and attenuation through buildings) or weather conditions (e.g., fog, rain, or humid air) can have a significant impact on the propagation of EM waves affecting the received power, low rectification efficiency at low input power.

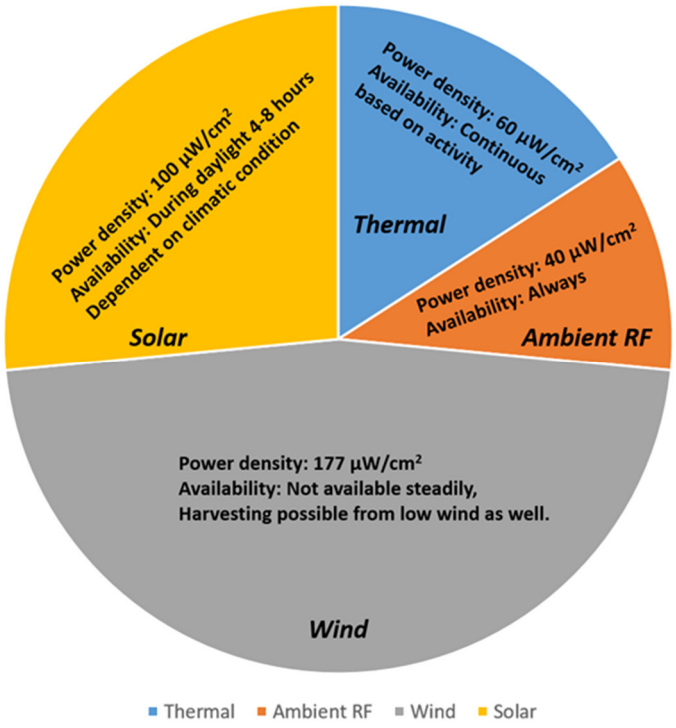

Figure 1.1 Overview of prominent ambient energy sources (based on the data in Table 1.1)

Table 1.2 Important metrics in the receiving antennas

Metrics	Reasons
Received signal amplitude, polarization, frequency, and bandwidth	Unknown received signal polarization in RFEH
Size	Low-profile antenna is required for compact harvester or portable devices.
Sensitivity	Ability to harvest energy and operate at low input power.
Directivity	Omnidirectional radiation pattern is required for ambient source. Unidirectional radiation pattern is required for known dedicated RF source.
Integrability with planar structure	Integration with PCB and matching network or rectification unit for practical applications.
Mechanical robustness	For long operation period or application in inaccessible/harsh environment or underwater
Stable performance with varying environmental condition	Temperature or humidity variation.
Circular polarization/ dual-polarization	Eliminate polarization mismatch for ambient source
Multi/wideband performance	To maximize harvested power, reception from multiple frequency.
Fabrication techniques	Performance trade-offs for low-profile and cost-effective manufacturing process

1.2 Challenges

Antenna design plays a crucial role in wireless systems, as the performance and reliability of these systems depend heavily on the antennas. However, there are several issues that

must be fixed in antenna design before wireless communication can be made more efficient and effective. Different wireless communication standards use different frequency bands, so it's crucial to design antennas that can work across a wide range of frequencies.

Also, the wireless power transfer system consists of two subsystems; transmitter and receiver. The core device of the receiver is the rectenna (rectifying antenna) which mainly consists of two components: a receiving antenna to harvest RF signals and a rectifier circuit to convert RF energy to DC power. The antenna plays a critical role in the rectenna system efficiency, as it is the front-end component to capture RF power from the transmitting device. Due to the small form factor of IoT devices, low-profile and efficient rectennas are required to remotely charge low-power IoT devices in WPT scenario. Over the past decades, WPT and RF energy harvesting (EH) technologies have introduced many types of receiving antennas [46-50]. These receiving antennas utilized typical patch antenna design techniques including simple rectangular patch [46, 48, 51], circular ring slot [49], sickle shaped patch like folded meanderline for long current path [50], etc. Antennas for low-power IoT devices should be compact and integrable with planar circuits as large antennas are less suitable to fit into the subsystem of small IoT devices and sensors due to large antenna dimension [49, 52, 53]. Nevertheless, designing a small-size antenna with a significant wireless signal capture capacity while attaining good gain and efficiency is incredibly challenging. Moreover, it is also difficult to achieve desired antenna structure with required performance using standard electromagnetic (EM) simulation (such as changing the patch shape or using different slot shapes) as they are limited to parametric study within a number of dimensional parameters.

Most of the antennas published in the literature for RFEH, WPT and wireless communication modules are based on traditional design approaches using

electromagnetic (EM) simulation with geometrical modifications such as variation of radiating element, changing the dimension of patches or the ground plane [48, 50, 54, 55]. However, the implementation of optimization algorithms to design antenna in the field of RFEH and WPT is relatively unexplored. Moreover, the emergence of different IoT applications poses new challenges in designing compact antenna as limited design space is available for the communication module which is comparatively difficult task using orthodox antenna design methods.

Moreover, in multi-antenna systems, isolation improvement is crucial for several reasons. In a multi-antenna system, the antennas are typically close together, which can cause coupling between the antennas. This coupling can result in interference, which can degrade the system's performance. By enhancing isolation, the level of coupling between antennas can be decreased, resulting in enhanced performance and dependability.

Optimal antenna performance can only be achieved through the application of sophisticated simulation and optimization methods, both of which are essential for overcoming these obstacles. The application of Computational Intelligence (CI) to complicated problems in antennas and propagation has received increasing attention recently. One of the main cornerstones of CI has always been evolutionary computation (EC). Evolutionary computation's primary unifying principle is based on the evolution principle from biology, which provides a methodology for embedding the principles of evolution within computer algorithms that can deal with complex engineering problems [56-59]. An evolutionary algorithm (EC) starts by creating a population of possible solutions of a problem. After that, the starting population is randomly varied to produce new solutions. Finally, all solutions are evaluated based on their task-solving ability. Evolutionary algorithms (EA) have been used to solve a wide range of antenna design problems, where EAs have been integrated with numerical approaches in

electromagnetics and yielded a variety of notable and effective outcomes [60]. Among the EAs applied in solving antenna design problems, Genetic Algorithm (GA) and Particle Swarm Optimization Algorithm (PSO) have been remained most prominent in the past decades [61-63]. These optimization techniques enable the investigation of designs that would otherwise be impossible to achieve using conventional methods. PSO has been employed in solving variety EM problems due to its straightforward and effective way in antenna design [63-65]. In applications involving antenna design, PSO has also been demonstrated to be more suited than other evolutionary optimization methods like genetic algorithms (GA), in context of algorithmic simplicity and feasibility of implementation. While the particle swarm optimizer shares the genetic algorithm's capacity to handle any nonlinear cost functions, its considerably simpler implementation and less computational budget requirement clearly illustrates its potential for wider usage in electromagnetic optimization. Further, the ability of PSO to efficiently handle various design goals contributes to its prominence in antenna designs [66, 67]. When dealing with multi-object or high-dimensional situations, the standard PSO technique suffers from early convergence issues and has difficulty processing them. Recently, it has been demonstrated that modified PSO algorithms have a greater way of searching for optimal solutions [68-71].

1.3 Research Objectives

Several objectives have been considered to address the challenges in state-of-the-art antenna design using pixelated configuration to develop and optimize different antenna designs. The objectives of this dissertation are listed below:

i. To design and optimize a low-profile defected ground antenna for dual-band application using pixelated configuration and binary optimization.

ii. To design a multi-layered multiband pixelated antenna using different pixel shapes with improved optimization performance and design flexibility.

iii. To investigate the performance of a multidirectional antenna with enhanced isolation using optimized pixelated patch configuration.

iv. To enhance the bandwidth of printed log periodic antenna using pixelated configurations.

1.4 Research Questions

This research aims to address the identified gaps and potential requirements for the widespread implementation of pixelated antenna design method by answering these research questions:

- How does the use of the proposed methods alleviate antenna performance?
- How can the use of different pixel shapes be leveraged to improve the process of antenna optimization?
- How the patch antenna can be optimized to operate at multiple frequency bands?
- Is it possible for pixelated antennas to achieve wider bandwidth compared with the conventional antennas?

1.5 Contributions

The key contributions of this dissertation are advancing receiving antenna methods or designs of receiving antennas for portable wireless devices or ambient RF energy harvesting and wireless power transfer. Specific contribution is investigation of binary

optimization based pixelization method in receiving antenna design with novel design topology where the conventional antenna design methods are limited upon certain shapes or geometric parameter optimization using standard electromagnetic simulation for antenna designs.

The first contribution is investigation and design of dual-band pixelated defected ground antenna (DGA). Compact antenna design can be achieved by making the best use of designated design space on the defected ground (DG) plane. Further, a V-shaped transfer function based BPSO with fast convergence allows us to implement the PDG technique efficiently. In the design procedure, pixelization is applied to a small rectangular region of the ground plane. The square pixels on the designated defected ground area of the antenna have been formed using a binary bit string, consisting of 512 bits taken during each iteration of the algorithm. The PDG method is concerned with the shape of the DG and does not rely on the geometrical dimension analysis used in traditional defected ground antennas. Initially, three single band antennas have been designed at 3.5 GHz, 5.2 GHz and 5.8 GHz using PDG technique. Finally, same PDG area has been used to design a dual-band antenna at 3.5 GHz and 5.8 GHz. The proposed antenna exhibits almost omnidirectional radiation performance with nearly 90% efficiency.

The second contribution is a stacked antenna for dual-band application at 5.2 GHz and 5.8 GHz bands. The proposed antenna topology consists of two pixelated layers of radiating patch which have been evolved using an enhanced binary particle swarm optimization algorithm (BPSO). The proposed technique offers essential aspects that are valuable in the design of compact single band or multi-band antennas for wireless systems. A binary string determines the shape of the radiating patches without depending on parametric study of conventional EM (electromagnetic) simulation. In the design

procedure, triangular-shaped pixels were used to form the principal radiating patch, while square-shaped pixels were implemented on the stacked parasitic patch. This approach provides considerable computational flexibility to achieve an optimal pixelated layout for the desired frequencies. The proposed design technique employs pixelization on both patch layers of the antenna and optimizes them simultaneously. With a compact design, the antenna achieved 4.7 dBi and 4.4 dBi gain at 5.2 and 5.8 GHz, respectively. The proposed antenna design exhibits characteristics nearly equivalent to larger and heavier alternatives that are often more challenging to develop and implement in practical scenarios.

The third contribution is a cubic antenna design with enhanced isolation and diverse radiation pattern for vehicular applications. The design consists of four radiating patches to take advantage of a nearly omnidirectional radiation pattern with enhanced isolation and high gain. The antenna system with four patches has been pixelated and optimized simultaneously to achieve desired performance and high isolation at 5.4 GHz band. The antenna achieved measured isolation of more than -34 dB between antenna elements. The overall isolation improvement obtained by the antenna is about 18 dB compared to a configuration using standard patch antennas. Moreover, isolation improvement is achieved through patch pixelization without requiring additional resonators or elements. The antenna achieved up to 6.9 dB realized gain in each direction. Additionally, the cubic antenna system is equipped with an E-shaped GPS antenna to facilitate connectivity with GPS satellite. Finally, the antenna performance has been investigated using a simulation model of the vehicle roof and roof rack. The reflection coefficient, isolation and radiation patterns of the antenna remains unaffected. The antenna prototype has been fabricated on Rogers substrate and measured to verify the simulation results. The measured results correlate well with the simulation results. The proposed antenna features low-profile,

simple design for ease of manufacture, good radiation characteristics with multidirectional property and high isolation, which are well-suited to applications where high isolation between multiple antennas is required.

The fourth contribution is the investigation of a bandwidth enhancement method using pixelated radiating element. As a design case, a log periodic patch antenna has been utilized. Pixelated dipole element has been used to design and optimize pixelated log periodic antenna with enhanced bandwidth. Two design cases has been investigated in this study where they achieved up to 22.2% increment in fractional bandwidth than the conventional design of printed log periodic antenna. Finally, the antenna prototype has been fabricated and measured to validate the design.

1.6 Thesis Organization

This thesis is organized as follows:

- Chapter 1: The first chapter provides introductory background of RF energy harvesting and wireless power transfer. The chapter also includes key roles of receiving antennas in RFEH and WPT. Research motivation, challenges and contribution are presented.

- Chapter 2: This chapter presents a well-rounded review of recent advancements of receiving antennas for RFEH and WPT. Antennas discussed in this chapter are categorized as low-profile antennas, multi-band antennas, circularly polarized antennas, and array antennas. A number of contemporary antennas from each category are presented, compared, and discussed with particular emphasis on design approach and performance.

- Chapter 3: This chapter presents design guideline and analysis of pixelated defected ground antenna. A dual-band pixelated defected ground antenna design has been proposed in this chapter along with a flexible design guide for different single-band antennas at different operating frequencies. The PDGA design is performed using the VBPSO algorithm. This chapter introduces the idea of utilizing pixelated defected ground for efficient antenna design without depending on geometric optimization of design parameters of defected ground area, unlike conventional DG antenna. The PDG configuration has the potential to achieve different antenna characteristics including, single or multi-band antenna design, gain or efficiency enhancement etc. using distinct configuration with a great degree of freedom. This leads to create multi-functional customized antennas for diverse applications.

- Chapter 4: This chapter presents a systematic approach to achieve optimal design of a Pixelated Stacked Antenna. An enhanced binary particle swarm optimization algorithm with a V-shaped transfer function has been utilized to obtain the pixelated layout of the patches on the bottom and top layers. By applying pixelization on the two radiating patches of the antenna, the antenna design enables simultaneous multilayer antenna optimization, which provides added benefits to the design procedure.

- Chapter 5: This chapter presents design of a cube shaped multidirectional pixelated antenna system. A pixelated multidirectional cubic antenna for automotive application has been designed. The evolution of the design of the antenna with a cube shape is based on a pixelated patch. The design technique and results indicate the benefits of the cubic configuration and the antenna's

characteristics. A binary optimization approach is used to design the antenna in order to obtain the specified operating band and better isolation. The isolation between antennas has been greatly enhanced in comparison to the same cubic antenna design with normal patch layout. High isolation is obtained without the use of extra hardware or filters.

- Chapter 6: The chapter presents an innovative technique to enhance bandwidth in log periodic antennas (LPA) using an enhanced binary particle swarm optimization approach. The resulting pixelated log periodic antenna (PLPA) design outperforms conventional printed LPAs in bandwidth. In the first design case, PLPAs achieved a 940 MHz bandwidth, showcasing a 13% fractional bandwidth increase. In the second case, the bandwidth extended to 1240 MHz, boasting a remarkable 22.2% improvement in fractional bandwidth. This method highlights the potential to create compact pixelated antennas with significantly enhanced bandwidth compared to traditional designs.

- Chapter 7: A summary of the thesis contents and achievements are given in the final chapter. Future work and plans to further develop this research topic are also discussed.

Chapter 2

Literature Review

2.1 Introduction

RF energy has the potential to wirelessly power a wide range of applications in situations when other ambient energy sources such as light, vibration, and thermal gradients are absent. RF energy harvesting refers to converting energy from electromagnetic field into electrical energy [72]. RF energy harvesting system or rectenna comprised of receiving antenna that captures RF signals, impedance matching network and rectifier circuit to generate DC power and power management unit. In radiative WPT a dedicated RF source transmits power toward a specific direction where the receiver is located. Emitted energy from electromagnetic radiation is transmitted via transmitting antenna from a power source to a receiving antenna by electromagnetic waves [38].

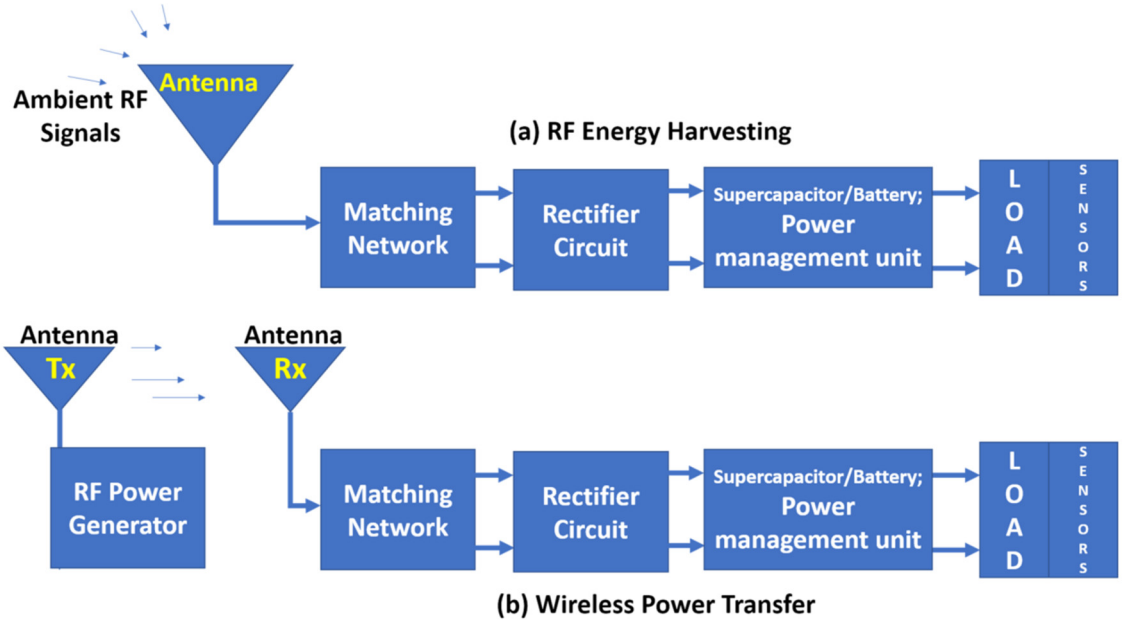

Figure 2.1 Block diagram of (a) RFEH and (b) WPT system

The communication channel could be the same for WPT and ambient RFEH scenarios,

but the signal source (transmitter) is different. Figure 2.1 and Table 2.1 provide basic illustration on ambient RFEH and WPT. RF signals are captured by the receiving antenna from various ambient sources like, TV towers, FM/AM radio station, mobile phones, base stations, wireless network or dedicated RF sources in case of WPT. The receiving antenna can operate on single band, multiband or broadband to receive power from different frequency bands simultaneously. The license-free ISM bands can be used for dedicated RF energy transfer. However, regulations are imposed on the maximum transmitting power of the dedicated RF sources by Federal Communications Commissions (FCC) [73, 74].

Table 2.1 Comparison of Ambient RFEH and WPT Techniques

	RFEH	WPT
Power source	Ambient sources such as wireless networks, radio/TV station, mobile tower, wireless router etc.	Dedicated RF power transmitting antenna
Known source (e.g. direction, polarization, frequency, transmitting power)	No	Yes
Receiving antenna properties (For ideal case)	Omnidirectional, multiband/wideband, capture RF energy from random polarization	High gain, multiband/wideband
Availability	Decreases due to lack of source, mostly in rural areas	Can be available on demand
Efficiency	Low efficiency in most cases (can be lower in low power density area)	High due to the availability of dedicated source

The path loss equation can be used to estimate power in RF energy harvesting scenario [75]. In addition, measurement of RF fields can be used to obtain the notion about maximum available power at different location in RFEH scenario. Table 2.2 depicts

example of maximum signal level available in different metropolitan areas in Australia “Table 2.2-A” and different locations (Metro stations and residential areas) in Canada “Table 2.2-B”. The table can demonstrate the feasibility of RFEH in civil environments.

`Table 2.2(A) Available RF Signal Level At Different Metropolitan Area In Australia At Different Frequency Ranges [76]

Location 1								
Frequency bands (MHz)	50	100	200	500	800	1000	2000	3000
Available signal level (dBuV) (Approx.)	70	110	78	110	97	88	80	41
Location 2								
Frequency bands (MHz)	50	100	200	500	800	1000	2000	3000
Available signal level (dBuV) (Approx.)	41	92	82	88	72	80	78	41
Location 3								
Frequency bands (MHz)	50	100	200	500	800	1000	2000	3000
Available signal level (dBuV) (Approx.)	96	101	78	100	68	70	72	40
Location 4								
Frequency bands (MHz)	50	100	200	500	800	1000	2000	3000
Available signal level (dBuV) (Approx.)	61	72	67	82	62	84	85	42
Location 5								
Frequency bands (MHz)	50	100	200	500	800	1000	2000	3000
Available signal level (dBuV) (Approx.)	87	104	88	108	78	99	95	83

Table 2.2(B) Available RF Signal Level At Various Areas In Canada Over Different Frequency Ranges [77]

Location 1 (Metro stations)							
Frequency bands	DTV	LTE700	GSM/LTE850	LTE1700/2100	GSM/LTE 1900	WiFi	LTE2600
Available signal level (dBm)	Max.: -19.97 Min.: -66.27	Max.: -19.08 Min.: -63.91	Max.: -19.73 Min.: -60.86	Max.: -27.11 Min.: -65.79	Max.: -20.16 Min.: -63.13	Max.: -58.25 Min.: -72.98	Max.: -34.34 Min.: -78.89
Location 2 (Residential areas)							
Frequency bands	DTV	LTE700	GSM/LTE850	LTE1700/2100	GSM/LTE 1900	WiFi	LTE2600
Available signal level (dBm)	Max.: -25.97	Max.: -37.38 Min.: -58.72	Max.: -41.62 Min.: -62.22	Max.: -44.17 Min.: -62.94	Max.: -42.95 Min.: -66.09	Max.: -59.80 Min.:	Max.: -54.26 Min.: -75.86

	Min.: -68.12					-74.53	

In case of WPT, the power received by an antenna at the receiving end of WPT system can be estimated by Friis transmission equation [75, 78],

$$P_r = P_t G_t G_r \left(\frac{\lambda}{4\pi R}\right)^2 \quad (2.1)$$

Where, P_r is the received power, P_t is the transmitted power, G_t denotes the transmitting antenna gain, G_r is receiving antenna gain, λ refers to the wavelength of RF signal, and R is the far-field distance from the transmitting antenna. This equation can provide a useful estimation for the possible upper limit of the range with a given transmitted power. However, it does not consider environmental attenuation that will affect available power at low levels.

An impedance matching network is required to decrease transmission loss and enhance voltage gain and sensitivity from the receiving antenna to the rectifier circuit [79]. Design of matching circuits requires a combination of real (resistor) and reactive (inductor or, capacitor) components to avoid power loss that may occur due to using only resistors. Performance of the matching circuit is crucial to achieve an optimum output from the whole system. The main challenge in designing a matching network is the non-linearity of the rectification device with input power and frequency (especially in ambient RFEH scenario). A wide input power range is required as the input power level fluctuates frequently in RF energy harvester. The RF signal received by the antenna is converted to DC voltage by the rectifier circuit [80].

2.2 Applications of Wireless Charging

Ambient RF energy harvesting and WPT are sustainable, cost-effective and green energy solutions. They can provide an alternative energy source for portable low-power devices that have a broad range of applications in different sectors such as agriculture, healthcare, manufacturing, mining, smart cities, etc. RFEH and WPT are expected to revolutionize the wireless charging technology of smart devices (smartphone, smart watch) and other consumer electronics (GPS devices, e-readers, wireless headphone, smart wearable sensors in medical healthcare) with true cordless experience. Smart farming or precision agriculture can be facilitated by remotely powered IoT sensors, wireless devices for tracking and monitoring of livestock and equipment, and sensing devices such as soil moisture, water tank level and temperature sensors. Other long-range application may include home automation and industrial control. On demand or schedule-based power can be also provided depending on the application requirements. The benefit of wireless power transfer solutions, is that the cost of manual labour can be reduced significantly in the case of large scale deployment of sensors [81]. Some of the application schemes are highlighted and explained in the subsequent sub-sections.

2.2.1 Wireless Sensor Networks

One of the major design constraints of wireless sensor networks (WSN) is the power scarcity associated with the sensors. Researchers are exploring new energy sources with enhanced reliability for WSNs. WSNs are comprised of many sensor nodes which are typically supplied by batteries. They are usually equipped with low processing power, short data storage capacity and limited power capacity [82, 83]. In addition to the finite life span of some batteries used as an energy source for WSNs, the problem of leakage current consumes the power even in unused low power states. Moreover, unavoidable

weather conditions (e.g. extreme temperature) may damage batteries which will also lead to environmental pollution. Two models of RFEH can be used in WSN. One with two radios, in which one radio is used for RF energy harvesting while the other one communicates with the rest of the sensor nodes. The other model employs the same radio for RFEH and communication purpose simultaneously. However, using a single radio model can minimize the design complexity of hardware as the dual-radio model may require separate antennas operating at different frequency [84, 85]. Moreover, dedicated RF sources using WPT can be used to keep sensors alive. In addition, simultaneous wireless information and power transfer (SWIPT) technology has the potential to combine power and information transfer aspects in modern wireless sensor networks [86]. The SWIPT concept merges the WPT schemes with WIT (Wireless Information Transfer) and introduces a new research direction, whereas WIT used to be a separate research area [87]. Nevertheless, the application area of RFEH and WPT in wireless sensor network is evolving. However, most of the literature that investigated the feasibility of RFEH and WPT in WSNs, did not consider long distance performance of the sensor network. Sensing devices that have a low power requirement are capable of utilizing harvested RF power [88]. Distance from the RF power source is vital to estimate the maximum input power available at the receiving end. In addition, the sleep time of sensors in the network is one of the major concerns during the charging process of the device [89]. Investigation of maximum time delay allowed between data transfer cycles is required in time-dependent applications. Table 2.3 provides an overview of RF powered WSNs using WPT and ambient energy harvesting techniques.

Table 2.3 Overview of RF powered WSNs

Refs.	Application	RF power source	Receiving antenna	Distance covered	Wireless power charging technique	Output	Remarks
[90]	Powering up autonomous WSN device in vehicles	Agilent N5158A	50 Ω COTS 3dBi antenna	1-4 meters	WPT (Dedicated)	Max. DC output 500µW-10 µW	At 4 meters distance the WSN device can transmit a packet at each 20 seconds of interval
[91]	Measurement of light level and temperature and transmission of measurement data wirelessly	1 MW UHF television broadcast transmitter, cellular base transceiver station	6dBi gain	10.4 km (From 1MW TV transmitter), 200 meters (From cellular base transceiver station)	Ambient RFEH	---	Fully ambient RF powered prototype, sensitivity -18dBm
[92]	Wireless humidity and temperature sensor	---	8.655 cm long quarter wave monopole antenna	2.5 m	Ambient RFEH	48 µJ; 1.8 V for 4 ms (1 operation cycle)	Picking up the sensing values and transmission is performed within 1 operation cycle (4ms); sensitivity -6 dBm
[93]	Autonomous Wireless Sensor Networks	Ambient RF energy at GSM-1800, UMTS-2100 and LTE-2600	Horn antenna; 0.8-18 GHz, 7-13 dBi gain	---	Ambient RFEH	Harvested power approx. 25 µW	Harvested power will suffice to power up temperature, humidity, Bluetooth transmitter, wake-up receiver and RFID based sensors. However, horn antenna has been user as the

							receiver in this experiment.
[94]	Powering wireless gas sensor node	Ambient RF energy at 900 MHz	---	---	Ambient RFEH	Charging of supercapacitor up to 5V by 400 seconds at 0 dBm input power	Perpetual operation of sensor node has been claimed. However, -20 to 10 dBm input power range has been considered in the application. The supercapacitor will take more time at less than 0 dBm input power changing the data transmission cycle.

2.2.2 Wireless Body Area Networks and Wearable Devices

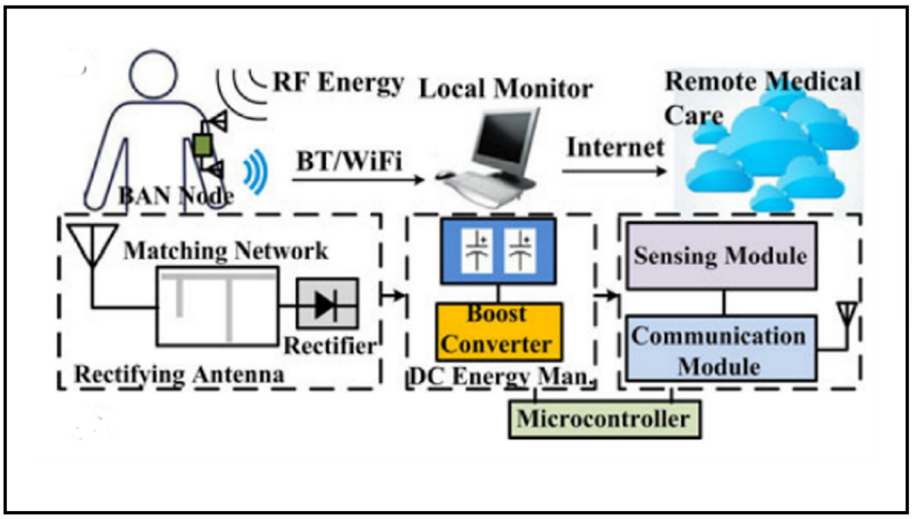

Figure 2.2 Future battery-less body area network sensor **[95]**

Long-term monitoring of health can be performed by wireless body area networks (WBANs) without affecting people's daily lives. WBANs provide a smart and inexpensive solution to health monitoring as a part of medical diagnostics [96, 97]. WBANs have received increasing recognition along with the emergence of wearable technology for Internet of Things (IoT) based healthcare applications [98].

Many low-power wearable communication and sensing technologies are being inspired for WBANs. Researchers emphasize wearable/on-body and implantable sensors to capture and transmit vital health parameters. On-body wearable devices or in-body implantable devices such as, pacemakers are expected to operate for long periods without replacing batteries. Moreover, batteries are usually the heaviest component in almost every WBAN devices [99]. Furthermore, most battery technologies come with corrosive electrolytes or flammable organics which is a health hazard and incompatible for in-body or wearable application from biomedical point of view [100]. RFEH and WPT provides an alternative green energy solution to wirelessly charge wearable or implantable devices.

Radiative near-field WPT based solutions can also be suitable for on-body or, implantable application. Moreover, this method is less prone to the misalignment issue between transmitter and receiver that happens in near-field coupling based WPT [101]. There are still challenges for RF powered wearable devices in context of flexibility; fabrics are broadly suitable for lightweight, low-cost and flexible performance [102]. Stable radiation pattern and reliable efficiency of the antenna in the receiving system is one of the most crucial factors if the person is mobile. In addition, reliability for interfacing rigid and flexible subsystems and efficient power management circuit for extremely low RF input power are required [102-104].

2.2.3 Internet of Things (IoT)

The quality of life is expected to be improved in large scale by the intelligent infrastructure of IoT, enabling the utilization of numerous devices connected through Internet. Most modern industries will see a new paradigm of advancement through IoT. IoT devices typically have wireless transceivers, sensors, processors, and a power source for data acquisition and communication [105]. However, power source issue is one of the

main constraints that have limited the full-scale adoption of IoT technology. RF energy scavenging and WPT can provide a sustainable energy solution for long term operation of IoT devices, where replacing or recharging batteries is not feasible. The efficiency of embedded systems in IoT framework has been advanced in recent years towards achieving the target of fully autonomous sensors with the help of low power radio and microcontrollers [106, 107]. Stability and viability of RFEH and WPT in IoT devices need to be considered by removing the local on-board energy sources, reducing environmental pollution and maintenance cost as well as making the device compact.

2.2.4 Smart Farming/Agriculture

The demand for food is rising prominently with the rapid growth of world population. Food security will be a significant concern as the population of the world is expected to be approximately 9.7 billion by the year of 2050 [108]. Deployment of wireless sensor networks (WSNs) has been an acceptable solution over the years for precision agriculture; smart agriculture with process automation [109, 110]. In addition, a paradigm shift in agricultural technology is emerging due to the application of IoT sensors along with the WSNs [108, 111]. However, power supply for autonomous sensors in the agricultural domain is still a dominant issue. Table 2.4 illustrates power consumption information of some sensor nodes available for agriculture. Solar power has been utilized to extend the battery lifetime of agriculture sensor kits such as the 'Davis 6345CSAU' [112]. Nevertheless, the dependence of solar power on climatic condition is inevitable.

Table 2.4 Wireless Sensor Nodes for Agriculture [110, 112, 113]

Name	Sensors included	Power consumption in active mode	Power consumption in sleep mode	Power supply

MICA2DOT	Accelerometer, temperature, light	15 mW (@3V)	75 µW	3V Coin cell battery
MICAz	Light, temperature, humidity, barometric pressure, accelerometer, GPS, RH, acoustic, video sensor, microphone, sounder, magnetometer	24 mW (@3V)	75 µW	2×AA Battery
MICA2	Light, temperature, humidity, barometric pressure, accelerometer, GPS, RH, acoustic, video sensor, microphone, sounder, magnetometer	24 mW (@3V)	75 µW	2×AA Battery
Cricket	Light, temperature, humidity, barometric pressure, accelerometer, GPS, RH, acoustic, ultrasonic, video sensor, microphone, sounder, magnetometer	24 mW (@3V)	75 µW	2×AA Battery
TelosB	Light,temperature, humidity	10 mW (@3V)	8 µW	2×AA Battery
IRIS	Light, temperature, RH, barometric pressure, acceleration, seismic, acoustic, magnetic and video	24 mW (@3V)	24 µW	2×AA Battery
Davis 6345CSAU [112]	Wireless Leaf & Soil Moisture/ Temperature Station	0.42 mW (@3V)	---	CR123A 3V Lithium battery (Extended lifetime by solar panel)

These sensors could be repowered by replacing the battery [110]. However, this becomes a significant challenge for mass deployment of sensors over large area, leading to great human effort as frequent change of batteries is not a viable solution for farmers. In such

cases, RFEH or WPT technology-based sensors can provide an alternative solution for self-powered operation or, extending the lifetime of sensors without having to replace batteries often. Architectures of WPT enabled IoT devices are of increasing interest to researchers. Figure 2.3 depicts a potential application architecture of RF Energy Harvesting/WPT based solution for remotely deployed wireless sensors in agricultural farmland. Extending the operating time of soil sensors in agriculture by RFEH/WPT can provide a long-term solution to remotely charge wireless sensor with minimum maintenance, irrespective of climatic condition. More controlled and reliable monitoring over agricultural services like irrigation, fertilization, pesticide spraying, animal and pastures can also be achieved.

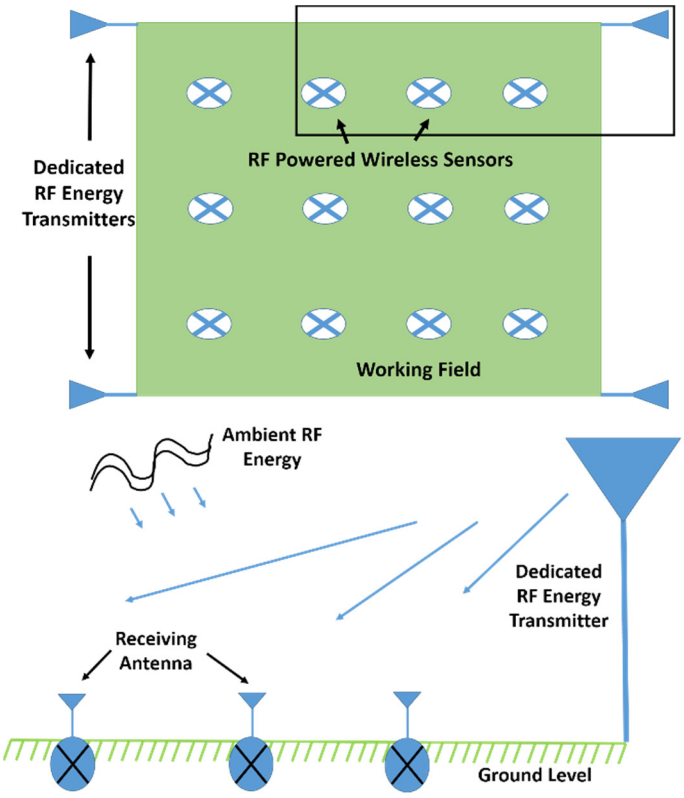

Figure 2.3 Potential Architecture of RF Energy Harvesting/WPT for Remotely Deployed Wireless Sensor

2.3 Antenna Design Requirements

Wireless communication receiver devices and RFEH system receives RF power from ambient sources which are usually unknown. Unlike RFEH, in case of WPT system, transmitting antenna comes into play, which is responsible for providing dedicated power to the rectenna. High gain transmitting antenna is preferred to overcome the challenge of long-distance transmission, as the transmitted power becomes radiated to the surrounding. Maximum efficiency in WPT can be achieved with the combination of high gain transmitting antenna and well-designed rectenna. In this chapter, we focus on the receiving antenna designs. The selection of receiving antenna is crucial for RFEH and WPT since antenna plays the key role in receiving electromagnetic wave from free space. Usually GSM900, GSM1800, UMTS2100, LTE2600 and Wi-Fi band 2.45 GHz bands are used for ambient RF energy harvesting due to wide availability. So, combining all available sources from different frequency bands is recommended for increasing scavenged power. However, in WPT scenario different factors of the transmitting antenna such as operating frequency, transmitting power, polarization, directivity, and gain are controlled and hence receiving antenna design is straightforward. In order to manage the separation distance, WPT receiving antennas should be designed to adapt with the properties of the known transmitting antenna, including bandwidth, polarization, and gain. Evidently, while WPT antennas work primarily in predictable propagation conditions, ambient RFEH antennas perform in unpredictable electromagnetic environments. The low RF power levels in the surroundings make efficient RF energy harvesting a very crucial issue. The scavengeable power levels can be affected by a variety of factors, including received signal parameters (frequency, bandwidth, polarization, power flux density etc.), telecommunication traffic densities and antenna orientation. Hence, RFEH antennas should be able to collect incoming waves with changing

polarization and bandwidth considering the unforeseeable conditions. The goal is to provide enough power to switch on the rectifier circuit which is challenging in real-world scenario with only one antenna. Several types of antennas including microstrip patch, spiral, inkjet printed, differentially fed, flexible, array, multiport etc. are found in literature for RFEH and WPT applications. Each type has their pros and cons. Below are the basic selection properties of receiving antennas.

2.3.1 Frequency

The operating frequency of the antenna depends on the available frequency at the targeted location of application. Multiband antennas are preferred for harvesting more power than single-band antennas. At higher frequency of operation, amount of received RF power reduces due to high free space path loss (FSPL) over long distances. Multiband antennas designed at reasonably low frequency can be used to avoid FSPL. However, capturing power from several frequency ranges can also be covered with wideband antenna. Wideband antennas have comparatively easier design and can be used in different countries with diverse frequency assignments [114]. Figure 2.4 illustrates the received power at different frequencies with the same transmitting power. The illustration is based on Friis law [75]. However, in realistic RFEH and WPT scenarios, there will be multi-path loss in real propagation environment hence, the amount of the received power will vary.

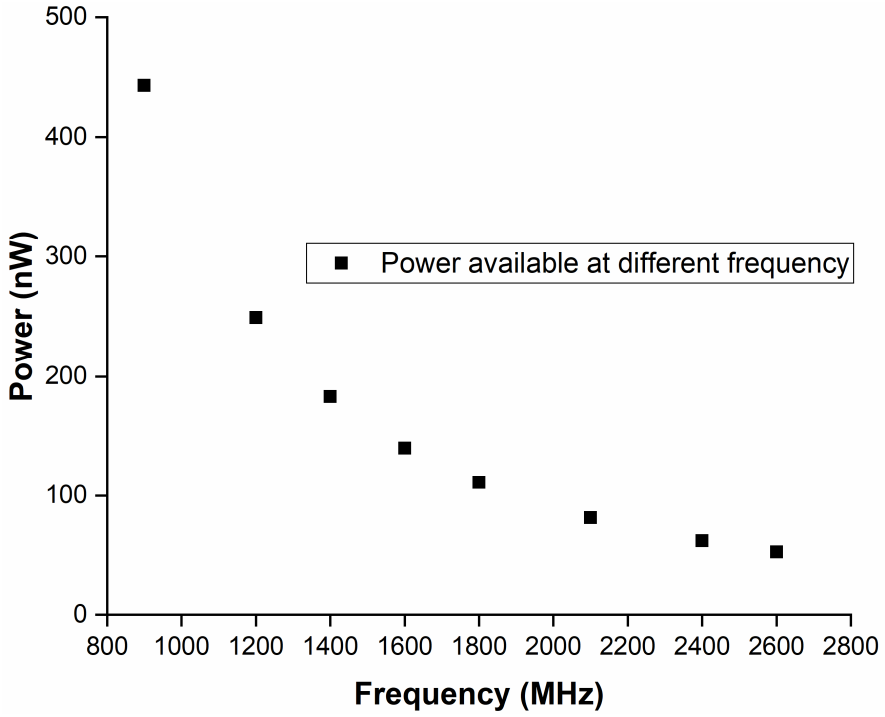

Figure 2.4 Variation of received power at different frequency, considering the receiving antenna (Grx=2 dBi) is 100 meters from the transmitting antenna (Gtx=16 dBi), transmitting power is 20 dBm

2.3.2 Radiation Pattern

Direction and shape of radiation pattern, beamwidth and polarization of the receiving antenna play significant role in capturing the electromagnetic wave. In ambient conditions, as the orientation of the incoming EM wave is unknown, an omnidirectional antenna is preferred. Unidirectional antenna is required for the dedicated RF transmitter for WPT to cover longer ranges.

2.3.3 Polarization

Polarization can be defined in terms of the direction of a transmitted or received wave from an antenna. A mismatch in the polarization of the antennas results in decreased received power. A circularly polarized (CP) antenna is useful because it can receive electromagnetic energy from a variety of polarizations. As a result, a wideband CP antenna can be advantageous for harvesting energy from random polarization especially

for RFEH. Moreover, dual linearly polarized antenna provides further advantage in receiving RF power by avoiding polarization mismatch [115], since achieving wide CP bandwidth using a compact structure is challenging. In case of WPT, the polarizations of the transmitted waves is known beforehand. Therefore, choice of receiving antenna can be broad having different kind of polarizations, including linear polarization (LP), right-hand and left-hand circular polarizations (RHCP/LHCP) as long as appropriate level of beam-pointing (from transmitter) and polarization matching can be established and maintained.

2.3.4 Gain

High gain antennas are useful in RFEH and WPT application. In RFEH scenario, increased dimension of an omnidirectional antenna can achieve more power. According to [116], higher directivity in antenna design does not improve harvested power in ambient RFEH. Hence, moderate amount of gain will suffice for ambient RFEH, as long as the antenna is efficient enough. However, high gain antenna will enhance the received power if the power is transmitted from a known source [117]. Gain and directivity are related according to the equation (2.2) [118]. Low-gain receiving antenna reduces the received power in WPT.

$$G = \mathcal{E}_R D \qquad (2.2)$$

Where G, $\mathcal{E}_R$, and D are gain, radiation efficiency and directivity of the antenna respectively [8, 119].

2.3.5 Bandwidth

The receiving antennas can be designed to operate at multiple frequency or single frequency. Wide bandwidth is preferred to harvest RF power from multiple RF sources simultaneously. Bandwidth of the antenna is related to antenna Q-factor by the following equation:

$$Q = \frac{f_r}{BW} \tag{2.3}$$

Where, Q is the quality factor, BW is the bandwidth and f_r is the resonant frequency of the antenna. This equation is applicable to resonant antennas. Bandwidth becomes narrower for high Q antenna. Moreover, the Bode-Fano criterion illustrates that, broader bandwidth can be achieved at the expense of higher value of reflection coefficient and good impedance matching is achieved at finite number of frequencies only [120].

Generally, dimension of wideband antennas tends to be larger compared to the narrowband antennas. Design of ultra-wideband antenna will be quite inefficient considering the antenna performance bounds. On the contrary, designing multiband antenna with stable radiation pattern, polarization and efficiency with wide frequency band is crucial and challenging. Achieving wideband performance in multi-band antenna design is difficult because of competing requirements. Broadband performance usually requires a wide frequency range, which can be challenging to maintain while keeping all desired bands at high efficiency, stable radiation patterns, and consistent polarization. Sophisticated design strategies as well as trade-offs on certain antenna performance elements are needed to balance these factors. Wide bandwidth multiband antennas are necessary for contemporary wireless communication systems. Because these antennas can function in different frequency bands, there is greater flexibility, better usage of the spectrum, and compatibility with a wider range of communication standards. Generally

antennas with reflection coefficient of less than -10 dB are accepted. However, the reflection coefficient requirements are met in most multiband antennas at the cost of degraded radiation efficiency at higher frequency [121, 122].

2.3.6 Efficiency and Size

Antenna efficiency is dependent on shape, size, material of antenna structure, frequency, and impedance of the antenna. The antenna efficiency decreases by reducing the physical size of the antenna [123]. A trade-off between antenna efficiency and size is expected in RFEH or WPT depending on the intended application.

2.3.7 Sensitivity

The ability to capture extremely low power in ambient condition is one of the main design limitations of designing rectifying antenna (Rectenna). Losses from dielectric substrate, rectification device, and matching network should be limited as much as possible to increase the rectenna sensitivity and to enable operation in ultra-low power environments [124]. Additionally, the choice of diodes and rectifier circuit design have foreseeable effects on sensitivity.

2.4 Antenna Technologies in RFEH, WPT and Wireless Communication

The antenna is the front-end component of every RF power receiving device, and its performance has a direct impact on the overall RFEH/WPT system efficiency. Hence, the selection and proper antenna design must be approached with particular care. The antennas for RFEH must face critical operational conditions like randomly changing incoming waves covering multiple polarization, ultra-low power density and fluctuating levels of incident power. However, receiving antennas for WPT are designed with the objective of capturing maximum power from a dedicated transmitting antenna in

deterministic propagation conditions (known source parameters). In this section, different state of the art designs and types of antennas have been discussed.

2.4.1 Low-Profile Antennas

The emergence of modern compact electronic devices enables the antenna engineers and researchers to design small antennas. Patch antennas are one of the most convenient antenna types as low-profile candidate that can be employed for RFEH and WPT. Patch antennas are extremely compatible with wireless devices considering their small foot-print, light weight and inexpensive fabrication cost. Different types of low-profile antenna designs are listed in Table 2.5 to provide an overview of the state of the art.

Table 2.5 Overview of different low-profile antennas

Refs.	Antenna type	Design technique/geometry/substrate	Dimensions	Operating frequency	Gain (dBi)	RF-DC efficiency of the rectenna (%)
[125]	Aperture-coupled dual linearly polarized patch antenna	Three layers based, 6 mm foam layer between Arlon A 25 N substrate, cross shaped slot on the patch	Patch size 34×34×7 mm^3, Area of foam unspecified, however bigger than the patch.	2.45 GHz	7.7	38.2 @ 1.5 $uWcm^2$ power density
[126]	Patch	Modified Koch fractal patch on high permittivity substrate, Rogers RO6010 with Rogers RO6002 superstate.	20×20 mm^2	2.45 GHz	-.25	---
[127]	CPW fed patch	T-shaped monopole loaded with interdigitated capacitor on FR4 substrate	101.8×46.5 mm^2	866 MHz	2	54 % @ 80 uW/cm^2 power density
[128]	Microstrip-fed dipole	Two poles of the antenna are folded on Rogers 5880 substrate, separated by a ground plane.	62×62 mm^2	900 MHz	1.84	---

[129]	coplanar strip-line fed	Slotted and folded dipole on Teflon substrate	53×17.375 mm^2	2.45 GHz	2.65-3.9	55% @ 1 mW/ cm^2 power density
[130]	Three-layer planar inverted-F	Circular shaped planar inverted-F antenna (PIFA) with two radiating layers, on 0.765 FR4 substrate	$3.14\times6^2\times1.584$ mm^3	915 MHz	-20.2	53% (Between 20 cm separation of Tx and Rx)
[131]	Folded dipole	Folded dipole using 0.1 mm thick copper sheet	30×30×10 mm^3	918 MHz	1	23% @ 1 mW input power
[132]	Patch	Slotted fractal radiating patch with partial grounding on 1.6 mm thick FR4 substrate	31×18.5 mm^2	2.15-2.9 GHz	2.2 @ 2.45 GHz	62% @ 0 dBm input power, 28% @ -10 dBm
[133]	CPW fed patch	CPW fed radiating patch with 4 rectangular slots	18 mm × 30 mm^2	2.45 GHz	5.6	42 % @ -10 dBm input power
[134]	Double layer Patch	Fractal patch with bent corners, helical patch between ground and main radiating patch, FR4 substrate	38×38 mm^2	2.45 GHz	3	24% @ -10dBm input power
[135]	Proximity coupled patch	Two annular slot-based patch on thin paper substrate	110×110 mm^2	0.79–0.96 GHz 1.71–2.17 GHz, 2.5–2.69 GHz 2.5–2.69 GHz	2.3 @ 940 MHz,	20% @ 2600 MHz, 22% @ 1800 MHz, 44% @ 900 MHz (Power density 1 uW/cm^2)
[136]	Rectangular patch	Double layer FR4 substrate based, separated by airgap	100x100x5 mm^3	2.45 GHz	8.35	---
[137]	Printed flat dipole antenna	Quasi-circular shaped, modified radiating structure from half-wavelength dipole antenna with rectangular loop on 0.8 mm thickFR4 substrate	110×60 mm^2	ISM 868-/915-MHz	2.6	25% @ 0.25 μW/cm^2 power density
[138]	Co-axial fed	Fractal geometry based radiating patch on 1.6 mm thick FR4.	60 × 60 × 1.6 mm^3	0.8–1.2 GHz,	1 @ 900	28% @ 900 MHz,

	square patch			1.6–2.1 GHz, 2.2–2.8 GHz, 3.1–4.0 GHz, 5.3–6.4 GHz, 7.0–7.8 GHz	MHz, 3@ 2 GHz, 5@ 5.5 GHz, 4@ 7 GHz	24% @ 2.5 GHz, 9% @ 1.8 GHz, 17% @ 3.5 GHz, 13% @ 5.5 GHz, 36% 7.5 GHz (input power 0 dBm)

According to the Table 2.5, one of the most common techniques used in compact antenna for RFEH application is employing fractal geometry in the patch antenna structure. Due to the property of self-similarity, embedding fractal geometry in antenna structure is a potential solution to design compact rectenna [126, 132, 134, 138-142]. With the increment of iteration order in fractal structure, the effective length increases. However, fractal geometry can be limited to a few iteration orders. As the number of iterations increases, the complexity of the design geometry increases, which is likely to increase the difficulty of fabrication. [132]. Introducing slots on a patch is also a popular technique to miniaturize antenna [129, 135, 143, 144]. Slots in antenna can effectively alter the surface current distribution of the antenna which can contribute to reduction of size and desired design goals. The proposed rectenna in [132] utilized both fractal and slotted geometry technique for the compact design of receiving antenna. The antenna design is depicted in Figure 2.5. Second iteration of the fractal shape is used in the patch, etched about in the middle of the radiating element on FR4 substrate with 1.6 mm thickness.

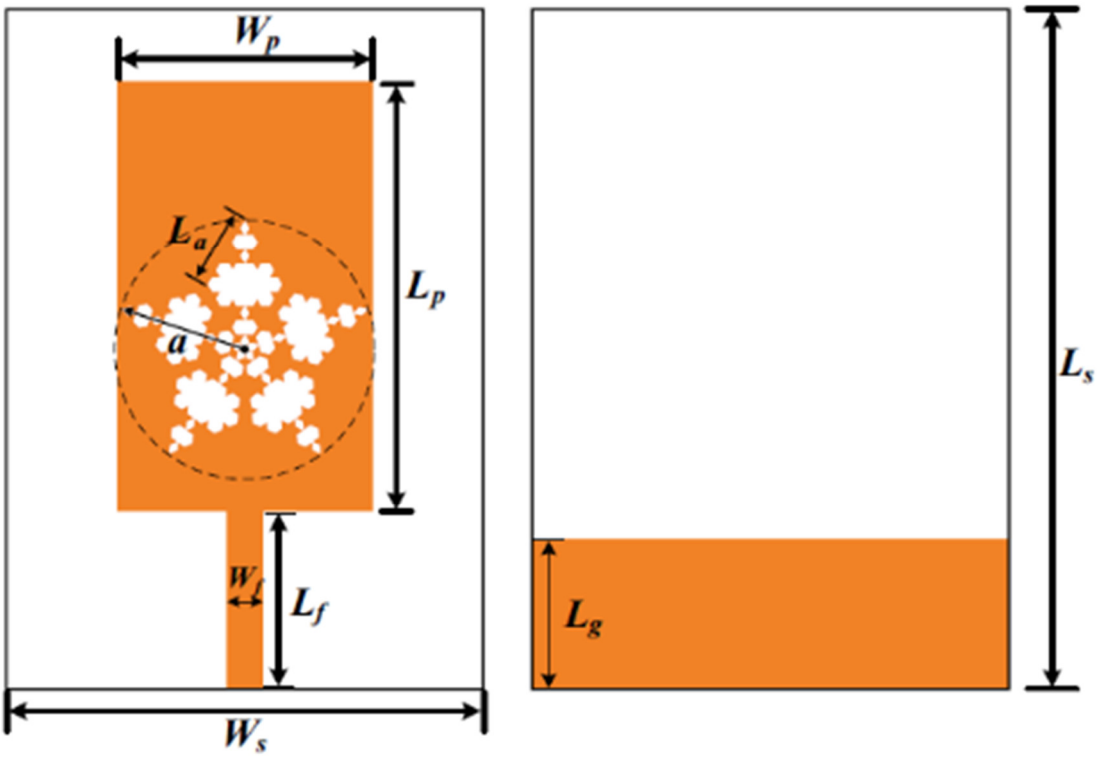

Figure 2.5 Slotted fractal antenna for RF energy harvesting [132].

The fractal geometry is achieved by the algorithm of iterative function system (IFS), an advantageous method to generate fractal structures based on different transformation techniques like rotation, translation and scaling. The final design of the antenna achieved a dimension of 31×18.5×1.6 mm3, which is quite compact for applications where more space is required for other circuitry. The antenna operating frequency ranges from 2.15-2.9 GHz. As the iteration of the fractal increased, the antenna obtained better impedance matching with optimum bandwidth of 850 MHz. RF-DC conversion efficiency of 28% is achieved by the rectenna employing the proposed antenna at 2.42 GHz, when the input power is -10 dBm. It can be assumed that, the RF to DC rectification efficiency of the rectenna reduces with the decrement of the antenna dimension. However, selection of antenna dimension should be considered based on the intended application.

Dedicated RF transmitter can be used as a source instead of ambient RF energy in WPT scenario, where it is required for application specific condition [145, 146]. For instance,

a tiny circular antenna has been proposed for a deep brain stimulation (DBS) device - a head-mountable device to perform experiment on animals [130]. The tiny planner inverted-F antenna is based on two layers of circular structure, employing meander-line, shorting and stacking technique for the miniaturization of the antenna on 0.765 mm thick FR4, depicted in Figure 2.6.

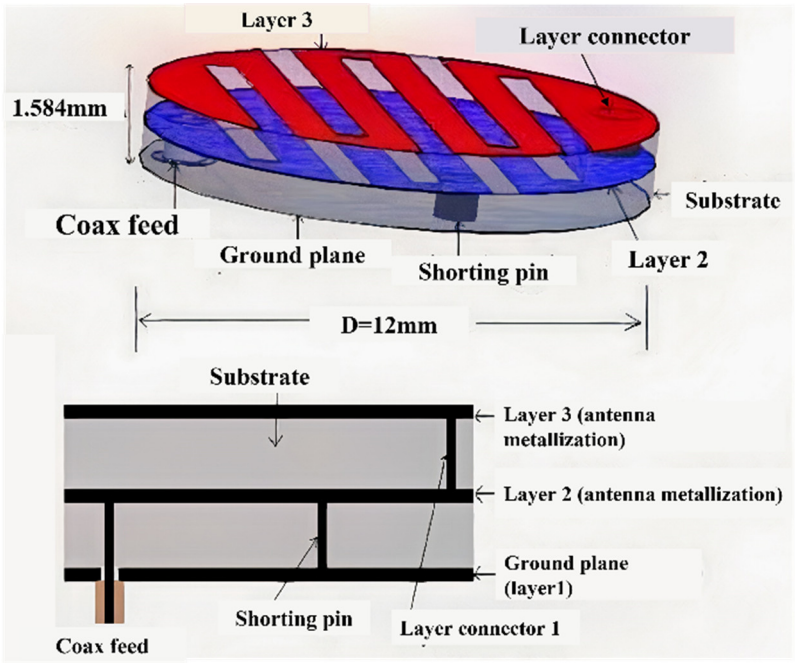

Figure 2.6 Design configuration of the double-layered PIFA antenna [130].

Effective current flow length has been increased in the antenna due to meandering and shorting techniques leading to two additional antenna miniaturization methods proposed in [147]. The PIFA structure is made circular to facilitate the utilization in the DBS device. The antenna layers are connected via shorting pin, where the location of the shorting pin is crucial in context of antenna performance. However, the antenna suffers from low gain and radiation efficiency due to substantial miniaturization [148, 149], which finally affected the rectenna performance. The proposed PIFA antenna achieved only −20.20 dB of gain, which is substantially smaller than conventional PIFA. Significant amount of

transmitting power, 34.77 dBm is required to receive only −3.193 dBm within a 20 cm distance.

The objective of miniaturizing antennas is to use the available space effectively to fit a compact antenna with competitive gain and efficiency performance compared with its equivalent conventional large antenna. An insightful discussion on antenna miniaturization has been documented in [150]. Meander-line, fractal geometry, ground plane engineering, use of capacitive or reactive loading and others are effective antenna size reduction techniques. Meandering technique can be useful in UHF [151] and implantable applications. However, high gain cannot be expected from meander-line antennas as the close radiating arms tend to cancel each other's respective radiation in the far field. Fractal antennas can be potentially used for miniaturization as well as multiband operation. Sierpinski gasket is one of the promising fractal geometries that can lead to multiband antenna design [152, 153]. Other fractal geometries include Sierpinski carpet, Giuseppe Peano, Koch snowflake. All of them have their own drawbacks such as limitation in applying at antenna edge, complex geometry and narrowband operation. However, the enhancement of bandwidth and miniaturization both have been reported by using complementary Minkowski fractal [154].

Ground plane engineering methods are usually associated with slots that can arise coupling or interference with nearby electronic devices which can further introduce electromagnetic incompatibility issues. Overall, the trade-off between low-profile antenna and antenna performance is huge, as different design techniques applied to compacting antenna come with the degradation of bandwidth, gain, efficiency and impedance mismatch [150].

Innovative antenna designs are required to provide a balanced trade-off between antenna dimension and size with a view to achieving maximum efficiency with minimum antenna size. Wheeler was the first one to illustrate the maximum dimension of electrically small antenna is to be '$\lambda/2\pi$' [149]. This can be defined further by '$ka < 0.5$', where 'k' is the radian/meter and 'a' is the sphere radius of the antenna's maximum dimension [155]. An electrically small antenna restricted by a volume limit, is followed by a minimum Q factor value. The impedance bandwidth decreases with higher Q factor value. Moreover, in comparison with radiation loss of antenna, losses in dielectrics, conductors and other materials in antenna have significant impact on electrically small antenna's efficiency η; illustrated as:

$$\eta = \frac{R_r}{R_r + R_m} \times (1 - \Gamma^2) \tag{2.4}$$

where, Rr and Rm are radiation resistance and resistance of material loss in the antenna and Γ is the reflection coefficient. In addition, due to the existence of capacitive input impedance of electrically small antenna, additional matching network might be required for the system to work, which can impact on overall antenna efficiency [156]. Nevertheless, this can be reduced by applying different antenna techniques such as capacitive loading or, inductive loading.

Applying topological optimization method of antennas can benefit in achieving low-profile receiving antennas [157, 158]. Pixelated antennas feature designing antennas within application specific boundaries. Three antennas are designed using pixelization technique for the same frequency with three different size that demonstrates the potential of this method in miniaturized antenna design [157]. Although the work focused mostly on impedance optimization, gain optimization is also possible.

Table 2.6 Overview of common antenna miniaturization techniques [150, 159-163]

Antenna design technique	Pros	Cons
 Meander-line antenna [159, 164]	• Reduction in antenna dimension by introducing meandered microstrip line consisting right angle bends. • Simple design structure. • Potential for lower UHF.	• Unable to provide high gain. • Low radiation efficiency.
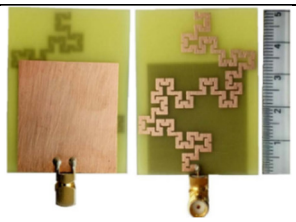 Fractal-based antenna [160, 161]	• Requires smaller area than Euclidean geometry-based antennas. • Can provide input impedance and radiation pattern like large antennas. • Efficient use of volume due to space filling geometry.	• Radiation efficiency degrades due to miniaturization. • May lead to sophisticated design and fabrication complexities. • Numerical design limitations.
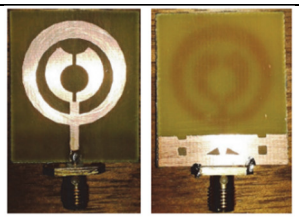 Defected-ground-structure-based antenna [162]	• Increased slow wave factor providing compact design. • Simpler to design and fabrication. • Easier realization of equivalent circuit. • Reduced dimension than photonic band gap (PBG) and electromagnetic band gap (EBG) structures.	• Embedded slots may create unwanted coupling. • Directivity may reduce due to unintended radiation. • Application limited to planer antennas.
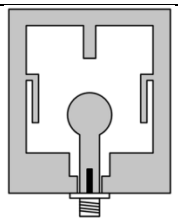 Other techniques [150, 165, 166]: Slot antenna example [167]	• Slotting • Optimizing geometrically, topological optimization • Using shorting pins • Using metamaterial, electromagnetic band gap (EBG) structures etc.	

The miniaturization of antenna is limited by the application specific RFEH or, WPT condition. It should be noted that common small communications antennas are

incompatible with RFEH and WPT. The amount of power received by the device is directly proportional to the effective aperture size and efficiency of the antenna. Regardless of those parameters, wireless communication antennas can be made compact, as the sensitivity of communication devices can be as low as -100 dBm. However, rectifiers can only operate at a particular power level. The practical challenge in designing antennas with small form factor for energy harvesting is to control the performance degradation with reduction of antenna size. Very tiny antennas will be impractical for ambient RF energy harvesting application. Autonomous implantable or wearable applications are also subjected to FCC rules [168].

2.4.2 Multi-band Antennas

Designing an antenna system that can perform well across a variety of frequency bands is necessary to achieve multi-band antenna performance. This requires setting considerable thought to a number of variables, including the choice of frequency band, kind of antenna, radiation pattern optimization, required bandwidth, choice of material, simulation, and testing. For constant coverage, radiation patterns must be optimized, and there must be enough bandwidth available to cover all of the frequencies in each band of interest.

Simultaneous power reception from different radio frequency bands can be useful where more than one RF source operate at different frequency bands. Moreover, the sources may be located at a random distance from the receiving antenna with varying power budgets [169]. The available RF signals in ambient condition are low in power, typically –5 to –30 dBm, usually multiple frequency bands are used to distribute the signals [170]. Hence, multiband antenna can enhance RFEH in such cases. This section discusses the multi-band antenna designs for RFEH/WPT. Multiband antenna/rectenna for RFEH is challenging due to non-linear variation of the rectifier input impedance with input power

level, frequency and load impedance. Input power of a multiband antenna is the summation of available input power at individual frequency bands, it can be illustrated as [171],

$$P_T = \Sigma_{i=1}^{n} P_{fi} \quad (2.5)$$

Where, n is the number of frequencies, Pfi is the power received at i'th frequency and PT is the total available power due to multiband operation. Table 2.7 summarizes some recent multi-band antennas for RFEH/WPT.

Table 2.7 Multi-band antenna/rectennas reported in literature

Refs.	Antenna design type	Operating bands	Size	Gain	Antenna efficiency	Single frequency rectenna efficiency (RF-DC)	Combined Dual/multi band rectenna efficiency (RF-DC)
[172]	π-shaped multilayered PIFA meandered strip on Rogers 3210	402 MHz, 433 MHz, 2.45 GHz	10×10×2.54 mm^3	-7 dB at 402 MHz, -11 dB at 433 MHz, -15 dB at 2.45 GHz	---	---	---
[173]	Intermittent meander-line on Duriod 5880	600 MHz to 2 GHz	52×50 mm^2	-2 to 6 dB	---	---	---
[174]	Slot loaded folded dipole on Arlon 25N	915 MHz, 2.45 GHz	60×60×29 mm^3	1.87 dB @ 915 MHz 4.18 @ 2.45 GHz	---	33% @ 915 MHz; 23 % @ 2.45 GHz (Input power -10dBm)	34% @ -10 dBm input power
[175]	Printed monopole with meander-lines on 0.83 mm thick Rogers 4003	900 MHz, 1800 MHz	46×30 mm^2	---	---	---	40.8% (Input power @ -20 dBm)
[170]	Planar cross dipole with bow-tie shaped patch on 1.6 mm thick FR4	550 MHz, 750 MHz, 900 MHz, 1.85 GHz, 2.15 GHz, 2.45 GHz	160×160 mm^2	2.5 dB @ 550 MHz, 3.4 dB @ 750 MHz, 3.6 dB @ 900 MH, 4.9 dB @ 1.85 GHz,	---	---	80% (Input power unspecified)

				5 dB @ 2.15 GHz, 4.4 dB @ 2.45 GHz			
[53]	L-probe stacked patch using Rogers 3003	925MHz, 1850 MHz, 2150 MHz	200×175× 46.6 mm^3	8.15 dB @ 915 MHz, 7.15 dB @ 1850 MHz, 8.15 dB @ 2150 MHz	---	25% @ 2170 MHz, 32 % @ 1820 MHz, 42% @ 925 MHz (-10 dBm input power)	50%
[176]	CPW fed patch with stepped ground plane on FR4	900 MHz, 1800 MHz, 2100 MHz, 2.4 GHz	48×42 mm^2	1.1 dB @ 900 MHz, 2.2 dB @ 1800 MHz, 2.1 @ 2100 MHz, 2.2 @ 2.4 GHz	---	38% @ 900 MHz, 27% @ 1800 MHz, (Input power 0 dBm)	---
[177]	Circular shaped printed monopole on FR4	900 MHz, 1800 MHz, 2100 MHz, 2.45 GHz	130×80 mm^2	2.6 dB @ 900 MHz, 3.6 @ 1800 MHz, 3.8 @ 2100 MHz, 4.7 @ 2.45 GHz	94-96%	25%@1820 MHz, 27% @ 2150 MHz (Input power – 7dBm)	---
[95]	Corrugated slot line based microstrip patch on Rogers RO4350	900 MHz, 2100 MHz, 2.36 GHz	70×66 mm^2	1 dB @ 900 MHz, 2.64 dB @ 2.025 GHz, -0.19 dB @ 2.36 GHz	42.2% at 0.9 GHz, 61.3% at 1.575 GHz, 72.6% at 2.025 GHz, 32.8% at 2.36 GHz	47 % @ 2.025 GHz, (Input power @ -11.1 dBm)	---
[178]	Printed monopole with fractal element on 0.8 mm thick Arlon substrate	900 MHz, 1800 MHz	100 × 60 mm^2	0.95 dB @ 870 MHz, 3.15 @ 1830 MHz	90% at 0.87 GHz, 83% at 1.83 GHz	62 % @ 880 MHz (15.9 $\mu W/cm^2$) 50% @ 1910 MHz (19.1 $\mu W/cm^2$)	---

[179]	Truncated square patch with slots on FR4 substrate	4.75 GHz, 5.42 GHz, 5.76 GHz, 6.4 GHz, 6.9 GHz, 7.61 GHz	40×45 mm^2	5.5 dB @ 4.75 GHz, 6.3dB @ 5.42 GHz, 6.75 dB @ 5.76 GHz, 7.1 dB @ 6.4 GHz, 7.1 dB @ 6.9 GHz	---	2% @ 4.75 GHz, 1% @ 5.76 GHz, 0-2 % @ 6.4,6.9,7.1 GHz (Input power -10 dBm)	---
[180]	Cube antenna using 3D printing and screen printing	900 MHz, 1800 MHz, 2100 MHz	50×50×50 mm^3	-0.8 dB @ 900 MHz, 4.7 dB @ 1800 MHz, 2.3 dB @ 2100 MHz	---	---	---
[52]	Differentially fed slot antenna using FR4 substrate and copper sheets	2.1 GHz, 2.4-2.48 GHz, 3.3-3.8 GHz	120×120× 30 mm^3	7 dB @ 2 GHz, 5.5 dB @ 2.5 GHz, 9.2 dB @ 3.5 GHz	85% at 2GHz, 75% at 2.49 GHz, 72% at 3.4 GHz	37% @ 2 GHz, 19% @ 2.5 GHz, 12% @ 3.5 GHz (Input power -15 dBm)	---
[135]	Nested annular slot based dual antenna approach on paper substrate	900 MHz, 1750 MHz, 2.45 GHz	110×110 mm^2	1.3 dB @ 900 MHz, 5 dB @ 1750 MHz, 5.5 dB @ 2.45 GHz	---	47% @ 900 MHz, 22% @ 1.8 GHz, 20% @ 2.6 GHz (At 1 $\mu W/cm^2$)	---
[181]	Stacked circular slotted patch	0.908-0.922 GHz, 2.35-2.50 GHz	120×120 mm^2	5.41 dB @ 918 MHz, 7.94 dB @ 2.48 GHz	---	19% @ 900 MHz, 17% @ 2.45 GHz (Input power -10 dBm)	---

Most multiband antennas are proposed to cover GSM-900, GSM-1800, 2100 MHz and 2.4 GHz bands due to the availability in environment. However, other bands are also considered like medical implant communication system (MICS) , industrial, scientific and medical (ISM) and C band [172, 179]. It has been shown that PIFA structures with meander stripes and π-shaped radiating element can obtain resonance in dual band [182, 183]. This method has been applied in implantable triple band rectenna design for

biotelemetry application [172]. The two fundamental frequencies are achieved by meander-line and stacking of the radiating strips. Excitation of a harmonic mode in the meander shaped strips enabled a third operating band at 2.45 GHz. Folding half-wave dipole antenna and introducing slots can provide dual resonances [174]. High gain dual band antenna using printed broadband Yagi antenna has been proposed for ambient RF power scavenging. Broad half power beamwidths (HPBWs) has been achieved, 110° and 170° at 2.15 and 1.85 GHz, respectively, which can facilitate less precise placement of the rectenna to achieve good power conversion efficiency (PCE) [184]. Dual band rectenna operation is introduced based on printed monopole antenna, inspired by second order Koch fractal based arm for low frequency and folded strip-line for higher frequency bands [178]. Multiband antennas based on spoof localized surface plasmons (LSP) resonator, dual-port L-probe feeding, multiple radiating line with stepped ground plane, slot loaded square patch, 3D printed cantor fractal, differentially fed slot have been also reported in literature for different rectenna applications [52, 53, 95, 176, 179, 180]. Impedance bandwidth of a quad band 'circular arc connected strip-line' patch based antenna has been improved by using stepped ground plane [176]. Proximity coupled feeding can help improving the impedance bandwidth of the receiving antenna as well [179]. Figure 2.7 illustrates some multiband antenna designs opted for RFEH/WPT. Several antenna techniques that have been reported for multiband RFEH/WPT are highlighted below.

- Slotted ring antenna
- Stack antenna
- Differential antenna
- 3D printed antenna

Resonance at multiple bands have been obtained by slotted ring antenna depicted in Figure 2.7(a). Multiple resonant modes have been achieved using annular ring slot patch

surrounded with T-shaped periodic array of slots. The degree of electromagnetic energy coupling has been enhanced using a metal disk by the end of the microstrip conductor and Rogers RO4350 has been used as the antenna substrate [95].

Back to back placement of patch antennas using stacking technique and dual port feeding is an effective way of achieving high gain with the ability to capture RF power from nearly all directions at GSM-900, GSM-1800 and UMTS-2100 bands [53]. L probe feeding method [185] is found to be improving the bandwidths of the operating bands as well. High isolation is provided by back to back placement of the ground plane, enabling similar performance for both antennas with unidirectional radiation. Rogers 3003 has been utilized as substrate and superstrate for this antenna.

Multiband antenna with differential feeding can be useful in suppressing harmonics with reduced cross-polarization levels while yielding larger output power than that of single ended patch antennas [52]. Multiband characteristics have been achieved by two square slots on the ground plane. The antenna is printed on 1.6 mm thick FR4 substrate and a metal reflector plane has been placed to enhance the gain.

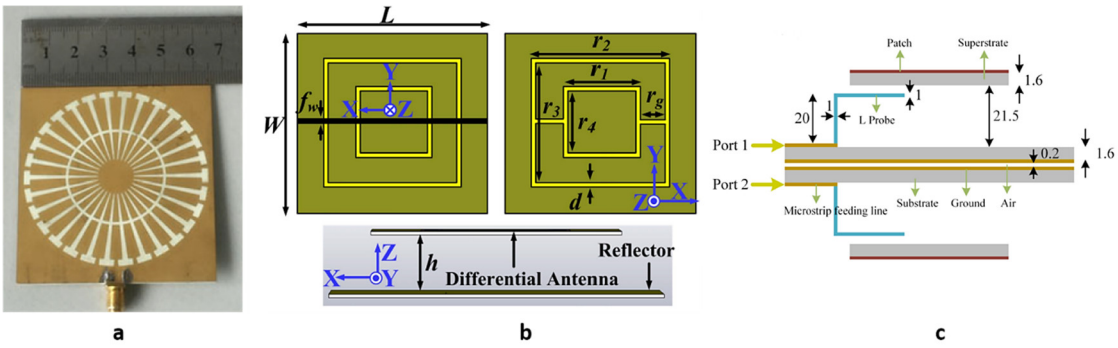

Figure 2.7 Multiband antennas for RFEH; (a) LSP resonator based annular ring slot [95], (b) slotted differentially fed with reflector [52], (c) stacked dual port with L probe feeding [53]

3D printing technology can facilitate low-cost fabrication of antenna and rectenna by proficient use of volume. A 3D printed multiband antenna based on system-on-package concept facilitated the rectenna circuit inside a cube structure [180]. Cantor fractal structures have been utilized in this antenna as multiband radiating element on different faces of the cube package.

Figure 2.8 illustrates the RF-DC power conversion efficiency of different rectenna based on multiband receiving antenna at different frequency bands. Antennas that operate at the lower end of the frequency spectrum captured more power. As seen from the figure, the rectennas achieved considerably low RF-DC efficiency at higher frequencies.

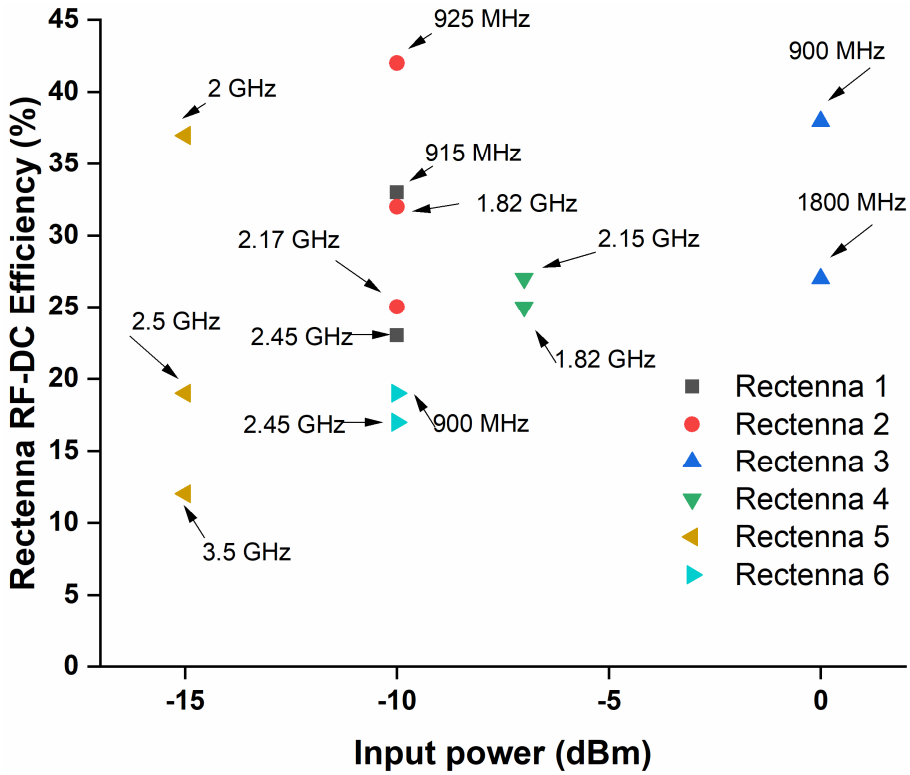

Figure 2.8 RF-DC efficiency of rectennas utilizing different dual/multiband antennas; Rectenna 1 [174], Rectenna 2 [53], Rectenna 3 [176], Rectenna 4 [177], Rectenna 5 [52], Rectenna 6 [181]

2.4.3 Antenna Polarization

Performance of an RFEH or WPT system could make significant difference based on the choice of circularly polarized (CP) or linearly polarized (LP) receiving antenna. Since electromagnetic waves are broadcast on single plane in linear polarization, a linearly polarized receiving antenna is required to be fixed upon the same plane as the transmitting antenna, to receive optimum RF power. Hence, a linearly polarized receiving antenna does not have much of freedom of orientation. However, greater range can be achieved by LP antennas due to concentrated emission, which is more than a CP antenna of same gain. Conversely, the vagueness of incoming ambient RF signals negatively affects the received power of the ambient RFEH system, if linearly polarized antennas are used. For instance, performance of wearable RF energy harvester can be degraded with the motion of the object or human. On the contrary, electromagnetic waves are emitted in a corkscrew style in CP antennas. Now, applications can decide the type of antenna to be used. If the orientation of the transmitting signal is known and receiving appliance can be located on the same plane of the transmitting antenna, a linearly polarized antenna can be considered. However, if the incoming RF signals' polarization is inconsistent, appliances could be benefited more by circularly polarized receiving antenna with stable performance. A comparison between LP and CP antennas is given in light of RFEH and WPT application in Table 2.8.

Table 2.8 LP antenna vs. CP antenna for wireless applications

Features [186-191]	Linearly polarized antenna	Circularly polarized antenna
Collection of RF energy from random polarization	No	Yes
Long range power transmission/reception	Yes	No
Variation of output voltage in rectenna due to change in Tx/Rx rotation	Yes	No
Fade resistant	Less	More

Alignment to the Tx antenna	Necessary	Not necessary
Feasibility of energy transmission to mobile devices	Less	More
Optimised global efficiency	Less	More
Multipath effects	Sensitive	Insensitive

A wave's polarization can be defined with regards to the radiated wave or received wave in a specific direction by an antenna [118]. CP antennas can provide better flexibility than linearly polarized antennas in wireless systems. CP antennas are well-found with certain advantages such as reduction of fading effect or multipath interference due to reflected RF signals from different objects and ground, independence of orientation between transmitter and receivers and immunity to the effect of 'Faraday rotation' in ionosphere [192-196]. RFEH and WPT system performance can be significantly enhanced by using CP antennas due to their improved invulnerability of polarization mismatch loss and multipath distortion which can facilitate RFEH or WPT system with greater flexibility of placement and signal reception [197]. Two orthogonal components of electric field are the requirements to achieve circular polarization in the far field region. A circularly polarized antenna design can be obtained, if the total electric field of the antenna has two orthogonal components with 90° phase difference and equal magnitudes [118, 192, 198, 199]. Generally, CP antenna performance is evaluated by considering axial ratio (AR) <3dB as a figure of merit. However, most conventional circularly polarized microstrip antennas suffer from low AR bandwidth [200]. Table 2.9 illustrates some of the basic CP antenna types and some common techniques to design circularly polarized antennas. Though most antennas reported for the application of RFEH or WPT system are linearly polarized [53, 133, 201-204] , applications such as RFEH and the WPT system will necessitate the development of novel circularly polarized antennas with great performance.

As seen from Table 2.9, dual or multiband CP antennas tend to have low axial ratio bandwidth. Most sophisticated and geometrically large CP antenna designs resulted in good performance in lower operating frequency bands [205-207]. These kind of antenna designs can be useful in RFEH or WPT at the cost of design complexity or large size.

However, cavity backed, and crossed-dipole antenna designs may not be potential for RFEH or WPT based portable applications due to their comparatively large structure [207-210]. In addition, CP antennas with omnidirectional radiation pattern provide additional advantage in RFEH system since these antennas can independently receive radio frequency irrespective of wave's polarization diversity and insensitive to multipath effects.

Table 2.9 Examples of CP antenna designs

Basic CP antenna types [192]	▪ CP Microstrip Patch Antennas ▪ CP Slot Antennas ▪ CP Wire Antennas ▪ Spiral Antennas ▪ Helix Antennas ▪ Quadrifilar Helix Antennas and Printed Quadrifilar Helix Antennas ▪ CP Dielectric Resonator Antennas ▪ CP Horn Antennas ▪ CP Arrays				
Refs.	CP Antenna Design type/technique	Operating frequency	3 dB AR bandwidth	Gain (dB)	Remarks
[205]	Bowtie dipole with co-axial feeding 90° hybrid feed network	0.94-1.7 GHz	51.8%	9	Gain increased by connecting bowtie patches. However, large reflector ground plane increased overall size. Supporting frame is required for mechanical stability.
[200]	CPW feed nesting L slot on the ground	1.77-6.06 GHz	60.9%	3.9 (Avg.)	Simple feeding structure is used with 80 mm reflector.
[211]	Ground slotted triangular monopole with branched microstrip feed	1.99-4.28 GHz	46.8%	2-2.6	Broadband circular polarization performance

					achieved with simple compact design structure.
[212]	Dual band dielectric resonator with modified patch	1.9 GHz, 2.4 GHz	3.16%, 5.06%	1.4, 1 (Avg)	Compact design with low AR bandwidth and gain.
[213]	Dual band printed monopole with semi-circular patch and Rectangular L-shaped adjusting stubs, ground connected complementary metal structure	2.5 GHz, 5.8 GHz	1.65%, 11.9%	<2 dB, 1.3-4.5 dB	Single fed, simple and compact antenna, advantageous for easy circuit integration.
[214]	Dual band folded annular slot with meta surface	2.5 GHz, 3.5 GHz	0.0032%, 4.28%	6.52, 7.04	Simple design but low AR bandwidth with moderate antenna size.
[215]	Square radiating element with cross slot and no-resistor feed network	0.961-1.204 GHz	6.8%	5.4	PTFE substrate-based design with a large height of 20 mm.
[216]	Radiating patch with inverted U-shape and I and L structured strips, simple square shaped frequency selective surfaced placed below the patch	2.4, 3.5, 5.3, 5.8 GHz	5.4%, 8.3%, 3.7%, 2.9%	5.95, 6.92, 6.37, 6.07	Simple design. However, overall antenna height is large, about 30 mm.
[217]	Slot loaded open ended ground plane with stair formed dielectric resonator and a stub with open circuit	3.844-8.146 GHz	46.0%	3.9	Wideband performance, 92% radiation efficiency with simple hybrid structure.
[206]	Crossed dipole with reflector, rotating circular and straight dipole printed on FR4 substrate	1.01-2.01 GHz	41.3%	6	Large in overall dimension with 50 mm antenna height.
[218]	Extended stub from square slotted ground plane, perpendicular to modified microstrip feedline	3.5-9.25 GHz	40%	0.8–4.5	Single fed, simple and compact antenna with 25×25 mm^2 size
[207]	Crossed stripped dipole with dual cavity backplane	1.9–4.4 GHz	66.7%	9.7	Overall antenna dimension increased due to dual cavity, 36 mm height.
[208]	Cross-looped parasitic radiator based cavity-backed crossed dipole	3.14-6.34 GHz	53.4%	10.2	Antenna mounted by semi-rigid coaxial cable with cavity backed structure. Could be vulnerable in context of mechanical stability during integration.
[219]	Multilayered patch fed by aperture coupling with dual Y shaped slot	3.28-6.76 GHz	50.4%	8.5	Compact design with large ARBW

[209]	Differentially fed cross dipole with parasitic patch and delay line phase shifter	1.5-2.8 GHz	31%	8	Large in dimension, 140×140 mm^2.
[210]	Parasitic element based crossed dipole with shorting pin	0.65-1.25 GHz	51.6%	4.03	Large in dimension, 138×138 mm^2, height 16.6 mm.
[220]	3D printed square patch with L-slot, loaded with shunt varactors at edges.	1.65-2.17 GHz (Tunable)	3%	2.6-4.5 (at different bias)	Complex antenna fabrication process.
[221]	Microstrip fed inverted L-shaped parasitic radiating element and modified slot loaded ground plane	3.2-8.4 GHz	82%	3.3	Compact and simple design with wide ARBW.

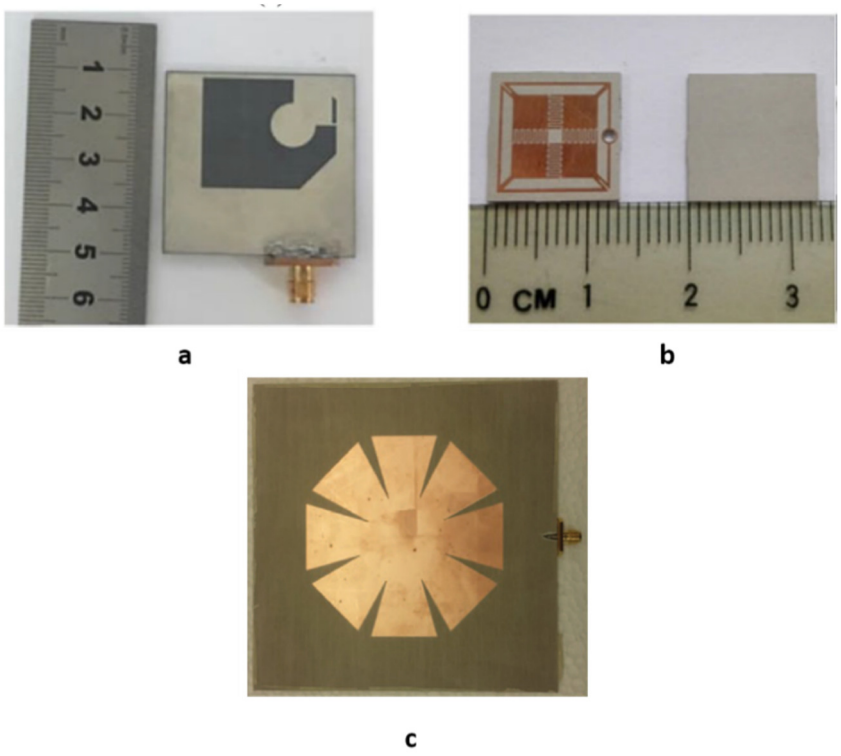

Figure 2.9 Circularly polarized antennas for WPT/RFEH; (a) wide slot [222], (b) implantable miniaturized [73] and (c) tapered slit [191]

CP microstrip antenna or CP slot antennas are good candidates for RFEH and WPT systems due to their low-profile, low manufacturing cost as well as ease of integration with power conversion circuitry [181, 223]. Figure 2.9 depicts different designs of

circularly polarized antenna for RFEH/WPT application. Recently, circularly polarized receiving antennas are being reported for RFEH and WPT [73, 224, 225]. Design of a patch antenna with dual circular polarization has been also illustrated for wireless power transmission [226]. The antenna is facilitated with harmonic rejection property by T-shaped slot and U-shaped resonator. A circularly polarized antenna design based on two cascaded skew planar wheel antenna has been reported for RF energy harvesting to power up IoT connected temperature sensor [227]. Other straightforward design methods of CP antenna include circular radiating patch along with L-shaped perturbation [191], adding diagonal slits at the edge of radiating patch and symmetrical meandered slits [222]. Gradually decreasing the length of tapered slots in diagonal direction on radiating element is also able to generate CP radiation effectively with simple antenna design for wireless power transfer and energy harvesting. Table 2.10 illustrates CP antenna design techniques reported in literature for RFEH and WPT. Nonetheless, a dual linearly polarized (LP) antenna may be found useful in some applications as it is difficult to achieve large CP bandwidth and CP beamwidth values with complex design. Dual-LP rectennas can extract orthogonal waves and combine them to form a DC signal using two rectifiers [228, 229].

Table 2.10 Different kind of CP antennas for RFEH/WPT applications

Refs.	Antenna design technique	Operating frequency (GHz)	3dB AR ratio bandwidth	Gain (dBi)	RF-DC Efficiency
[188]	Coaxial fed circular patch with unbalanced circular slots on FR4	2.45	1.22%	3.6	55% @ 10mW/cm^2 Power density
[226]	Square patch with 45° rotated U-shaped resonator inserted in T-shaped slot on FR4	2.45	4.08%	8	70% @ 10 dBm input power
[190]	Circular shorted annular ring-slot on appropriate position of the Arlon 25 N substrate	2.45	8.34%	5.25	50% @ 10 μW/cm^2

[225]	Coaxial fed circular patch with e-shaped slot on Rogers 4003	2.4	1.24%	5	---
[222]	Circular radiating patch along with L-shaped perturbation and wide slot on Teflon substrate	5.8	37.7%	6.4	63% @ 10 mW/cm^2 power density
[73]	Diagonal slits at patch edge and symmetrical meandered slits on Rogers 3010	.915	1.21%	-29	N/A (Intended for implantable application)
[191]	Gradually decreasing in length tapered slots in diagonal direction on radiating element printed on Rogers 4003 and feedline and ground printed on another Rogers 4003	.900	3.3%	5.6	40% @ 10dBm input power
[230]	Square loop slotted patch fed by a feed network containing microstrip feedline, phase shipter, Wilkinson power divider, Y-structured feeding stubs using Rogers 4003 substrate	1.68-2.8 GHz	48.4%	2.9-4.5	42% @ 15 $\mu W/cm^2$ (2.4 GHz)

2.4.4 Antenna Arrays

Some applications require more power than a single rectenna can provide. Mobile phone manufacturers and researchers have been already racing to develop self-charging devices using RFEH or WPT techniques [231-233]. Powering unmanned aerial vehicles (UAVs) wirelessly while in mid-flight is a great area of interest for research as well [234, 235]. In such cases, single antenna is unable to suffice the power-hungry application. For instance, array antenna inspired microwave powered mini electric vehicles were introduced in 2007 [236]. The received power could be more useful for power hungry applications if a

rectenna array or antenna array is used to capture RF power rather than using a single rectenna in RFEH or WPT application.

Electromagnetic waves can be captured using two or multiple antennas. An antenna is referred to as array antenna, if the total received signal power is enhanced using two or more antenna elements by combining the output of each antenna [237]. Improved performance over a single antenna is obtained through combination and processing of signals from multiple antennas. The signal combination through feed network is equally vital as the antenna elements of the array. Advantage of array antennas include overall increment in gain, rejection of interference, beam steering for sensitivity towards a fixed direction, diversity reception etc. There are some factors that control the radiation characteristics of an array of identical elements, such as, design configuration of overall array, relative structure of different element, amplitude of element excitation, distance among elements of array and array element's phase of excitation [118, 237, 238].

It has been investigated and illustrated that an increase in the number of antenna elements in an array can lead to better performance of the DC-combiner. The research was conducted using a planar 2×2 array antenna, as higher available RF power leads the rectifier to work in a higher efficiency region, [239]. Recently, more attention is being given to antenna array design for WPT and RFEH. Different designs including Printed Yagi antenna array [240], square patch array [241], dielectric resonator antenna array [242], differentially fed array [243] and solar-cell integrated antenna array [244] have been reported in literature recently. Figure 2.10 depicts some designs of antenna array reported for RFEH or WPT.

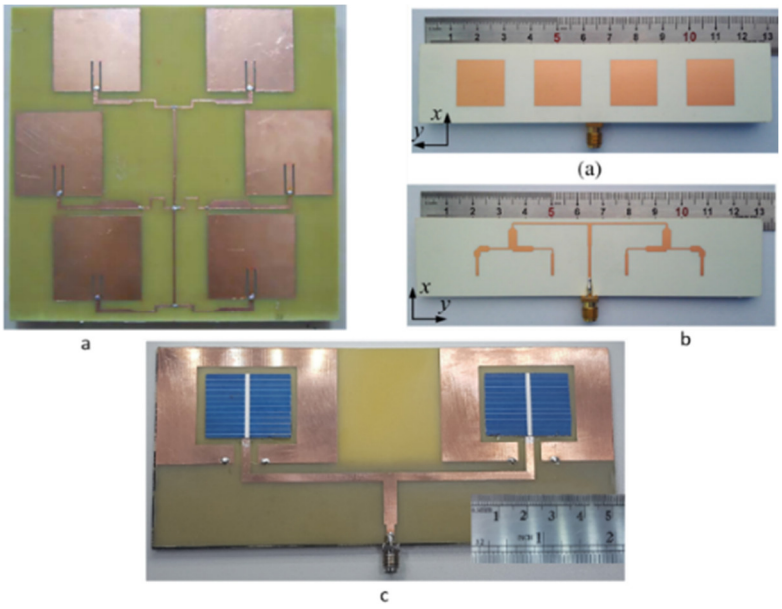

Figure 2.10 Array antenna for RFEH/WPT; (a) microstrip antenna array [241], (b) 1×4 patch array [245], (c) solar cell antenna array [244]

Collected RF energy can be enhanced by antenna arrays with large aperture dimension. Antenna arrays with uniform excitations distribution are typically used as the receiving components of rectennas in order to maximize the amount of captured power. The amount of harvested RF power sharply decreases with the variance of incident angle of incoming wave, if the beamwidth of the receiving array is relatively narrow. Rectenna arrays with enhanced beamwidth could address the issue [245]. On the flip side, rectenna arrays may suffer degraded efficiency due to close position of antenna elements and inter-coupling effect. Investigation of isolation structure in rectennas are performed to decrease level of coupling effect, raising efficiency and gain of the array [246, 247]. Recently, rectenna designs based on solar cell integrated antenna array are also proposed in literatures [244] , [248, 249]. Transparency of the antenna materials can be an issue since the incident light may be absorbed by the material. This will likely affect the efficiency of solar cell. Moreover, fabrication process of these kind of transparent antennas is expensive.

Nevertheless, array-based RF power harvesting system can be comprised of two different array configurations. These two topologies have been used in conjunction with 2×2 antenna and rectenna elements to compare the performance [239]. One of them is to arrange the antenna array to channel the RF power to a single rectifier. Due to the higher power delivered to a single rectifier, this architecture harvests more power near the main beam. Another strategy is to use a different rectifier for each antenna in order to harvest DC power independently. The DC power harvested from all rectifiers can then be combined in a variety of ways, including parallel, series, and hybrid configurations. Using this design, more received power is obtained with a broader pattern, which made the arrangement less sensitive to incident angle variations.

Though array antenna designs are reaching a level of maturity with the advent of modern design methods and technology [250-253], new rectenna research based on innovative array antenna with additional features is still in infancy. Antenna array design and investigation in WPT/RFEH system design is one of the most important research issues for rectenna. Compact array structures overcoming the constraints of RFEH or WPT receiving network scheme and array configuration have potential research scope. The price of using attractive features of array antenna is paid by increased cost and complexity. The issues related to array antenna feed network are balanced and traded-off with the mechanical constraints of single elements. However, inexpensive and effective feeding network can be designed and fabricated with the advanced application of solid-state technology [118]. The discussion below briefly highlights some of the array antenna design aspects and techniques.

2.4.4.1 Feed Network

Distribution of excitation in feed network is one of the major steps in designing antenna array. It is a significant challenge to reduce the complexity of the feeding network while maintaining efficiencies that are comparable to the theoretical maximum. Since each antenna element is responsible for gathering the impinging RF wave and converting it to DC power, it is preferable for the feed network in receiving arrays to be simple, light, and straightforward [254]. A microstrip array antenna design method has been documented based on efficiency of power transmission optimization [241, 255, 256]. Feasibility of feed network fabrication is investigated based on the optimization procedure. Amplitude and phase distribution of incident wave on antenna elements are generated by the optimization. The optimized values of phase and amplitude have been used to design the feeding network of the antenna, depicted in Figure 2.10(a). The feeding network of the 4-element antenna depicted in Figure 2.10(b) is designed using a distribution of optimal excitation. In [244], solar cell based two element antenna array feed network is designed using parallel microstrip feedline. Simple 2-element series-fed network based array antenna and 4-element cascaded array based T-junction power divider and two 2-element series-fed array are also reported for WPT application [257].

2.4.4.2 Uniform and Non-uniform Arrays

Uniform array antennas are those consisting of uniformly excited radiating elements with similar layouts. In non-uniform arrays, amplitude distribution is non-uniform while the inter element spacing remains uniform. High directivity with smaller beamwidth is achieved in uniform array [258]. In WPT scenarios, uniform transmitting arrays can facilitate simplicity and ease of maintenance [254].

Table 2.11 Overview of array antennas for RFEH/WPT

Refs.	Design configuration	Antenna array elements	Operating frequency	Size	Gain (dBi)	Radiation efficiency (%)	RF-DC efficiency (%)
[239]	Modified Koch-fractal structure based radiating element on high dielectric	2×2	2.45 GHz	360×340 mm^2	4.5	---	70% (Input power unspecified)
[259]	Printed quasi-yagi with double sided parallel feeding on RT/Duroid 5870 substrate	1×4	1.8-2.2 GHz	190×100 mm^2	10.9 dB @ 1.85 GHz	---	34% @ 1.8 GHz (Input power -20 dBm); 50% expected @ -10dBm input power
[241]	Square patch array with inset feeding on FR4 substrate	3×3	915 MHz	300×300 mm^2	10.5	84.14	41% @ 10 dBm input power
[260]	Dual monopole array with folded 3D meandering on 0.1 mm thick flexible substrate	2-element folded structure	900 MHz	35×56×12 mm^3	0.3 dB	48	---
[242]	Rogers TMM10i material based dielectric resonators on 0.1 mm copper ground plane	5×5	5.5 GHz	148×122.6 mm^2	---	65% (Power absorbing efficiency)	---
[245]	Dual Rogers-4350B substrate based patch array, feedline and patch printed on opposite substrate	1×4	5.8 GHz	129×30 mm^2	---	---	50% @ 1276 $\mu W/cm^2$ Power density
[243]	Differentially fed Dolph-Tschebyscheff on RT Duroid substrate	1×6	5.8 GHz	---	14.29 dB	---	22% @ -10 dBm input power (Approx.); 82.4% at 232 $\mu W/cm^2$
[244]	Multicrystalline solar cell based	1×2	2.4 GHz	---	6.24 dB	54.5	35% @ 6 mW/m^2

	planar array on FR4 substrate						power density

2.4.4.3 Beamforming, Beam Scanning and Beam Steering

Beamforming technique using antenna arrays can result in high-gain multiple beams simultaneously with controlled beamwidth. Steering and changing the direction of a single main beam of an array is referred to as beam scanning. The beam scanning method is potentially a promising technique to direct microwave power after finding the location of receiving appliance in WPT scheme [261-263]. The pivotal component for beamforming and beam steering is phased array antenna [264]. Electronic beam steering has certain advantages over mechanical beam steering in terms of compatibility with different application, size and speed [265]. Printed microstrip-fed reflect array antennas are advantageous in the application of WPT system as transmitting antenna. High gain directive performance can be achieved from reflector antennas along with beam steering facility [266]. Nevertheless, adaptive beamforming technique can provide solution to transfer radiated power towards desired direction, if the location of receiving device remains unknown or power required by multiple remote devices [267]. Above all, a robust and efficient antenna array with impeccable scanning performance and high gain is a vital requirement of wireless power transmitting system. Major design challenges in WPT beam scanning antenna array includes, mutual coupling of array elements, beam steering capability of ±45° and antenna efficiency [268].

2.5 Summary

The performance of a wireless communication system and WPT or RFEH system is significantly dependent on the antenna module. This chapter reports the state-of-the-art

and recent progress in antenna designs for RFEH and radiative WPT. This chapter is intended to help the reader understand the current receiving antenna trends in different circumstances. It started with an introduction of RFEH and WPT, their applications and enveloped a range of topics including wireless charging, the required receiving antenna specifications and state-of-the-art antenna technologies and designs for RFEH/ WPT. Different antennas are reviewed with a focus on design architecture and performance. This study has explored various antenna designs while categorizing them in context of low-profile, multiband, LP/CP and antenna arrays. Performance and advancements of the antennas are compared considering practical realization of antenna design for future multistandard applications.

Chapter 3

Dual-band Low-Profile Defected Ground Antenna

3.1 Introduction

The quality of life is being transformed by the internet of things (IoT), which is creating an ecosystem of smart and highly diverse devices that can support a wide range of new applications. The internet of things (IoT) is the next generation of global wireless platform of connectivity comprised of a diverse range of electronic circuits, integrated radio frequency (RF) sensors, and antenna systems. The IoT is continually and rapidly expanding, as new technologies are introduced and existing technologies are adapted to new applications including intelligent home control, precision farming, driver-less cars, simultaneous wireless information and power transfer, energy harvesting, logistics control and location tracking [2, 30, 269-274] . In IoT devices, antenna is an essential part of wireless communication modules [275, 276]. Several antenna design challenges arise from the vast range of IoT applications including compact dimensions for small IoT devices and multistandard antenna with a low profile structure [277-282].

Variety of antenna designs have recently been presented in the literature for IoT devices including single and multi-band antennas with low profile, covering different frequency bands. In recent years, the design of compact and easily integrable antennas have attracted a lot of attention because of the increased need for multi-frequency and multi-function antennas in IoT communication technologies [283] as well as in small IoT devices for ambient radio frequency energy harvesting [284, 285] and wireless power transfer [51] application. Moreover, the IoT applications demand low-profile and lightweight antenna that can be easily integrated with multistandard IoT devices.

Defected ground (DG) refers to the compact geometrical slots embedded in the ground plane. The DG has also been proven to improve the bandwidth, gain, radiation property and other characteristics of microstrip antennas [286]. DG has acquired prominence among other strategies stated in literature for achieving desired antenna performance parameters. Several kinds of DG shapes are used in antenna design such as, U-slot [287], "L", extended arc, asymmetric arc-shaped [288], etc. A U-slot DG approach has been proposed as an effective way to design a low-profile dual-band antenna [287]. However, the antenna has negative gain and quite narrow bandwidth at the lower band. Nevertheless, the conventional methods of DG are based on traditional EM simulation which are restricted by modifications of geometrical design parameter. It becomes difficult to select the proper defected ground shape with desired antenna performance. Conversely, pixelated DG configuration using V-shaped Binary Particle Swarm Optimization (VBPSO) algorithm has not been investigated in antenna design yet. The DG slot has the ability to alter the current path by perturbing the current distribution on the ground plane which directly impacts the antenna characteristics. Hence, subdividing a single DG slot into many little DG slots or pixels using the pixelization approach will enable antenna design flexibility by accessing the unexplored part of the defected ground area with different pixelated configurations.

The majority of existing antennas are based on electromagnetic (EM) simulations with geometrical alterations, such as changing the radiating element, patch shape, or ground plane, as the primary design technique. Also, for the case of defected ground antenna design using conventional approach, it is challenging to select the proper defected ground shape with desired antenna performance. The main benefit of using PDG in antenna design is the freedom in efficiently exploring complicated defected ground shapes that can contribute to its prominence in antenna designs. For instance, when designing a low-

profile single-band or dual-band antenna, the pixelated defected ground technique can be used to explore the designated ground area and find a balance between improved gain, operating frequency, bandwidth and size. By applying PDG topology, this work proposed a compact dual-band antenna with balanced performance in terms of gain and bandwidth in both bands considering a limited defected ground space. Figure 3.1 depicts a general idea of obtaining desired antenna for IoT application using PDG technique. The PDG technique can be employed to achieve multistandard and customized antenna performance for application specific conditions.

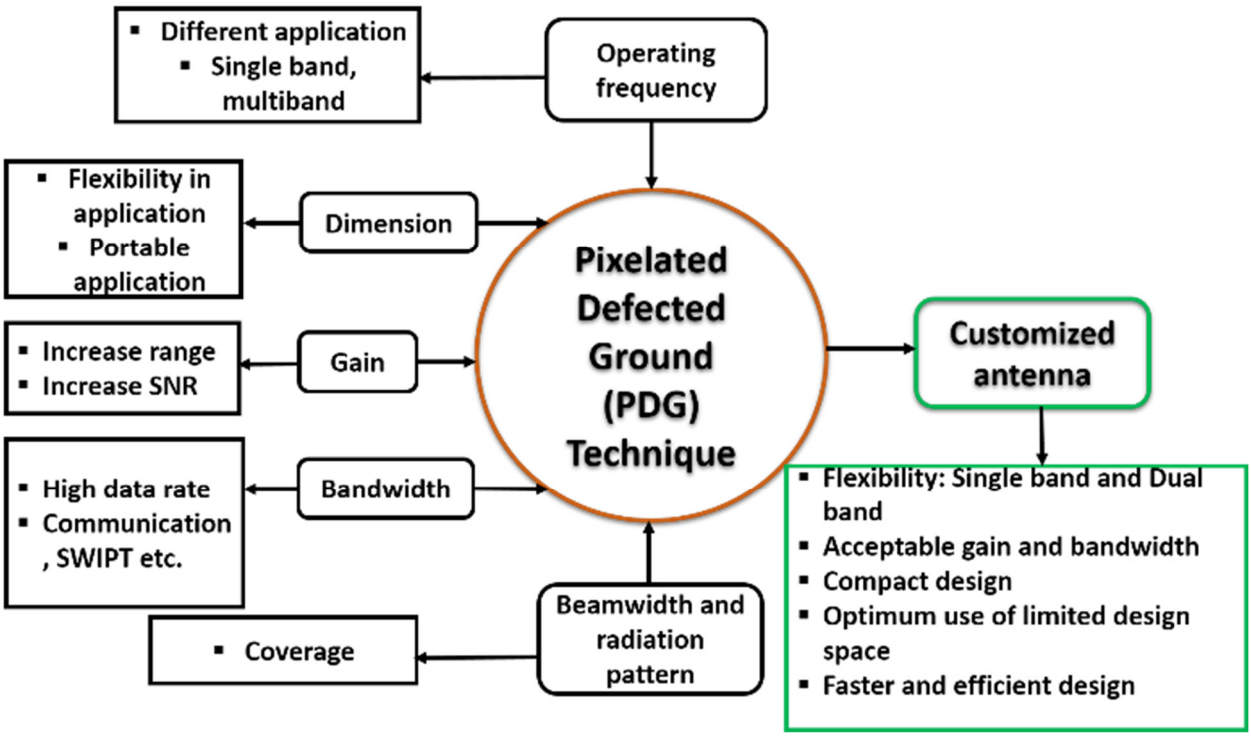

Figure 3.1 Customized antenna design for IoT application using pixelated DG technique

In this chapter, a low-profile pixelated defected ground antenna has been presented for dual-band application. The pixelated defected ground antenna (PDGA) design is performed by VBPSO. To the best of our knowledge, the pixelated defected ground antenna topology using VBPSO algorithm proposed in this chapter has not been

implemented in any prior work. The main contribution of this work is flexibility of achieving single-band and dual-band antenna within a compact structure (with reasonable performance metrics such as acceptable gain, bandwidth, dual-radiation pattern etc.) only by exploring the pixel configurations in the DG area. The VBPSO algorithm has been applied to explore the degree of freedom in pixelated DG configuration due to VBPSO's faster convergence speed and ability to avoid falling into local minima. Initially, three single-band antennas have been designed to explore the flexibility of the design methodology and finally a dual-band antenna design is performed. The proposed antenna exhibits dual-band operation at 3.5 GHz and 5.8 GHz. Unlike the typical defected ground antenna simulation, this method emphasizes on the pixelated DG shape rather than any dimension based DG analysis. The proposed antenna with PDG achieved 5.63% fractional bandwidth with 2 dBi measured gain at the lower band and 4.1% fractional bandwith with 3.1 dBi measured gain at the higher band. The antenna also achieved dual radiation pattern characteristics with nearly omnidirectional radiation patterns having different polarization at both operating bands. The antenna has potential for multipurpose application in IoT platform.

3.2 PDG Antenna Design Methodology

This section presents a detailed description of the antenna design methodology. First, a brief overview of binary particle swarm optimization is presented. Subsection 3.2.1, describes the PDG antenna design method, beginning with a simple patch antenna. Problem formulation and simulation method are discussed in subsection 3.2.2.

3.2.1 BPSO and VBPSO

The Particle Swarm Optimization (PSO) algorithm was first introduced in 1995 by Eberhart and Kennedy [289]. The PSO's initial version only works with continuous search

spaces. Following that, in 1997, the binary variant of the PSO (BPSO) was introduced in response to the high demand for binary or discrete search space optimization problems [290]. In PSO, a swarm or population of candidate solutions moves around the search space. The velocity of the particles is varied based on their own experiences and in accordance with the best one, which is obtained by swarm in the search area. The velocity equation of BPSO is mathematically modelled as [290]:

$$v_i^{t+1} = wv_i^t + c_1 \times rand \times (pbest_i - x_i^t) + c_2 \times rand \times (gbest - x_i^t) \quad (3.1)$$

Where, w denotes a weighting function, v_i^t indicates *i*-th particles velocity at iteration *t*, c_1 and c_2 are acceleration coefficients, *pbest* is the *i*-th particle's best solution, x_i^t represents the position of *i*-th particle at iteration number *t*, and *gbest* designates the best result of the swarm that has been obtained till current iterations.

Equation (3.1) obtains the real values of velocity. However, the BPSO algorithm deals with binary-valued (0 or 1) position vectors. So, a transfer function is required to convert real values of velocities to binary values as depicted below:

$$T(v_i^k(t)) = \frac{1}{1+e^{-v_i^k(t)}} \quad (3.2)$$

Where, $v_i^k(t)$ denotes *i*-th particle's velocity in the *k* dimension at *t*-th iteration. After that, the *i*-th particle's position at *t*-th iteration is updated according to equation (3.3).

$$x_i^k(t+1) = \begin{cases} 0, & if\ rand\ < T(v_i^k(t)) \\ 1, & if\ rand\ > T(v_i^k(t)) \end{cases} \quad (3.3)$$

The transfer function in equation (3.2) refers to the original version of BPSO. The position update function is the fundamental difference between the PSO and the BPSO,

where the probability of any binary variable change is determined by particle velocity. This is accomplished by using the transfer function to convert velocity to probability. The chances of a bit change in a particle's position vector is determined by this probability. BPSO is utilized generally in discretized applications, unlike the PSO which only deals with real numbered variables. In some engineering problems and other applications where the search space is discretized, 0 and 1 can be utilized as degrees of freedom in variables. However, the standard BPSO suffers from the issue of local minima and slower convergence. As a result, the algorithm struggles to discover the optimal solution to the optimization or antenna design challenge. As previously stated, transfer functions define the likelihood of changing elements of a position vector from "0" to "1" and vice versa. Transfer function is the vital part of the BPSO algorithm, and BPSO performance can be enhanced significantly by selecting a proper transfer function. When dealing with multi-objective or high-dimensional situations (as in the case of pixelated DG antenna design with hundreds of pixels), the traditional BPSO approach has difficulties with early convergence and processing local minima. Recently, it was proved that updated BPSO algorithms perform better at finding optimal solutions. As an approach to improve the BPSO, six new transfer functions have been proposed, and their performance have been analyzed [71]. They were divided into two different families, namely "S-shaped" and "V-shaped". The findings demonstrate that the newly introduced V-shaped family of transfer functions can considerably improve the performance of the original BPSO in terms of avoiding local minima and convergence rate by using their unique approach of updating position vectors. Some initial simulations have been performed using the three new transfer functions of the V-shaped family to select the transfer function for designing PDG antenna. The following transfer function (3.4) from V-shaped family showed promising results. So, we have utilized VBPSO using the following transfer function (4) from the

V-shaped family for the PDG antenna design. The V-shaped family of transfer functions differs from the S-shaped family, and they follow entirely new position updating rules in (3.5), where position of particle *i* is denoted by $x_i^k(t)$ and $v_i^k(t)$indicates velocity of particle *i* at iteration *t* in *k*-th dimension. The complement of $x_i^k(t)$ is $\left(x_i^k(t)\right)^{-1}$. This approach has the advantage of encouraging particles to remain in their current places at low velocity. The name V-shaped binary particle swarm optimization (VBPSO) is based on the shape of the characteristics curve of the new family of transfer functions. The shape of the characteristics curve of the transfer functions resembles the English letter 'V'. Hence, the name V-shaped binary particle swarm optimization algorithm (VBPSO) is given to this algorithm [71].

$$T\left(v_i^k(t)\right) = \left|\frac{\left(v_i^k(t)\right)}{\sqrt{1+\left(v_i^k(t)\right)^2}}\right| \tag{3.4}$$

$$x_i^k(t+1) = \begin{cases} \left(x_i^k(t)\right)^{-1} & \text{If rand } < T\left(v_i^k(t+1)\right) \\ x_i^k(t) & \text{If rand } \geq T\left(v_i^k(t+1)\right) \end{cases} \tag{3.5}$$

3.2.2 Pixelated Defected Ground (PDG) Antenna

The PDG antenna design starts with a basic patch antenna. The initial antenna consists of a small rectangular patch with a dimension of *Lp*×*Wp* and a rectangular ground plane with the size of *Lg*×*Wg*. The antenna ground plane is modified by introducing a rectangular slot, inspired by defected ground antenna design. The antenna geometry and design dimensions are illustrated in Figure 3.2 and Table 3.1. The rectangular slot on the ground plane is introduced to define an area for pixelization to realize single-band or dual-band performance. The dimensions of the defined area for pixelization is inspired by the sizes of different DG shapes available in state-of-the-art literature [287, 288].

Additionally, the dimensions of rectangular slot should be able to accommodate adequate number of pixels for satisfactory optimization. DG is used in the field of microstrip antennas for enhancing performance as the anomaly on the ground plane disrupts the current distribution of the ground plane. Followed by this disruption, slot inductance and slot capacitance are introduced, which can change the characteristics and performance of the antenna [162]. However, in conventional approaches, DG design is limited by geometric change of design parameters (usually with different slot shapes) which makes the method difficult to design and select proper DG shapes for the antenna. On the flip side, pixelization technique is not bound by this limitation. Hence, we used pixelization method to effectively design the defected ground slot area based on the positions of binary bits from the VBPSO, which is discussed further in the following section. The patch antenna is excited by co-axial feeding method. A shorting pin has been used to provide miniaturization to the proposed antenna as the resonant frequency of the patch antenna can be lowered down with shorting pin than the unloaded patch antenna's lowest operating frequency [291]. The design dimensions of the antenna are included in Table 3.1. The following section provides the design methodology of the proposed PDG antenna.

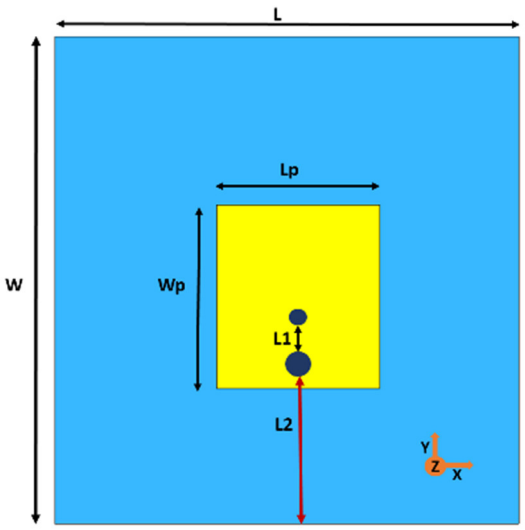

(a)

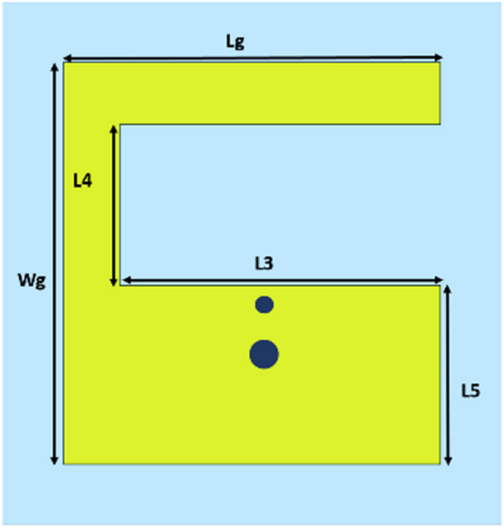

(b)

Figure 3.2 Initial defected ground antenna design with a rectangular slot on the ground plane of the antenna, (a) top view- rectangular patch (b) ground plane with rectangular slot; blue area defines substrate.

Table 3.1: DG Antenna Design Dimensions

Parameters	Value (mm)	Parameters	Value (mm)
L	24.8	Lg	18.8
W	26	Wg	20
Lp	8.95	L3	16
Wp	9.850	L4	8
L1	2.5	L5	8.9
L2	5.5		

In the proposed antenna design, the PDG structure is achieved by using the binary strings originated from the VBPSO algorithm. Figure 3.3 depicts the defined area of the antenna ground plane for PDG, divided into 32×16 array consisting of 512 square pixels. The pixel size is 0.5 mm × 0.5 mm. Increasing the number of pixels will result in large search space for the algorithm, which affects the algorithm performance to determine the optimum

structure of the defected ground region. In contrast, if the number of pixels is decreased the pixel size needs to be increased. For instance, if the pixel size is increased to 1mm×1mm the defined DG area can accommodate only 128 pixels (the defined DG area is 16mm×8mm). This limits the exploration of the DG configuration during the simulation. Also, the chosen pixel size (0.5mm×0.5mm) is only about 0.58% of the wavelength at the lower frequency (3.5 GHz). Further reducing the size would increase the simulation time. To balance the trade-offs between these scenarios we have used 512 pixels in the PDG region.

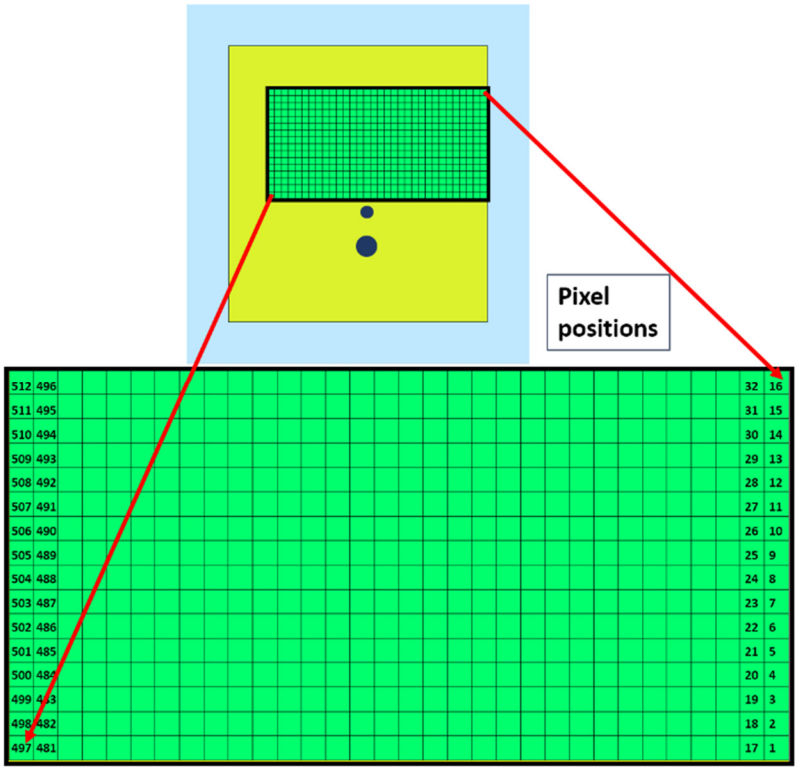

Figure 3.3 Pixelization of the defected ground area

The binary bit string obtained from the position of every particle in each iteration of the algorithm and sets the position of conductor or air. If the bit value is 1, the respective pixel position is filled with a conductor. If the bit value is 0, it keeps the pixel as empty space.

3.2.3 Problem Formulation and Simulation of Single-band and Dual-band PDG Antenna

The PDG antenna design can be defined as a minimization problem in the VBPSO, using the initial geometry depicted in Figure 3.2. The design challenge is to obtain single-band and dual-band operating frequency using the defined space as DG area on the ground plane. PDG is discretized within a defined area into many rectangular cells using the VBPSO.

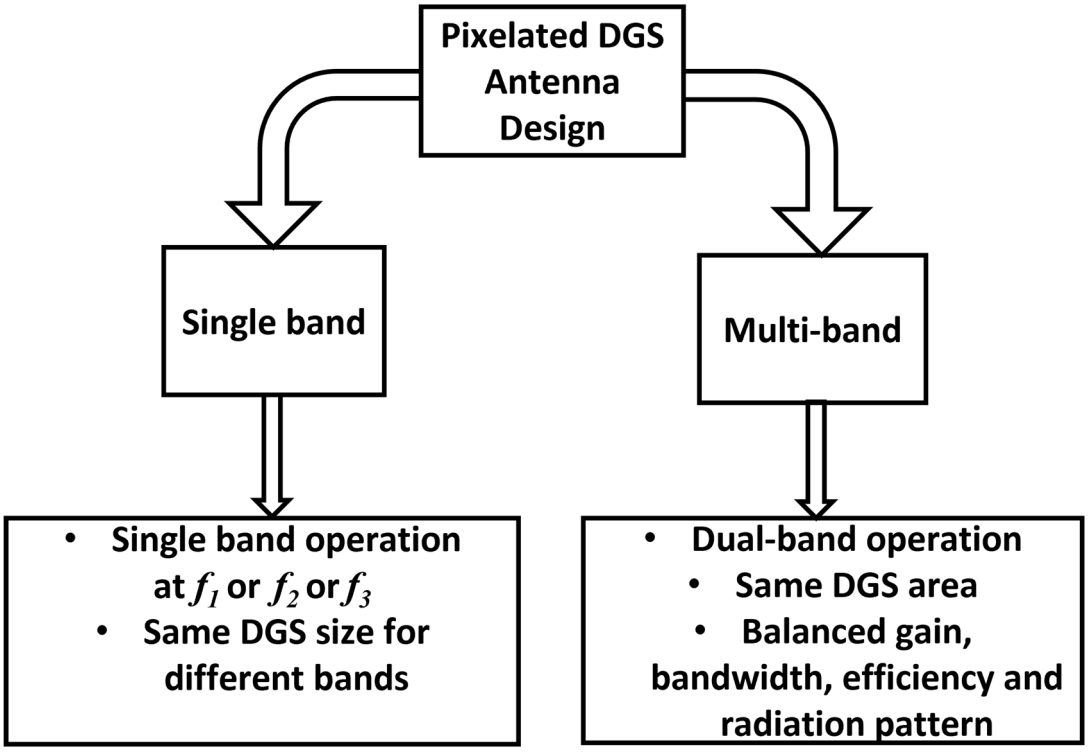

Figure 3.4 Single-band or multi-band antenna design flexibility using pixelated DG configuration.

Figure 3.4 illustrates the flexibility of antenna design at different frequency bands by adopting pixelated DG configuration. Antenna sections are assigned to a preset area in many applications. The traditional method requires alteration of antenna size, shape etc. in order to obtain the desired performance at a certain frequency. However, in the suggested antenna design using PDG technique antenna size and shape do not need to be

altered. Antennas with different resonance frequency, gain, bandwidth, etc. can be designed using this method on a given defective ground region. Different frequency of operation can be achieved by changing the pixel configuration only. We can achieve single-band operation at multiple frequency or dual-band performance only by using the same defected ground area with different pixelated configuration. Initially, the design goals of the pixelization are to achieve single band coverage at three different commercial frequency bands 3.5 GHz (f_1), 5.2 (f_2) GHz and 5.8 (f_3) GHz to demonstrate the capability of PDG in single-band antenna design. After that, the same PDG area is used to achieve dual-band coverage of 3.5 GHz (f_1) and 5.8 GHz (f_3) for potential applications. The lower band can support application in LTE band and emerging 5G mid-band [292, 293] and the higher band could be utilized for industrial, scientific and medical (ISM) band. Hence, the objective functions for the antenna design problems become:

Fitness function $FF_1 = \min(S11_{f_1=3.5\ GHz})$ (3.6)

Fitness function $FF_2 = \min(S11_{f_2=5.2\ GHz})$ (3.7)

Fitness function $FF_3 = \min(S11_{f_3=5.8\ GHz})$ (3.8)

Fitness function $FF_4 = \min(S11_{f_1=3.5\ GHz}, S11_{f_3=5.8GHz})$ (3.9)

Equation (3.5), (3.6), and (3.7) are defined to improve the antenna reflection coefficient at single bands (denoted as f_1, f_2, f_3). Equation (3.8) is defined to improve the antenna reflection coefficient at two desired frequencies (f_1 *and* f_3). Figure 3.5 shows the design procedure of the proposed PDG antenna using a flow chart. The VBPSO algorithm has been implemented in Matlab and then connected to electromagnetic (EM) simulator software (CSTMWS) [294]. The bit string from VBPSO is imported to the EM simulator using a pre-simulation module implemented in Matlab and decodes the bits to the

respective simulation model.

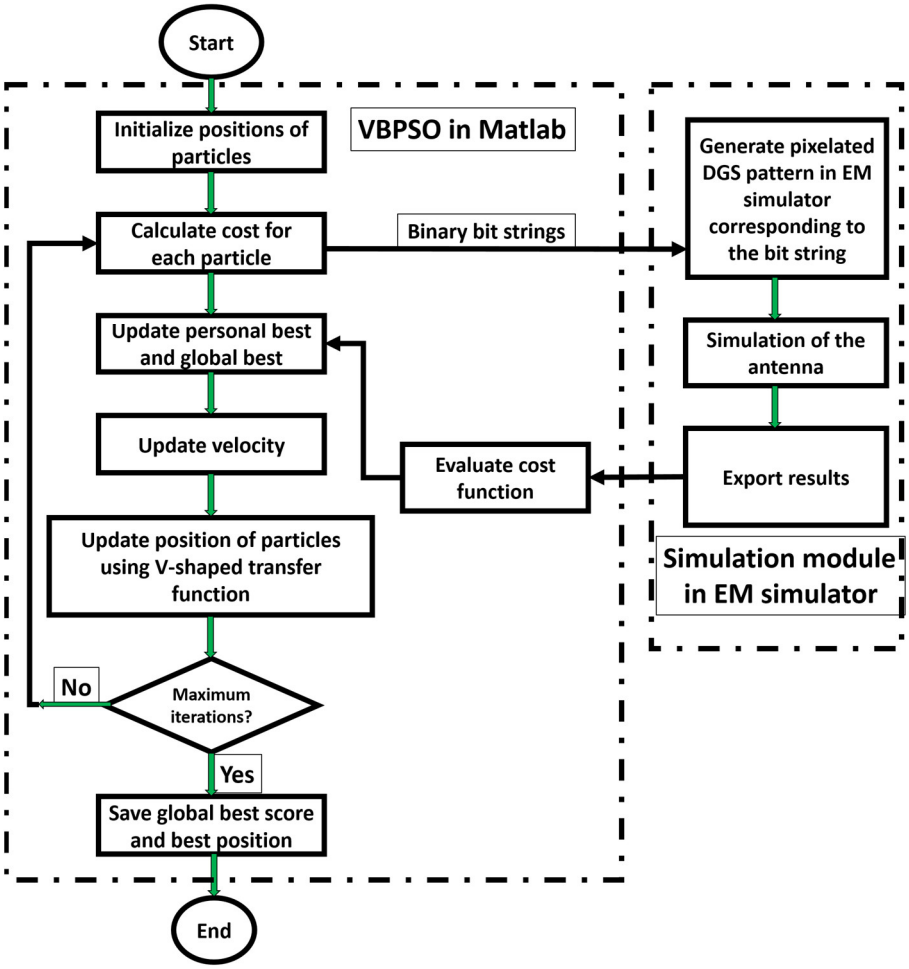

Figure 3.5 Proposed PDG antenna design methodology

The underlying mechanism of PDG is based on the interaction between the reflection coefficient and PDG pattern, which cannot be found using commercial EM solvers' built-in optimizers. Our approach focuses on the defected ground shape rather than its dimensions. Hence, the pixelization technique entails deciding which part of the defected ground area should be covered with metal and which should not (etched). Simulation of the antenna model in CSTMWS is performed in Time Domain Solver. A workstation computer has been utilized to perform the simulation. The hardware specification of the computer is illustrated in Table 3.2 beow. After performing the simulation, the results of reflection coefficient are exported to Matlab to evaluate the objective function in equation

(3.6). Based on that, personal best score and global best score in VBPSO are updated. The velocity and particle position are updated according to equations (3.4) and (3.5), respectively. After reaching the maximum number of iterations, the pixelization stops and provides the best positions of the binary bits for pixelated area.

Table 3.2: Hardware Specification of the Computer

Subsystems	Type
Processor	Intel(R) Xeon(R) Gold 5217 CPU @ 3.00 GHz, 2 (processors)
RAM	64 GB
System type	64-bit operating system
GPU	NVIDIA Quadro RTX 4000
GPU memory	8 GB

3.3 Results and Discussions

Simulation of the proposed PDG antenna has been performed in CSTMWS for 100 iterations with 13 particles to keep the number of function evaluations low and also, to avoid extended simulation time over the iterations with increased number of particles [295]. The selection of the number of particles has an impact on the convergence rate and fitness value of the objective function. Number of fitness function evaluations (EM simulation) in every iteration is determined by the number of particles. Adding more particles increases number of fitness function evaluation and simulation time. If the number of fitness function evaluation is higher, the optimization should improve in ideal case (fitness value and convergence). Nevertheless, using many particles may not always achieve meaningful results. So, there is a trade-off between both scenarios, and the number of particles can be tuned to produce optimal results with acceptable total

simulation duration. However, setting the number of particles to less than 10 has been found to reduce the convergence rate and make it more difficult to improve the fitness value, which is directly related to the antenna's reflection coefficient. Time varying inertia weight has been used to maintain balance between local and global search in the BPSO. The acceleration coefficients c_1 and c_2 are tuned to obtain optimum results. The pixel positions are obtained based on each particle's position during each iteration.

Firstly, pixelization of the defected ground area has been performed for single-band antenna designs as illustrated in equation (3.6), (3.7) and (3.8) to achieve operating band at 3.5 GHz (Antenna A), 5.2 GHz (Antenna B) and 5.8 GHz (Antenna C) respectively. The same pixelated defected ground area has been utilized to design the Antenna A, Antenna B and Antenna C. Different pixelated configuration of the defected ground area result in three different single band antenna operating at different frequency. The different pixelated configurations are obtained from separate optimization process using VBPSO. Figures 3.6, 3.7 and 3.8 clearly demonstrate that pixelated DG can be utilized for single-band antenna design at different frequencies.

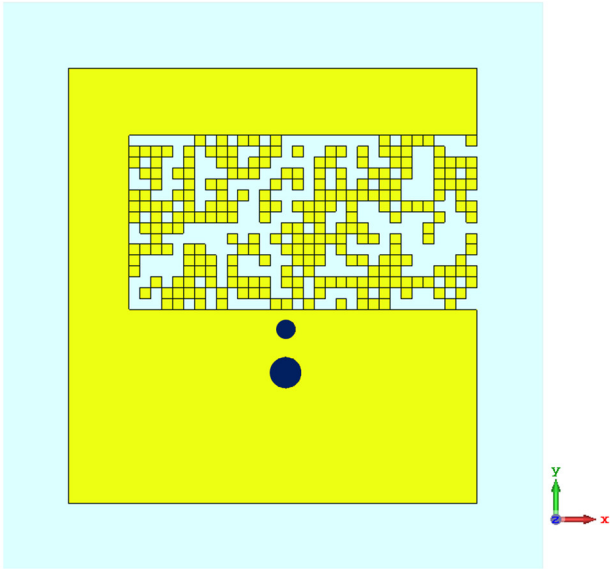

(a)

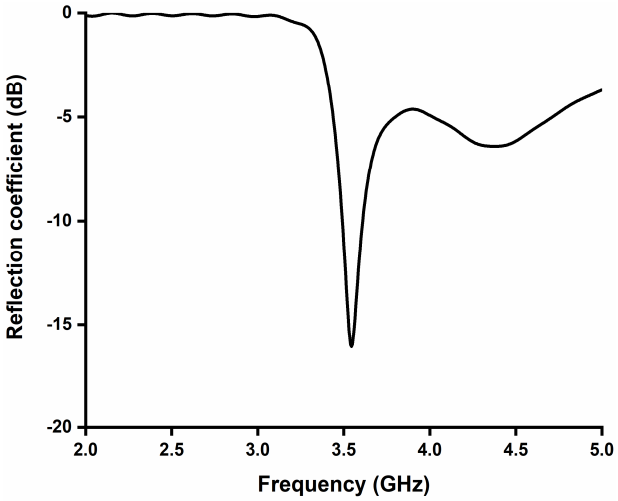

(b)

Figure 3.6 Design configuration and results of the antenna with optimized pixel positions for FF_1 (a) Pixelated layout of Antenna A (3.5 GHz), (b) reflection coefficient of Antenna A

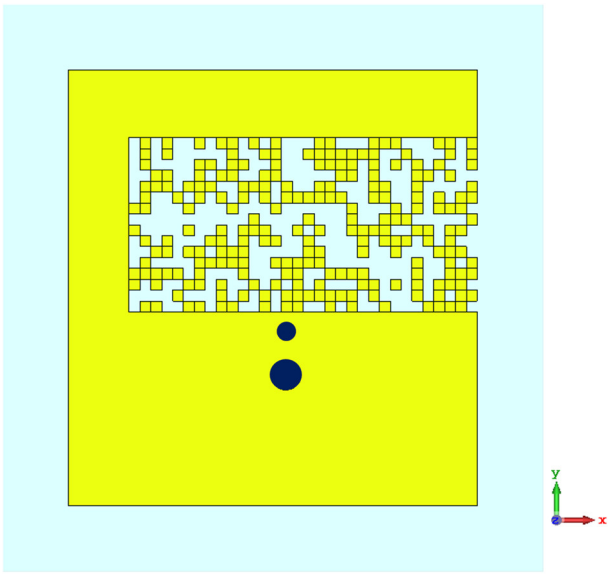

(a)

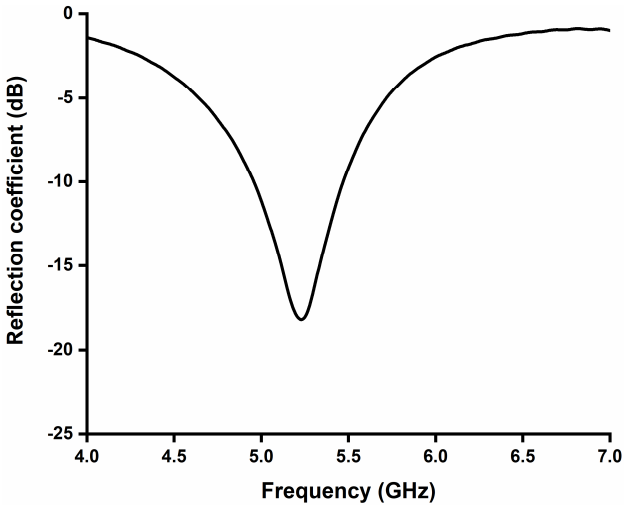

(b)

Figure. 3.7 Design configuration and results of the antenna with optimized pixel positions for FF_2 (a) Pixelated layout of Antenna B (5.2 GHz), (b) reflection coefficient of Antenna B

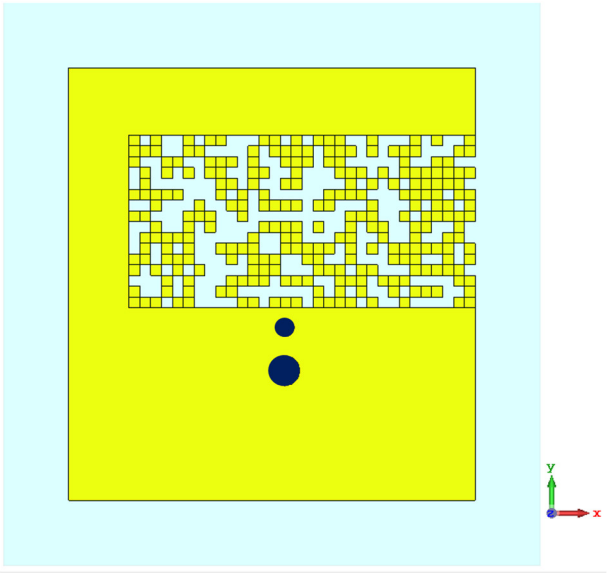

(a)

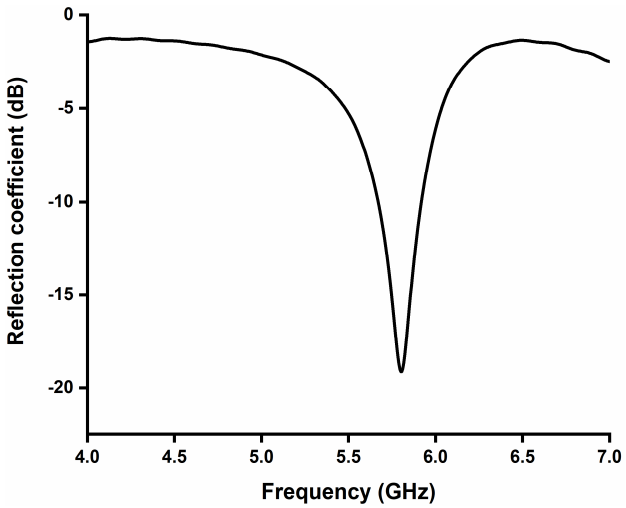

(b)

Figure 3.8 Design configuration and results of the antenna with optimized pixel positions for FF_2 (a) Pixelated layout of Antenna C (5.8 GHz), (b) reflection coefficient of Antenna C

The proposed pixelated defected ground antenna design method can be utilized to design dual-band antenna as well. Finally, to illustrate the flexibility of antenna design process for dual-band antenna, pixelization of the same DG area as previous antennas (Antenna A, B and C) has been performed for dual-band operation at 3.5 GHz and 5.8 GHz (Antenna D) using equation (3.9). The optimal placement of pixels has been achieved after 96 iterations using VBPSO. After 96 iterations, the optimal values of the bit strings are obtained as the best position for pixels and are depicted in Figure 3.9. The bit values resemble the numbering of pixels illustrated in Figure 3.3.

Figure 3.9 Optimal bit values for pixel positions

Figure 3.10 (a) depicts the pixelated layout of the PDG antenna (Antenna D) resulted from the VBPSO algorithm and the convergence curve of the pixelization process, which were obtained from the objective function (9) using both the VBPSO and BPSO. The small yellow squares represent the pixels and hence, existence of metal. From the convergence curves of Figure 3.10(b), it is apparent that the VBPSO outperforms the BPSO in Pixelated DG antenna design. Further, the VBPSO obtained a much better average fitness value for balancing the goals, and the convergence rate is faster than BPSO. This is due to the different method of updating position using equation (3.5) in V-shaped transfer

function. This approach has the advantage of avoiding local minima and fast convergence by encouraging particles to remain in their current postion at low velocity instead of forcing particles to take 0 or 1 values [71].

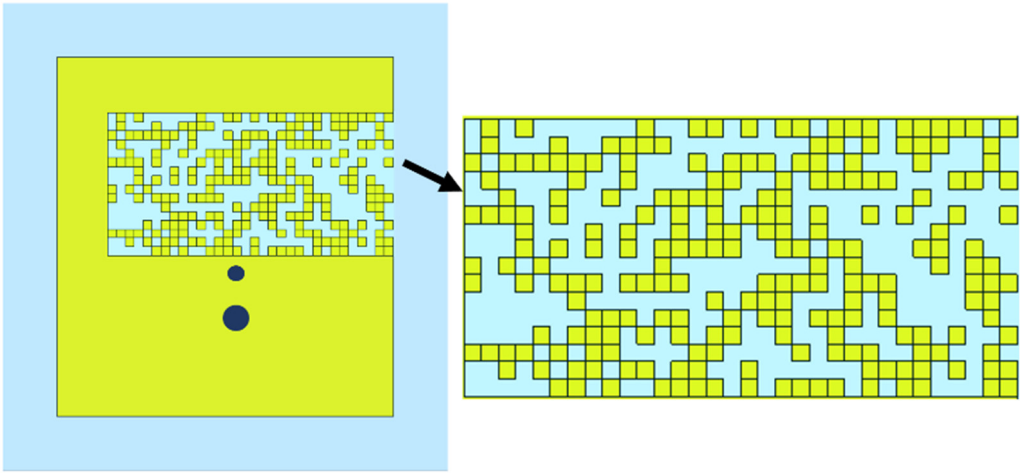

(a)

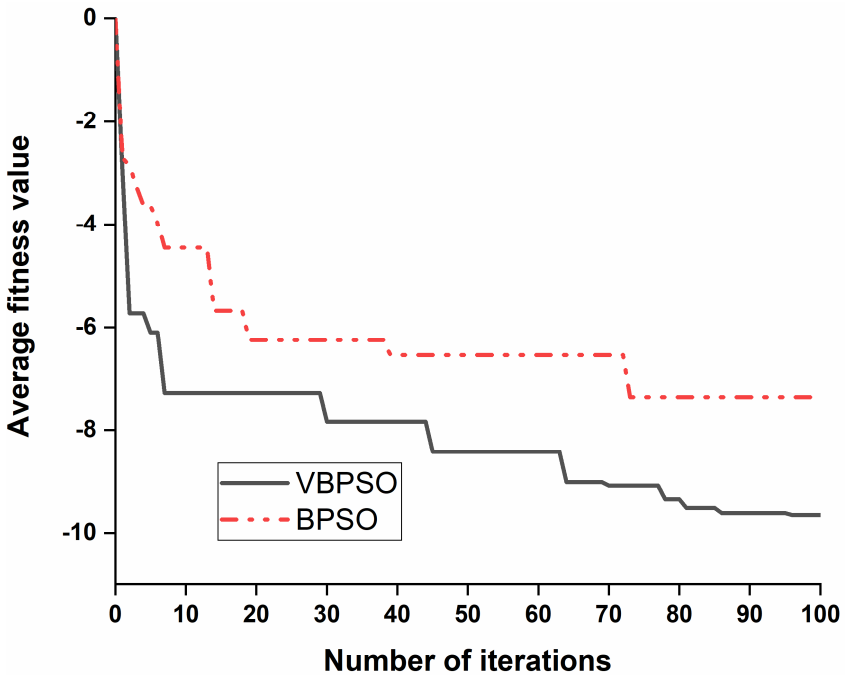

(b)

Figure 3.10 Design configuration and results of the antenna with optimized pixel positions for FF_4 (a) Final PDG layout of the proposed antenna (Antenna D), (b) Comparison of convergence curves obtained by using VBPSO and BPSO

To confirm the feasibility of the antenna design methodology using VBPSO, Figure 3.11 represents the reflection coefficient of the PDG antenna at different iterations. Also, Table 3.2 provides a comparison of pixelization results between VBPSO and BPSO. The results show that the performance of standard BPSO is below satisfactory level as expected. As can be seen from Figure 3.11 (a), BPSO only goes close to the design goal once at iteration 39. However, in the next iterations, it failed to improve the results further. Conversely, the reflection coefficient of the antenna resulting from VBPSO algorithm appears to improve gradually as the iteration increased, depicted in Figure 3.11 (b). The comparison in Table 3.3 further illustrates the performance of BPSO and VBPSO for PDG antenna design at different iterations. For example, at iteration 73, BPSO obtained an average fitness value -7.359, whereas VBPSO obtained a better average fitness value -7.836 at iteration 30. The best obtained average fitness value using VBPSO is -9.650, where BPSO remains stuck at -7.359 from iteration 73 to 100.

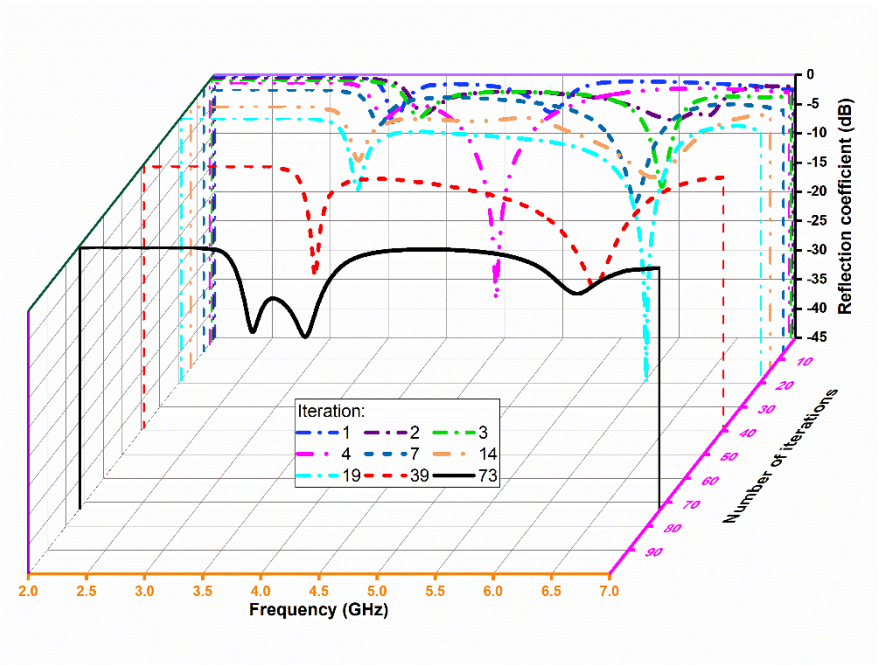

(a)

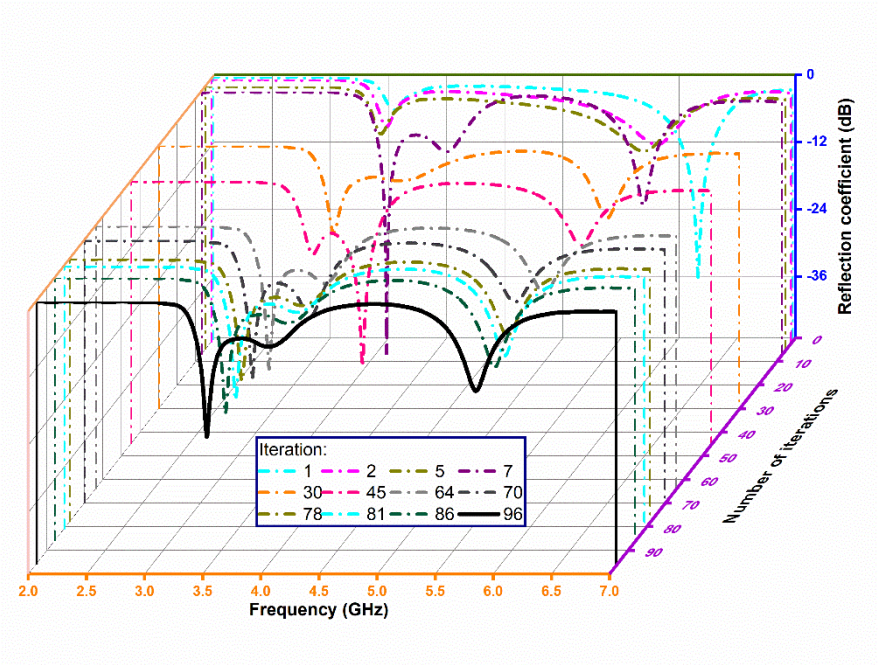

(b)

Figure. 3.11 Simulated reflection coefficient of the antenna at different iterations

(a) BPSO, (b) VBPSO

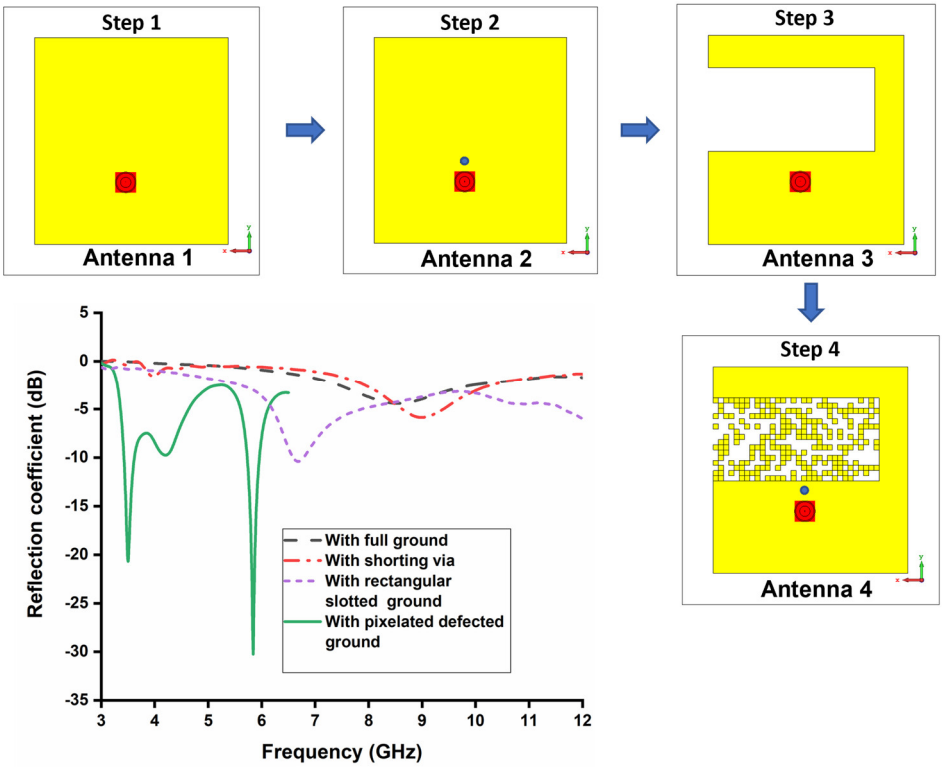

(a)

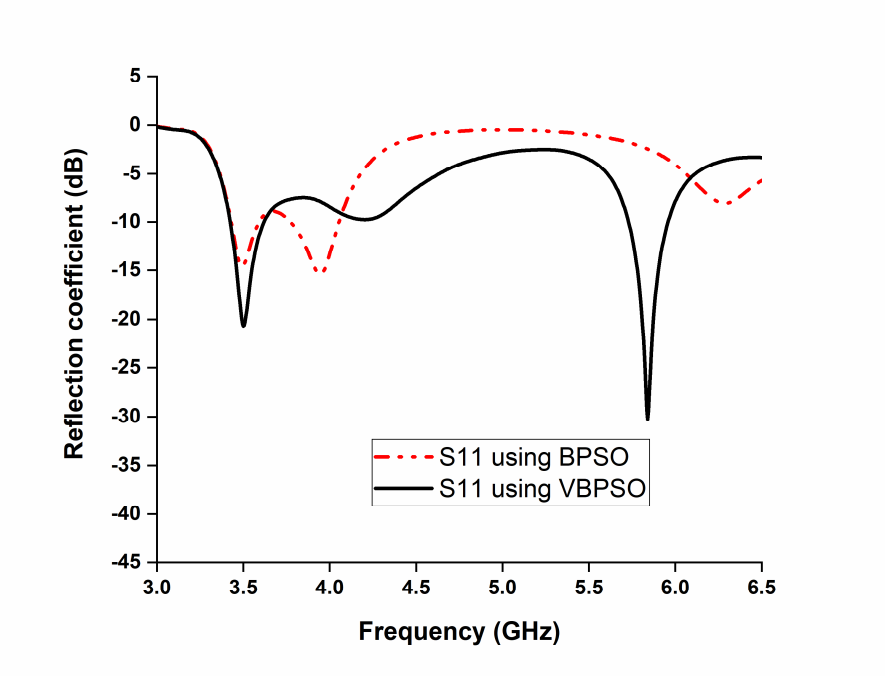

(b)

Figure 3.12. (a) Evolution of the antenna; Antenna 1-with full ground and patch, Antenna 2-with shorting via, Antenna 3-with rectangular slotted ground, Antenna 4-with pixelated defected ground, Software used: CST Microwave Studio 2019 (b) Simulated reflection coefficient of the antenna with VBPSO vs. BPSO

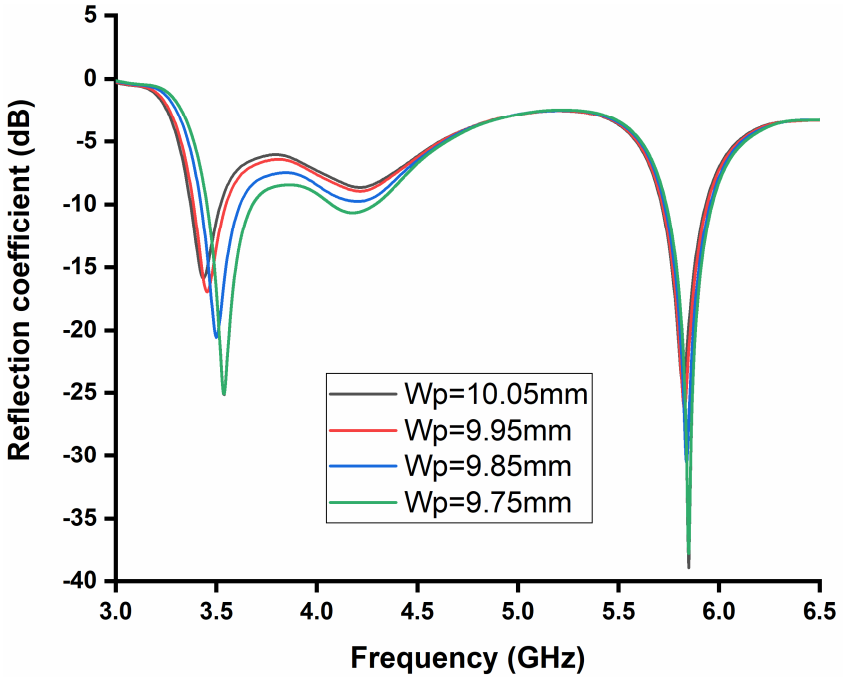

(a)

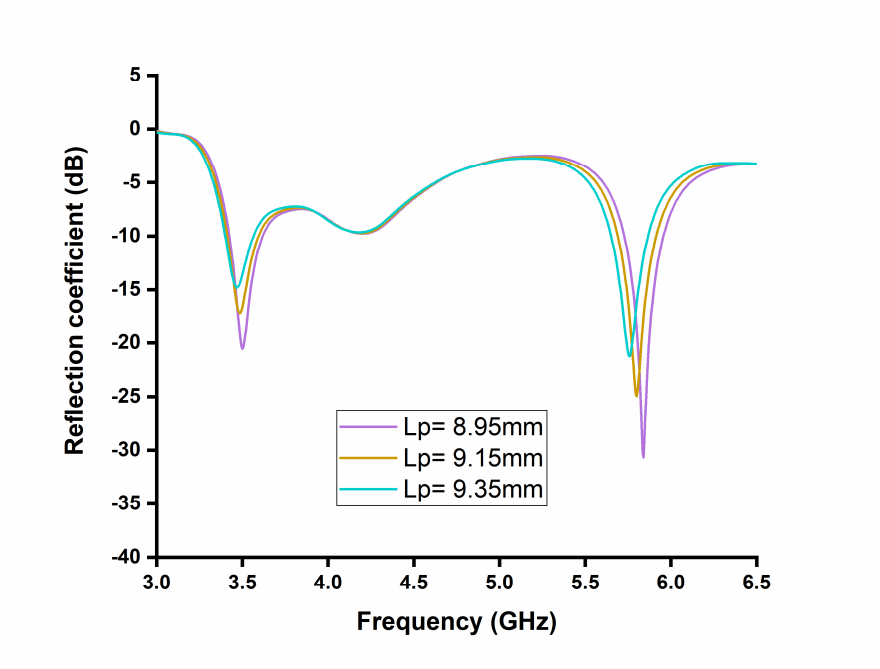

(b)

Figure 3.13 Simulated reflection coefficient of the antenna due to change in length and width of the patch (a) effect of Wp, (b) effect of Lp

The proposed antenna design using VBPSO has successfully achieved dual-band at 3.5 GHz and 5.8 GHz. Fig 3.12(a) depicts the design evolution process of the antenna. It can be seen that the antenna achieved desired dual-band performance in lower bands using PDG with shorting pin. Figure 3.12(b) compares the reflection coefficient of the antenna using the final pixel positions from VBPSO and BPSO. It is evident that PDG antenna using BPSO struggles to achieve the desired results. The results presented in Figure 3.12 supports the effectiveness of pixelated defected ground antenna design by achieving and exploring better pixel positions for the PDG area using the V-shaped binary particle swarm optimization.

Table 3.3: Comparison of pixelization results using VBPSO and BPSO

V-shaped BPSO				Standard BPSO			
Iteration	FF value	S11 @3.5 GHz (dB)	S11 @ 5.8 GHz (dB)	Iteration	FF value	S11 @3.5 GHz (dB)	S11 @ 5.8 GHz (dB)
1	-2.992	-4.39	-5.67	1	-2.711	-5.57	-1.14
2	-5.723	-8.31	-11.41	2	-2.858	-0.63	-6.46
5	-6.096	-8.23	-11.39	3	-3.267	-0.62	-11.28
7	-7.284	-6.98	-20.35	4	-3.629	-6.00	-1.35
30	-7.836	-15.44	-11.17	6	-3.988	-5.82	-0.50
45	-8.426	-9.30	-9.71	7	-4.456	-5.91	-14.52
64	-9.016	-24.84	-10.66	14	-5.675	-7.44	-9.97
70	-9.088	-13.25	-8.96	19	-6.252	-11.04	-10.34
78	-9.351	-19.48	-13.18	39	-6.544	-15.86	-17.76
81	-9.516	-19.05	-15.94	73	-7.359	-14.54	-2.16
86	-9.614	-17.16	-15.76	100	-7.359	-14.54	-2.16
96	-9.650	-20.56	-18.64	-	-	-	-
100	-9.650	-20.56	-18.64	-	-	-	-

The achieved -10 dB impedance bandwidth is 200 MHz (3.45-3.65 GHz) for the lower frequency band and 240 MHz (5.97-5.73 GHz) for the higher band (Figure 3.12), covering 5.63% and 4.1% fractional bandwidth, respectively. The operating frequency of the antenna can be further tuned by changing the length and width of the patch (value of *Wp* and *Lp*). The impact of *Wp* and *Lp* on the reflection coefficient is shown in Figure 3.13 (a) and (b). The length is tuned from 9.75mm to 10.05mm, and it is observed that changing *Wp* affects most on the lower band. This indicates that *Wp* can be used to regulate the difference between lower and higher bands. Increasing the *Wp* shifts the lower band towards lower frequency with degraded reflection coefficient levels. Moreover, change in

Lp influences both the higher and lower bands. The frequency shift is approximately similar in both bands due to a change in the length of *Lp*.

The antenna's mechanism is further investigated by observing the surface current distribution at both operating frequency bands, shown in Figure 3.14. At 3.5 GHz, the current is primarily distributed at the left and right sides of the patch, as well as the edge of the pixelated region of the ground plane, with some on the PDG area, as shown in Figure 3.14 (a). This is due to the fact that the current goes to the ground through the shorting pin making the PDG part of the antenna. The resonant frequency of the lower band f_1 can be approximated by considering the patch and PDG dimension using equation (3.10) [296, 297]:

$$f_1 = \frac{c}{(2W_p+2L_3+L_4)\sqrt{\varepsilon_{eff}}} = 3.35\ GHz \tag{3.10}$$

where, c denotes the speed of light and ε_{eff} is the effective dielectric constant of the substrate, W_p indicates the patch width, L_3 is the length of the PDG slot area and L_4 represents the width of PDG slot. ε_{eff} is given by $\varepsilon_{eff} = (\varepsilon_r + 1)/2$ =2.275, where the relative permittivity of Rogers 4003 is $\varepsilon_r = 3.55$. At 5.8 GHz, the current is mainly concentrated around the top, right and bottom edges of the radiating patch as well as through the middle of the PDG area, travelling the approximate path length L_4 (Fig 3.10 (b)). The resonant frequency of the second band f_2 can roughly be estimated using equation (3.11) [296, 297], which is also close to our desired band.

$$f_2 = \frac{c}{(2L_p+W_p+L_4)\sqrt{\varepsilon_{eff}}} = 5.6\ GHz \tag{3.11}$$

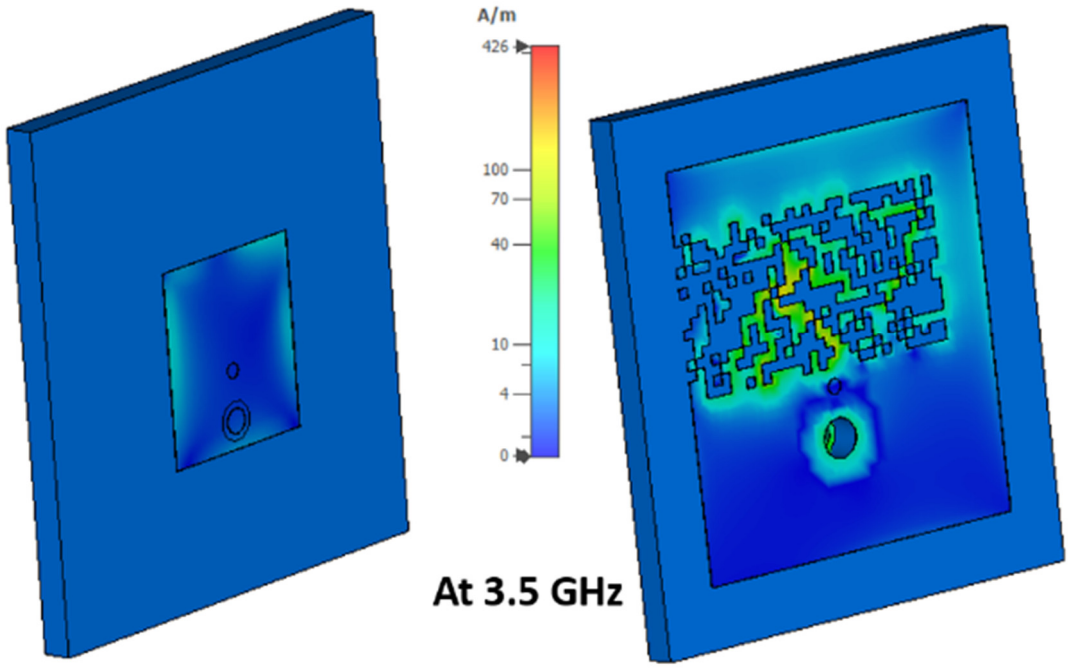

(a)

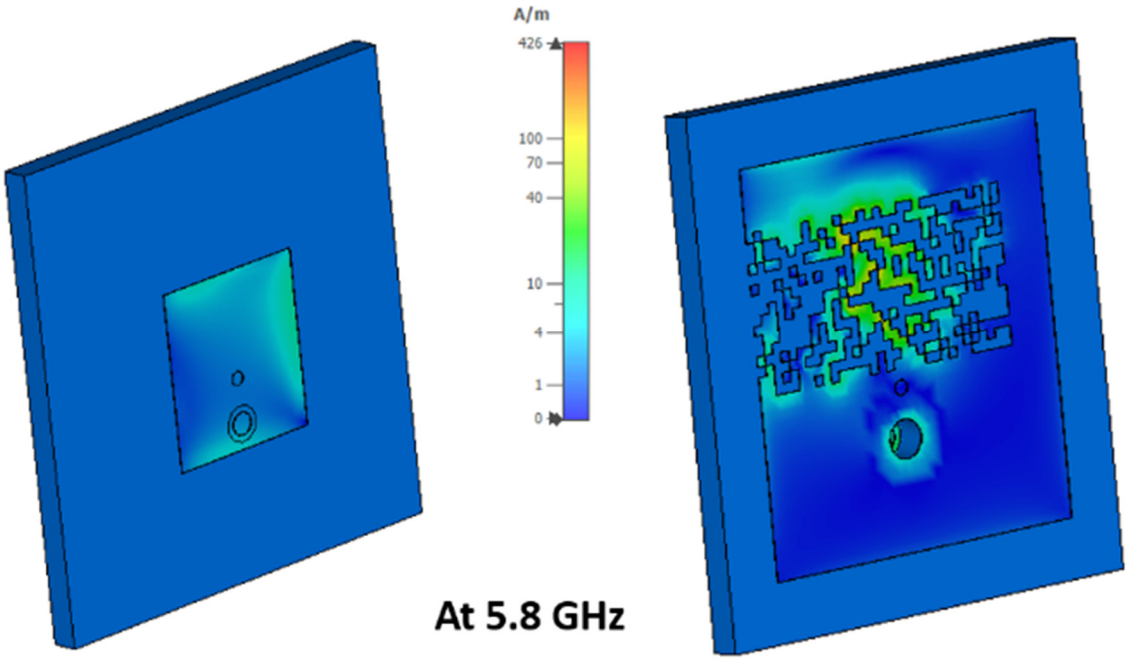

(b)

Figure 3.14 Simulated surface current distribution of the antenna, Software used: CST Microwave Studio 2019, (a) surface current distribution of the PDGA at 3.5 GHz, (b) surface current distribution of the PDGA at 5.8 GHz,

The optimal dual-band PDG antenna design depicted in Figure 3.10(a) has been fabricated using 1.52 mm thick Rogers 4003 substrate with dielectric constant of 3.55 and measured to verify its performance. The total antenna dimension is 24.8mm×26mm. Figure 3.15 depicts the fabricated antenna prototype and experimental set-up of the antenna under test (AUT). The reflection coefficient characteristics of the antenna were measured using a Rohde and Schwarz ZVA40 vector network analyzer.

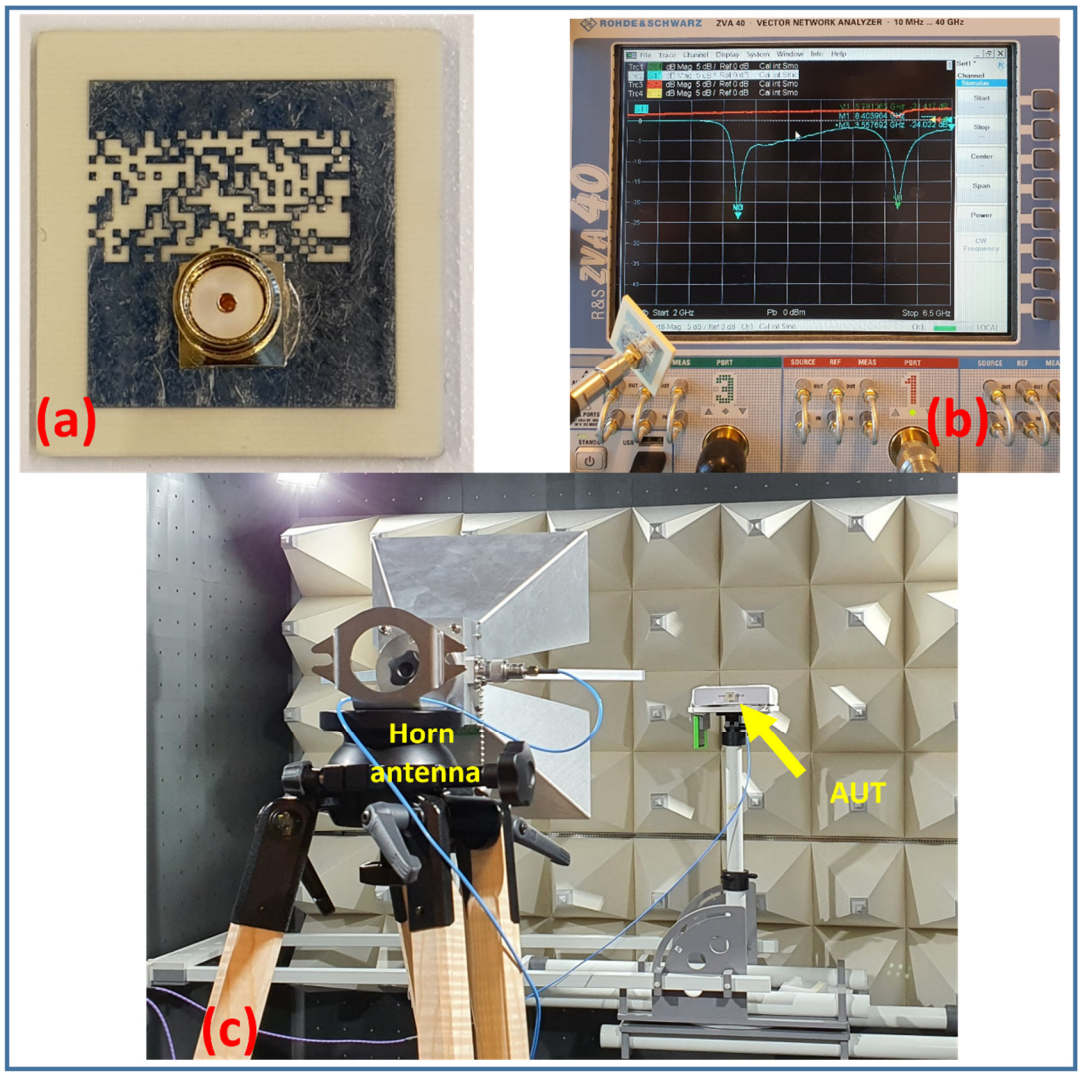

Figure 3.15 Fabricated prototype of the final PDGA (Antenna D) and measurement set up in RF and Communication Technologies (RFCT) Laboratory, UTS (a) Fabricated prototype of the proposed antenna (b) reflection coefficient measurement, (c) radiation pattern measurement

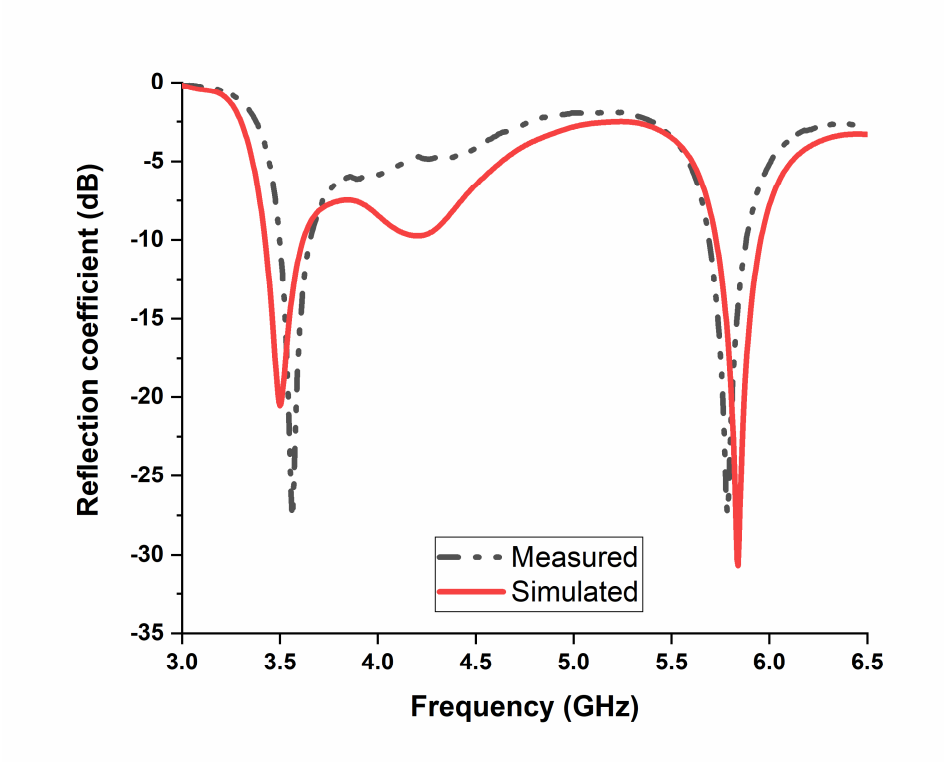

Figure 3.16 Simulated and measured reflection coefficient of the PDGA

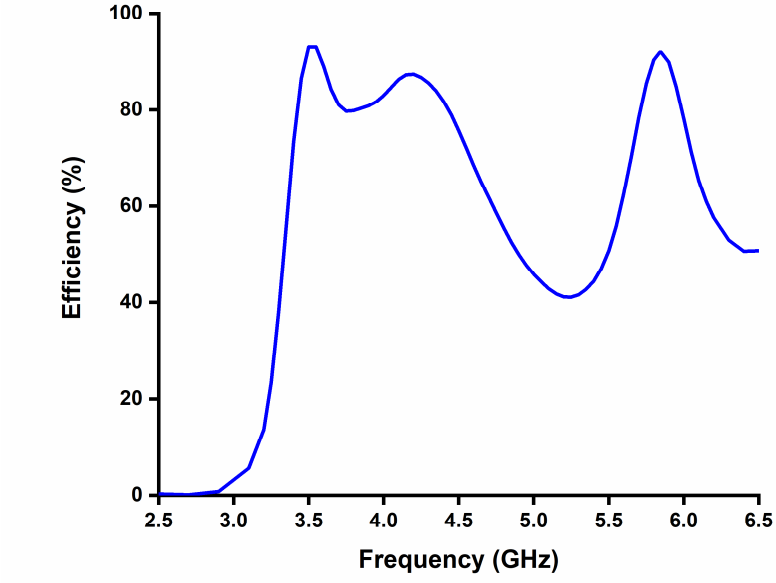

(a)

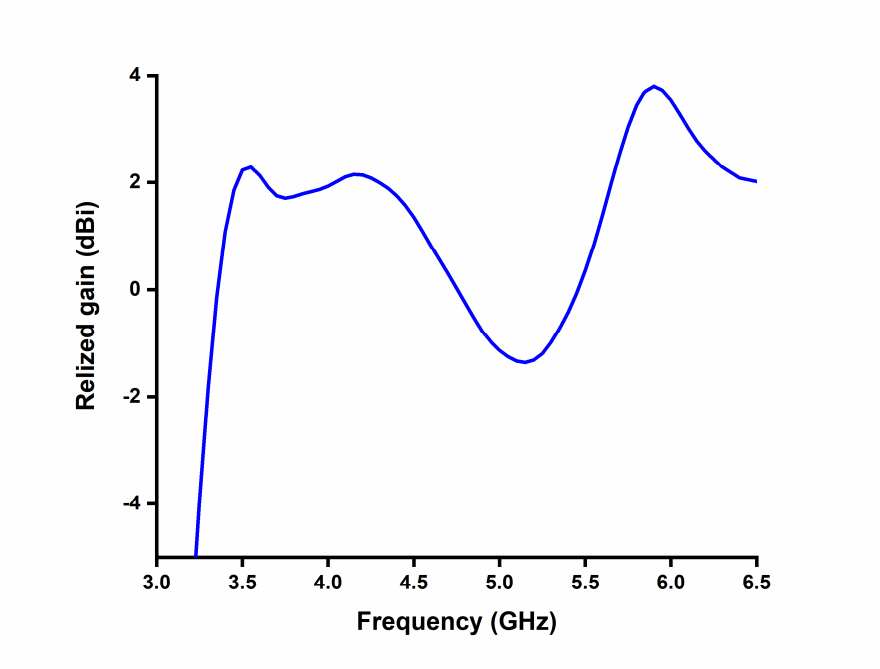

(b)

Figure 3.17 Simulated (a) efficiency and (b) realized gain of the PDGA antenna

Figure 3.16 shows the simulated and measured reflection coefficient of the proposed antenna. The measured reflection coefficient coincides well with the simulation results. The measured –10 dB impedance bandwidth at both frequency bands are almost similar to the simulated results. The simulated gain and efficiency of the proposed antenna are presented in Figure 3.17. The antenna obtained 2 dBi and 3.24 dBi realized gain at 3.5 GHz and 5.8 GHz, respectively. The achieved computed efficiency is more than 90% at both operating frequency bands and the measured antenna gain are 2 dB and 3.1 dB at 3.55 GHz and 5.8 GHz, respectively.

The normalized radiation patterns from simulated and measured results of the proposed antenna at 3.55 GHz and 5.8 GHz are provided in Figure 3.18. The simulated and measured radiation patterns are in good agreement. The pattern is nearly omnidirectional in both XZ plane at 3.55 GHz and YZ plane at 5.8 GHz. The proposed antenna has

monopole-like omnidirectional patterns in two operating frequency bands and, it is evident that the measured patterns generally meet IoT application requirements.

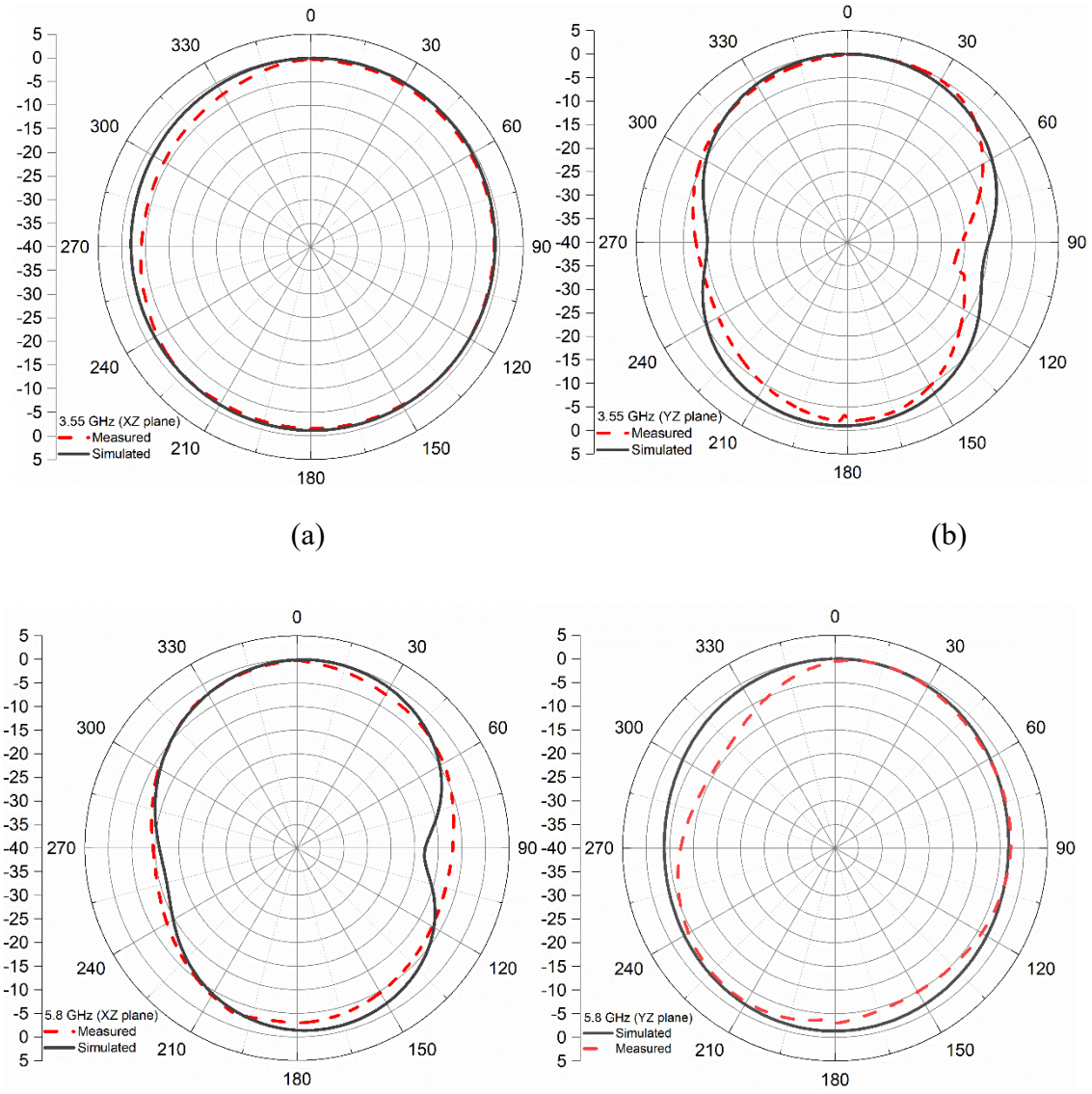

Figure 3.18 Normalized radiation patterns of the proposed antenna at (a) 3.55 GHz (XZ plane), (b) 3.55 GHz (YZ plane), (c) 5.8 GHz (XZ plane) (d) 5.8 GHz (YZ plane)

It can be seen that the proposed antenna has approximately similar radiation patterns with different polarizations at the two resonant frequencies. This is associated with the direction of surface current at both operating frequencies. Also, as depicted in Figure 3.14, the resonance frequency at both lower and upper bands are dependent on the length of *Wp*

and *Lp* respectively. The schematic of the surface current direction on the patch is depicted in Figure 3.19. Dense current is placed around the edges of the patch. The co-axial feed excites current across the patch edges. The direction of dominant current is along Y direction at 3.5 GHz that is helping the radiation of the patches which conforms to the radiation patterns of the antenna at the lower frequency band. At the higher band, the current flow is along X direction with some along Y on the right edge. However, the net dominant current flow is along X direction, which can be attributed to the radiation patterns at the higher band.

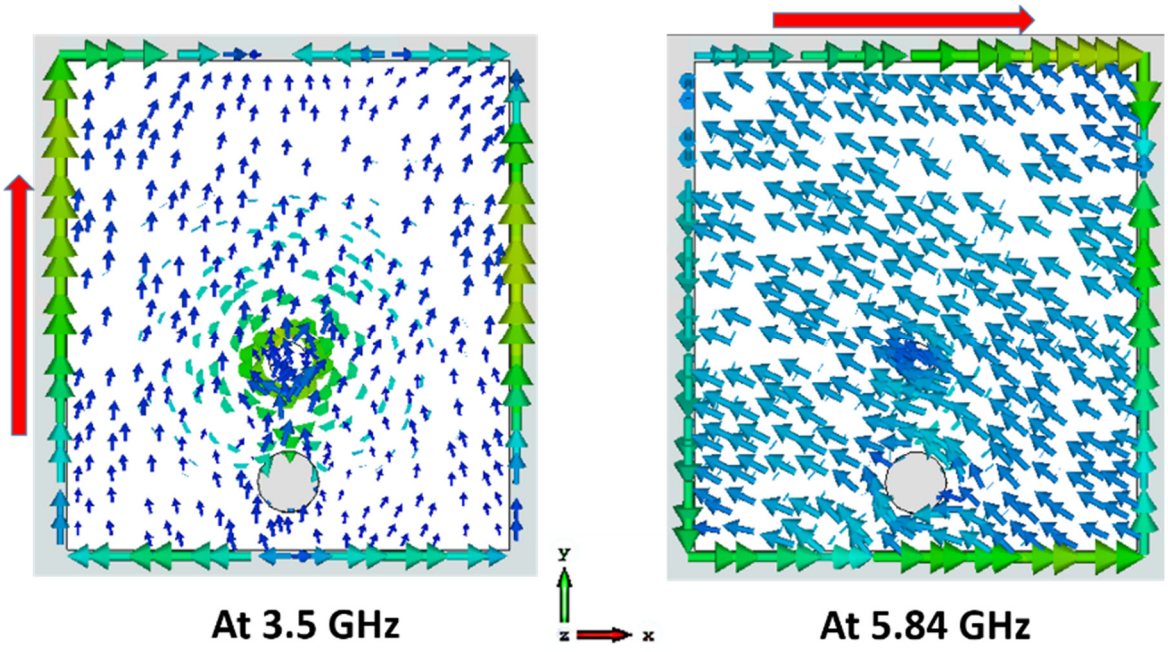

Figure 3.19 Schematic of surface current direction on the patch

Potential application of the proposed new dual-band antenna with dual patterns can be illustrated by the schematic in Figure 3.20. One possible scenario for IoT application using portable device is shown. The two bands can be used to receive or transmit wireless signal to different transmitter or receiver that are positioned in different directions. This

type of antenna design can support efficient communication in small IoT devices/sensors, creating more flexible positioning possibilities.

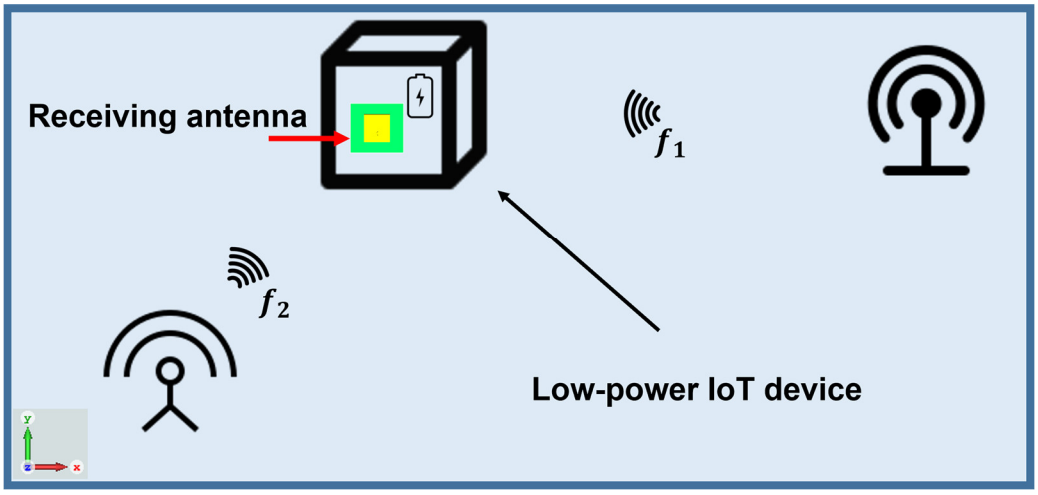

Figure 3.20 Schematic of potential applications of the proposed dual-band, dual pattern antenna

Table 3.4 compares the proposed antenna with other antennas in the literature for IoT applications, designed by conventional EM simulation methods. The proposed pixelated DG antenna is certainly advantageous over other designs, considering the total size, and excellent performance in dual-band. Moreover the proposed method of PDG antenna design has the capability of designing single-band or dual-band antenna according to the requirements of application specific IoT platforms. The greatest challenge addressed in this work is the trade-off between design complexity and achieving multiple functions; same DG area and size for single band antenna or dual-band, dual-pattern antenna with good gain, bandwidth and compact size.

In summary, the compact dual-band antenna design inspired by pixelated DG starts with a very straightforward initial geometry. Moreover, the implementation of VBPSO provides an efficient design of a novel pixelated DG with good antenna performance without any geometrical analysis on the DG area. Also, this approach of PDG does not restrain the DG to any particular shape, nor does it provide symmetry that can constrain

the output of the pixelization process. The antenna exhibits excellent performance with a low profile in comparison with antennas designed by traditional EM simulation. Antennas with these features are comparatively easy to integrate with circuits and embedded electronics. Also, their size is small enough to fit into portable devices (e.g. IoT devices). The proposed antenna can be a potential candidate to be used in IoT application. This research also reveals that the VBPSO algorithm is an effective and powerful optimizer for PDG antenna design.

Table 3.4 Comparison of the proposed PDG antenna with relevant antenna designs proposed for IoT applications

Refs.	Antenna type	Single/dual-band design flexibility using same DG design space	No. of bands and operating frequency (GHz)	Gain (dBi)	Bandwidth (%)	Antenna length (λ Considering lowest resonance frequency)	Planar circuit integration feasibility for portable IoT device	Dual-band dual vertical radiation pattern
[298]	Ground plane modified monopole	No	UWB; 3.1-8.5	-0.16 to -0.78	122	0.19 λ	Yes	No
[163]	Modified meanderline	No	1; 2.4	1.73	6	0.33λ	Yes	No
[299]	Additively manufactured folded 3D	No	2; 0.9, 1.8	0.9,1.7	8.9,33.3	0.32λ	Less feasible due to 3D footprint with 43.6 mm height	No
[300]	Square spiral loop patch	No	2; 0.92, 2.45	1.85,4.1	8.69,11.8	0.49λ	Yes	No
[301]	Cavity backed slot	No	1, 0.9	2.4	6.7	0.23λ	Yes. However, antenna height 15mm	No
[302]	Folded strip slot antenna	No	1, 2.45	Not specified	5.09	0.51λ	Yes	No

This work	Pixelated DGA using VBPSO	Yes, using different configuration of PDG with same space of DG; Can be designed for signle bands at 3.5, 5.2 5.8 GHz and dual-band at 3.5 and 5.8 GHz	2;3.5, 5.8	2, 3.24	5.7, 4.1	.30λ	Yes	Yes

3. 4 Summary

A dual-band pixelated defected ground antenna design has been proposed in this chapter along with a flexible design guide for different single-band antennas at different operating frequencies. The proposed PDGA design is performed using the VBPSO algorithm. This chapter introduces the idea of utilizing pixelated defected ground using VBPSO for efficient antenna design without depending on geometric optimization of design parameters of defected ground area, unlike conventional DG antenna. The PDG configuration has the potential to achieve different antenna characteristics including single or multi-band antenna design, gain or efficiency enhancement etc. using distinct configuration with a great degree of freedom. This leads to create multi-functional customized antennas for diverse applications. The advantage of using VBPSO in the antenna design process is the V-shaped transfer function, which provides enhanced and faster searchability of pixel positions for the PDG antenna. The defined area for defected ground is pixelated using a binary string from the algorithm, and the objective function has been evaluated for single band as well as dual-band performance. The final PDGA operates at 3.5 GHz and 5.8 GHz bands with 5.63% and 4.1% fractional bandwidth, respectively. To validate simulation results, the proposed antenna has been fabricated and measured. The measured and simulated results are in excellent alignment. The proposed

antenna has a nearly omnidirectional radiation pattern with 2 dBi and 3.1 dBi measured gain at 3.55 GHz and 5.8 GHz, respectively. The simulated efficiency is more than 90% at both operating bands. The proposed antenna can be a potential candidate to be applied in different applications in IoT platform including device to device communication, wireless power transfer in low power IoT devices, etc.

Although the antenna is generally resilient to manufacturing errors, precautions have been taken to address potential issues stemming from contact between two pixels. Specifically, a small conducting area, designed to match the fabrication tolerance, has been incorporated at the contact point. This proactive measure has proven effective in preventing fabrication errors and has contributed to achieving favorable measured results for the antenna. Moreover, the frequency limitations of the antenna design can be estimated using standard equations commonly applied in patch antenna design. However, for lower frequencies, it is crucial that the optimization area and pixel size do not deviate significantly from the wavelength associated with that frequency. Also, the chosen pixel size can be up to 0.5% of the wavelength at the lowest operating frequency. Further reducing the size would increase the simulation time due to the number of mesh cells required in the EM simulator.

Chapter 4

Multi-service Stacked Antenna with Different Pixel Shapes

4.1 Introduction

The Internet of Things (IoT) has experienced a massive rise in interest, as IoT solutions are being expanded to almost every aspect of life. IoT is bringing about a paradigm shift in emerging applications that will enhance the quality of life by connecting a wide range of smart devices and physical objects [301]. As the number of wireless IoT devices is expected to experience exponential growth in the near future, many emerging applications will benefit from utilizing a wide range of IoT systems [2, 278, 285, 303-307]. Antenna is a vital part of the wireless communication modules in IoT devices that performs crucial role in the system operation and performance. Due to the wide variety of IoT applications, designing antennas can be challenging. Antennas for low-power IoT devices should be compact and integrable with planar circuits as large antennas with bulky dimension are less suitable to fit into the subsystem of small IoT devices and sensors [49, 52, 53, 302]. Recent antenna designs for IoT applications include shared aperture slot antenna [308], meander line antenna with parasitic element [163], transparent loop antenna [309], frequency-tunable inverted-F antenna [310], inkjet-printed antenna [311], and multi-standard MIMO antenna [312]. A handbag zipper antenna has been reported for IoT applications [305]. The structure makes use of the zipper of the handbag as antenna. However, it has a larger size compared to the common types of antennas with reasonable performance. A small monopole antenna with a slit ground plane has been proposed for ultra-wide band (UWB) IoT applications [298]. Nevertheless, the antenna's average gain is low due to miniaturization. Besides communication, the lifespan of IoT devices can be

extended by radio frequency energy harvesting and wireless power transfer technology where antenna also plays a key role[15, 30, 76, 278, 284]. Over the past decades, wireless power transfer and radiofrequency energy harvesting technologies have introduced several types of receiving antennas [46-50]. However, low-profile and efficient receiving antennas are required to remotely charge low-power IoT devices due to the small form factor of IoT devices.

With certain shapes and techniques, the aforementioned and other relevant antennas have achieved reasonably good performance. However, the majority of the antennas are designed using traditional EM simulation by changing patch or ground shape. As a result, the enhancement space for the antenna is limited, particularly in terms of gain, operating frequency, and radiation pattern. Nevertheless, designing a small-size antenna with a significant capacity to capture wireless signals, while attaining good gain and efficiency is incredibly challenging. Most antennas published in the literature are based on traditional design approaches using electromagnetic (EM) simulation with geometrical modifications such as variation of radiating element, changing the dimension of patches or the ground plane [48, 50, 54, 55, 313, 314].

Evolutionary Algorithms (EA) have been used to solve a wide range of antenna design problems, where EAs have been integrated with numerical approaches in electromagnetics and yielded a variety of notable and effective outcomes [56, 57, 59]. Among the EAs applied in solving antenna design problems, Genetic Algorithm (GA) and Particle Swarm Optimization (PSO) algorithm have remained the most prominent in the past decades [61-63]. PSO has been employed in solving variety of EM problems due to its straightforward and effective way in antenna design [63-65]. Further, the ability of PSO to efficiently handle various design goals contributes to its prominence in antenna

designs [66, 67]. When dealing with multi-object or high-dimensional situations, the standard PSO technique suffers from early convergence issues and has difficulty processing them. Recently, it has been demonstrated that modified and updated PSO algorithms provide an improved way of searching for optimal solutions [68-71].

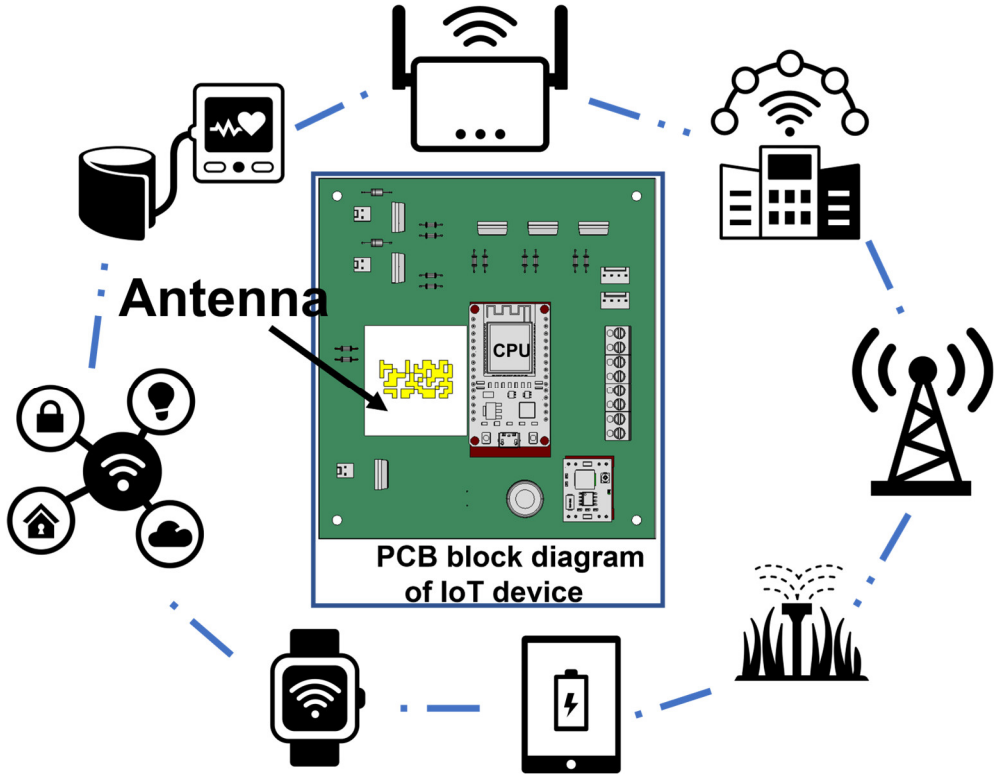

Figure 4.1 Potential application scenario of optimized pixelated stacked antenna in IoT devices

The emergence of different IoT applications poses new challenges in designing compact antenna as limited design space is available for the communication module. It is comparatively challenging using orthodox antenna design methods. Since antenna sections are assigned to a preset area in many applications, space management in antenna designs for communication module is as critical as cost reduction. Dual-band antennas can have a smaller footprint than two distinct antennas operating at different frequency bands. Additionally, dual-band antenna is advantageous when a device needs to transmit or receive over two frequency bands. Recent research has featured dual-band antenna

designs that incorporate elements such as the Sierpinski carpet fractal, paired L-shape slots, and an inset-fed patch with a partial ground [315-317].

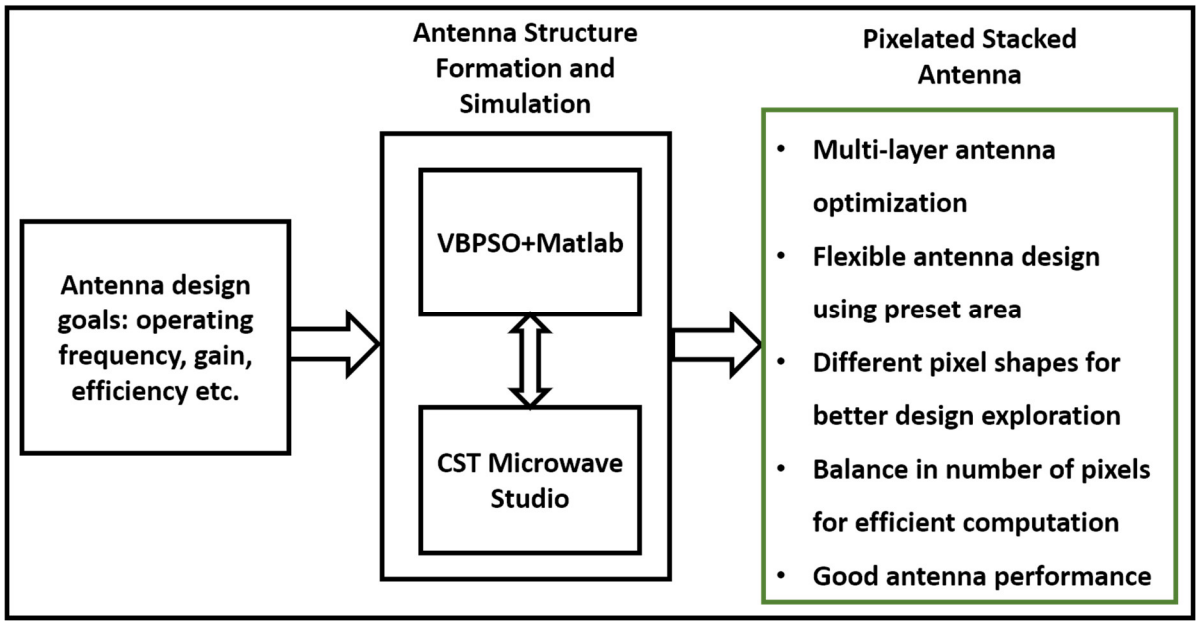

Figure 4.2 Pixelated stacked antenna design methodology

In this chapter, a multi-service low-profile Pixelated Stacked Antenna (PSA) is proposed for dual-band applications at 5.2 GHz wireless local area network (WLAN) and 5.8 GHz Industrial Scientific and Medical (ISM) bands. These bands are established in Australia and globally for radio local area network equipment, ISM applications, network access points, radio Local Area Networks (LAN), WiFi and wireless LAN applications, wireless audio, and video system [318, 319]. Figure 4.1 illustrates a potential application scenario of the proposed antenna topology in IoT environment. The traditional antenna design methods require alteration of antenna size, shape etc. to obtain the desired performance at a certain frequency. Antenna shape and size significantly impact performance metrics such as operating frequency, gain, and efficiency for IoT devices. The ideal antenna should blend with the device's circuit and casing. A generic commercial antenna may be used if it achieves the desired performance. However, fitting such an antenna into a small

space like a planar printed circuit board (PCB) can be challenging, limiting its effectiveness. This is where the proposed antenna topology serves a critical purpose as it can deliver optimized performance in these challenging conditions where preset limited design space is available for the antenna. The antenna can be designed and optimized for different resonance frequency, gain, efficiency, etc. only by considering a predefined area.

Figure 4.2 briefly highlights major advantages of designing pixelated stacked antenna using the proposed methodology. In the proposed antenna design using PSA technique, antenna size and shape do not require to be altered. Antennas with different resonance frequency, gain, bandwidth, etc. can be designed using this method on given patch regions. Different frequency of operation can be achieved only by changing the pixel configuration. Also, the proposed method does not require a comprehensive understanding of EM (electromagnetic) formulations, or models. The proposed antenna design consists of two pixelated radiating patches, enabling simultaneous dual-band operation of the proposed antenna at desired bands. To the best of authors' knowledge, pixelated stacked antenna design that simultaneously employs pixelated radiating patch with different pixel shapes in multilayers, has not been implemented in any prior work. BPSO algorithm with a V-shaped transfer function optimized the antenna's pixel position for dual-band operation while maintaining satisfactory performance.

Simultaneous optimization of multilayers of the structure avoids the need for multiple separate optimizations of the same structure for each component or part of the antenna. The primary patch utilizes triangular pixels to provide major flexibility in the design process considering the number of required pixels in the design. The proposed antenna design methodology offers greater feasibility in designing single band or dual-band antenna. This work also investigates the performance of eight different transfer functions

of binary particle swarm optimization algorithm from S-shaped and V-shaped families for the antenna design. The transfer function with the best initial result has been implemented to achieve final pixelated layers of the antenna. The proposed antenna achieves dual-band performance at 5.2 GHz and 5.8 GHz bands. The achieved measurement results indicate that the proposed methodology is an effective strategy for designing compact, dual-band, pixelated stacked antenna with excellent performance.

The rest of the chapter is organized as follows: The design configuration and utilization of BPSO with different transfer functions are described in Section 4.2. Section 4.3 evaluates the best transfer function and impact of pixels' shape, size, and number on antenna performance. This section also demonstrates single or dual-band antenna design flexibility. Results of the optimum design are presented in Section 4.4, and concluding remarks in Section 4.5.

4.2 Pixelated Stacked Antenna Design

This section presents a detailed description of the antenna design methodology. First, a brief overview of PSO, BPSO and different transfer functions (S-shaped and V-shaped) is presented in Subsection A. Subsection B, describes the pixelated stacked antenna (PSA) design evolution and formation of pixelated antenna configuration, beginning with a simple patch antenna. Finally, Subsection C illustrates pixelization on dual-layers of the antenna and problem formulation for optimization.

4.2.1 PSO, Binary PSO and Different Transfer Functions

The PSO is an evolutionary algorithm that is inspired by the social behavior of animals and is one of the most extensively used evolutionary algorithms in antenna design [62, 289]. The particles in PSO move through the search space, where their positions are

updated by two optimum values. The first is the best solution (fitness) to date. This value is referred to as *pbest*. The other one is the best value obtained globally by any particle in the swarm. This optimal value is denoted by *gbest*. Following the determination of the *pbest* and *gbest*, the velocity update rule is vital in a PSO algorithm. The current position, current velocity, distance to their personal best solution (*pbest*), and the distance to the global best solution (*gbest*) should all be taken into consideration by each particle in PSO, while modifying its position and velocity. The following equations are used to update the velocity and position of each particle for each problem dimension in PSO [289]:

$$v_i^{t+1} = wv_i^t + c_1 \times rand \times (pbest_i - x_i^t) + c_2 \times rand \times (gbest - x_i^t) \quad (4.1)$$

$$x_i^{t+1} = x_i^t + v_i^{t+1} \quad (4.2)$$

where, the velocity and position of particle i at iteration t is denoted by v^t_i and x^t_i, respectively. c_1 and c_2 denote acceleration coefficient and w represents a weighting function. A random number between 0 and 1 is represented by *rand*.

Based on equations (4.1) and (4.2), the PSO algorithm only deals with continuous search spaces. However, new optimization challenges arise when dealing with discrete binary search spaces. They need binary algorithms to solve their problem as required in automated pixelated antenna design methodology. Kennedy and Eberhart proposed the binary variant of PSO (BPSO) in 1997 [290]. Two distinct components distinguish the continuous and binary versions of PSO; a new position updating method and a new transfer function to transform a continuous search space into a binary search space. Mapping a sigmoid function's continuous-valued output to binary values (0 or 1) based on a threshold is the goal of the transfer function. The sigmoid function produces

continuous-valued outputs that represent probabilities. The BPSO algorithm's transfer function is essential in discretizing the continuous search space into a binary search space, which enables the algorithm to find optimal solutions in a binary domain with efficiency. The corresponding binary position can either be 1 or 0, as determined by the transfer function by applying a threshold to the sigmoid function's output. Using equation (4.3), all real velocities are converted to probability values in the interval of 0 and 1 where, v^k_i is the particle i's velocity at iteration t in dimension k. After converting velocities to probabilities, position vectors could be updated with equation (4.4) [290].

$$T\left(v_i^k(t)\right) = \frac{1}{1+e^{-v_i^k(t)}} \tag{4.3}$$

$$x_i^k(t+1) = \begin{cases} 0 & \text{If } rand < T\left(v_i^k(t+1)\right) \\ 1 & \text{If } rand \geq T\left(v_i^k(t+1)\right) \end{cases} \tag{4.4}$$

The transfer function has a great significance in optimization performance of BPSO. However, this standard variant of BPSO is affected by trapping into local minima. To address this issue, recently 6 new transfer functions for the BPSO algorithm have been proposed [71]. A study on 25 benchmark functions has been performed using total of 8 transfer functions to evaluate the performance of BPSO. They were classified into two families called S-shaped and V-shaped transfer function due to the shape of their characteristics curve, which are provided in Table 4.1. The V-shaped family of transfer functions differs from the S-shaped family, and they follow entirely new position updating rules in (4.5) [71]. This approach has an advantage of encouraging particles to remain in their current places at low velocity.

$$x_i^k(t+1) = \begin{cases} \left(x_i^k(t)\right)^{-1} & \text{If rand } < T\left(v_i^k(t+1)\right) \\ x_i^k(t) & \text{If rand } \geq T\left(v_i^k(t+1)\right) \end{cases} \tag{4.5}$$

Table 4.1: S-Shaped And V-Shaped Transfer Function For BPSO [71]

Name	Transfer functions	Family
BPSO1	$T(x) = \frac{1}{1+e^{-2x}}$	S-shaped
BPSO2	$T(x) = \frac{1}{1+e^{-x}}$	
BPSO3	$T(x) = \frac{1}{1+e^{(-x/2)}}$	
BPSO4	$T(x) = \frac{1}{1+e^{(-x/3)}}$	
BPSO5	$T(x) = \left\lvert \text{erf}\left(\frac{\sqrt{\pi}}{2}x\right)\right\rvert = \left\lvert \frac{\sqrt{2}}{\pi}\int_0^{(\sqrt{\pi}/2)x} e^{-t^2}dt \right\rvert$	V-shaped
BPSO6	$T(x) = \lvert\tanh(x)\rvert$	
BPSO7	$T(x) = \left\lvert (x)/\sqrt{1+x^2}\right\rvert$	
BPSO8	$T(x) = \left\lvert \frac{2}{\pi}\arctan\left(\frac{\pi}{2}x\right)\right\rvert$	

The study on these transfer functions reveals that the new V-shaped family of transfer functions can considerably improve the original BPSO's performance in terms of avoiding local minima and convergence rate. These results, however, are illustrative and may not apply to all electromagnetic (EM) optimization situations. Also, the No Free Lunch theorem implies that there is no superior algorithm. The main reason for implementing new or modified algorithms is the possibility of performing better than others in certain problem categories [320-322]. One BPSO algorithm with a specific transfer function could perform better or worse than another BPSO with different transfer function. Hence, the modified versions of BPSO with different transfer functions are worth testing and applying the suitable one in solving our proposed pixelated stacked antenna design

problem. So, this chapter also investigates the performance of BPSO in solving a pixelated stacked antenna design problem with different transfer functions.

4.2.2 Proposed Antenna Design Methodology

The proposed antenna design methodology has the advantage of considering a specific region of the antenna for varied resonance frequencies, gain, efficiency, etc. This is particularly important for practical applications where only a predefined area is allocated for antenna module. It becomes challenging to determine the correct patch or ground shape with desired antenna performance using conventional design methodology or by using EM solvers' built-in optimizers. In contrast, the pixelization technique subdivides the predefined regions into small pixels and determines the optimum shape using suitable binary optimization algorithm. Additionally, our proposed method combines the advantage of two different pixel shapes (Square and Triangular) that efficiently explores optimum configuration for the patches. Figure 4.3 depicts the design configuration of the proposed antenna. The proposed pixelated stacked antenna (PSA) consists of two substrate layers with pixelated radiating patch. Triangular pixels are used on one layer and square pixels are used on the second layer (parasitic layer). The total height of the antenna with both layers is 3 mm. As a starting point, a typical rectangular radiation patch is used for the initial design stage. The width and length of the patch can be approximately determined by the following equation (4.6)-(4.9) [323, 324], where c is the speed of light, f_r denotes the desired operating frequency, and ε_r denotes relative permittivity of the substrate.

$$f_r = \frac{c}{2W}\sqrt{\frac{2}{\varepsilon_r+1}} \tag{4.6}$$

The length of the patch can be calculated as

$$L = \frac{\lambda}{2} - 2\Delta L \tag{4.7}$$

where,

$$\frac{\Delta L}{h} = 0.412 \frac{(\varepsilon_{\text{eff}}+0.3)\left(\frac{W}{h}+0.264\right)}{(\varepsilon_{\text{eff}}-0.258)\left(\frac{W}{h}+0.8\right)} \tag{4.8}$$

$$\varepsilon_{\text{eff}} = \frac{\varepsilon_r+1}{2} + \frac{\varepsilon_r-1}{2}\left[1 + 12\frac{h}{W}\right]^{-1/2} \tag{4.9}$$

where, ε_{eff} is the effective permittivity of the substrate and h is the substrate height.

However, a standard rectangular patch antenna with simple radiating patch is incapable of providing high antenna performance in terms of reflection coefficient, gain, efficiency, radiation patterns, etc. Slots on the radiation patch can significantly alter the antenna's performance due to variations in the surface current path. A rectangular slot has been introduced to accommodate pixels from the bit string of BPSO. The length and width of the slot can be approximated by equation (4.10) considering one-wavelength distribution of current along the circumference of the slot at the lowest operating frequency [325], where l_1 and w_1 are length and width of the slot, respectively. After that, the parasitic pixelated patch is positioned above the main pixelated patch as an electromagnetically coupled patch to achieve enhanced optimized performance from the antenna [326].

$$f_L = \frac{c}{2(l_1+w_1)} \tag{4.10}$$

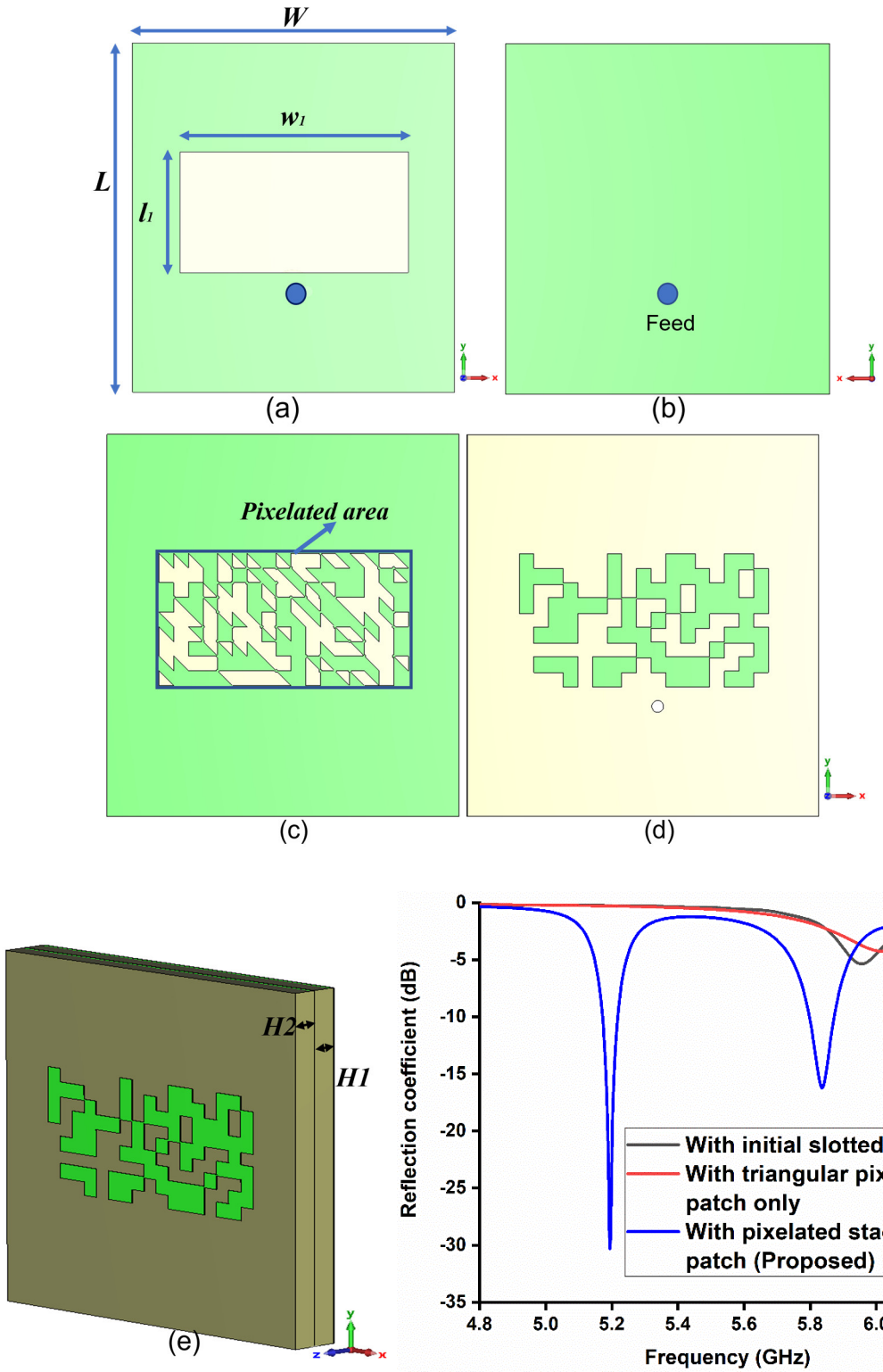

Figure 4.3. Design evolution and configuration of the proposed pixelated stacked antenna; (a) initial slotted patch, (b) ground plane, (c) pixelated layout of the main radiating patch, (d) parasitic pixelated patch, (e) perspective view of the proposed pixelated stacked antenna, and (f) reflection coefficient of different stages of the antenna. (Green: Metal; Brown: Substrate)

4.2.3 Problem Formulation and Pixelization on Multilayers

Following the methodology discussed in the previous section, a pixelated stacked antenna has been designed. The proposed antenna is designed to achieve dual-band operation at 5.2 GHz and 5.8 GHz. The dimensions of the antenna substrate are 26 mm×24 mm. Rogers 4003 has been used as substrate and superstrate for the antenna. The height of both substrates *H1* and *H2* are 1.52 mm. *W* and *L* are the dimensions of the radiating patch and ground plane. w_1 and l_1 are the dimensions of the slot on the bottom and main patch. The main radiating patch is pixelated by triangular shaped pixels and the stacked parasitic patch utilizes square shaped pixels. The triangular shape of pixel has been utilized on the slot of the principal radiating patch as the principal patch is directly connected with the feeding. Further, a small change on the principal radiating patch has more impact on the resonance frequency of the antenna than the parasitic staked patch. Also, this combination serves the purpose of using less pixels (binary bits) for efficient search of pixel positions. Table 4.2 provides the design dimensions of the proposed antenna.

Table 4.2 Dimensions of the Antenna

Dimensional Parameters	Dimension (mm)
W	24
L	26
w_1	17
l_1	9
H_1	1.52
H_2	1.52

The correlation between the resonance frequency and geometric shape of the designated region for pixelization serves as the basis for the design mechanism of the proposed pixelated stacked antenna. Automated shape generation is not achievable using

commercially available electromagnetic (EM) solvers' built-in optimizers. The built-in optimizers can optimize a simulation model based on different geometrical parameters only (e.g. length, width, etc.). On the contrary, our PSA design approach provides a solution that deals with the multilayered geometry or shape of the designated part of the antenna to achieve desired results. Further, it aids the shape optimization with better efficiency by employing square and triangular shapes of pixel.

The rectangular slot and the stacked parasitic patch are considered for pixelization in the proposed antenna design method. Initially, the rectangular slot of the main radiating patch is divided into 17×9 rectangular pixels with a resolution of 1 mm×1 mm as shown in Figure 4.4. Though the rectangular pixelization provides freedom to the generated pixelated shape based on the binary string from BPSO, it still limits the structure within rectangular pixelization, which in turn limits the exploration of new patch shapes. Also, increasing the resolution of pixels may provide potentially better outcomes as it can facilitate more evaluation of small change in the design space. However, reducing the size of square pixels gives significant rise to the number of required pixels and corresponding binary bits. The presence of a large number of pixels (bits) dramatically increases the solution space of the optimization technique, which results in the algorithm failing to attain convergence with good results (shown in the following section). To address this issue, each square pixel (1 mm×1 mm) on the main radiating patch is divided into two triangular pixels, depicted in Figure 4.3. The triangular pixels not only facilitate better shape exploration, but also provide a balance in the number of pixels in the BPSO, as significantly increased number of pixels will result in unsatisfactory performance from the optimization algorithm. The proposed methodology adopts a total number of 459 binary bits to represent pixels on the antenna, 306 pixels to represent triangular pixels on the main radiating patch and 153 square pixels on the stacked parasitic patch depicted in

Figure 4.5.

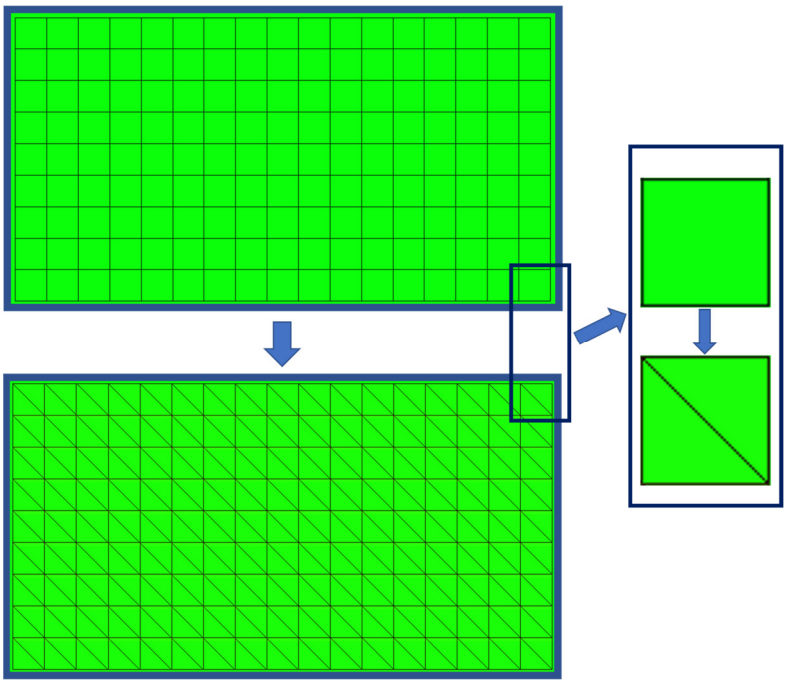

Figure 4.4 Pixelization area on the main patch divided into triangular pixels.

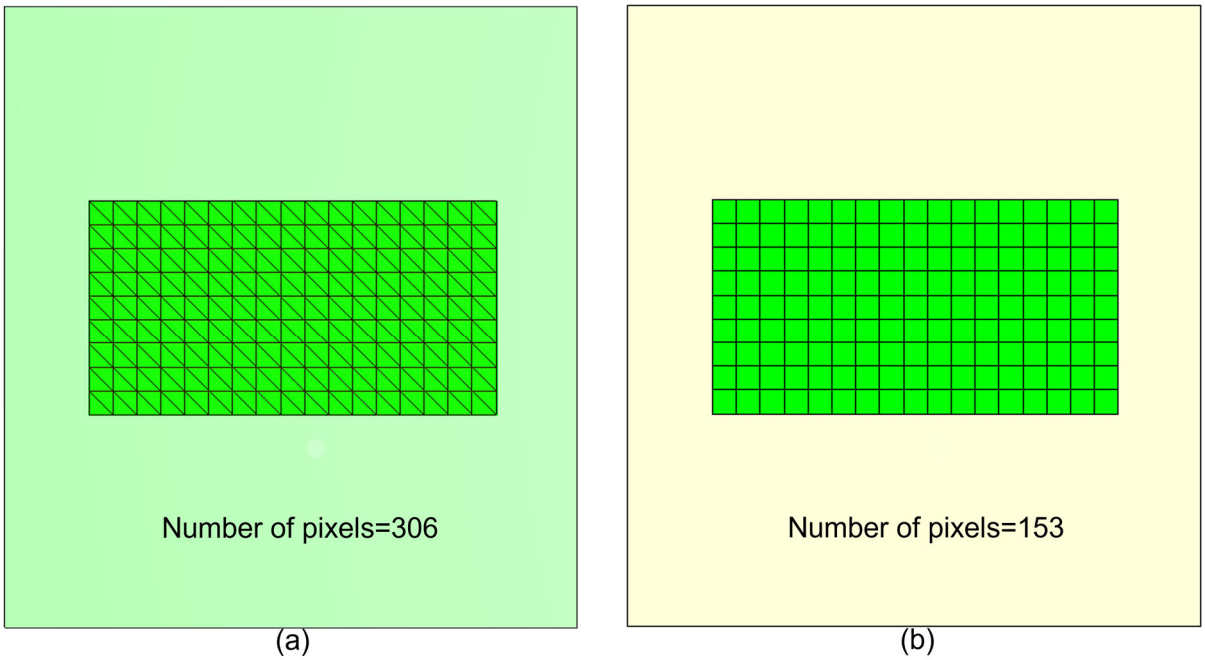

Figure 4.5 (a) Main radiating patch on the bottom substrate; (b) parasitic patch area on the top substrate

Every optimization technique necessitates the use of a fitness function in order to find

a potential solution. The fitness function can be constructed from the results of an electromagnetic simulation while designing antennas with optimization algorithms. The dual-band PSA design can be defined as a minimization problem in BPSO. The design challenge is to obtain dual-band operation using the defined space on the bottom substrate and the top substrate. Design goals of the pixelization are to achieve dual-band coverage of 5.2 GHz (f_1) and 5.8 GHz (f_2) simultaneously for potential applications. Hence, the objective or fitness function for the antenna design can be formulated as:

$$FF = w_1\left(S11_{f_1=5.2\ GHz\ band}\right) + w_2\left(S11_{f_2=5.8GHz\ band}\right) \tag{4.11}$$

Equation (4.11) is defined to minimize the antenna reflection coefficient at the desired frequencies (f_1 and f_2). W_1 and w_2 are two weighing coefficients that can be tuned to achieve optimal solution. The flowchart in Figure 4.6 illustrates the design methodology of the proposed antenna. BPSO with V-shaped transfer function is implemented in Matlab while the EM simulator is interfaced with Matlab. Computer Simulation Technology Microwave Studio (CSTMWS) is used to evaluate the EM simulation model of the antenna. After initialization, BPSO sends the binary bit string to the EM simulator. Pixelated shape is then generated based on the binary bits, where 1 and 0 in the bit string represents metal and empty space (etched) inside the defined area. After the simulation, the EM simulator is called to send the required antenna performance to BPSO and evaluate its fitness function. Based on the fitness value, personal best score, and global best score in BPSO are updated. As iterations in the BPSO continue, the algorithm searches for the right position of particles. This method is repeated until the end conditions have been fulfilled. In this approach, the pixelization stops after reaching the maximum number of iterations, and then offers the best binary bits for the pixelated area.

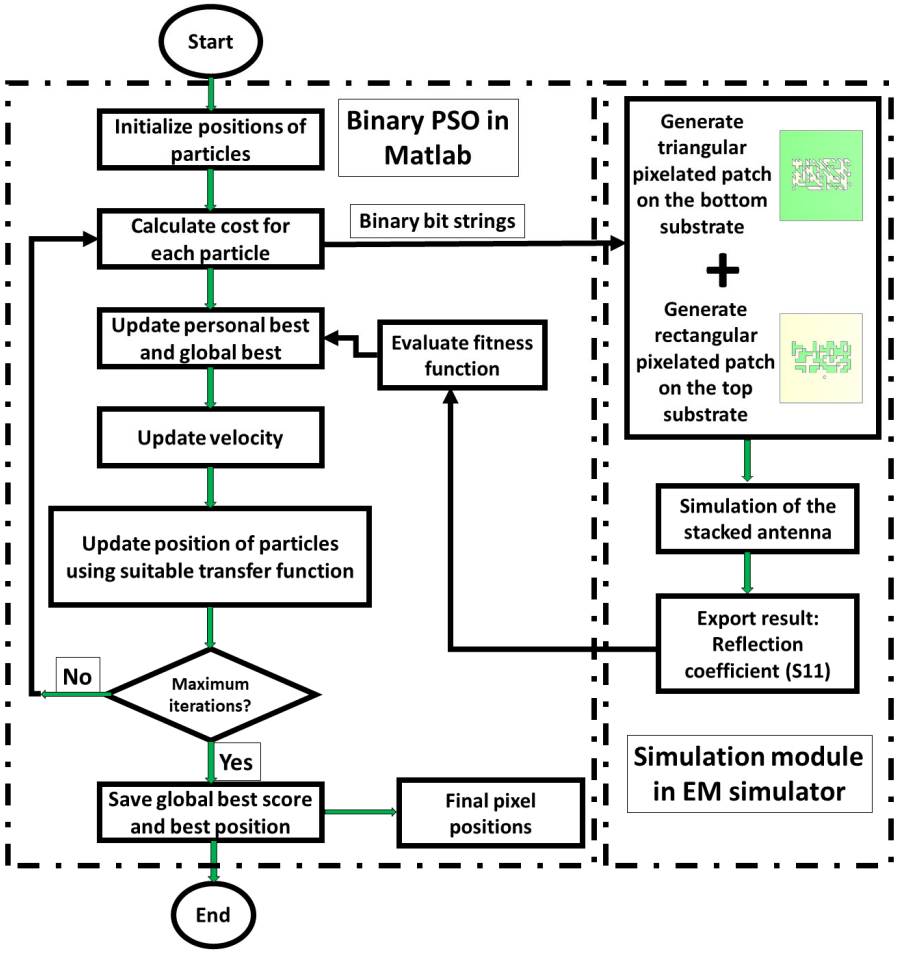

Figure 4.6 Flowchart of the proposed pixelated stacked antenna design methodology

4.3 Antenna Simulation

This section presents the simulation results of the proposed antenna using different transfer functions of BPSO in subsection 4.3.1. In Subsection 4.3.2, a case study on the pixelated stacked antenna design using different pixel size and combination of different pixel shape is presented. Simulation results demonstrate the feasibility of the proposed design method for single band and dual band antenna.

4.3.1 Simulation Using Different Transfer Functions

Initial simulations have been performed to determine the suitable transfer function to be used in the design of the proposed antenna. As mentioned earlier, BPSO can perform

differently with different variants of transfer functions. The main objective of these simulations is to observe which transfer function of BPSO provides potentially good solution to achieve dual-band operation of the antenna. These simulations are performed for 100 iterations using 13 particles in BPSO to keep the number of function evaluations low. Each transfer function listed in Table 4.1 is utilized in 8 independent runs to optimize the fitness function of PSA design in Equation (4.11). Illustration of the convergence curves of various variants of the BPSO algorithm with different transfer functions is presented in Figure 4.7(a). BPSO4 has the lowest performance as it has stopped updating the fitness value around iteration 38. It is obvious that the BPSO algorithm with V-shaped family of transfer function performs better than the S-shaped family. BPSO6 and BPSO8 performed almost similar in context of achieving the best fitness value. However, it may not always indicate that they achieved the optimization goals successfully. Further clarification can be obtained by looking at Fig 4.7(b), which presents the reflection coefficient of the antenna. As the design goal is to achieve operation at two different frequencies, BPSO6 and BPSO8 failed to achieve the two design goals simultaneously, rather they emphasized on one goal towards achieving the higher band, which may be mitigated by changing the cost function definition. On the contrary, BPSO7 outperforms the others in achieving both the optimization goals with a fitness value of -7.9. Reflection coefficient values of -15 dB and -14.39 dB have been achieved at 5.2 GHz and 5.78 GHz, respectively. Results from these initial simulations can be attributed to the modified position updating rules which are used in the different transfer functions of BPSO. It is possible that BPSO7's improved findings and faster convergence are the consequence of a streamlined exploitation procedure, that places more emphasis on exploration initially than on exploitation. It suggests that BPSO7 has improved ability of exploration for the optimum pixel positions for the pixelated patch of the antenna. Also, BPSO7 belongs to

the V-shaped family of the transfer functions that performed well in optimizing a diverse range of benchmark functions, including composite benchmark functions with complex structure similar to real world optimization problem [71]. Applying a proper transfer function can be crucial in pixelated antenna design as the particle positions serve as the pixel position and there is a direct relationship between the pixel position and antenna performance. Based on the results obtained, BPSO7 is utilized for further simulations in this work.

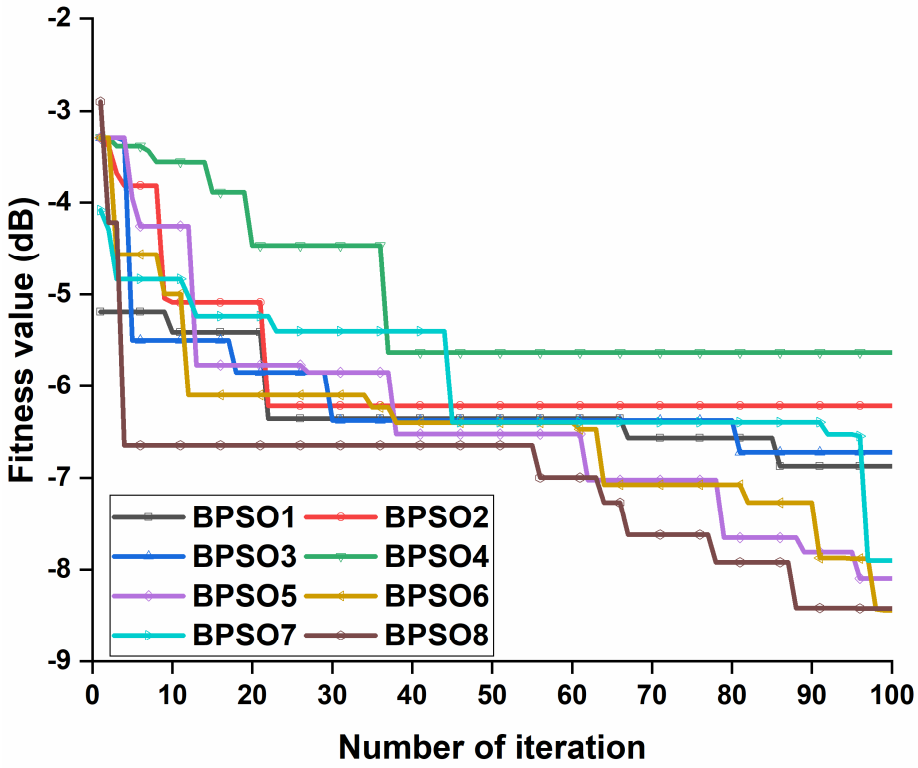

(a)

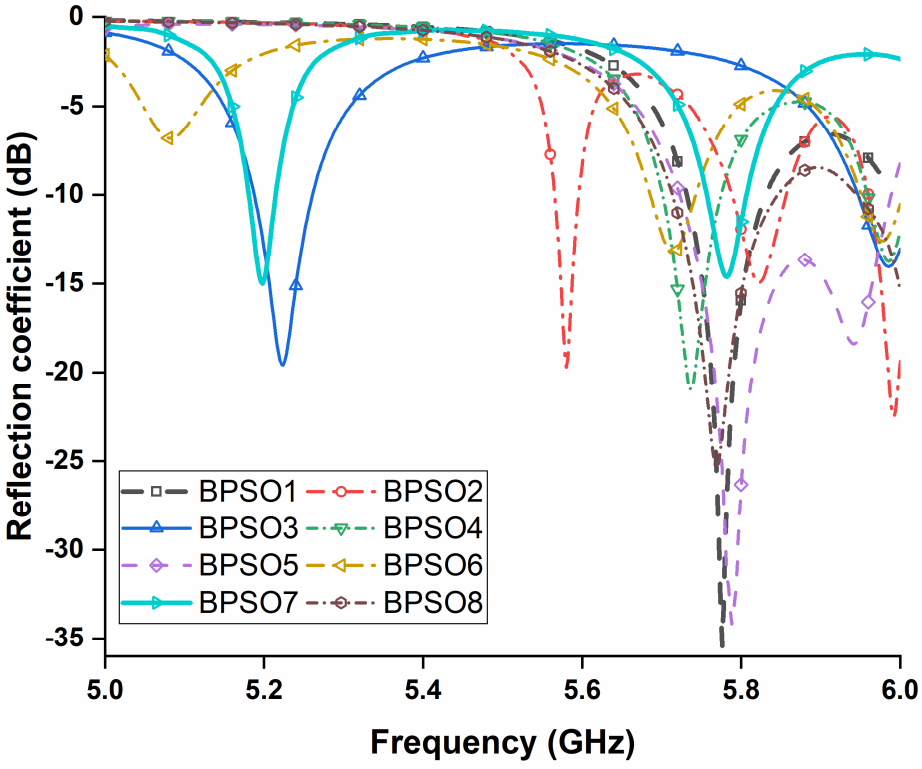

(b)

Figure 4.7 (a) Convergence curve of different BPSO with different transfer functions, (b) achieved reflection coefficient of the antenna using different transfer function in BPSO.

4.3.2 Simulation with Different Pixel Size and Shape

In this section, a design case with smaller pixel size and increased number of pixels has been investigated to compare the results with the proposed antenna design with triangular pixels. The pixelization designated space for each of the bottom and top substrates are discretized into 18×34 pixels, where the square pixel size has been decreased to 0.5 mm×0.5 mm. Hence, the total number of pixels on the whole antenna design space becomes 1224. The same fitness function (4.11) is utilized to perform the simulation using BPSO7 with 20 particles and 100 iterations. Figure 4.8(a) illustrates the convergence plot of the two different design topologies for stacked pixelated antenna. As it can be seen, the convergence rate achieved by the antenna with triangular pixels is better. Moreover, the triangular pixelated antenna successfully achieved the optimization goal with better

reflection coefficient levels with −30.24 dB and −16.29 dB at 5.19 GHz and 5.83 GHz respectively.

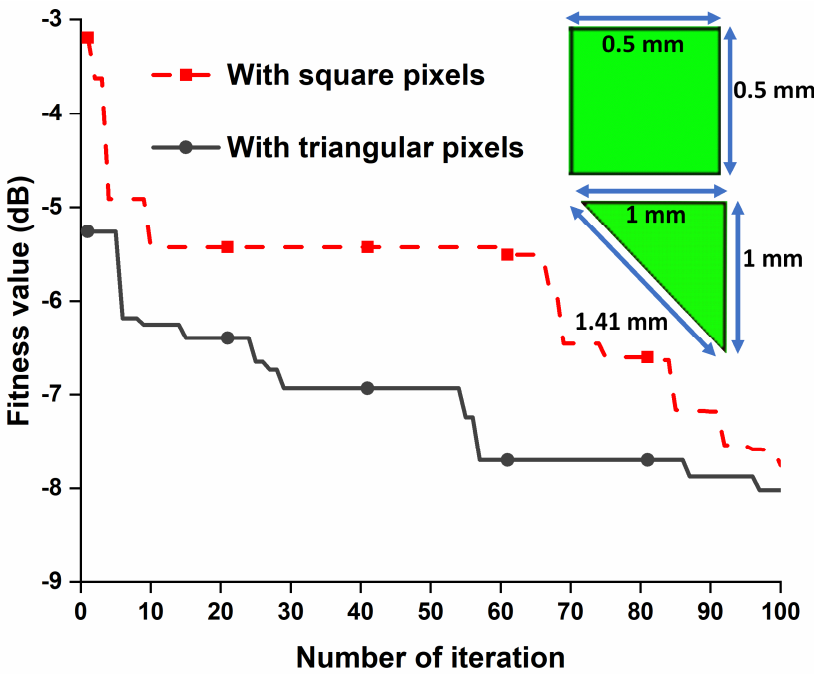

(a)

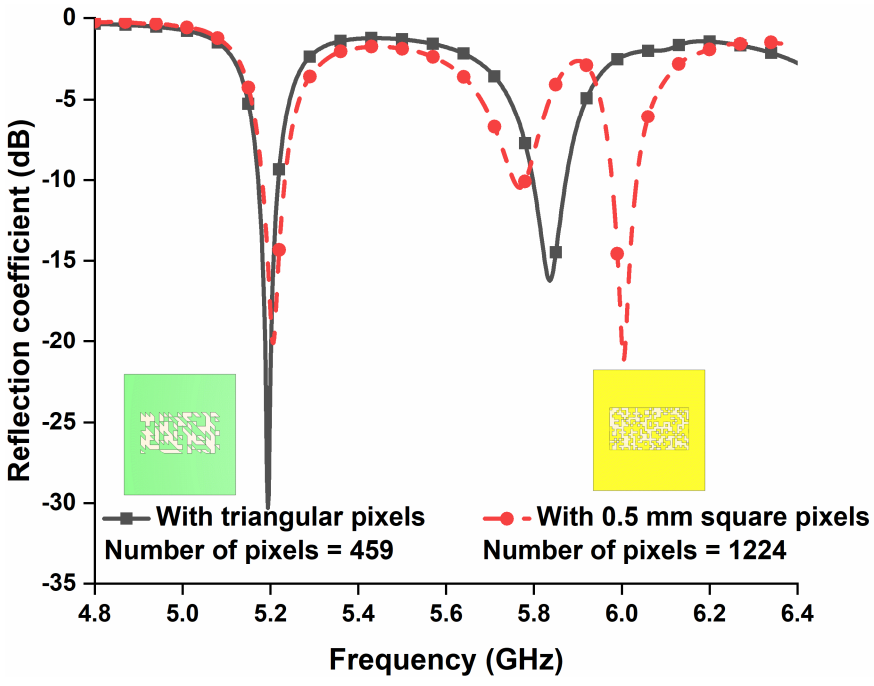

(b)

Figure 4.8 (a) Convergence curve of the antenna for different design topology (b) reflection coefficient of the antenna with different number of pixels.

The results illustrated in Figure 4.8(a) and Figure 4.8(b) clearly indicate that, significantly

increased number of pixels on the antenna design space is more likely to result in unsatisfactory performance from both the algorithm and antenna under optimization perspectives. This poor performance is related to incomparable number of particles with the dimension of solution or search space. The solution space for pixelated antenna with 1224 pixels is too large for the optimizer using 20 particles. Moreover, if the number of particles is increased, a substantial number of iterations is required for the particles to converge, resulting into a significant rise in computational cost [295, 327]. Table 4.3 provides a detailed comparison between the two optimization methods. Further, Figure 4.8(a) and Figure 4.8(b) demonstrate the effectiveness of the proposed design method using the combination of triangular and square pixels, to avoid utilization of increased number of small pixels in the pixelated antenna design. This method provides a balance among algorithm parameters, antenna performance and computational cost, leading to a satisfactory outcome.

Table 4.3 Comparison of Optimization Results

Antenna	With square pixels	With triangular and square pixels
Total number of pixels	1224	459
Number of particles	20	20
Number of iterations	100	100
Fitness value	−7.75	−8.0198
Reflection coefficient	−20 dB @ 5.20 GHz and −10.42 @ 5.76 GHz	−30.24 dB @ 5.196 GHz and −16.29 @ 5.83 GHz
Average simulation time in each function evaluation	95.9 Seconds	69.93 Seconds
Total optimization time	53.33 Hours	38.47 Hours

Table 4.4 illustrates the antenna simulation results from 20 independent runs using the proposed design methodology. The results indicate that 17 out of 20 independent runs

achieved the antenna design goal for dual-band operation. The results demonstrate that the proposed methodology of the pixelated stacked antenna design is an effective technique for designing compact, dual-band stacked antennas with excellent optimization success capability. Figure 4.9 depicts the convergence curves of the 20 test runs.

Table 4.4. Simulation results of different independent optimizations

No.	Fitness value (dB)	Reflection coefficient	Obtained performance at dual-band	No.	Fitness value (dB)	Reflection coefficient	Obtained performance at dual-band
Test run 1	−7.90	−15 dB @ 5.19 GHz, −14.39 dB @ 5.78 GHz	Yes	Test run 11	−11.40	−16.17 dB @ 5.25 GHz, −16.62 dB@ 5.79 GHz	Yes
Test run 2	−7.97	−17.8 dB @ 5.26 GHz, −17.32 dB @ 5.75 GHz	Yes	Test run 12	−9.66	−26.21 dB @ 5.19 GHz, −19.46 dB @ 5.82 GHz	Yes
Test run 3	−10.74	−29.21 dB @ 5.23 GHz, −10.22 dB @ 5.86 GHz	Yes	Test run 13	−6.50	−30.55 dB @ 5.78 GHz	No
Test run 4	−9.17	−13.81 dB @ 5.23 GHz, −17.57 dB @ 5.79 GHz	Yes	Test run 14	−10.12	−18.92 dB @ 5.20 GHz, −17.93 dB @ 5.79 GHz	Yes
Test run 5	−7.1205	−20.4 dB @ 5.75 GHz	No	Test run 15	−9.59	−16.04 dB @ 5.19 GHz, −13.59 dB @ 5.78 GHz	Yes
Test run 6	−8.0198	−30.24 dB @ 5.19 GHz, −16.29 dB @ 5.83 GHz	Yes	Test run 16	−8.40	−22.20 dB @ 5.20 GHz, −10.24 dB @ 5.86 GHz	Yes
Test run 7	−8.89	−15.56 dB @ 5.19 GHz, −21.51 dB @ 5.78 GHz	Yes	Test run 17	−8.30	−23.37 dB @ 5.19 GHz, −17.57 dB @ 5.80 GHz	Yes
Test run 8	−9.24	−26.5 dB @ 5.23 GHz, −13.3dB @ 5.75 GHz	Yes	Test run 18	−9.47	−16.08 dB @ 5.18 GHz, −25.08 dB @ 5.81 GHz	Yes
Test run 9	−9.57	−13.33 dB @ 5.23 GHz, −10.17 dB @	Yes	Test run 19	−9.74	−20.25 dB @ 5.20 GHz, −15.60 dB @5.78 GHz	Yes

		5.75 GHz					
Test run 10	−7.07	−23.88 dB @ 5.25 GHz, −12.10 dB @ 5.85 GHz	Yes	Test run 20	−6.77	−14.11 dB @ 5.81 GHz	No

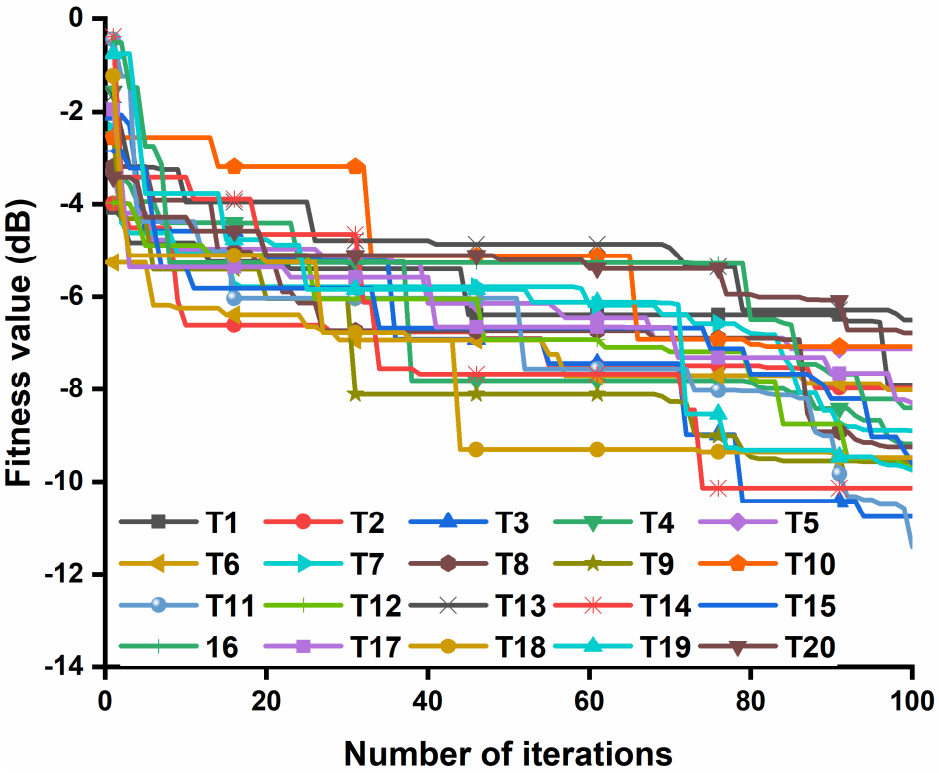

Figure 4.9 Convergence curves of 20 test run. 'T' in figure indicates test run.

Furthermore, to demonstrate the flexibility of the proposed antenna topology for single band and dual band antenna design, the pixelization and optimization of the antenna have been performed to achieve single bands at 5.2 GHz and 5.8 GHz, and dual-band performance at 5.8 GHz and the emerging Wi-Fi 6E bands. The same predefined areas of the antenna have been used to achieve different goals. Three sample antennas (Antenna X, Antenna Y, Antenna Z) have been considered using following cost functions:

$$FF_X = \left(S11_{f_1=5.2\ GHz\ band}\right), \tag{4.12}$$

$$FF_Y = \left(S11_{f_2=5.8GHz\ band}\right), \tag{4.13}$$

$$FF_Z = w_1\left(S11_{f_1=5.8\ GHz\ band}\right) + w_2\left(S11_{f_2=WIFI\ 6E\ band}\right) \tag{4.14}$$

Figure 4.10 and 4.11 clearly demonstrate that the PSA can be used as single band antenna at different bands. Figure 4.12 depicts that the same design with different pixelated configuration can be utilized for dual-band performance at different frequencies.

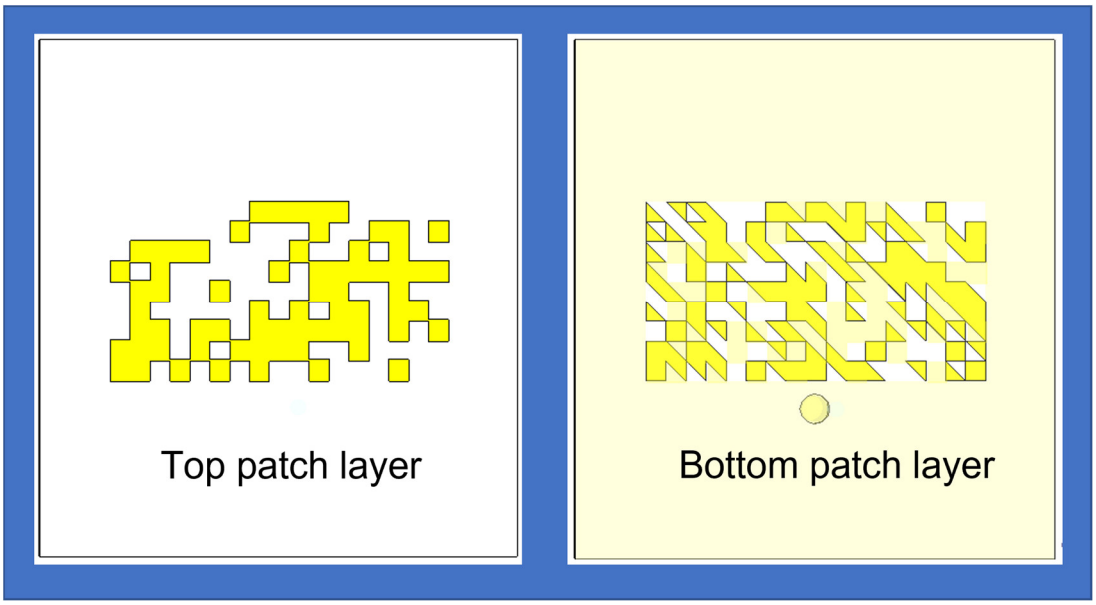

(a)

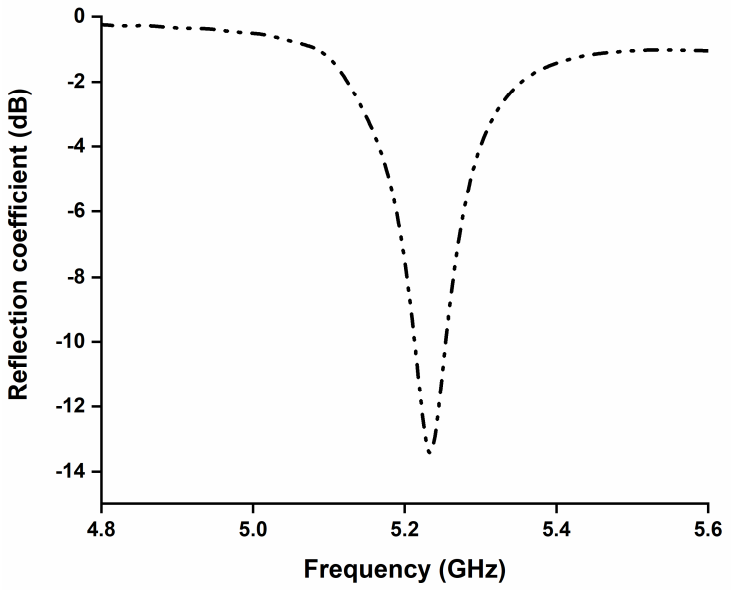

(b)

Figure 4.10 (a) Antenna X configuration, (b) Reflection coefficient of Antenna X at 5.2 GHz band

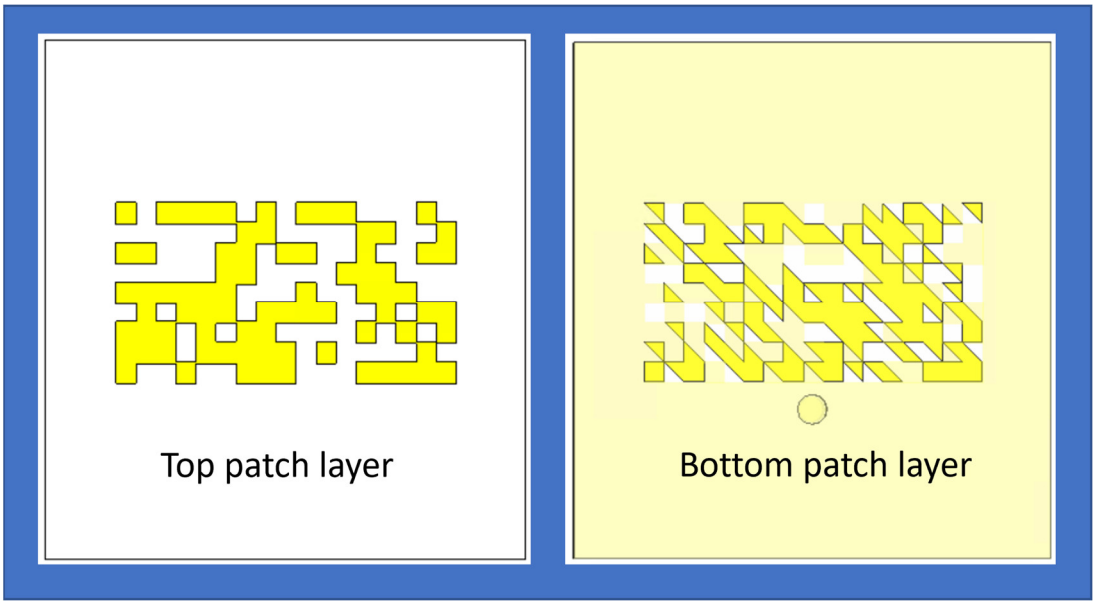

(a)

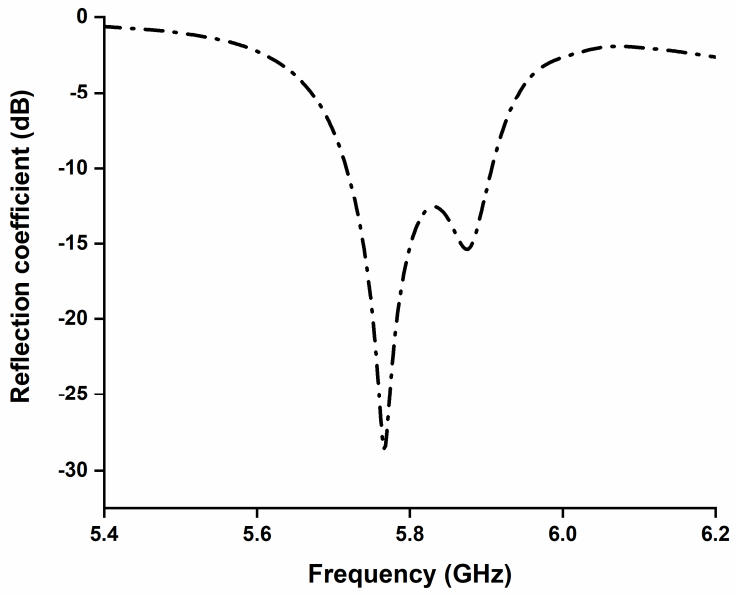

(b)

Figure 4.11 (a) Antenna Y configuration, (b) Reflection coefficient of Antenna Y at 5.8 GHz band

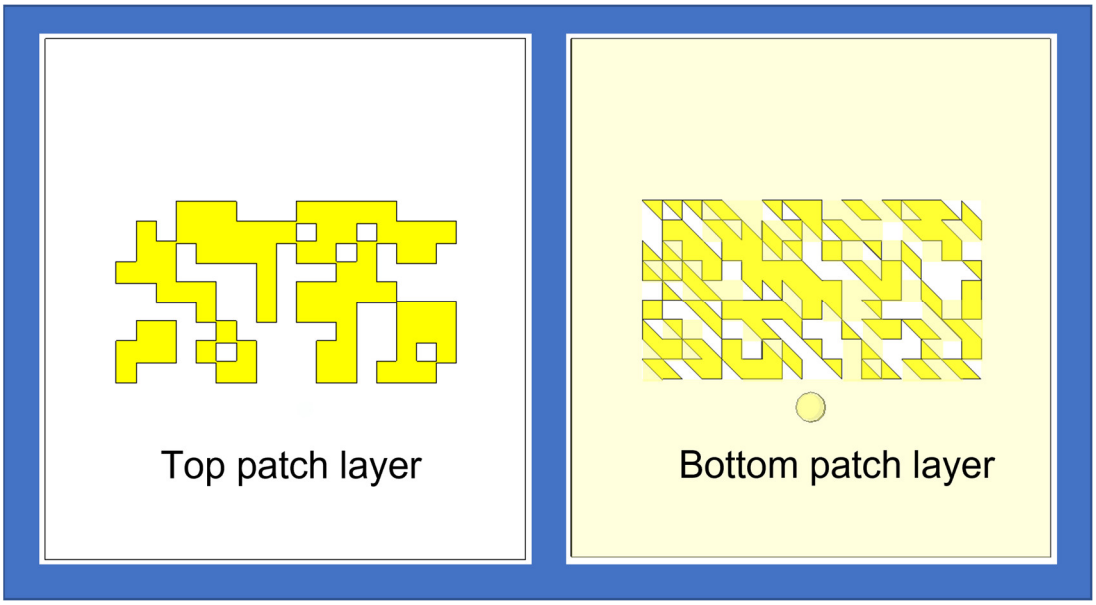

(a)

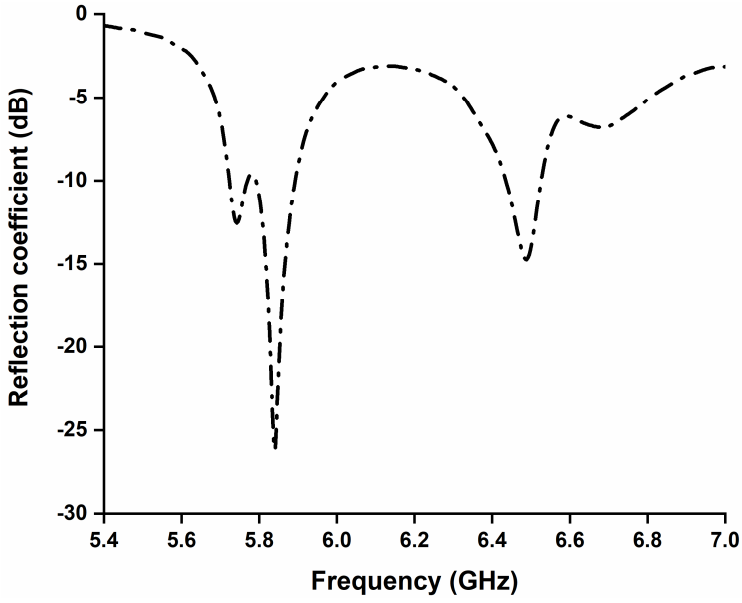

(b)

Figure 4.12 (a) Antenna Z configuration, (b) Reflection coefficient of Antenna Z at 5.8 GHz and WiFi 6E bands

4.3 Results and Discussion

The dual-band antenna prototype shown in Figure 4.13(a) is fabricated in accordance with the design specifications in Table 4.2 and the pixelated layout in Figure 4.3. The

main radiating patch of the antenna is fed by coaxial feeding method using SMA connector. The final pixelated layout on the top and bottom layer is selected based upon the pixelization results of 20 independent runs using BPSO (Table 4.4). The design with the best result (Test run 6) with good reflection coefficient and gain is finalized for fabrication and measurement. Figure 4.13 depicts the fabricated antenna prototype and experimental set-up of the antenna under test (AUT). The reflection coefficient and radiation patterns of the antenna are measured using Rohde and Schwarz ZVA40 vector network analyzer and Rohde and Schwarz HF907 double-ridged waveguide horn antenna. Comparison between the simulated and measured reflection coefficients of the antenna is depicted in Figure 4.14. Based on the measurement results, it is evident that, the proposed antenna satisfies the desired optimization goals, and achieves operation at 5.2 GHz (WLAN) and 5.8 GHz (ISM) bands successfully. At 5.2 and 5.83 GHz, the simulated results are found to be −30 dB and −16.29 dB, respectively, which correlate fairly well with the measured values of −15 dB (at 5.2 GHz) and −17.7 dB (at 5.85 GHz), respectively. The slight difference between the simulated and measured reflection coefficient is due to manufacturing tolerance.

The simulated efficiency of the proposed pixelated stacked antenna is depicted in Figure 4.15. The antenna's efficiency is 70 percent at 5.2 GHz and 82 percent at 5.83 GHz, respectively. The simulated and measured realized gain of the proposed antenna is depicted in Figure 4.16. The PSA achieved 4.7 dBi and 4.4 dBi realized gain at 5.2 and 5.83 GHz in simulation, respectively. Also, the measured gain is 3.82 dB at 5.2 GHz, and 3.46 dB at 5.8 GHz.

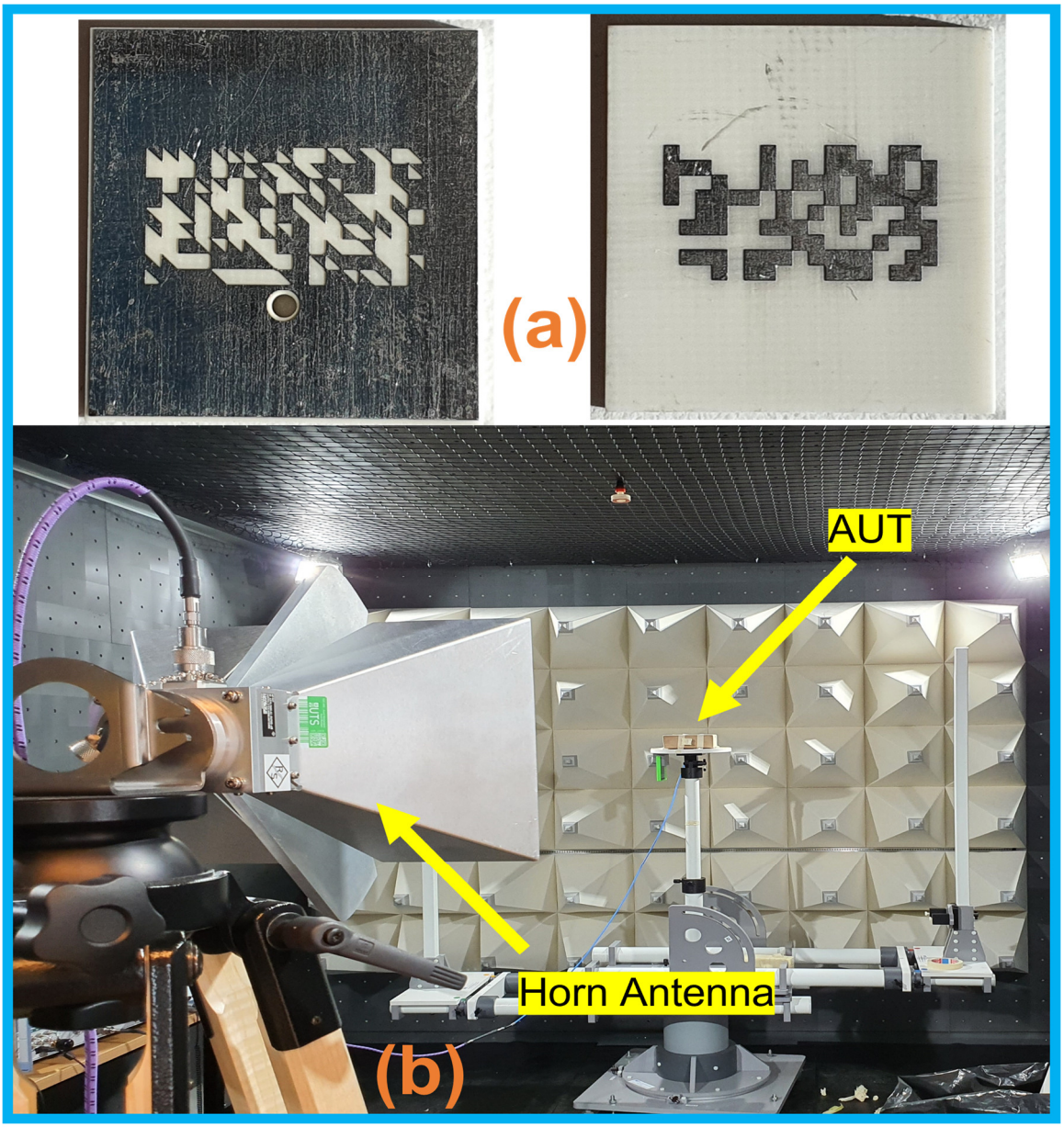

Figure 4.13 (a) Fabricated prototype of the PSA, and (b) measurement setup of the antenna in RF and Communication Technologies (RFCT) Laboratory, UTS.

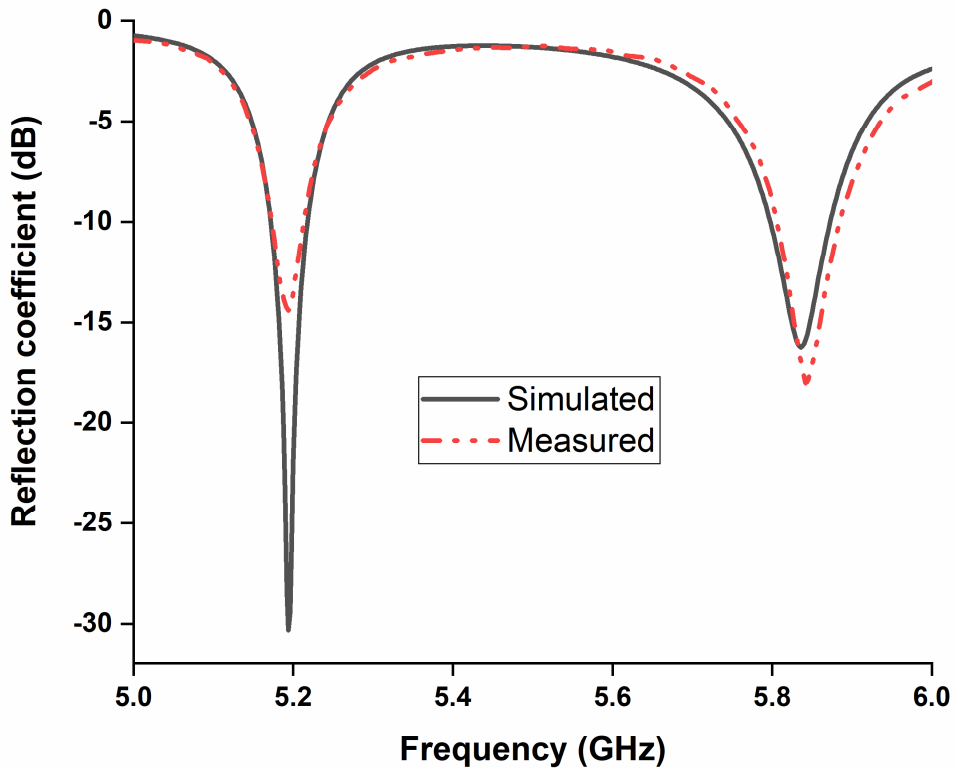

Figure 4.14 Simulated and measured reflection coefficient of the PSA

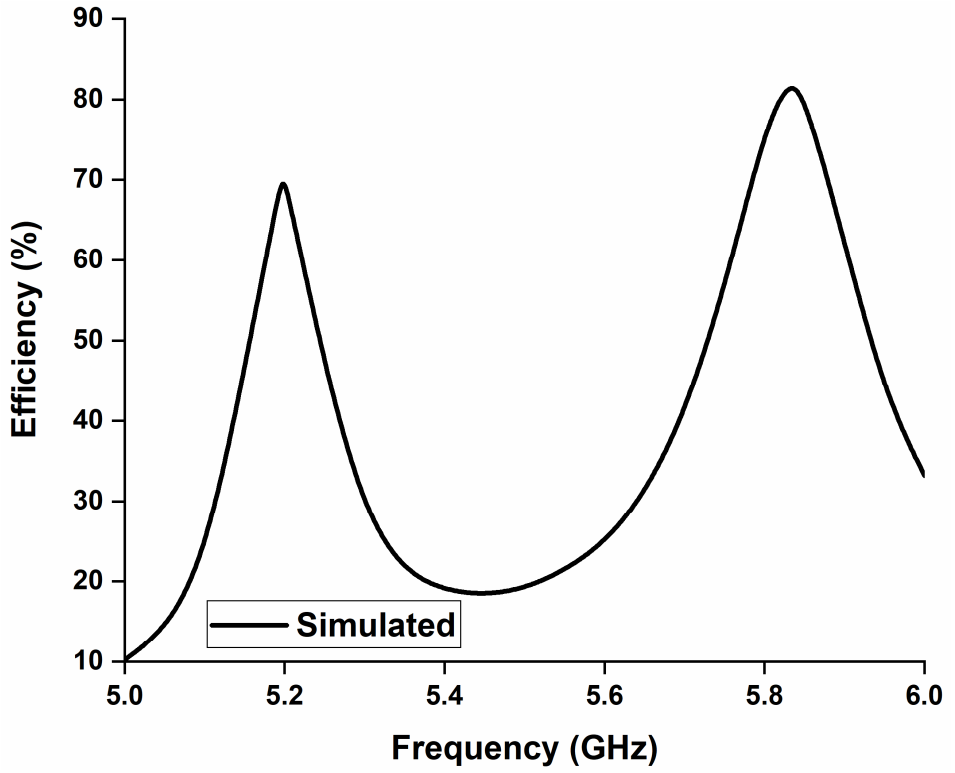

Figure 4.15 Simulated efficiency of the PSA

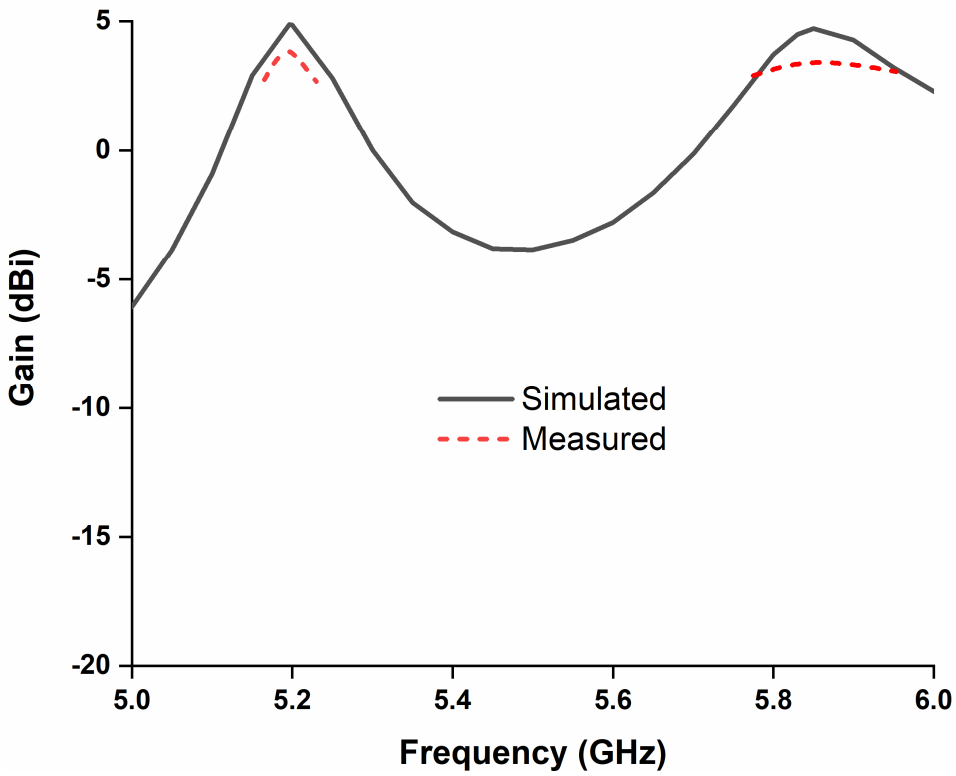

Figure 4.16 Simulated and measured realized gain of the PSA

The simulated surface current distribution at 5.20 GHz and 5.83 GHz are presented in Figure 4.17. Surface current is concentrated mostly around the pixelated areas of the antenna at both frequencies. However, compared with that at 5.83 GHz, the currents on the pixelated patches are stronger at 5.20 GHz, which can be attributed to enhanced impedance matching at 5.20 GHz. In consequence, the obtained gain at the lower frequency band is slightly higher than that of the higher frequency band.

Figure 4.18 shows the simulated and measured far-field radiation patterns in the XZ- and YZ-planes at 5.2 GHz and 5.8 GHz. The radiation patterns of the proposed antenna are stable in both operating frequencies. The antenna exhibits consistent directional radiation patterns at both operating bands. The simulated and measured radiation patterns of the antenna at XZ and YZ plane at both operating bands are in good agreement. At 5.20 GHz, the maximum cross-polarization levels are -0.59 dB in XZ plane and -0.54 dB in YZ

plane. At 5.83 GHz, the maximum cross polarization levels are -1.82 dB in XZ plane and -4.39 dB in YZ plane. The minor discrepancy between the levels of cross polarization in XZ-plane and YZ-plane could be attributed to the asymmetrical position of the feeding coaxial probe and asymmetrical pixelated structure. This level of cross polarization is reasonable as added advantages in many circumstances and has many potential applications, especially in portable devices for communication, wireless energy harvesting and wireless power transfer.

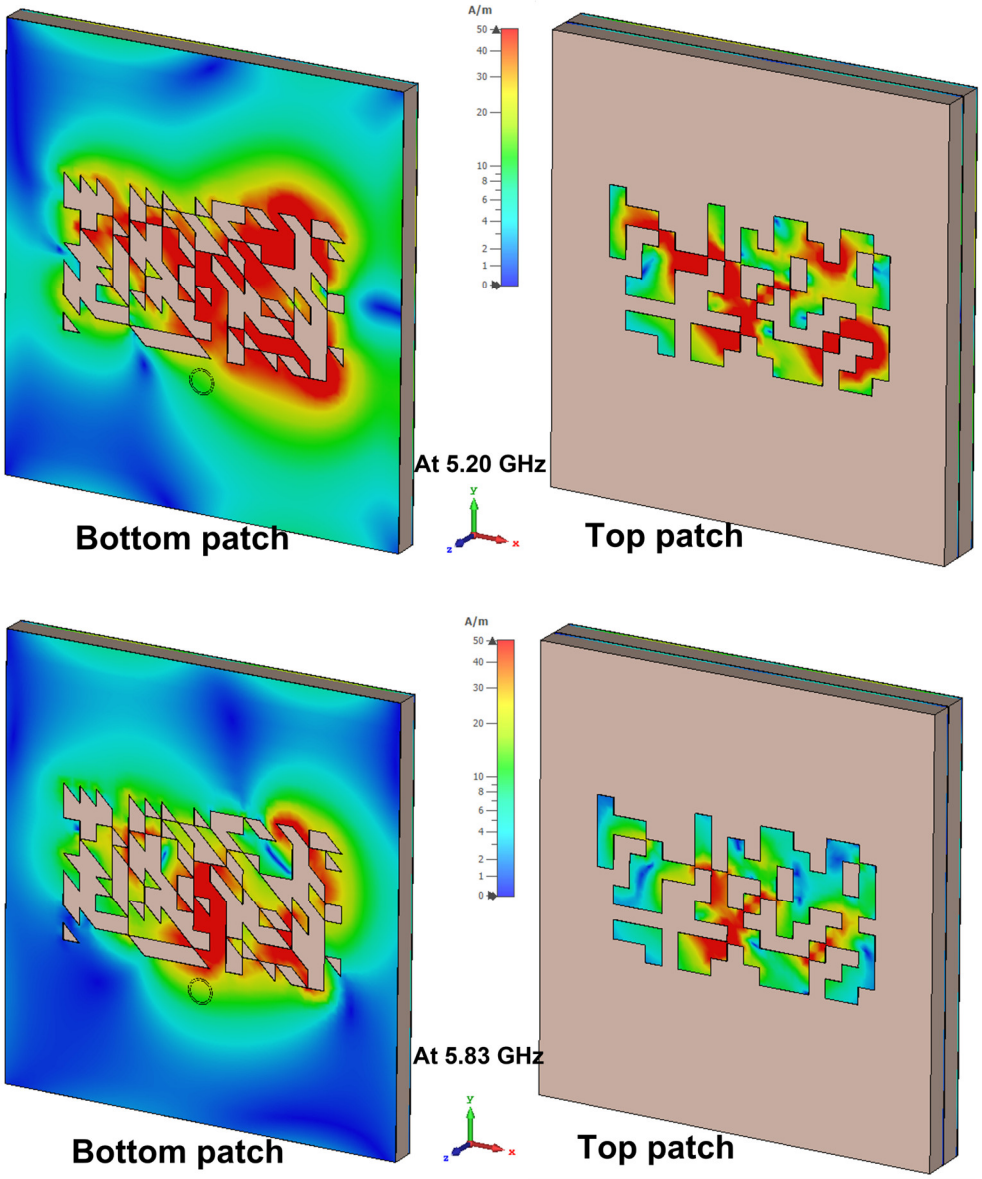

Figure 4.17 Surface current distribution of the proposed antenna at 5.20 GHz and 5.83 GHz

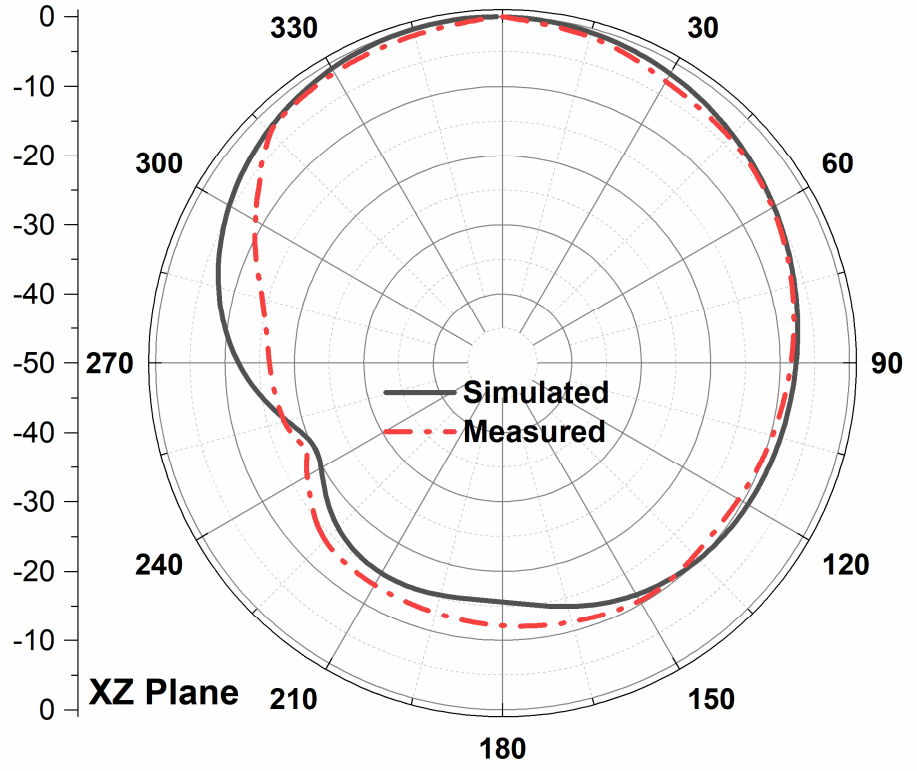
0
-10
-20
-30
-40
-50
-40
-30
-20
-10
0
330
30
300
60
270
90
240
120
210
150
180
Simulated
Measured
XZ Plane

(a)

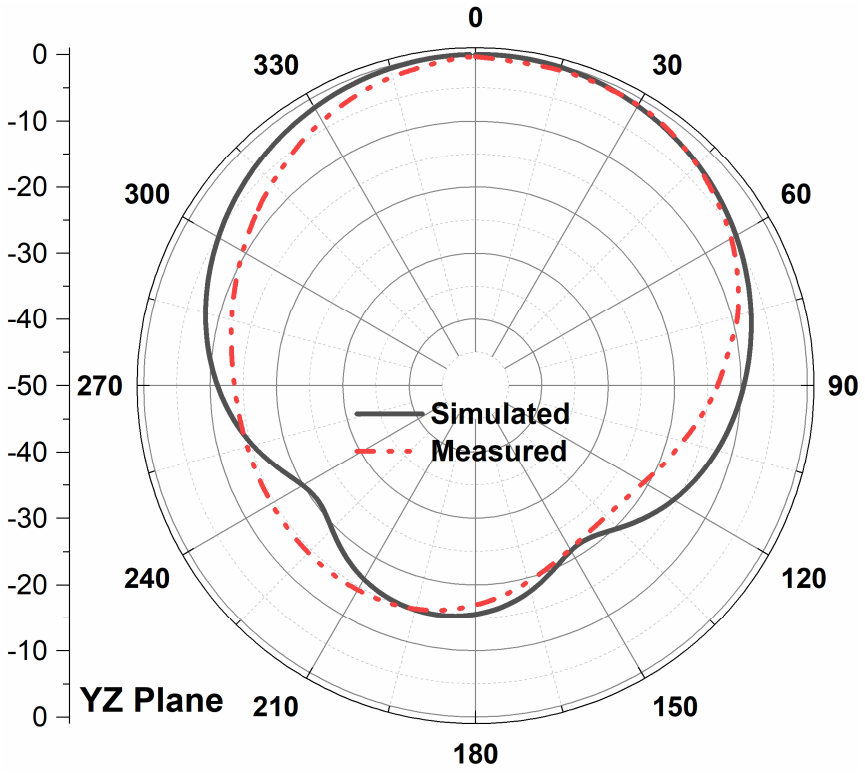
0
0
-10
-20
-30
-40
-50
-40
-30
-20
-10
0
330
30
300
60
270
90
240
120
210
150
180
Simulated
Measured
YZ Plane

(b)

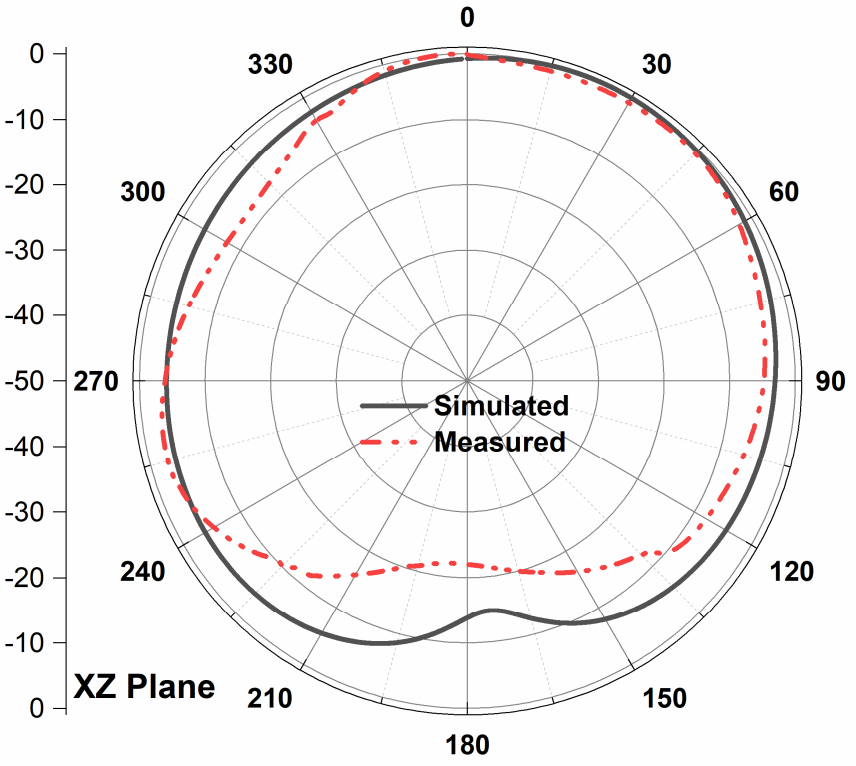
0
30
60
90
120
150
180
210
240
270
300
330
0
-10
-20
-30
-40
-50
-40
-30
-20
-10
0
Simulated
Measured
XZ Plane

(c)

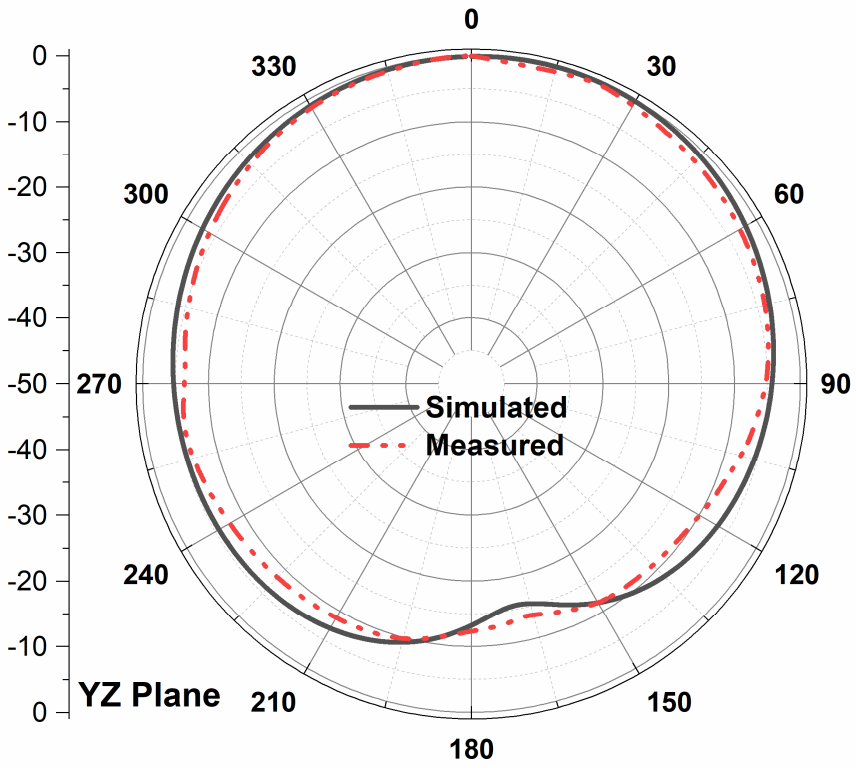
0
30
60
90
120
150
180
210
240
270
300
330
0
-10
-20
-30
-40
-50
-40
-30
-20
-10
0
Simulated
Measured
YZ Plane

(d)

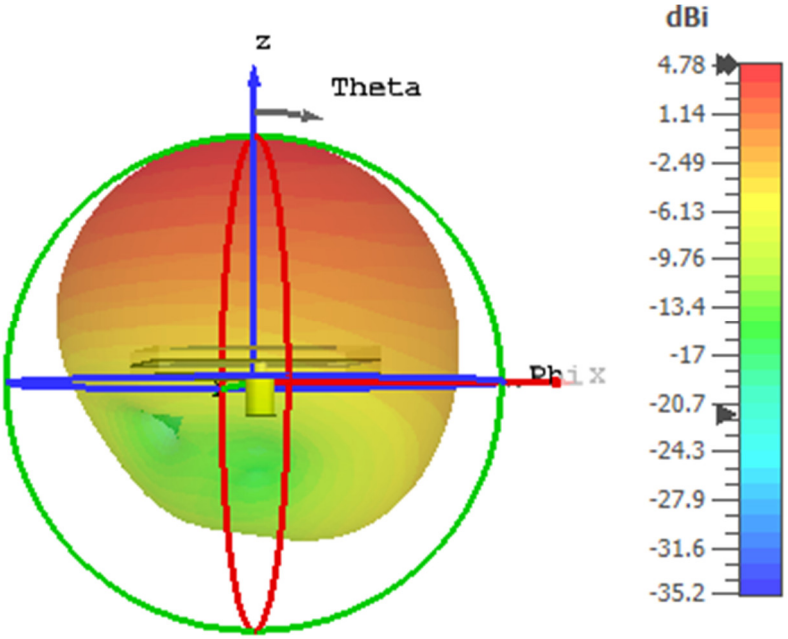

(e)

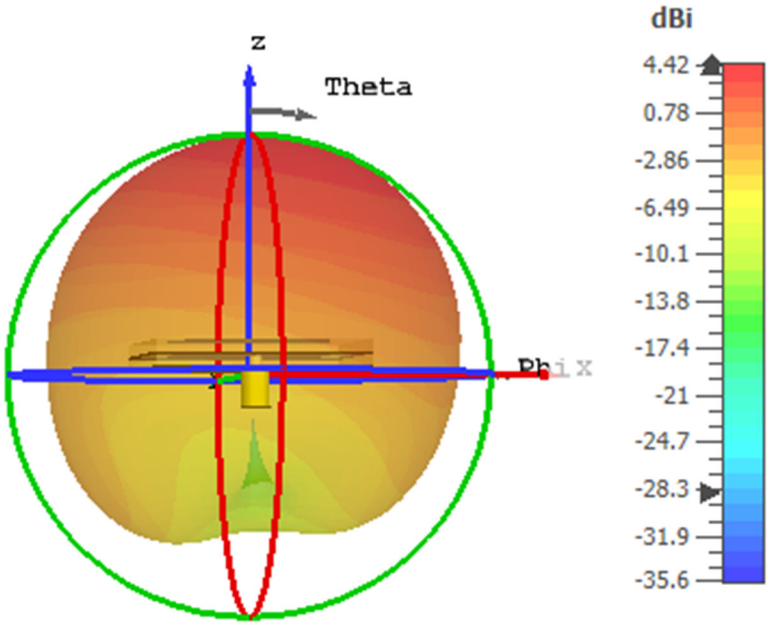

(f)

Figure 4.18 Radiation patterns of the proposed antenna (a) 5.2 GHz XZ plane, (b) 5.2 GHz YZ plane, (c) 5.8 GHz XZ plane, (d) 5.8 GHz XZ plane, (e) simulated 3D radiation pattern at 5.2 GHz, (f) simulated 3D radiation pattern at 5.8 GHz

Table 4.5 compares our proposed antenna design methodology with previously published antennas. It can be noted that most of the antennas are designed by traditional design approach using commercially available EM simulator. On the contrary, the proposed antenna design is achieved by intelligent EM simulation assisted with V-shaped BPSO,

employing both triangular and square pixelated radiating patch. The innovative concept is to use an initial design area that will produce the desired results, while exploring the radiating structure with two different pixelated shapes simultaneously. The proposed approach achieves dual-band performance comparable to other antennas, while being simpler to construct within comparatively smaller size than the other antenna topologies. The antenna design exhibits characteristics nearly equivalent to larger and heavier alternatives that are often more challenging to develop and implement in practical scenarios.

Table 4.5. Comparison of the proposed pixelated stacked antenna with other reported antennas in literature for different wireless applications

Refs.	Antenna type	Design simulation method	No. of Bands	Operating frequency	Gain (dBi)	Antenna Efficiency	Overall Size	Height	Planar circuit integrability for small IoT devices/sensors	Antenna design flexibility with preset
[301]	Cavity backed slot	Traditional EM simulation	1	0.915 GHz (0.896-0.958 GHz)	2.4 (Measured)	79%	0.23 λ × 0.23 λ (77mm×77mm)	15mm	Yes. However, large antenna height	No
[50]	Slotted patch	Traditional EM simulation	2	2.4; 5.8 (2.1-2.7 GHz; 5.6-5.9 GHz)	1.48; 3.83 (Simulated)	Not specified	0.352 λ × 0.264 λ (44mm×33mm)	1.6mm	Yes	No
[302]	Folded strip slot	Traditional EM simulation	1	2.45 (2.37-2.47) GHz	Not specified	73%	0.51 λ ×0.40 λ (62mm×50mm)	1 mm	Yes, however large size	No
[222]	Wide slot	Traditional EM simulation	1	5.8 (4.2-6.2 GHz)	6.4 (Measured)	Not specified	0.80 λ × 0.77 λ (41mm×40mm)	0.8mm	Yes	No
[49]	Reconfigurable monopole	Traditional EM simulation	1	5.8 (5.1-5.8 GHz)	4.84(Simulated), 4.48(Measured)	Not specified	1.73 λ × 3.08 λ (90mm×160mm)	0.803mm	Yes. However, large antenna size.	No

[52]	Differentially fed stacked	Traditional EM simulation	3	2, 2.5, 3.5 (1.95-2.05 GHz, 2.45-2.55 GHz; 3.4-3.6 GHz)	7, 5.5, 9.2 (Measured)	85 %, 75%, 72%	1.06 λ × 1.06 λ (160mm× 160mm)	28mm	Larger antenna height with large metal reflector could be an issue	No
[53]	L-prob dual port stacked patch	Traditional EM simulation	3	0.9, 1.8, 2.1 (0.9-0.97GHz; (1.8-2.2 GHz)	8.15, 7.15,8.15 (Measured)	Not specified	0.525 λ × 0.60 λ (175mm× 200mm)	46.2mm	Larger antenna height could be an issue	No
[46]	Reconfigurable microstrip antenna	Traditional EM simulation	1	5.2/5.8 (5.15-5.25 GHz; 5.77-5.87 GHz)	4.3/6.4 (Simulated)	Not specified	0.785 λ (Length 45.2 mm)	.803mm	Yes	No
[328]	Dual layer patch	Traditional EM simulation	1	5.8 (5.75-5.87 GHz)	7 (Measured)	Not specified	0.8 λ × 0.8 λ (40mm×40mm)	1.6mm	Yes	No
[329]	Multilayer-slot	Traditional EM simulation	1	5.8 (5.7-5.88 GHz)	6.84 (Measured)	Not specified	0.425 λ × 0.80 λ (22mm×41.6mm)	7.2mm	Yes	No
[313]	T-shaped patch	Traditional EM simulation	2	2.4, 5.8 (2.4-2.48 GHz; 5.72-5.87 GHz)	3.09, 0.64 (Simulated); 0.56, -1.59	Not specified	0.25 λ × 0.37 λ (30mm×45mm)	3.2mm	Yes	No
[314]	U-slot square patch with circular substrate	Traditional EM simulation	2	2.45, 5.8 (2.39–2.54 GHz; 5.6–6.14 GHz)	1.37, 4.37 (Measured)	Not specified	0.50 λ Diameter (61.6mm)	6.3mm	Large height and dimension	No
This work	Pixelated stacked-patch	Intelligent EM Simulation: Pixelization using triangular and square shaped pixels and BPSO	2	5.2, 5.8 (5.16-5.21 GHz; 5.79-5.86 GHz)	4.7, 4.4 (Simulated), 3.82, 3.46 (Measured)	70%, 82%	0.415 λ × 0.45 λ (24mm×26mm)	3mm	Yes	Yes
*λ is the wavelength of the lowest operating frequency of each antenna										

4.4 Summary

A systematic approach to achieve an optimal design of a pixelated stacked antenna has been presented in this chapter. The antenna design uses pixelization on the two radiating patches to enable simultaneous optimization of multiple layers, resulting in improved optimization balance. The design methodology utilizes a combination of triangular and square pixel shapes to achieve the design goals. Moreover, this method has an advantage in reduction of the solution space for pixelated layout using cost-effective computation, while maintaining the balance between antenna and optimization performance. The proposed method significantly reduces computational cost in the optimizer. Optimum design of the antenna can be achieved by reduced number of cost function evaluations, contributing to decreased computational time. Also, this method depicted an excellent optimization success capability with 17 successful optimizations for dual-band antenna out of 20 test runs. The consistency between simulated and measured dual-band characteristics proves the accuracy of the design methodology. The optimized antenna achieved 4.7 and 4.4 dBi gain at 5.20 GHz and 5.83 GHz with up to 70% and 82% efficiency. The proposed methodology can also be applied to design single or dual-band antennas at different frequencies. The proposed antenna is suitable for communication modules in IoT devices and other wireless systems.

Chapter 5

Multidirectional Cubic Antenna with Enhanced Isolation

5.1 Introduction

The use of wireless technology is ubiquitous in our everyday lives. After a few decades of focusing on the development of wireless systems, there is now increased attention to vehicular communications [330, 331]. Communication between vehicles can be incorporated into a telemetric platform to supply the driver with real-time information. To provide a better user experience, mobile and wireless connectivity in vehicles is gaining increasing interest from academia and industry. A wireless local area network (WLAN) system for internet access from any location, as well as vehicle-to-vehicle communication systems for safe driving control could be included in future vehicles. Radio frequency (RF) systems such as Satellite Digital Audio Radio Service (SDARS), Global Positioning System (GPS), Vehicle to-Everything (V2X) communication, cellular communication, and Wireless Local Area Network (WLAN) are increasingly installed in modern automobiles for navigation, communication, and entertainment purposes [330, 332-335].

A vehicle's antenna design is challenged by stringent requirements. Vehicular communication modules require low-profile antennas with multi-standard characteristics, such as good radiation performance with the ability to communicate in multiple directions, enhanced isolation from antenna elements, high gain and high bandwidth. Increased coverage, enhanced robustness to multipath, and resistance to signal interception and interference are some of the benefits that smart antennas offer over

standard antennas. Also, smart antennas have the ability to determine the direction of arrival (DOA) of an incoming signal and adjust the radiation pattern to enhance smart vehicular localization systems [336, 337].

5.1.1 Multidirectional Antenna and Challenges

A multidirectional antenna system is a promising approach to meet the requirements of vehicular technologies. There is a greater chance of improved signal reception if the antenna has more radiators. Because of this feature, the antenna can establish a reliable connection even when the vehicle is in motion. Simple omnidirectional patch antennas can be utilized for this purpose as omnidirectional antennas may receive signals from any direction (both in terms of elevation and azimuth), but their gain is typically quite low [338]. In such a scenario, the receiver may feature a number of antennas oriented in various directions to detect signals in its various polarizations. The quality of the received signal is enhanced by employing appropriate switching/selection or combining strategies.

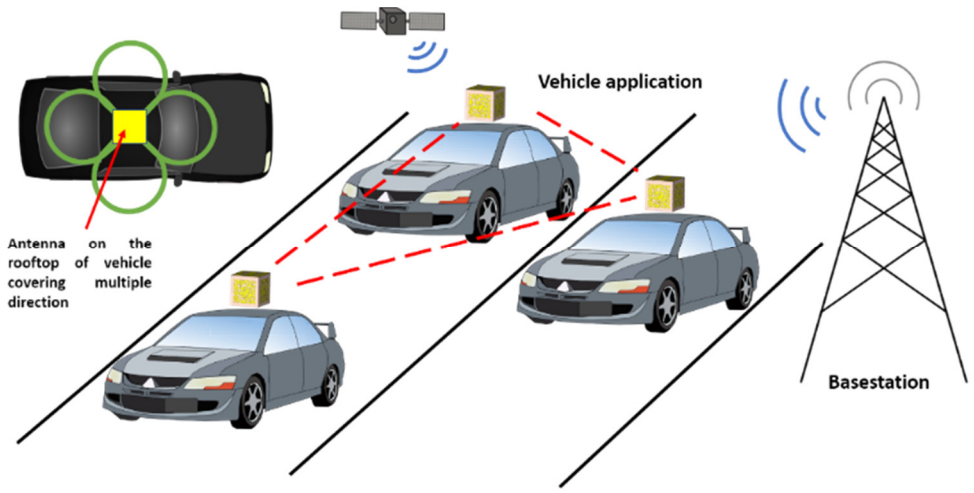

Figure 5.1 Potential vehicular application scenario of the proposed multidirectional antenna in outdoor environment.

In such a scenario, the issue of mutual coupling comes into effect when multiple antenna elements are closely placed together. Antennas should be as far apart as possible from one another to minimize interference from nearby radiators and maintain signal quality. Therefore, the best way to establish a solid connection is through increased isolation [334, 339, 340]. The maximum amount of mutual coupling that closely packed antennas can withstand varies depending on several variables, such as the demands of the particular application, the performance metrics that are wanted, and the antenna's design limitations. However, for many useful antenna system designs, a maximum mutual coupling of about -15 dB is can be generally regarded as acceptable. Different attempts have been made by the antenna research community to improve isolation. The defected ground structure (DGS) is a common technique for reducing mutual coupling [306, 341, 342]. Nevertheless, antenna radiation performance is impacted when the DGS is used as a decoupling element. As a result, improved isolation comes at the expense of radiation performance. Considerable separation between the antenna elements is required to reduce mutual coupling using the split-ring resonators (SRR) [343] and electromagnetic bandgap (EBG) [344] structures [345]. In addition, other mutual coupling reduction techniques for patch antennas include slotted meander-line resonators (SMLR) [346], metamaterial structures [347] and parasitic elements [348] between antennas. However, such methods involve utilization of extra space within the antenna structure, as they are mostly used as separate elements or resonators to suppress mutual coupling. In addition to increasing the antenna size, they may affect the antenna performance.

5.1.2 Advantages of Multidirectional Antenna System

As seen in Figure 5.1, multidirectional antenna systems can facilitate real-time, traffic-based adjustment of the coverage area. High-efficiency and energy-saving

communication is therefore possible. Vehicle antennas should be able to communicate in multiple directions to provide communication dependability between the vehicle and other wireless infrastructure, particularly in the case of long-distance, wide-area coverage, and high-speed data transmission.

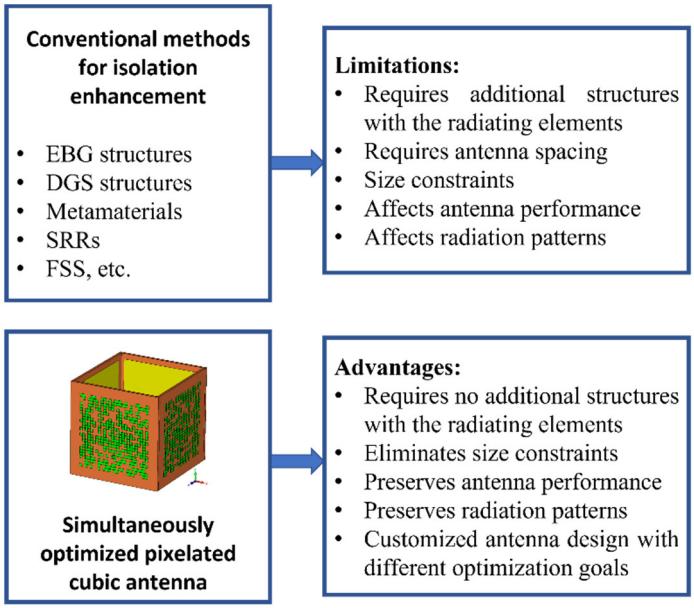

Figure 5.2 Overview of the proposed antenna method: advantages over traditional design technique to enhance isolation.

In this chapter, we propose a multidirectional cubic shaped antenna system with enhanced isolation and high gain. The structure consists of four antennas with pixelated configurations on the patches. The antenna design is based on binary optimization of the radiating patches while focusing on two design goals of reflection coefficient at the desired frequency (5.4 GHz) and isolation improvement. This work suggests combining polarization diversity measures to simultaneously take advantage of omnidirectional patterns with high gain. To increase the possibility of capturing wireless signals, multiple directional antennas are arranged in the cubic structure configuration. The antenna is designed using a binary optimization algorithm with pixelization of the radiating patches.

No extra resonator or parasitic element is placed between the antennas, leading to a compact antenna profile, while maintaining desired performance with increased isolation. Moreover, an edge-to-edge gap between the radiating elements is not required in this design. Figure 5.2 illustrates the proposed antenna design advantages over conventional methods to enhance isolation. The proposed antenna achieved up to 6.9 dBi realized gain. The measured results demonstrate that the isolation between the antennas is better than 34 dB. The overall improvement of 18 dB isolation is achieved in comparison to a standard patch antenna system. Additionally, an E-shaped patch has been placed on top of the cubic structure, which operates at GPS frequency of 1.57 GHz.

5.2 Pixelated Multidirectional Antenna Design

This section outlines the design and optimization of the proposed cubic antenna. The antenna design initially starts with a standard patch antenna technique using simple rectangular radiating patches.

5.2.1 Design Using Standard Patch Antenna

The basic microstrip patch antenna is used to design and analyze the first configuration, in which the maximum lobe of the pattern is perpendicular to the patch. To take advantage of the cubic shape from a geometric point of view, the four microstrip patch antennas were placed in opposite and perpendicular directions. Each antenna is designed to operate at 5.4 GHz on Rogers 4003 substrate. The configuration is depicted in Figure 5.3. In this configuration, each antenna has about 5 dBi realized gain with only 60 degree beamwidth. However, using standard patch antenna design is not suitable for this configuration, as the mutual coupling between antennas is high, as depicted in Figure 5.3. The maximum isolation between antennas achieved in this configuration is only about 18 dB (S21). Also,

the simulated efficiency is around 55% in cubic configuration. Nevertheless, the efficiency of each antenna is 66.3% with 6.6 dBi of realized gain, when each patch antenna is simulated separately. A key challenge in multi-antenna system is the reduction of mutual coupling between antennas that affects each antenna element's radiation performance. Figure 5.3(b) shows a mutual coupling of about −13 to −18 dB between the antennas. This configuration has degraded efficiency and radiation performance.

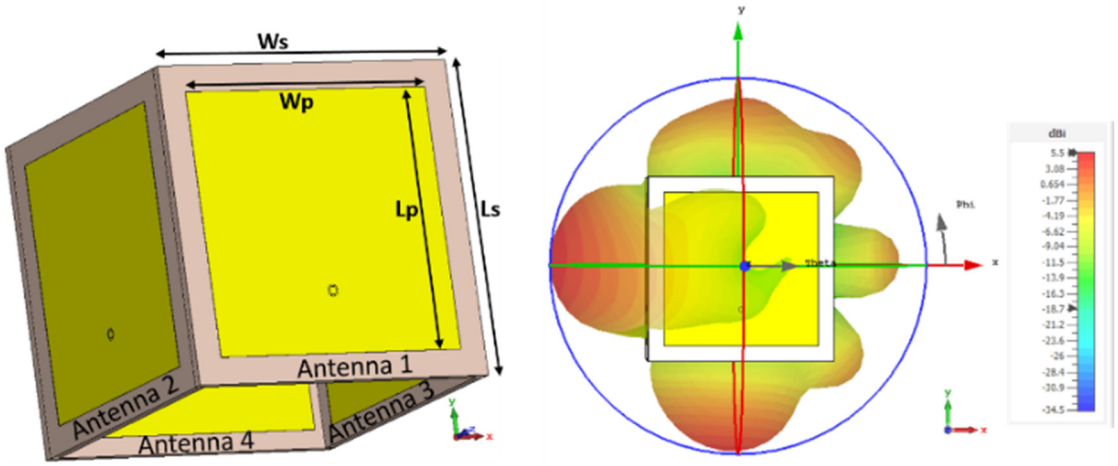

(a)

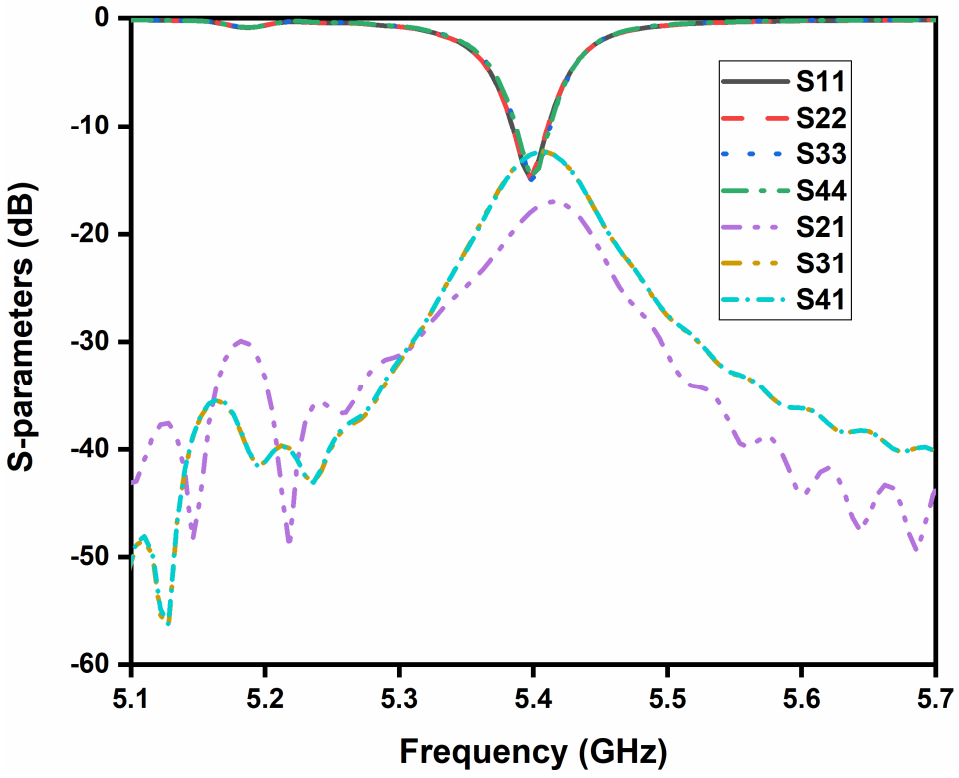

(b)

Figure 5.3 Configuration of four simple patch antennas in a cubic structure and the simulation results; Ws=Ls=50 mm, Wp=Lp=41.6 mm.

5.2.2 Pixelated Cubic Antenna Configuration

To address these challenges, in the proposed antenna design, pixelization technique is used to reduce the mutual coupling effect while maximizing performance of each antenna in the cubic configuration. In this design, pixelization of the four patch antennas is performed simultaneously to achieve operating frequency at the desired band with high isolation. Unlike any previously reported methods, our design approach is based on patch shape optimization without placing any decoupling resonator. This also results in shrinking the antenna profile because only the defined area of the patch is considered.

Figure 5.4(a) depicts the initial configuration of the proposed antenna. The antenna is designed on Rogers 4003 substrate with dielectric constant of 3.55 and 1.52 mm thickness. Each antenna of the cubic structure is fed by the co-axial feeding technique. The patch as a radiating element is subdivided into 26×26 array of total 676 pixels. The array of pixels occupies 39mm×39mm, smaller than the standard patch size simulated in Figure 5.3. Each pixel size is 1.5mm × 1.5mm. Then each pixel is given a value of 0 or 1, denoting the elimination and presence of the copper layer in each pixel's defined area, respectively. Table 5.1 depicts the initial design dimensions of the antenna. Mirror technique has been employed to avoid using a large number of pixels, as shown in Figure 5.4(b). The same pixel configuration is applied in all antennas during simulation, where all antennas are considered simultaneously for the optimization process. Additionally, patches of antenna 1 and antenna 2 are arranged differently from antenna 3 and antenna 4 to achieve better isolation. The pixel configuration of antennas 3 and 4 is the reverse

(side-by-side) of antennas 1 and 2. The feed point of the patch remains as a conductor during the optimization process to ensure excitation to the patch at all times. The ground plane of the antenna is not continuous. They are kept separated to achieve ease of fabrication.

Table 5.1 Design dimensions of the proposed antenna

Parameters	Value (mm)	Parameters	Value (mm)
Wsp	50	Lsp	50
Wpp	39	Lg	44
Lpp	39	Wg	44

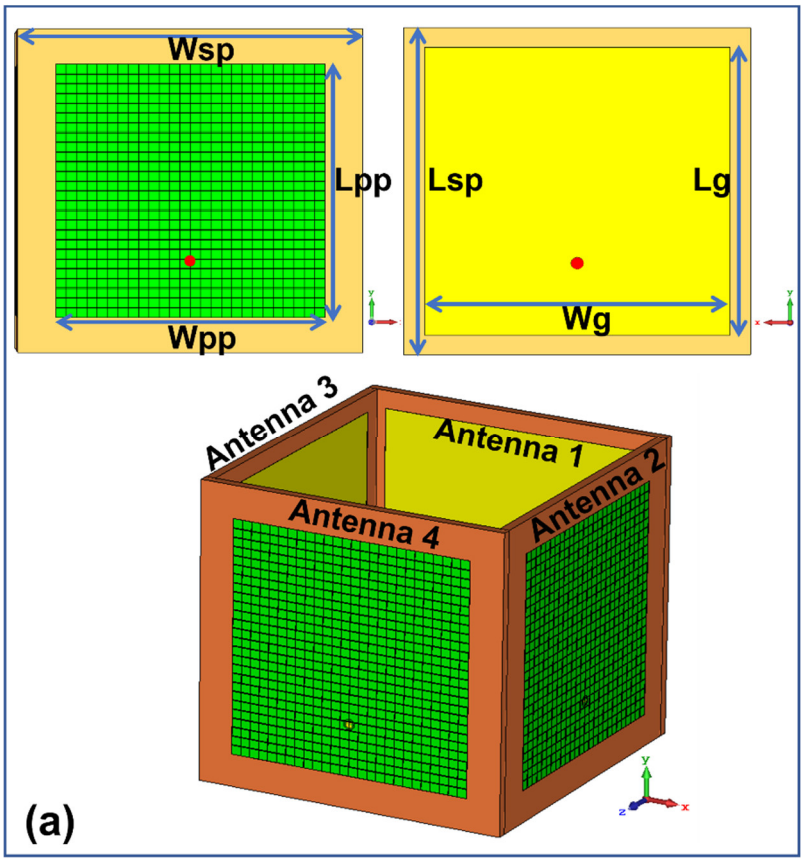

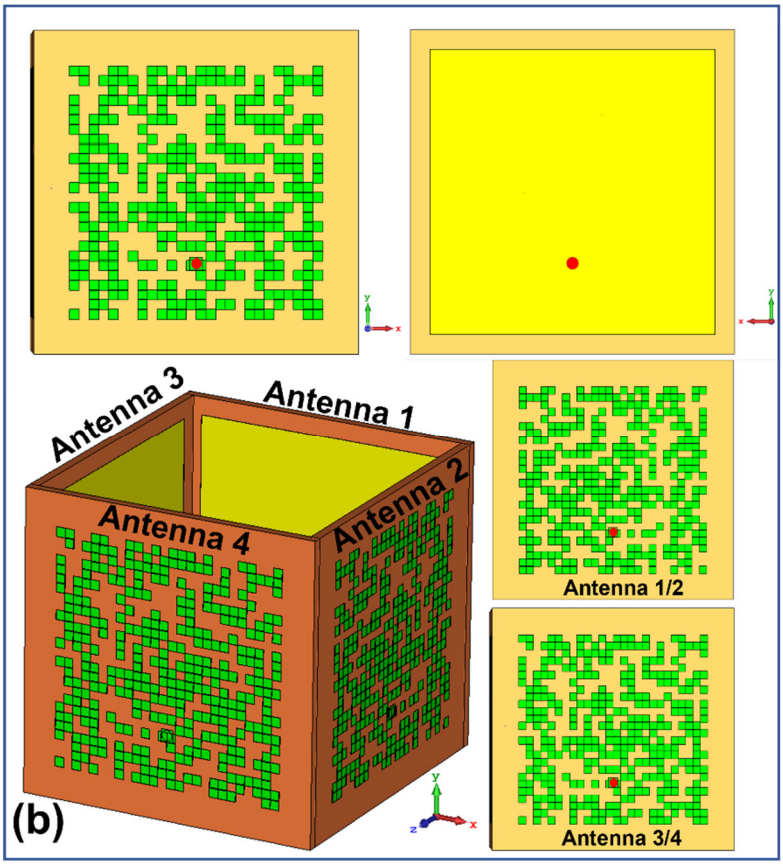

Figure 5.4 Design Configuration and evolution of the proposed antenna (a) pixelization of the structure, (b) optimized pixelated configuration of the antenna.

5.2.3 Optimization of the Antenna

The underlying mechanism of the optimization process is based on the inherent relationship between the pixel configuration and S-parameters of the antenna. Each generated pixel configuration introduces mini slots on the antenna patch. Slots on the radiation patch can significantly alter the antenna's performance due to variations in the surface current path. The pixelization process of the patches is performed using a binary particle swarm optimization (PSO) algorithm with V-shaped transfer function (VBPSO) [71]. The configuration of pixel positions is optimized by the VBPSO. The following equations alter the particle's position and velocity in accordance with its prior position and velocity.

$$v_i^{t+1} = wv_i^t + c_1 \times rand \times (pbest_i - x_i^t) + c_2 \times rand \times (gbest - x_i^t) \quad (5.1)$$

$$x_i^{t+1} = x_i^t + v_i^{t+1} \quad (5.2)$$

Where, the velocity and position of particle i at iteration t is defined by v^t_i and x^t_i respectively. c_1 and c_2 denote the acceleration coefficient, and w represents a weighting function. A random number between 0 and 1 is shown by *rand*. Based on equations (5.1) and (5.2), the PSO algorithm only deals with continuous search spaces. However, new optimization challenges arise when dealing with discrete binary search spaces. Hence, a binary algorithm is required to solve these problems as required in the automated pixelated antenna design methodology. Two distinct components distinguish the continuous and binary versions of PSO; a new position updating method and a new transfer function to transform a continuous search space into a binary search space. The following V-shaped transfer function in Equation (5.3) is adopted for the BPSO in the proposed antenna design to avoid local minima and premature convergence [71].

$$T(x) = \left|(x)/\sqrt{1+x^2}\right| \quad (5.3)$$

$$x_i^k(t+1) = \begin{cases} \left(x_i^k(t)\right)^{-1} & \text{If rand } < T\left(v_i^k(t+1)\right) \\ x_i^k(t) & \text{If rand } \geq T\left(v_i^k(t+1)\right) \end{cases} \quad (5.4)$$

Using equation (5.3), all real velocities were converted to probability values in the interval of 0 and 1 where, v^k_i is the particle i's velocity at iteration t in dimension k. After converting velocities to probabilities, position vectors can be updated using Equation (5.4). Table 5.2 illustrates the parameters used in the algorithm during optimization.

Table 5.2 Parameters used in the BPSO algorithm

Number of particles in optimization	20
Number of iterations	60
c_1	1.5
c_2	2.5

Two design goals are considered in the proposed antenna design: achieving operation and enhancing isolation at 5.4 GHz frequency band. Nevertheless, the frequency band can also be changed by altering the design goal in cost function. In order to achieve desired performance, the fitness function for the VBPSO optimizer is set by capturing the S parameters from EM simulator following several trials. We set the fitness function as a minimization problem. The reflection coefficient of antenna 1 (S11) is considered in Equation (5.5), where the transmission coefficients (S21, S31, S41) between all antennas are included. The reflection coefficients of all other antennas remain mostly similar due to the same pixel configuration on the patch.

$$FF = w_1\left(S11_{f=5.4\ GHz\ band}\right) + w_2\left(\left(S21 + S31 + S41\right)_{f=5.4GHz\ band}\right) \tag{5.5}$$

The co-simulation is performed using binary optimization algorithm implemented in Matlab along with CST Microwave Studio EM simulator simultaneously. The following are the individual steps that were taken in the simulation and optimization process:

Step 1: Initialize particle positions. Set the number of maximum iterations.

Step 2: Calculate each particle's fitness value in accordance with equation (5.5). A binary bit string with 676 bits is sent to the EM simulator to generate pixel configurations. After simulation, the values of S parameters are sent back to Matlab to calculate the fitness value.

Step 3: Analyze each particle's fitness value. Then, update the personal best and global best position of particles.

Step 4: Velocity value is calculated and updated according to Equation (1). The position of particles is updated in accordance with Equations (5.2) and (5.3).

Step 5: Check the number of iterations. If the current number of iterations is less than the maximum iterations, return to Step 2. If maximum iterations are completed, proceed to Step 6.

Step 6: Save global best score and best position. The best position of particles provides the optimum pixel configuration of the antenna.

It takes up to 41 hours to complete the optimization procedure. However, a significant amount of simulation time is taken by the EM simulator to generate pixel configurations and simulate the cubic antenna structure. A small amount of time is required by Matlab for implementing the algorithm. The fitness function used in Equation (5.5) resulted in efficient antenna optimization. Figure 5.5 depicts the convergence curve of the optimization. As can be seen, the VBPSO algorithm converged at iteration 43. The fitness value decreased to a minimum value of -13.014 when the maximum number of iterations is completed.

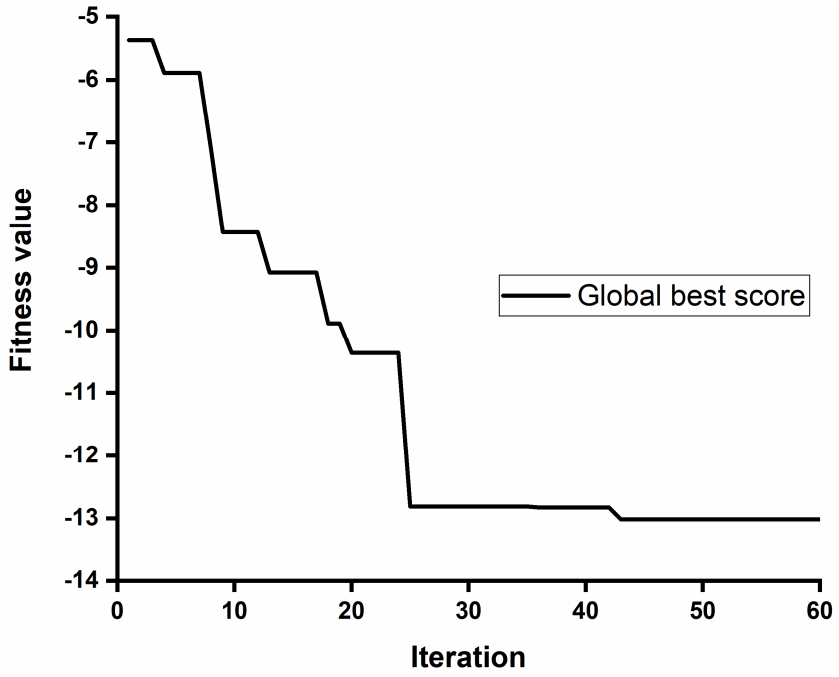

Fig 5.5. Convergence curve of the optimization.

5.2.4 E-Shape GPS Antenna as an Additional Feature

Additionally, a simple GPS patch antenna is placed on the topside of the cube shaped structure to facilitate the antenna system communication with GPS satellite. A simple E shaped radiating patch has been utilized to achieve an operating frequency of 1.57 GHz for the GPS antenna. The antenna is also designed on a Rogers 4003 substrate with 1.52 mm thickness. Figure 5.6(a) depicts the design configuration of the E-shaped GPS antenna. Figure 5.6(b) presents the position of GPS antenna on the topside of the pixelated optimized antenna. Table 5.3 provides the dimensions of GPS antenna.

Table 5.3. Dimensions of the GPS antenna

Parameters	Dimensions (mm)
Lg	48.75
Wg	46
L1	48.75
L2	38.5
W1	46
W2	8
W3	9

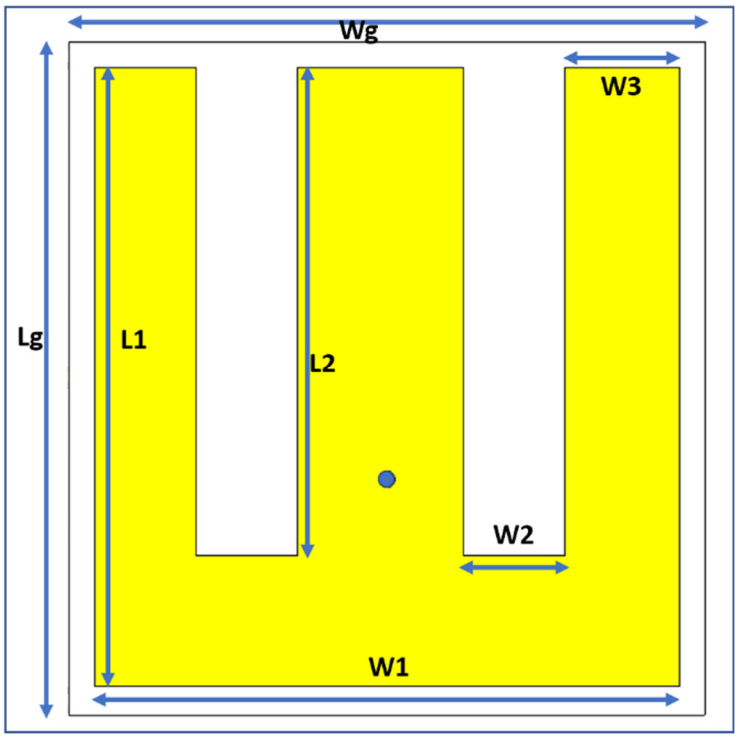

(a)

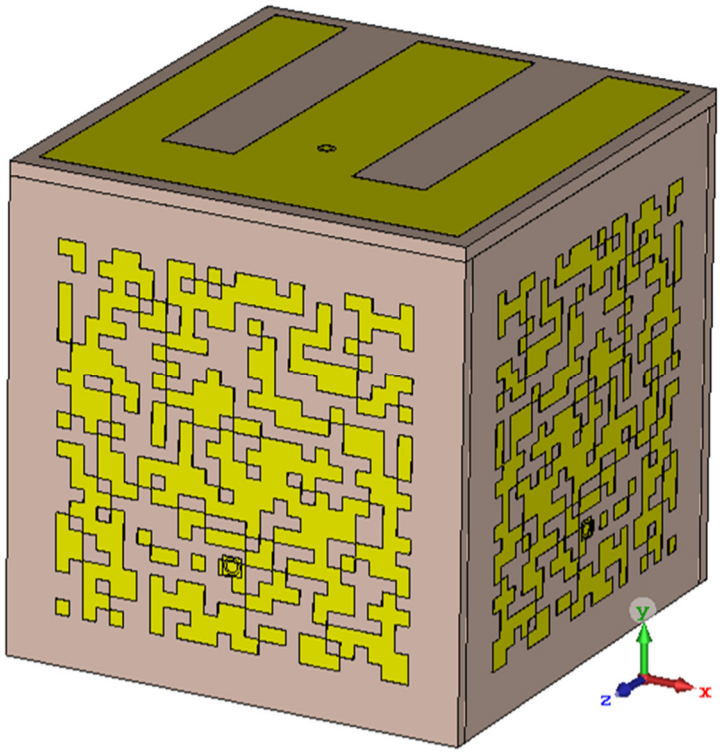

(b)

Figure 5.6 (a) E-shaped GPS antenna (b) placement of the antenna with cubic structure

5.3 Simulated and Measured Results

5.3.1 Results in Free Space

The antenna prototype is fabricated and tested to validate the performance of simulation model. The antenna with optimized pixel configurations has been fabricated on Rogers 4003 substrate and its performance has been measured. Photographs of the fabricated prototype and measurement setup are presented in Figure 5.7. The simulated and measured results of the antennas' reflection coefficient are presented in Figure 5.8. The simulated operating band is from 5.35 GHz to 5.47 GHz. The measured results illustrate that all four antennas resonate at a nearly similar frequency band. They achieved −10 dB impedance bandwidth from 5.33-5.43 GHz. Good agreement between simulations and measurements is observed; nonetheless, a minor disparity is noted which may be attributable to fabrication imperfections.

(a)

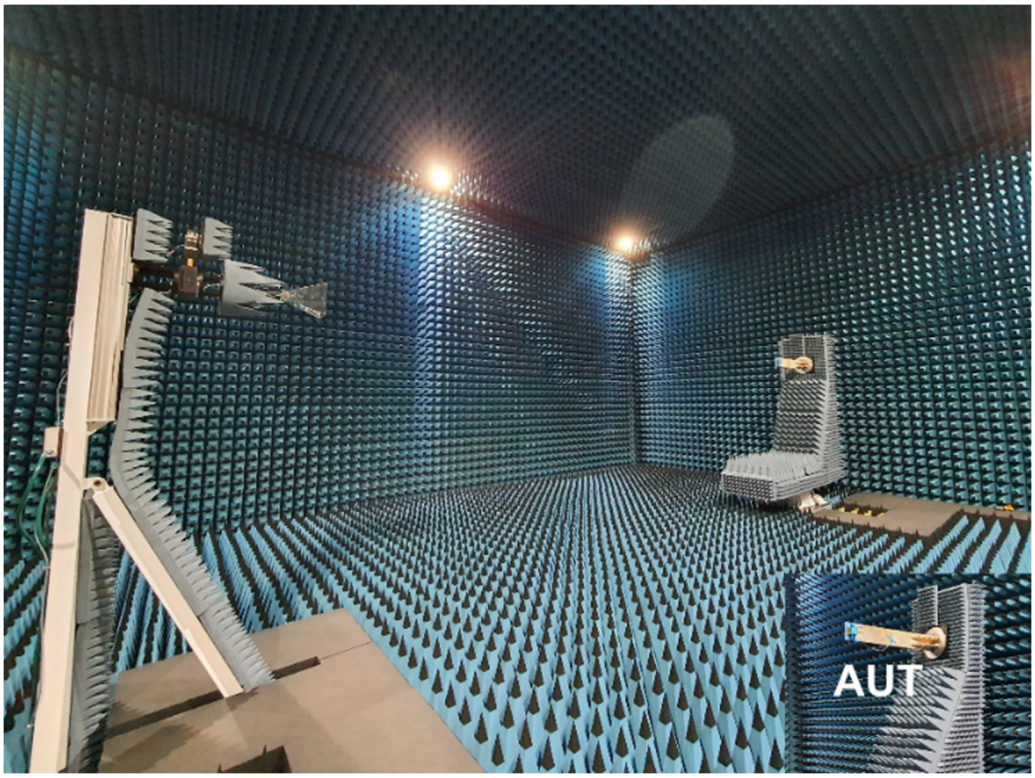

(b)

Figure 5.7 (a) Fabricated prototype of the pixelated multidirectional antenna (b) measurement setup of the antenna under test (AUT) in anechoic chamber

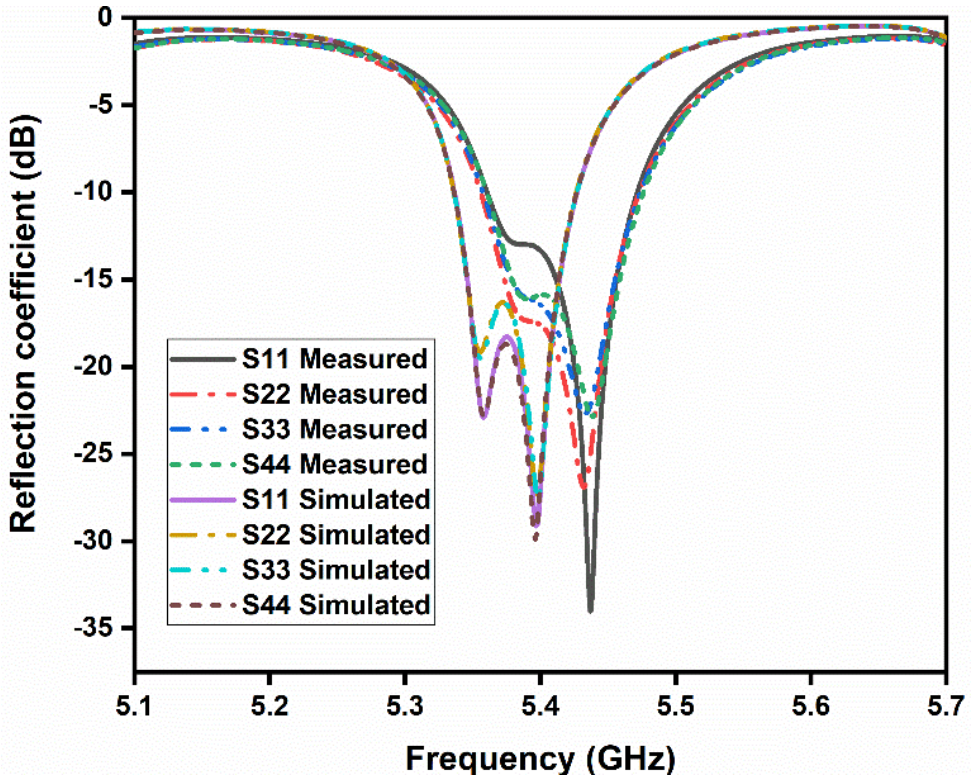

Figure 5.8. Simulated and measured reflection coefficients of the antennas (Antenna 1, Antenna 2, Antenna 3 and Antenna 4)

Enhancing the isolation between antennas is the second design goal of the cubic antenna structure. Figure 5.9 represents the simulated and measured S-parameters of the antennas. The antennas in the cubic structure are tightly packed, leading to large mutual coupling, as depicted in Fig 5.1. Hence, the isolation is enhanced using pixelated patch configuration without any decoupling resonator or components. The isolation value is below 34 dB at 5.4 GHz in simulation, and below 37 dB in measurement results. The maximum achieved isolation is 45 (S31 at 5.4 GHz) dB in simulation, while in measurement the maximum value is 42.5 dB (S31 at 5.43 GHz).

Surface current distribution is plotted in Figure 5.10 to demonstrate the influence of pixelated patch configuration on the antenna elements in the cubic shaped structure. In Figure 5.10 (a), when the antenna 4 is excited, the surface current is coupled from one antenna to another. However, the surface current is suppressed after the patch layout is optimized using pixelated configuration. The induced surface current in the nearby antenna has been significantly reduced and as a result, the isolation between antennas has increased.

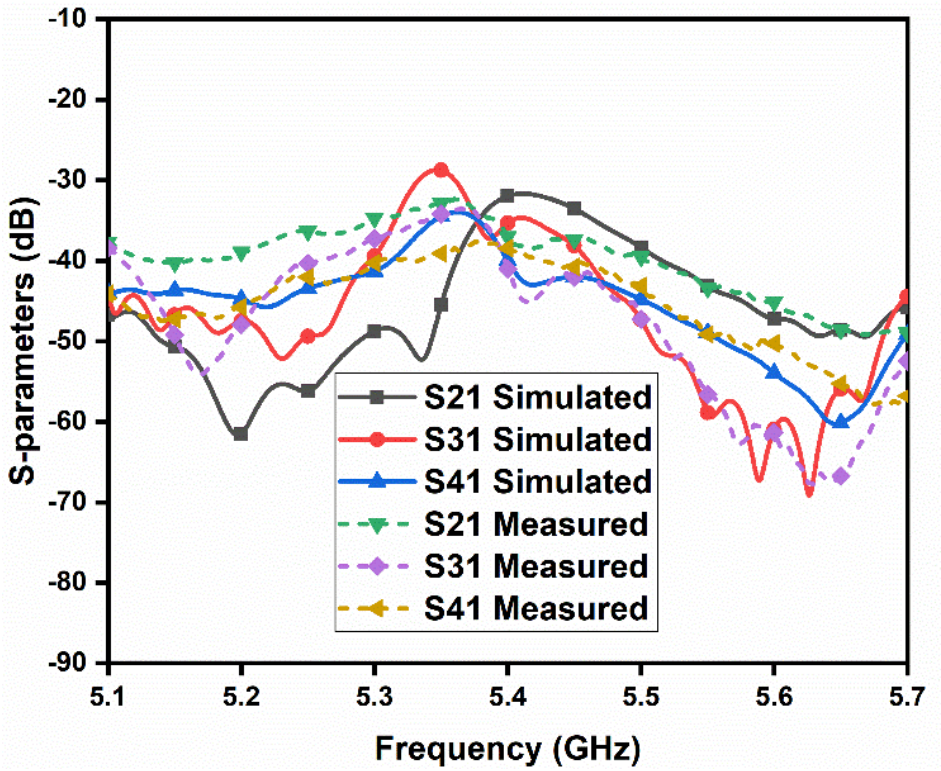

Figure 5.9 Simulated and measured S-parameters of the antennas.

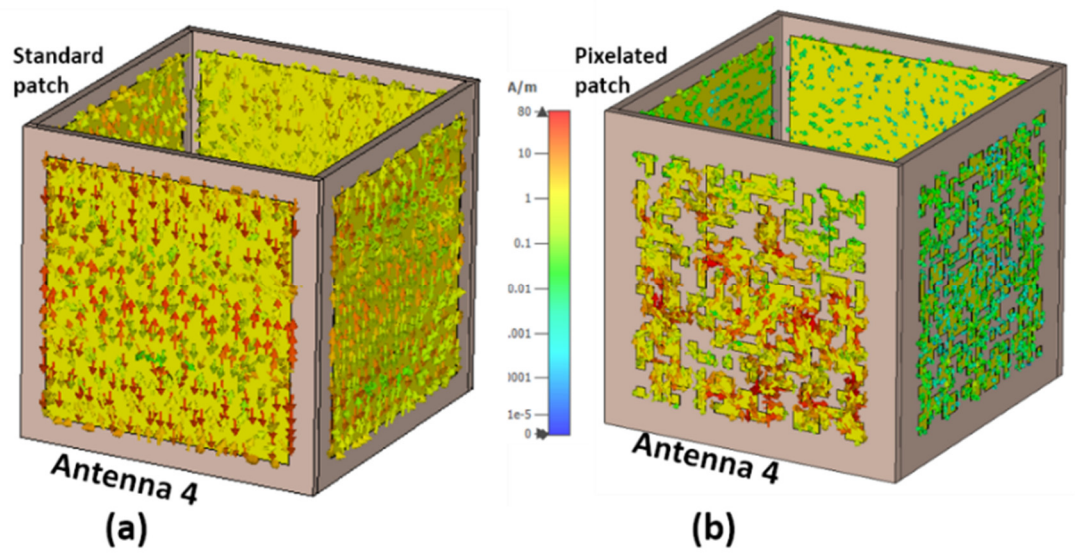

Figure 5.10. Simulated surface current distribution, (a) with standard patch at 5.4 GHz (b) using optimized pixelated patch at 5.4 GHz

Figure 5.11 presents the simulated and measured reflection coefficient of the GPS antenna. The antenna has been simulated and measured considering the placement on top of the four pixelated antennas structure. The measured results correlate well with the simulated results.

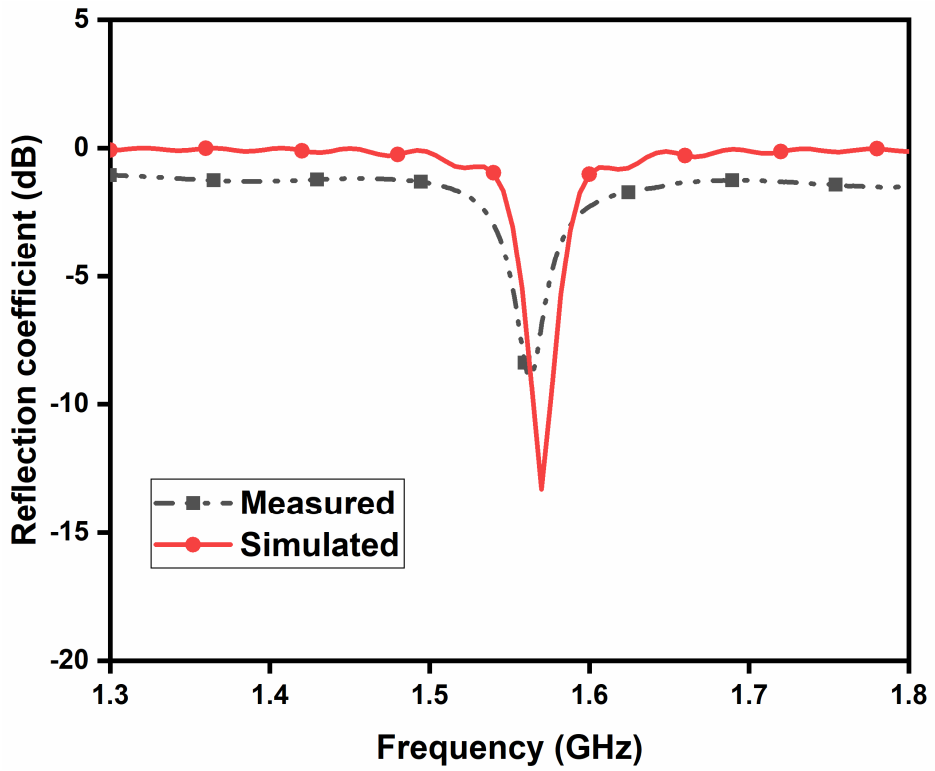

Figure 5.11 Simulated and measured reflection coefficient of the GPS antenna

The simulated and measured H-plane and E-plane radiation patterns of the pixelated cubic antenna are shown in Figure 5.12 and Figure 5.13 respectively. The radiation patterns measurement is performed in the anechoic chamber shown in Figure 5.7. The measured results of radiation patterns coincide well with the simulated results. The combined radiation pattern of four antennas covers all propagation directions in both planes. Moreover, it should be noted that, due to isolation enhancement using pixelated patch

technique, the radiation patterns are not affected. The achieved maximum measured gain is 6.4 dBi, which is close to the simulated realized gain of 6.9 dBi.

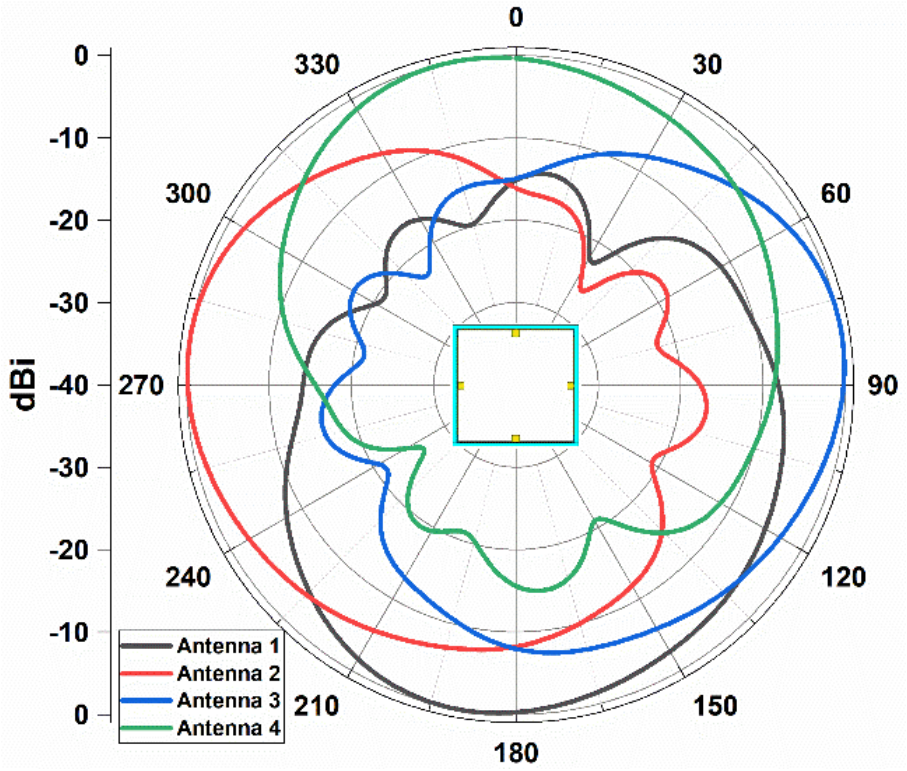

(a) Simulated

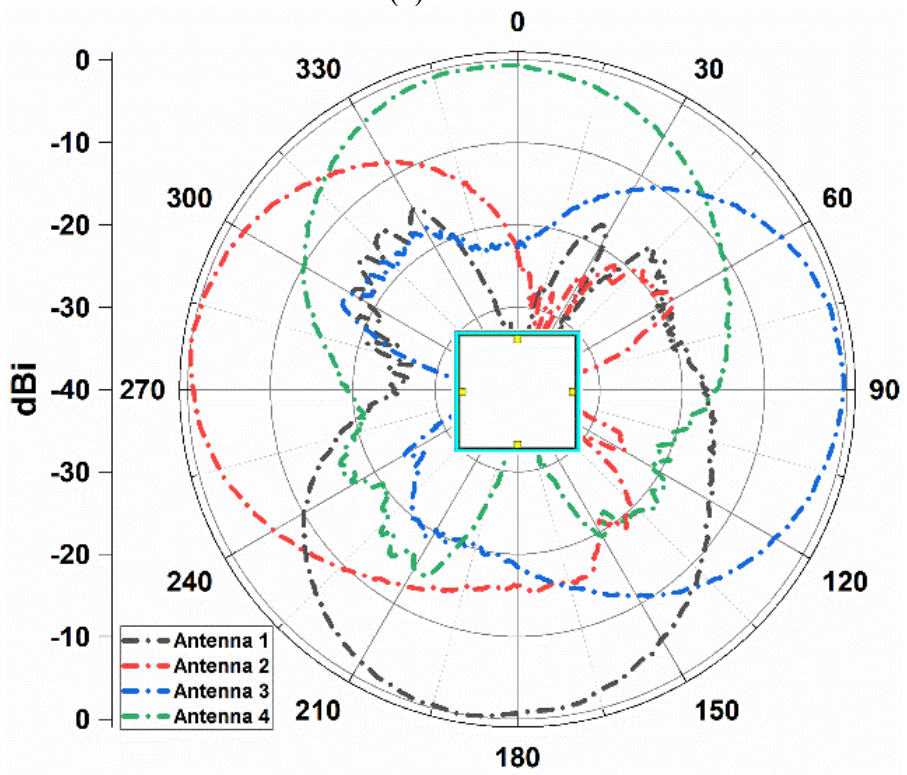

(b) Measured

Figure 5.12 Simulated and measured H-plane radiation patterns of the optimized pixelated antennas.

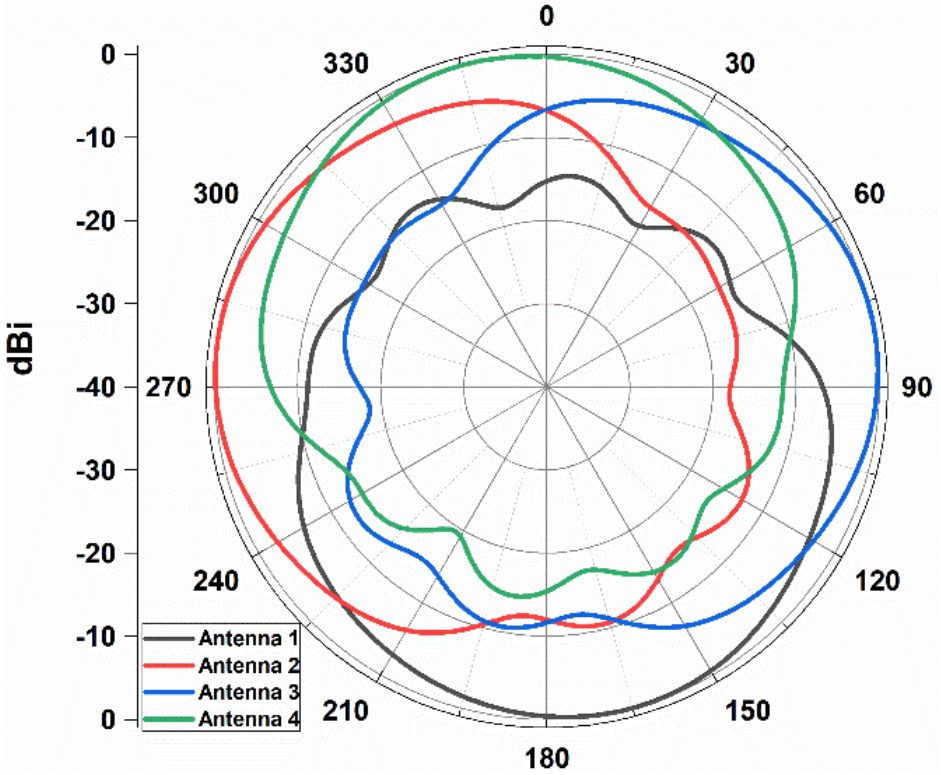

(a) Simulated

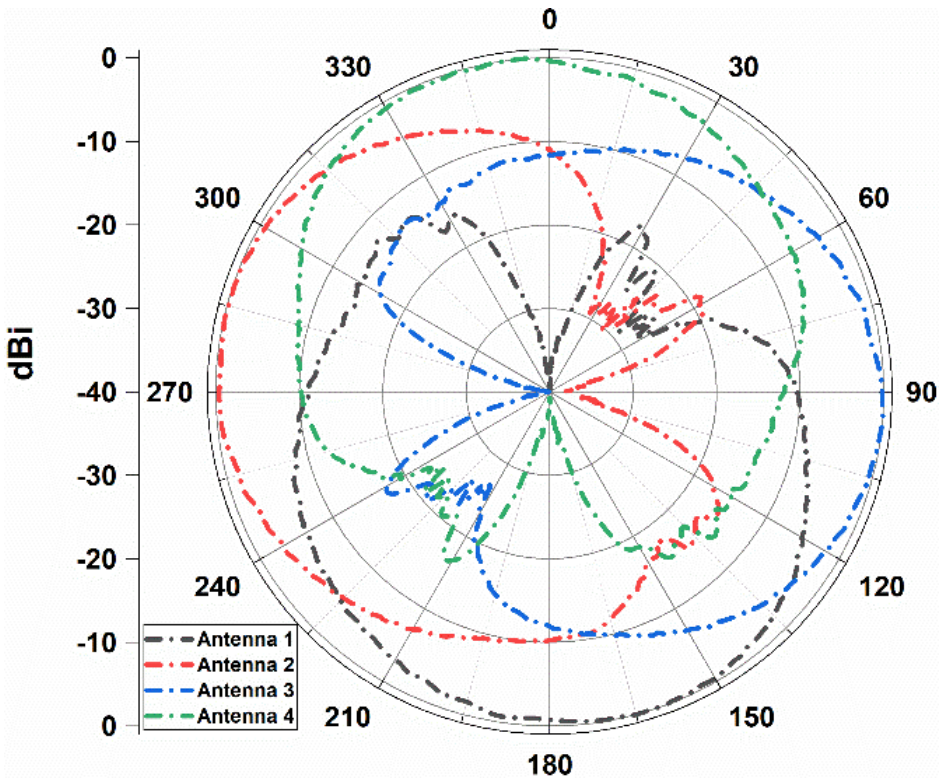

(b) Measured

Figure 5.13 Simulated and measured E-plane radiation patterns of the optimized pixelated antennas

Figure 5.14 represents the simulated and measured H-plane and E-plane radiation pattern of the GPS antenna. The measured realized gain of GPS antenna is 0.9 dBi. Good agreement between the simulated and measured radiation patterns has been observed. The ripples in the measured patterns can be attributed to the presence of a metal plate in the measurement setup in the anechoic chamber.

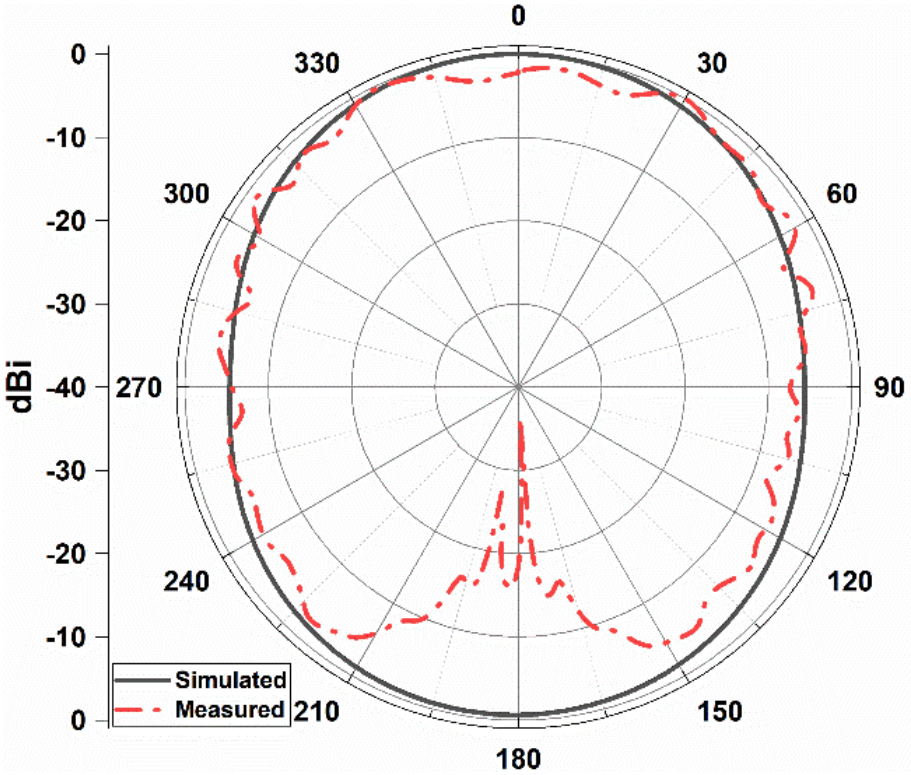

(a)

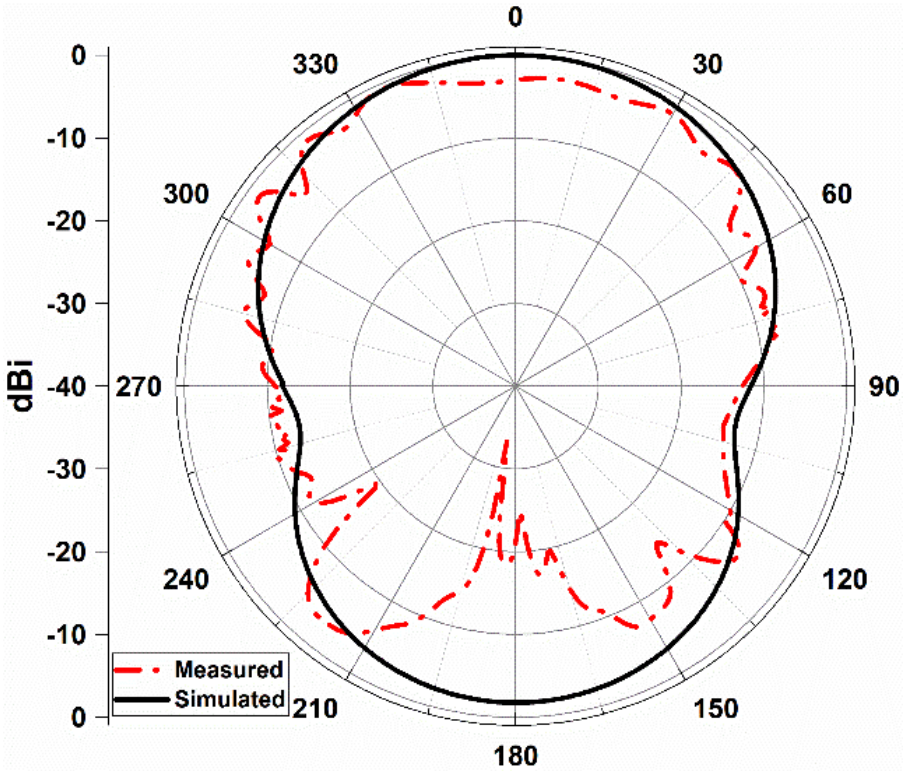

(b)

Figure 5.14 Radiation patterns of the E-shaped GPS antenna (a) H-plane, (b) E-plane

5.3.2 Investigation of Antenna Performance with Vehicle Roof and Roof-rack

Figure 5.15 illustrates further investigation of the proposed antenna performance on the vehicle roof. Antenna performance can be significantly impacted by the configuration and dimensions of the vehicle roof [349]. A metal plane with 105 cm length and 105 cm width is considered as a vehicle roof. The antenna is then placed on the metal plane. Perfect electric conductor (PEC) is used as the metal plane to reduce the requirement of computational resources. The antenna is placed on the middle of the computational roof model. Simulation is performed considering different gap between the antenna and roof model, denoted by D in Figure 5.15. D is varied from 0 to 25 cm. Figure 5.16 depicts the impact of the vehicle roof model on the reflection coefficients of the proposed antenna.

With varying gaps between the antenna and metal plane, the impedance bandwidth is hardly affected. However, the isolation between antennas has been slightly affected when the antenna is placed closest to the metal plane (D=0) as depicted in Figure 5.17. The isolation is 30 dB for S21, 27 dB for S31 and 29 dB for S41 at 5.4 GHz, which is still a lot better than the isolation between antennas with standard patch as shown in Figure 5.3. However, the maximum isolation is achieved when the gap between antenna and roof is D=5 cm. At this position, S21 is 35 dB, S31 is 41 dB and S41 is 40 dB at 5.4 GHz.

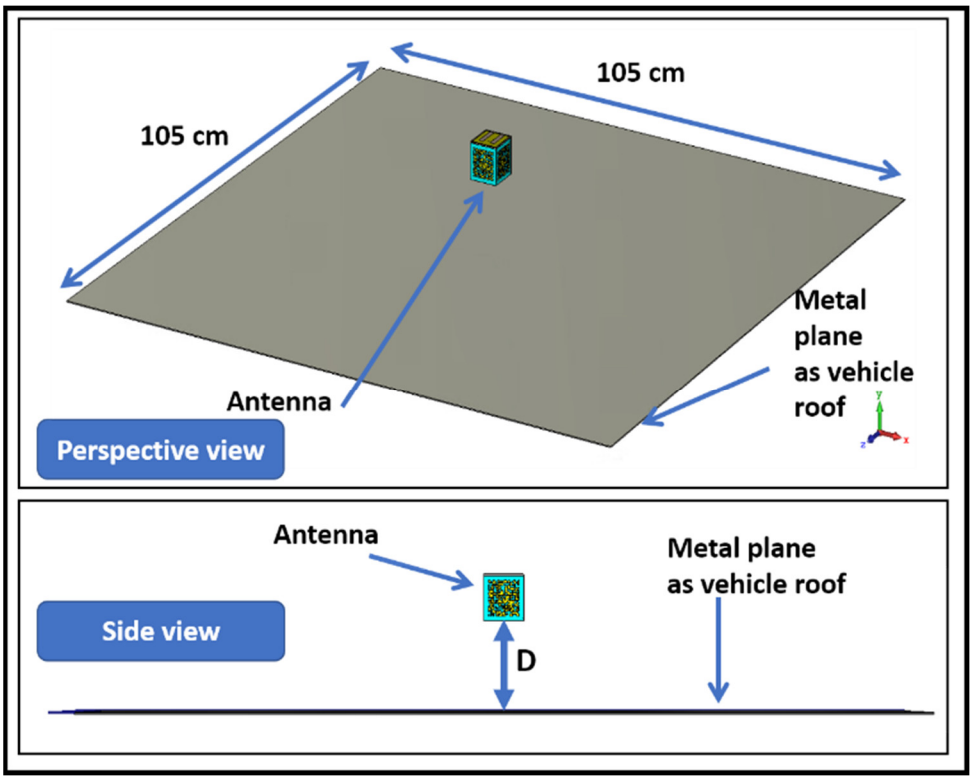

Figure 5.15 Simulation of the proposed antenna for vehicular applications considering placement on vehicle roof.

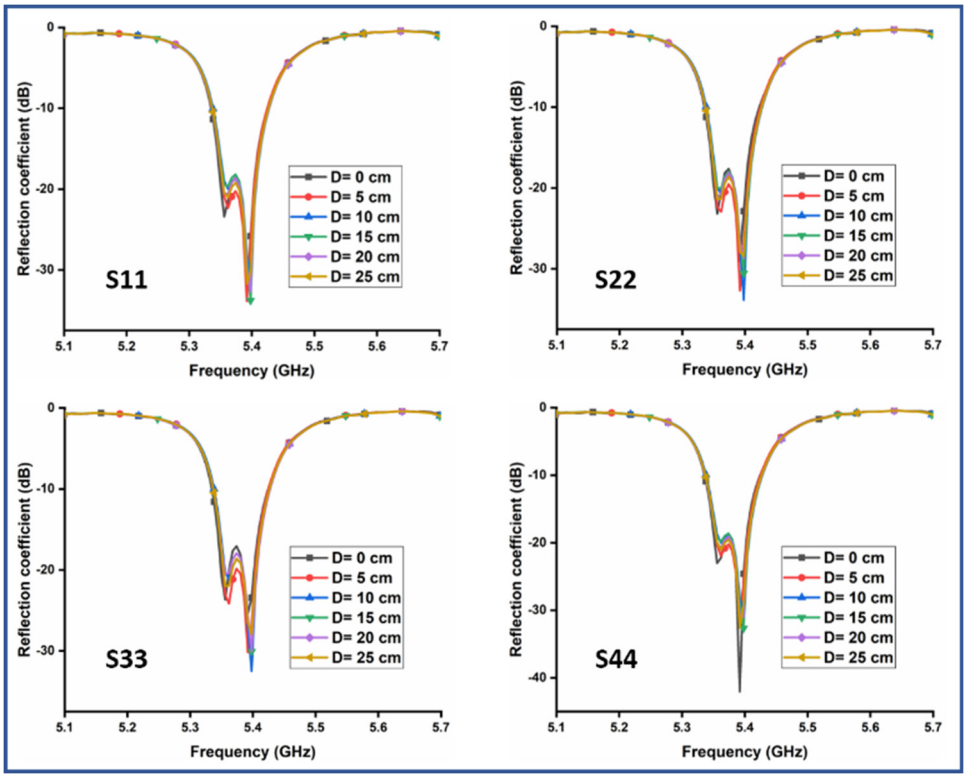

Figure 5.16 Reflection coefficients of the antennas (S11, S22, S33, S44)

Radiation patterns of the proposed antenna with metal plane is shown in Figure 5.18 when D=5 cm. The beamwidths of the patterns are similar to the original radiation patterns in Figure 5.12. In summary, although the presence of vehicle roof has negligible impact on the isolation of the proposed antenna, the reflection coefficient and radiation patterns maintain original performance that can contribute to reliable vehicular communications. Also, the minor decrease in isolation when D=0 cm is expected as it is the closest position of the antenna to the metal plane. Required isolation level can be maintained by placing the antenna on the vehicle rooftop with a proper gap, such as D=5 cm.

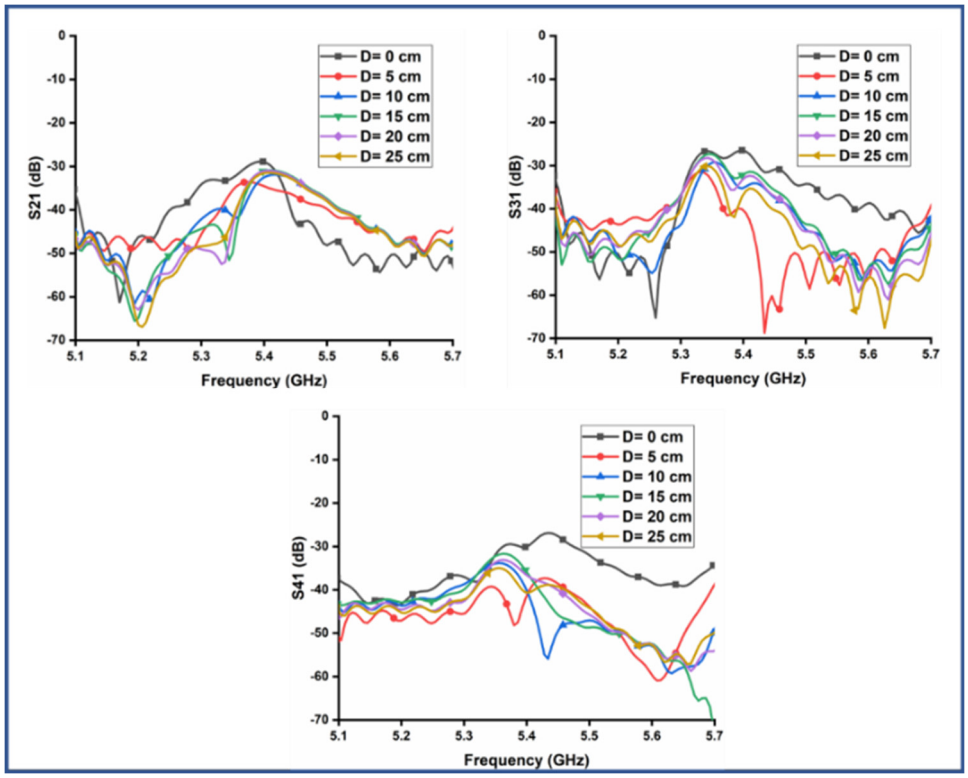

Figure 5.17 S-parameters of the antenna with metal plane

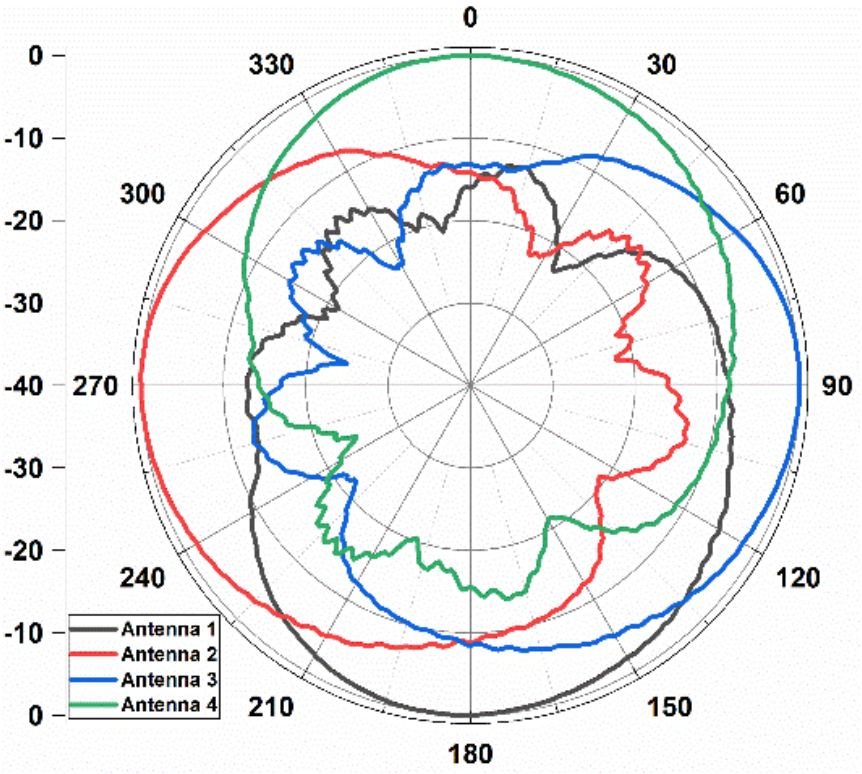

Figure 5.18 Radiation patterns of the optimized pixelated antennas with metal plane

Another simulation setup of the proposed antenna is shown in Figure 5.19, where the antenna is positioned at the corner of a car roof rack, as it can achieve the highest coverage with least interference from obstacles. Since the roof usually remains open and high above the ground, an automobile's roof or roof rack can be chosen by car manufacturers for the antenna placement. In general, a car's antenna should be placed practically at a higher place off the ground. The position aids in getting a high reception rate in nearly all antenna directions. The simulation setup in Figure 5.19 considers a realistic car roof rack. Aluminium has been used as the material of the roof rack. A foam has been considered below the antenna as a holder for the antenna. The height of the foam holder is 2.5 cm. Simulation is performed to investigate the S-parameters and the radiation pattern of the antenna with roof rack. Figure 5.20 presents the S-parameters of the antenna when placed at the corner of car roof rack. Reflection coefficients of the antenna is similar to the reflection coefficient of the antenna in free space, resonating at 5.4 GHz for all four antennas. The values of isolation ranges from 32 dB to 44 dB for S21, S31 and S41. The isolation is still 18 dB higher in comparison to the results of the antenna with standard patch in free space illustrated previously in Figure 5.3. Figure 5.21 represents the H plane radiation patterns of the antenna while mounted on the roof rack. There are some apparent ripples in the radiation patterns of antenna 1 and antenna 2, preserving the original radiation patterns in all directions. The slight variations could be attributed to the presence of uneven metallic structure of the vehicle roof rack. Despite the slight alterations brought on by the roof rack arrangement, the antenna radiates effectively within the desired directions as determined by the radiation patterns in free space (Figure 5.12 and Figure 5.13). The pixelated cubic antenna may be installed in a variety of locations because of its relatively compact structure in relation to the vehicle roof.

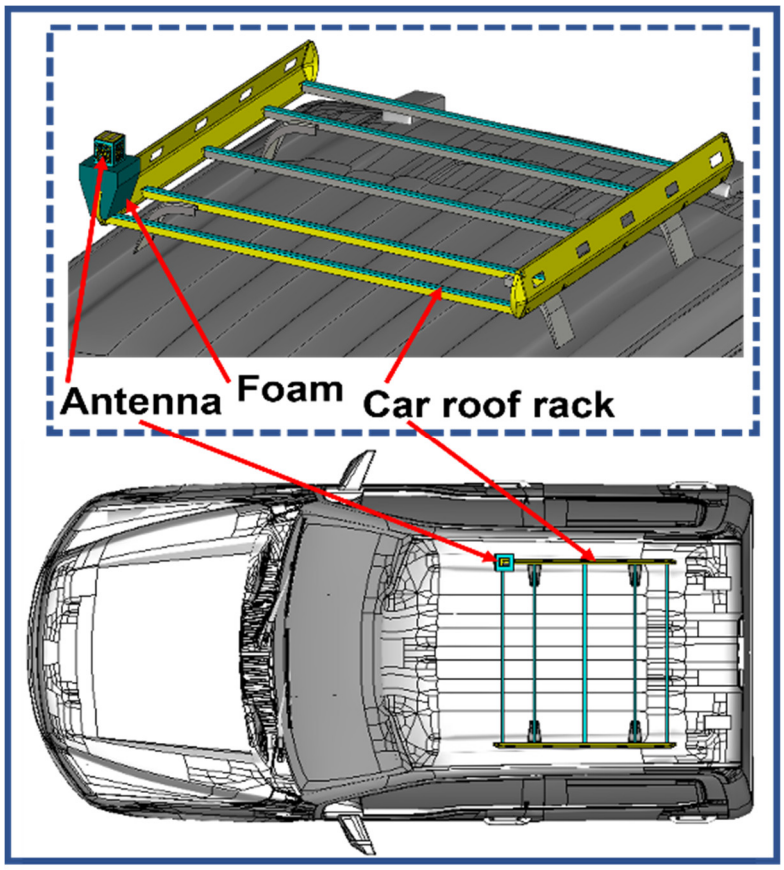

Figure 5.19 Simulation of the proposed antenna for vehicular applications considering placement on a car roof rack.

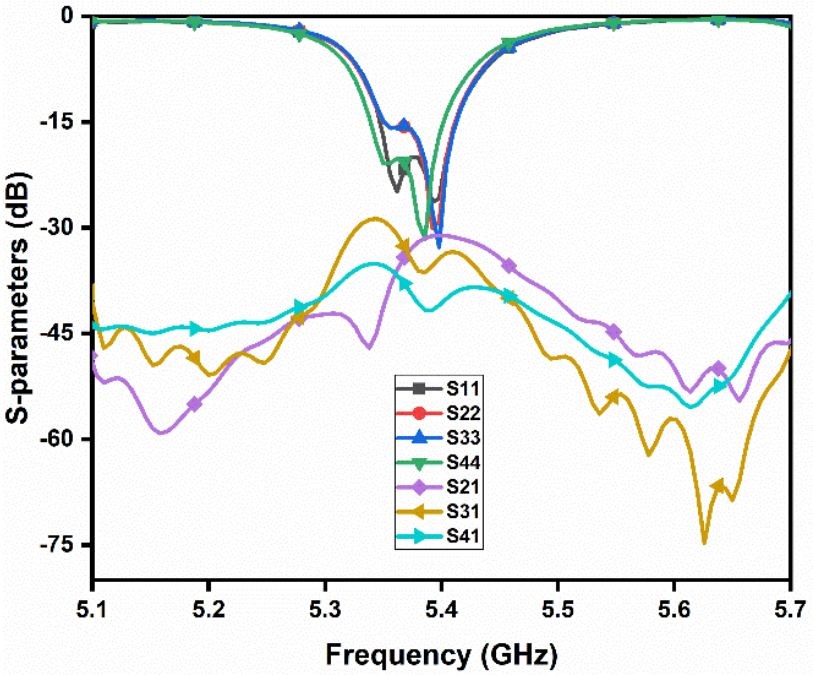

Figure 5.20 S-parameters of the proposed antenna when placed on a car roof rack

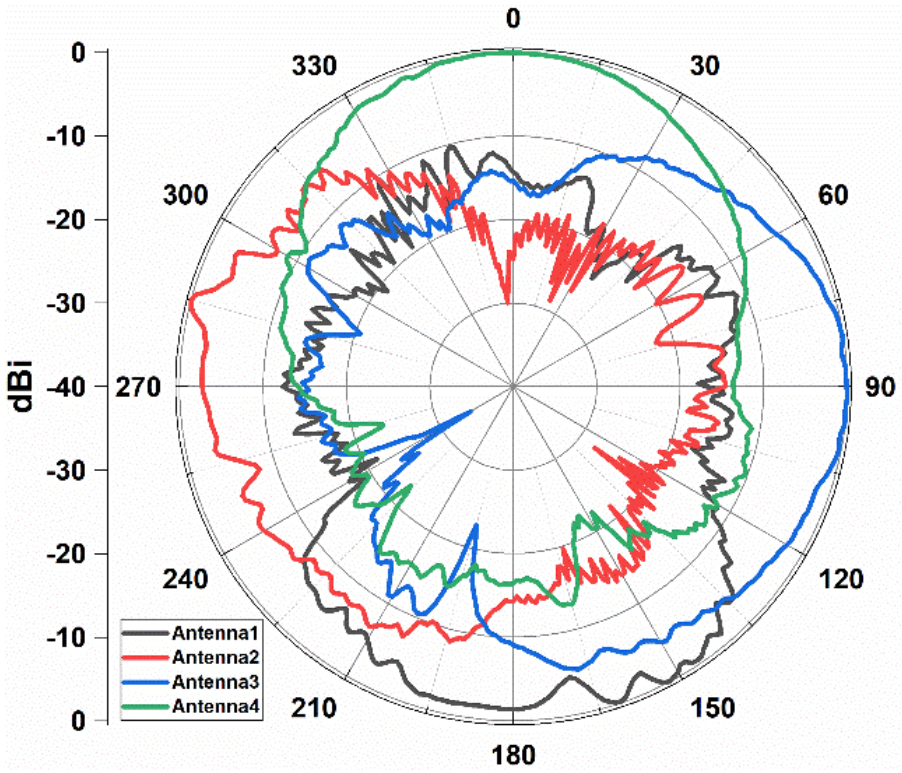

Figure 5.21 Radiation patterns of the proposed antenna when placed on a car roof rack

5.3.3 Experimental Results of the Antenna with Vehicle Roof-rack

To demonstrate the potential practical application of the proposed antenna, an experiment has been performed to measure the level of received power of the proposed antenna system with a real roof rack, illustrated in Figure 5.22. The antenna has been placed on a car roof rack. A metal plane has also been placed to represent the metallic car roof right below the roof rack. A signal generator has been used to transfer 0 dBm power at 5.4 GHz using a horn antenna with 10.8 dB gain at 5.4 GHz (Rohde and Schwarz HF907). A spectrum analyzer (Rhode & Schwarz, FSH8, 9 kHz-8 GHz) has been utilized to measure the received signal power level.

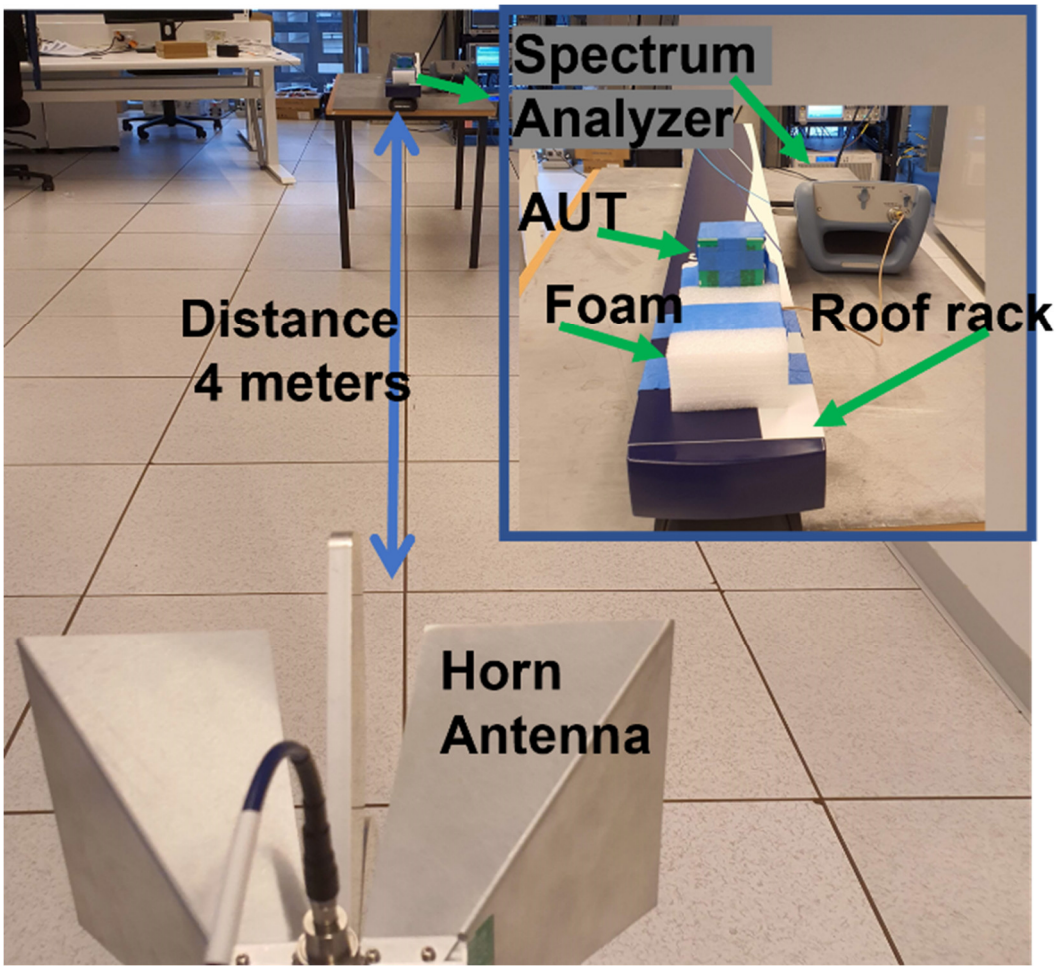

Figure 5.22 Experimental setup of the power measurement using the proposed pixelated multidirectional antenna as receiving antenna in RFCT Laboratory, UTS

The received power has been measured for all four antennas by rotating the roof rack to cover all four directions. 4 meters of distance has been considered between the transmitting horn antenna and the receiving multidirectional pixelated cubic antenna. Figure 5.23 depicts the received power level of the 4 pixelated antenna used in the cubic antenna configuration. The power levels of the Antenna 1, Antenna 2, Antenna 3 and Antenna 4 are -43.3 dBm, -44.2 dBm, -43.2 dBm and -44.4 dBm respectively. The experimental results entails that the proposed antenna system is capable of receiving wireless signal efficiently from multiple direction in vehicular or automotive system.

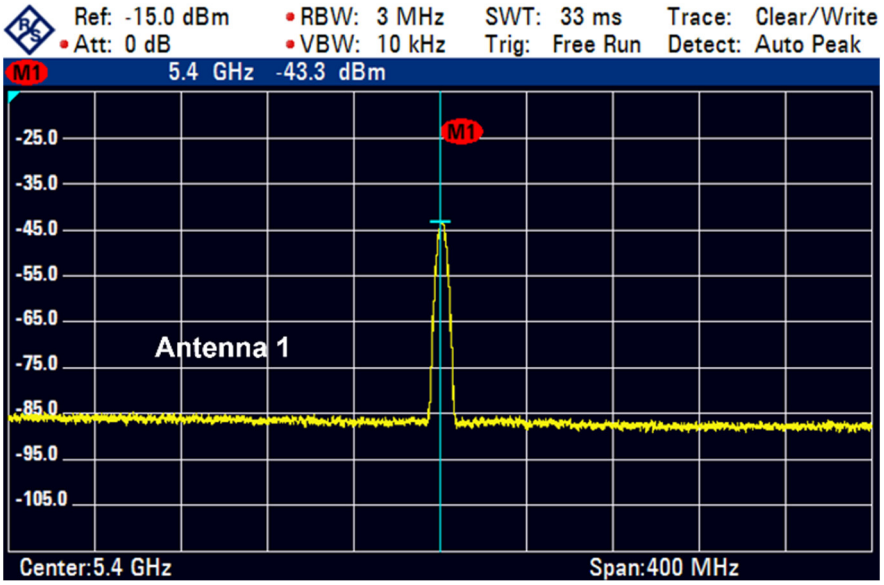
Ref: -15.0 dBm
Att: 0 dB
RBW: 3 MHz
VBW: 10 kHz
SWT: 33 ms
Trig: Free Run
Trace: Clear/Write
Detect: Auto Peak
M1
5.4 GHz -43.3 dBm
-25.0
-35.0
-45.0
-55.0
-65.0
-75.0
-85.0
-95.0
-105.0
Antenna 1
Center:5.4 GHz
Span:400 MHz

(a)

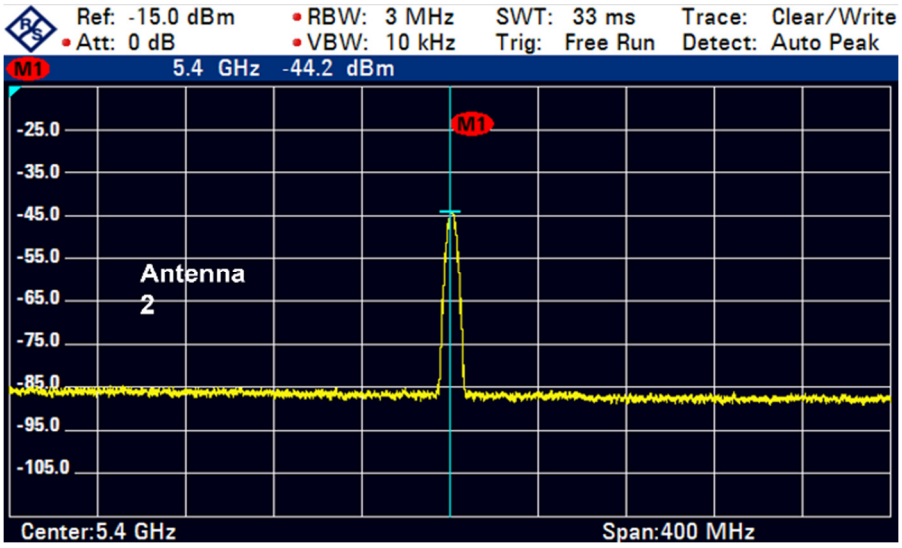
Ref: -15.0 dBm
Att: 0 dB
RBW: 3 MHz
VBW: 10 kHz
SWT: 33 ms
Trig: Free Run
Trace: Clear/Write
Detect: Auto Peak
M1
5.4 GHz -44.2 dBm
-25.0
-35.0
-45.0
-55.0
-65.0
-75.0
-85.0
-95.0
-105.0
Antenna 2
Center:5.4 GHz
Span:400 MHz

(b)

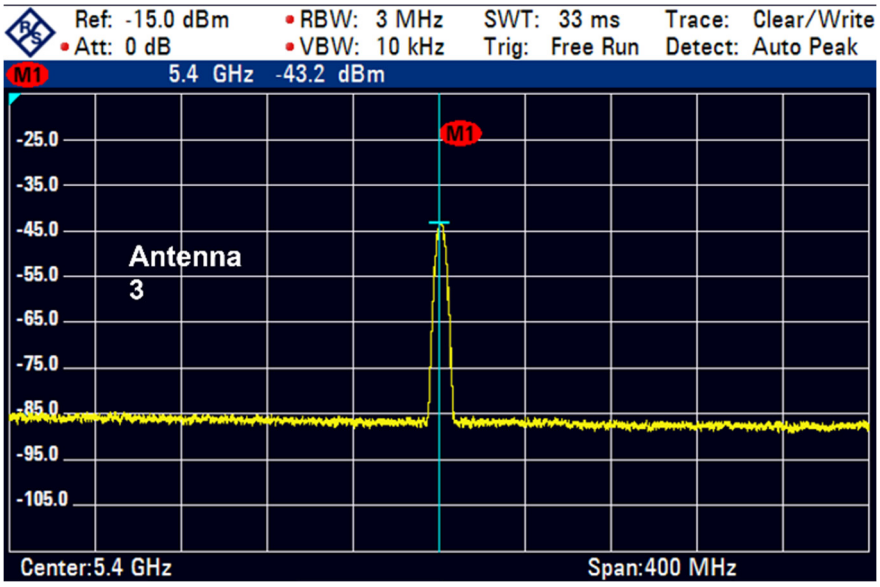

(c)

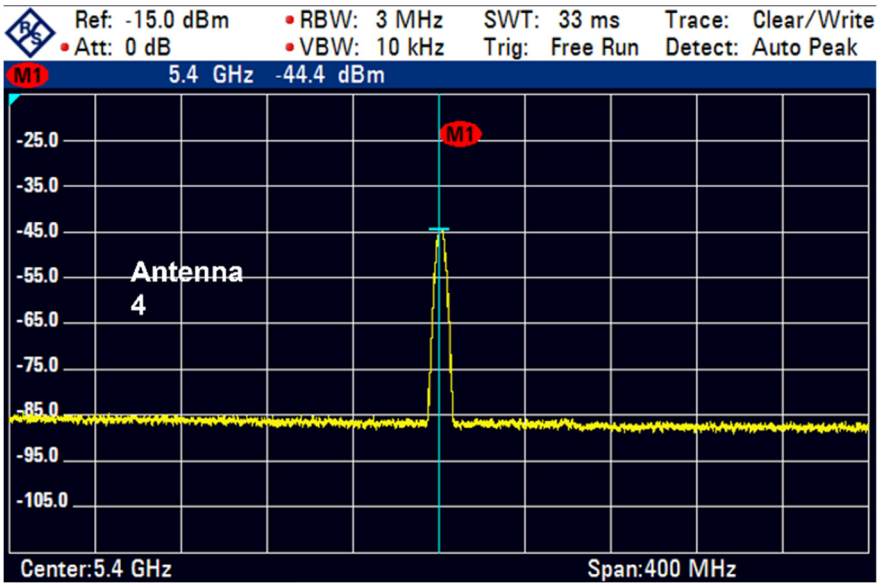

(d)

Figure 5.23 received power by the proposed vehicular antenna; (a) Antena 1, (b) Antenna 2, (c) Antenna 3, (d) Antenna 4

5.4 Summary

In this chapter, a pixelated multidirectional cubic antenna has been proposed for vehicular applications. The design evolution of the cube shaped antenna is based on a pixelated patch. The design methodology and the results demonstrate the advantages of the cubic configuration and merits of the proposed antenna. The antenna is designed with a binary

optimization algorithm to achieve a desired operating band and enhanced isolation. The isolation between antennas has been significantly improved considering the counterpart cubic antenna design with standard patch configuration. High isolation is achieved without using any additional hardware or filters, while the measured gain in each direction is about 6.4 dBi. The antenna performance has also been investigated by placing the antenna on a vehicle roof and roof rack model in CST software. The antenna performance is nearly unaffected by the presence of a metal plane on the vehicle roof and roof rack. There is no requirement for metallic components or grounding on the bottom side of the antenna which simplifies installation at different areas of the vehicle. Featuring compact size, enhanced isolation, multidirectional radiation pattern, lightweight, low cost, straightforward design, and simple manufacturing, the proposed antenna is well-suited for vehicle systems.

Chapter 6

Optimized Log Periodic Antenna with Pixelated Configuration for Enhanced Bandwidth

6.1 Introduction

Antennas with a broad frequency range are needed for a variety of telecommunications applications. Recent years have seen rapid advancements in wireless communication technology, leading to a dramatic increase in the demand for small, low-profile antennas with a wide frequency range. Due to many attractive characteristics, including its light weight, low volume, low cost, low profile, small dimensions, and ease of production and conformality, etc., patch antennas have remained a strong candidate for consideration in practical applications [118, 350]. Antenna design remains a challenging issue, particularly for applications that require a wideband antenna. Broadband antenna properties are required in communication systems, electromagnetic field (EM) metrology, and EM field sensing, for instance. In addition, certain systems, such as cognitive radio, require an antenna capable of emitting and/or receiving signals in the desirable frequency ranges in a dynamic and autonomous manner [351]. Moreover, in MIMO, WLAN, and similar applications, communication systems require that they be equipped with an antenna that can support a wideband or even ultra-wideband (UWB) frequency range [352, 353].

The inherent narrowband performance of patch antennas restricts their application to broadband systems. Microstrip antennas in the low microwave frequency range are typically too large to be installed in a mini-system. Thus, the issue of attaining a large impedance bandwidth in a small antenna has remained a paramount concern in contemporary antenna design.

A diverse range of techniques has been documented to enhance the bandwidth of microstrip patch antennas. Initial research were based on utilizing low permittivity substrates, thick substrates, and wide patch [354]. Adopting metamaterial concept is one of the recent approaches to enhance bandwidth of patch antennas [355] [356]. A novel bandwidth enhancement technique has been suggested, which capitalizes on increasing the average substrate thickness in the vicinity of the metal patch, while keeping the rest of the dielectric substrate thin [357]. Other efficient methods to improve bandwidth includes using E-shaped patches [358], U-shaped-slot patches [359], Folded patch [360] etc.

The log-periodic dipole array (LPDA) antenna is be one the best candidates for wideband applications due to its relatively excellent broadband characteristics. Microstrip-based LPDA antennas are simple to design and implement. In the 1950s and 1960s, the geometry and electrical properties of log-periodic antennas were developed. The microstrip based LPDA antennas are very useful in practical applications. Nevertheless, they do have some drawbacks, to achieve excellent periodic performance, the antenna should have many dipoles, which increases its size [361]. Several methods have been reported to achieve desired performance using printed LPDA antenna where different types of dipoles are used including, meandered dipole, dielectric loaded dipole, Koch-dipole, and parasitic element loading [362-365].

In this chapter, a pixelated log periodic antenna (PLPA) with enhanced bandwidth has been proposed. The PLPA is designed using an enhanced binary particle swarm optimization. In the design process, pixelated dipole configuration has been utilized as the dipole elements.

The optimization process depends on how the pixels are arranged and how this affects the antenna's behaviour, measured by S-parameters. Changing the pixel layout introduces small slots on the antenna, which can alter how the antenna's surface currents flow and, as a result, impact its performance. The optimized pixelated log periodic antenna achieved significantly enhanced bandwidth than the counterpart conventional printed log periodic antenna of similar size. The antenna operates at 1.62 GHz to 2.56 GHz covering a wide band.

6.2 Pixelated Log Periodic Antenna Design Methodology

This section illustrates the proposed antenna design methodology. To achieve wideband performance, a pixelated configuration is used in the initial design of a log periodic antenna element. Broadband antennas are essential in various use cases such as wireless personal area networks, satellite communication, and radar systems. The Log-periodic dipole array (LPDA) antennas offer numerous benefits, including consistent gain, extensive bandwidth, and cost-effectiveness. As a result, they are highly suitable for a wide range of wideband wireless communication systems.

6.2.1 Conventional Log-Periodic Antenna

The initial design of the proposed antenna is based on a conventional log-periodic antenna, that consists of multiple dipoles and a transmission line. Log-periodic antennas are employed in wireless applications due to their ability to achieve a wide frequency range while maintaining high directivity and low cross-polarization ratio.

An initial design of the log-periodic patch antenna has been simulated as Figure 6.1(a). The antenna has been designed on FR4 substrate with 1.6 mm thickness. The dimension of the initial antenna is 60mm × 55mm. The antenna has been designed to operate at 2-

2.7 GHz frequency range. The design process consists of several essential steps. The first step entails determining the scaling factor τ, spacing factor σ, and number of dipole elements N [118, 366]. In this initial design, number of dipole elements N=6 is chosen where the scaling factor τ=0.88 and spacing factor σ=0.09. The corresponding design dimensions can be initially estimated according to the equations (6.1-6.5) [366]. The length of the longest dipole that responds to the lowest resonance frequency can be approximated by (6.1).

$$L_1 = \frac{\lambda_{\text{eff max}}}{4} \tag{6.1}$$

$$\lambda_{\text{eff max}} = \frac{c}{f_{min}\sqrt{\varepsilon_{eff}}} \tag{6.2}$$

Where, $\lambda_{\text{eff max}}$ corresponds to longest operating wavelength and it can be determined by the following equation. ε_{eff} is the effective dielectric constant and c denotes speed of light in free space. Also, for the initial dipole case, the effective dielectric constant for microstrip lines can be used to approximate the ε_{eff} according to following equation. In the equation, W_1 represents largest dipole width.

$$\varepsilon_{eff} = \frac{\varepsilon_r+1}{2} + \frac{\varepsilon_r-1}{2}\frac{1}{\sqrt{1+\frac{12h}{W_1}}} \tag{6.3}$$

Additionally, the following equation can be used to estimate the relationship between dipole spacing and element length. Once the longest dipole element's length is obtained, the lengths of the remaining dipole elements can be estimated with the following formula.

$$S_{n+1} = 4\sigma L_n; \text{ where } n = 1,2,..,5. \tag{6.4}$$

$$\frac{L_{n+1}}{L_n} = \frac{W_{n+1}}{W_n} = \tau \tag{6.5}$$

Based on the initial dimensions enlisted in Table 6.1, the initial antenna has been designed, depicted in Figure 6.1(a). The antenna achieved operating bandwidth at 2.00-2.77 GHz. To achieve impedance matching within the desired frequency band, the PLPDA's dimensions as shown in Table 6.1 have been tuned.

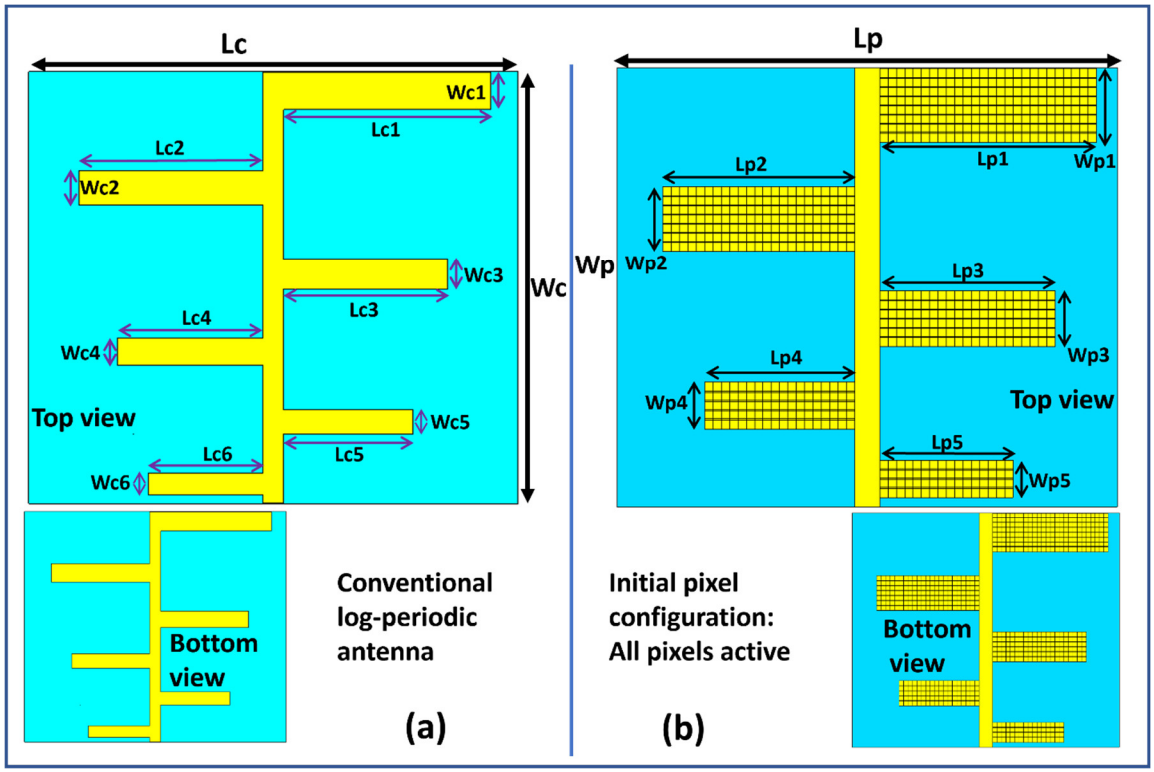

Figure 6.1 Initial design of the log-periodic antenna (a) and pixelization of the initial layout (b).

Table 6.1: Design dimensions of the antenna

Conventional LPDA (mm)				Pixelated log periodic antenna (PLPA) (mm)			
Lc	60	Wc	55	Lp	60	Wp	48.2
Lc6	14	Wc6	2.7	Lp5	16	Wp5	4
Lc5	15.8	Wc5	3.1	Lp4	18	Wp4	5
Lc4	17.8	Wc4	3.4	Lp3	21	Wp3	6
Lc3	20	Wc3	3.8	Lp2	23	Wp2	7
Lc2	22.6	Wc2	4.3	Lp1	26	Wp1	8
Lc1	25.3	Wc1	4.8				

Overall antenna size 0.48λ×0.44λ×0.012λ	Overall antenna size 0.42λ×0.33λ×0.012λ. Overall antenna size reduced by 34.3%.
λ is the free-space wavelength of the center frequency of conventional LPDA	λ is the free-space wavelength of the center frequency of PLPA design case 1

6.2.2 Pixelated Log Periodic Antenna Design

After that, considering the initial design of the conventional LPDA, the proposed design configuration, the dipoles of the antenna have been divided into pixels as seen in Figure 6.2. A binary particle swarm optimization (BPSO) algorithm has been utilized to optimize the pixel positions. To reduce the number of pixels on the design five poles has been considered in the design for optimization. The design dimensions of the antenna are enlisted in Table 6.1. All poles of the antenna in each side have been discretized into 649 small pixels with a dimension of 1 mm × 1 mm. The top side and the bottom side of the antenna represent similar pixel configuration.

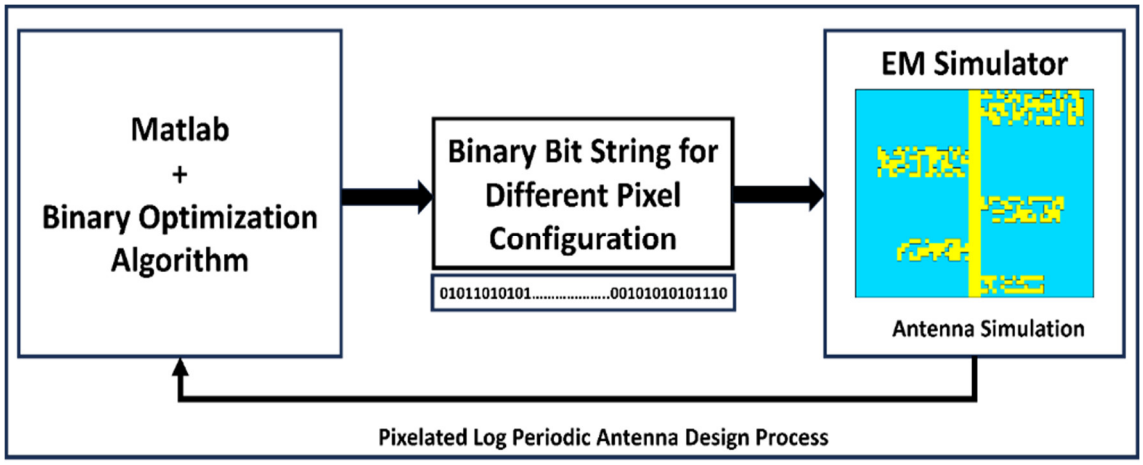

Figure 6.2 Block diagram of the antenna design procedure

The optimization process relies on the intrinsic connection between the arrangement of pixels and the antenna's S-parameters. By generating different pixel configurations, small slots are introduced on the antenna poles. These slots can bring significant changes in the antenna's performance by affecting the path of surface currents. Each pixel is given a

binary value of 0 or 1, with 1 indicating that the copper layer is left intact on the surface and 0 indicating that it should be removed.

The pixelization process of the patches is performed using a binary particle swarm optimization (PSO) algorithm with V-shaped transfer function (VBPSO) [71], implemented in MATLAB and applied to optimize the binary values of the bits. This algorithm searches the solution space for the optimal way to reach optimization goals using a population of candidate solutions (each solution is a particle). Particles maintain their inertia using a straightforward formula that allows them to accelerate to both their own and the population's highest levels of prior experience [290, 295, 367, 368].

6.2.3 Problem Formulation and Optimization for Enhanced Bandwidth

The objectives of our optimization are to increase the antenna's bandwidth while maintaining its radiation pattern with satisfactory gain. In order to accomplish these objectives, the cost function (CF) that the optimization procedure aims to minimize was defined as follows:

$$\mathrm{CF} = w_1 \cdot C_1 + w_2 \cdot C_2 \tag{6.6}$$

$$C_1 = S_{11}^{[\mathrm{dB}]}(f_L - f_H);\ \left|S_{11}^{[\mathrm{dB}]}(f_L - f_H)\right| < 10 \tag{6.7}$$

$$C_2 = Average\ gain\ (f_L - f_H) \tag{6.8}$$

Where, C_1 and C_2 are the two terms of the cost function of the optimization goals and w_1 and w_1 are weighting coefficients. In (6.7) C_1 considers the value of reflection coefficient in EM simulator after each simulation based on the pixel positions. By this definition, C_1

considers the antenna reflection coefficient values which are better than -10 dB over the desired operating band ($f_L - f_H$). C_2 is related to the conservation of satisfactory gain with radiation pattern in specific direction in H-plane. Different gain values were considered at specific angles of the H-plane radiation pattern over the desired operating band from the EM simulator after each simulation of the antenna with different pixel configuration. It is worth mentioning that the desired operating bandwidth can be controlled by defining the CF properly. The weighting coefficients can be tuned to provide balance between the two terms of the cost function (6.6). The following are the individual steps that were taken in the simulation and optimization [71] process:

Step 1: Initialize particle positions. Set the number of maximum iterations.

Step 2: Calculate each particle's fitness value in accordance with equation (5). A binary bit string with 649 bits is sent to the EM simulator to generate pixel configurations. After simulation, the values of corresponding result values are sent back to Matlab to calculate the fitness value.

Step 3: Analyze each particle's CF value. Then, update the personal best and global best position of particles.

Step 4: Velocity value is calculated and updated accordingly. The position of particles is updated accordingly. They follow the equations illustrated in [71], which have been mentioned in earlier chapter 1.

Step 5: Check the number of iterations. If the current number of iterations is less than the maximum iterations, return to Step 2. If maximum iterations are completed, proceed to Step 6.

Step 6: Save global best score and best position. The best position of particles provides the optimum pixel configuration of the antenna.

A link was established between the binary algorithm (implemented in MATLAB) and CST Microwave Studio (as the full-wave electromagnetic simulator) for the pixel position optimization procedure. By considering 17 populations the optimization has been performed for 60 iterations for both design cases. The convergence was achieved at the 50th iteration for case 1 and at the 47th iteration and desired bit strings were obtained. Figure 6.3 illustrates the convergence curves of the optimization process.

6.2.4 Optimization Outcome

In this study, two design cases have been considered. The desired operating band as 1.6-2.6 GHz has been considered in 'case 1' and 1.7-2.9 GHz in 'case 2'. Figure 6.4 and Figure 6.5 represent the pixelated configurations of the optimized antenna for the two design cases. The reflection coefficients of the conventional LPDA and pixelated LPDA have been illustrated in Figure 6.6. The conventional LPDA achieved operating band at 2.00-2.76 GHz. The pixelated LPDAs have achieved operating bandwidth of 1.62-2.56 GHz and 1.67-2.91 GHz in design case 1 and case 2 respectively. The conventional LPDA has a bandwidth of 760 MHz with 31.9% fractional bandwidth. The pixelated LPA in case 1 has achieved 940 MHz bandwidth with 13% increment in fractional bandwidth. Also, the PLPA in case 2 has achieved a bandwidth of 1240 MHz with 22.2% increment in fractional bandwidth. These results clearly demonstrate that the proposed pixelated log periodic antenna design methodology has potential in designing pixelated antennas with enhanced bandwidth with compact dimension than their conventional counterpart design.

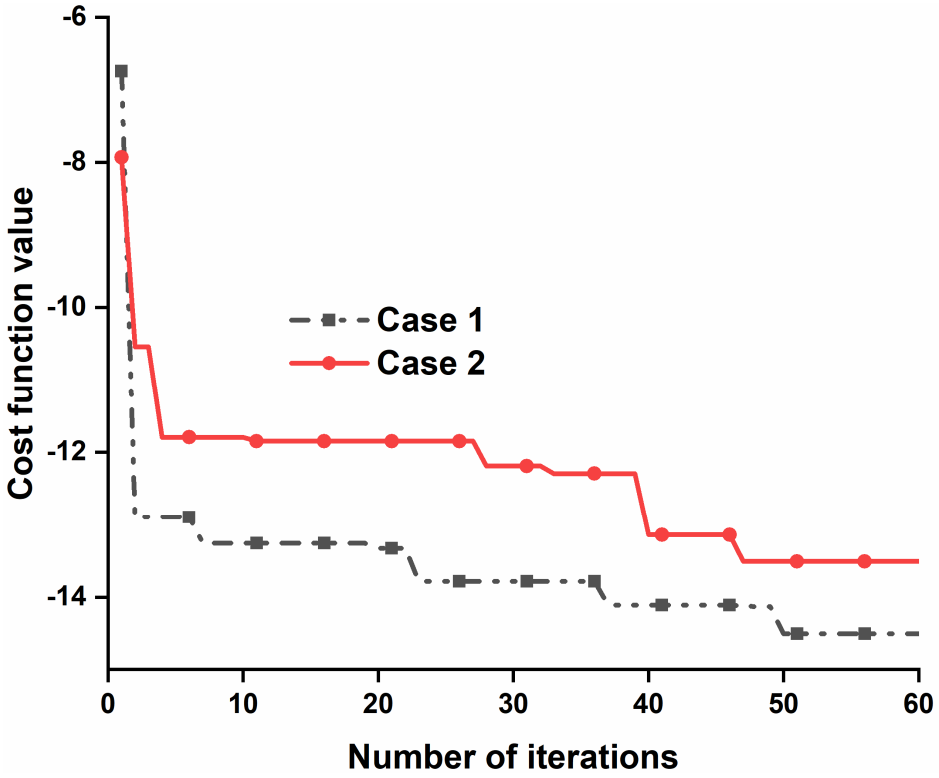

Figure 6.3 Convergence curves of optimization

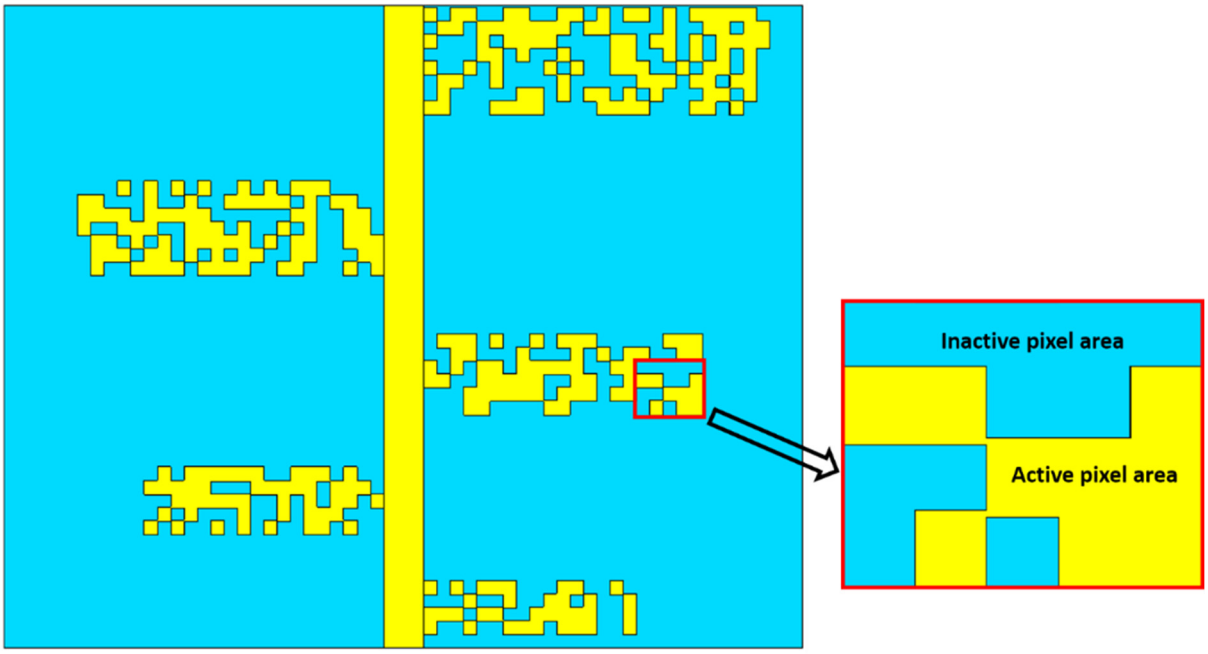

Figure 6.4 Pixelated log periodic antenna (Case 1)

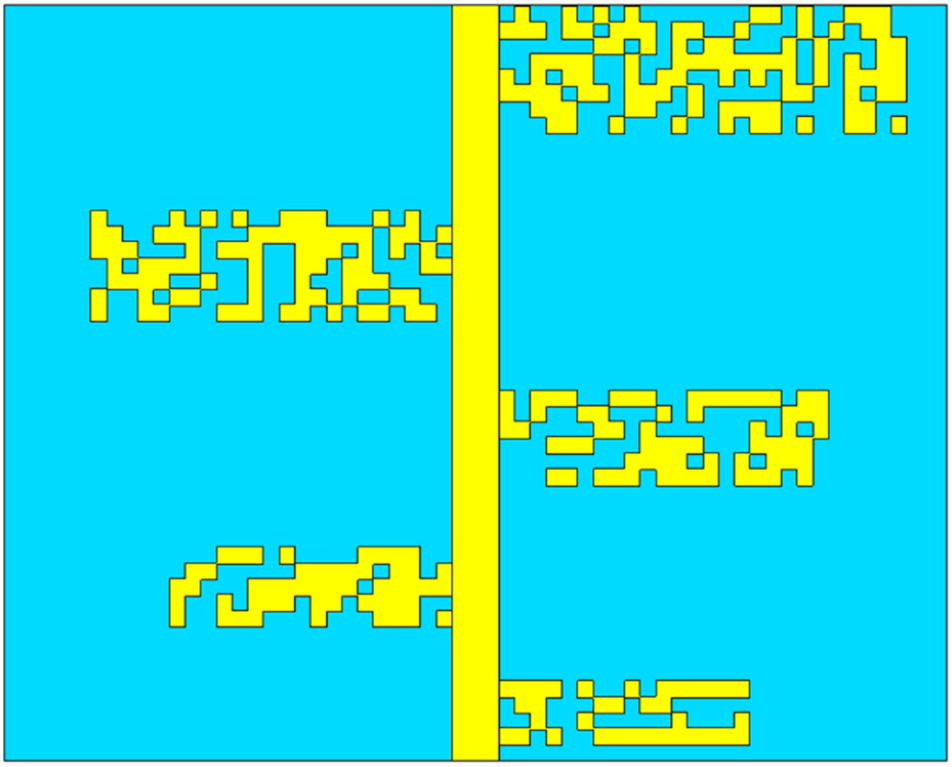

Figure 6.5 Pixelated log periodic antenna (Case 2)

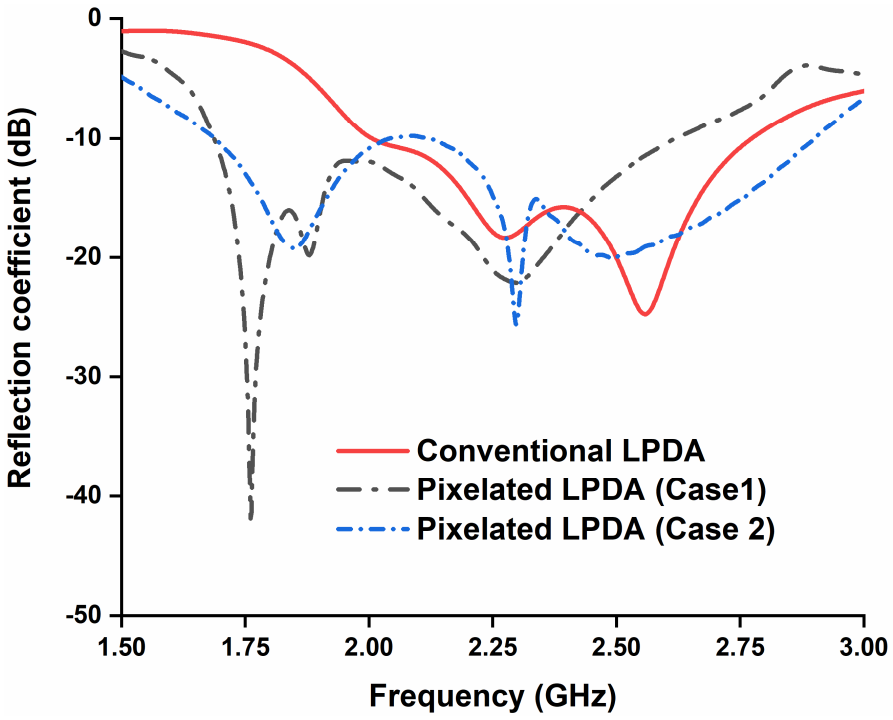

Figure 6.6 Simulated reflection coefficient of different log periodic antenna

6.3 Results and discussion

A prototype of the pixelated log periodic antenna has been fabricated and measured to validate the proposed antenna design and methodology. The optimized pixelated configuration in ‘Case 1’ has been fabricated on FR4 substrate with 1.6 mm thickness. Figure 6.7 illustrates the fabricated prototype and the measurement set-up of the antenna in anechoic chamber in Figure 6.8. The simulated and measured reflection coefficient of the proposed antenna has been depicted in Figure 6.9. The antenna achieved operating bandwidth at 1.62-2.56 GHz in simulation.

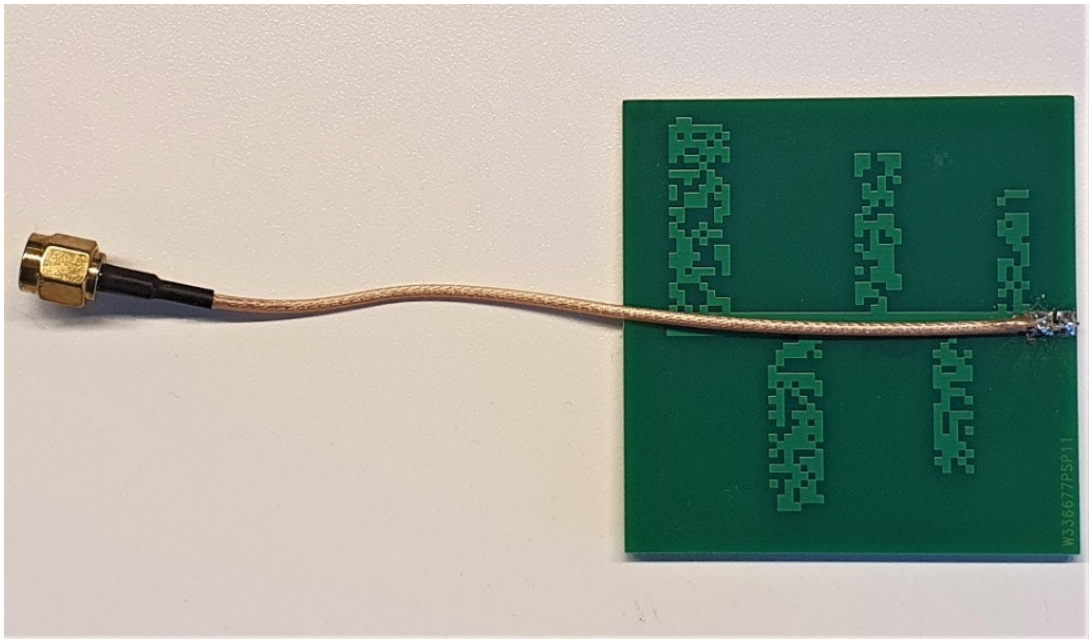

Figure 6.7 Fabricated prototype of the proposed pixelated log periodic antenna

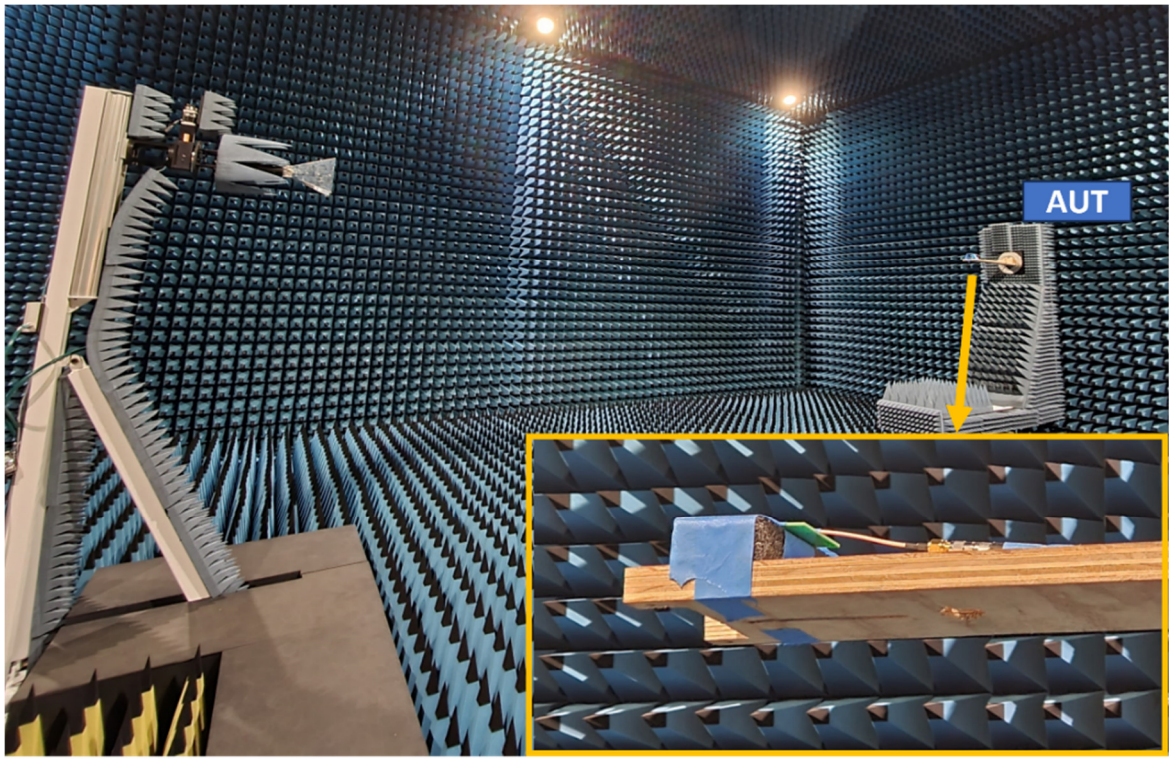

Figure 6.8 Radiation performance measurement set-up of the proposed antenna in anechoic chamber

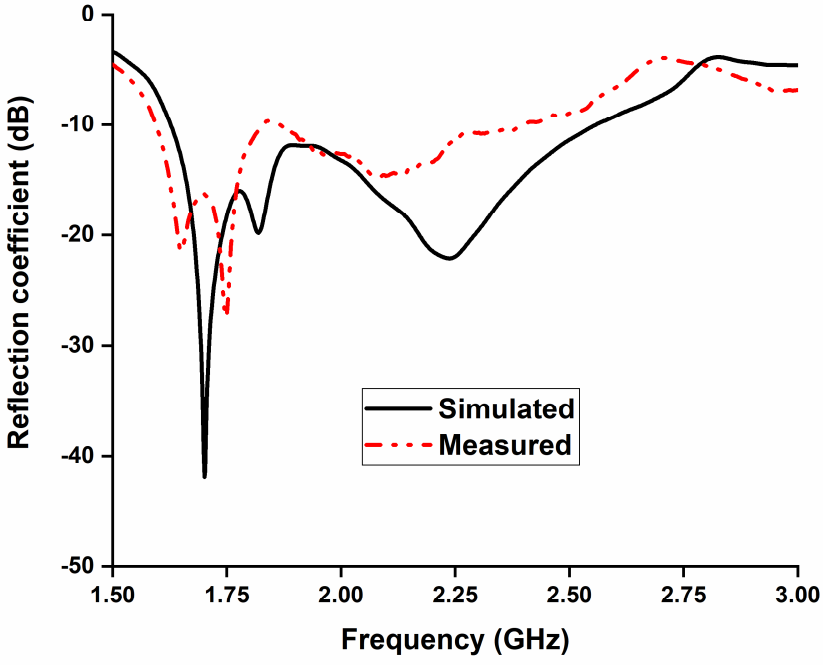

Figure 6.9 Simulated and measured reflection coefficient of the proposed pixelated log periodic antenna

In the measured results of reflection coefficient, the antenna operates at 1.58-2.49 GHz. The simulated and the measured results are in good agreement. In Figure 6.9, the operating frequency range has shifted slightly, which can be attributed to fabrication tolerances and the type of coaxial cable used to connect and excite the antenna. The simulation did not account for the effects of the coaxial cable, leading to a discrepancy between the simulated and actual operating bands.

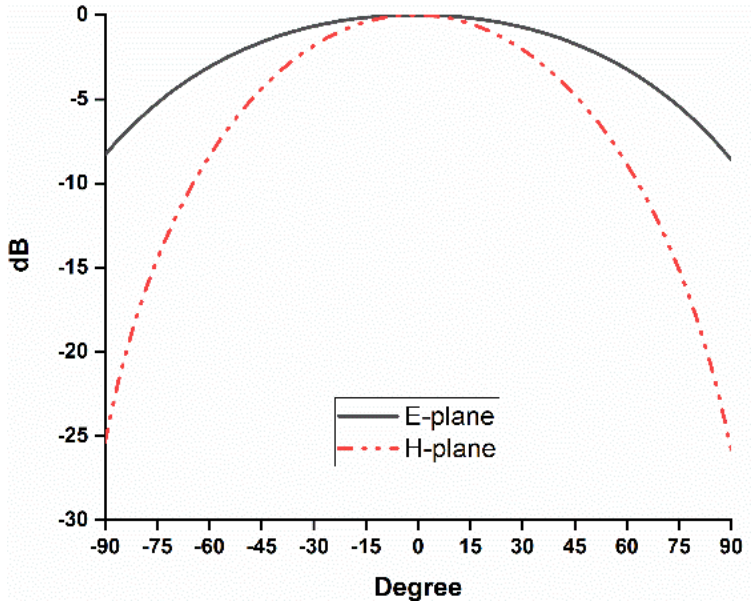

(a)

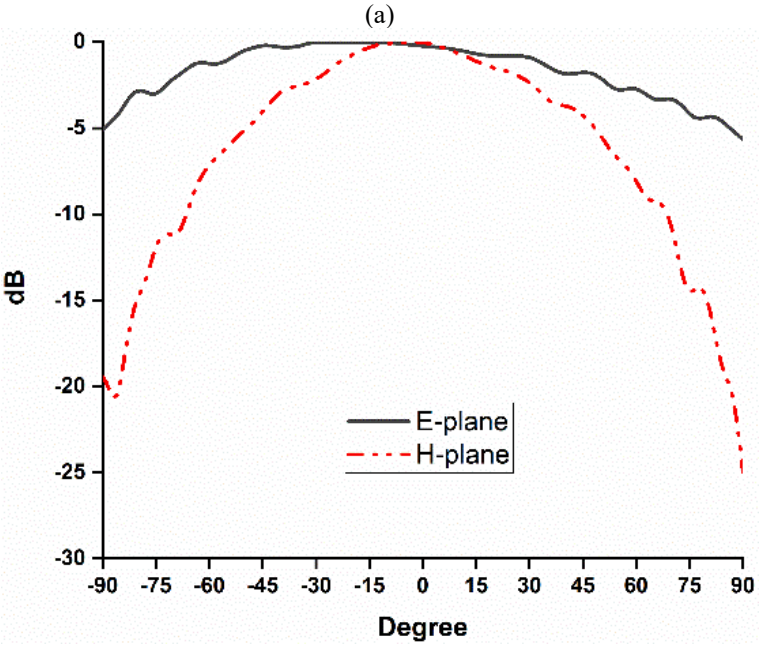

(b)

Figure 6.10 Simulated and measured radiation patterns at 1.7 GHz (a) Simulated (b) Measured

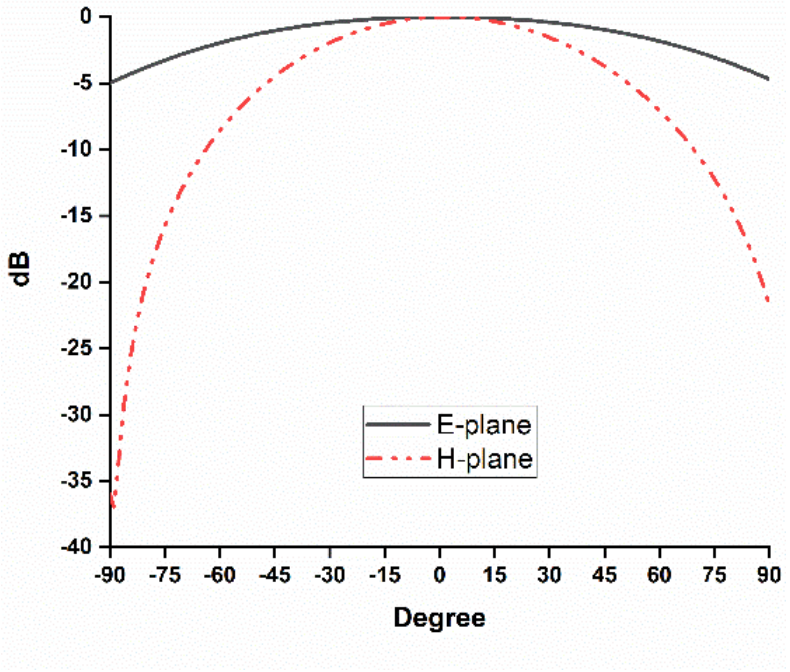

(a)

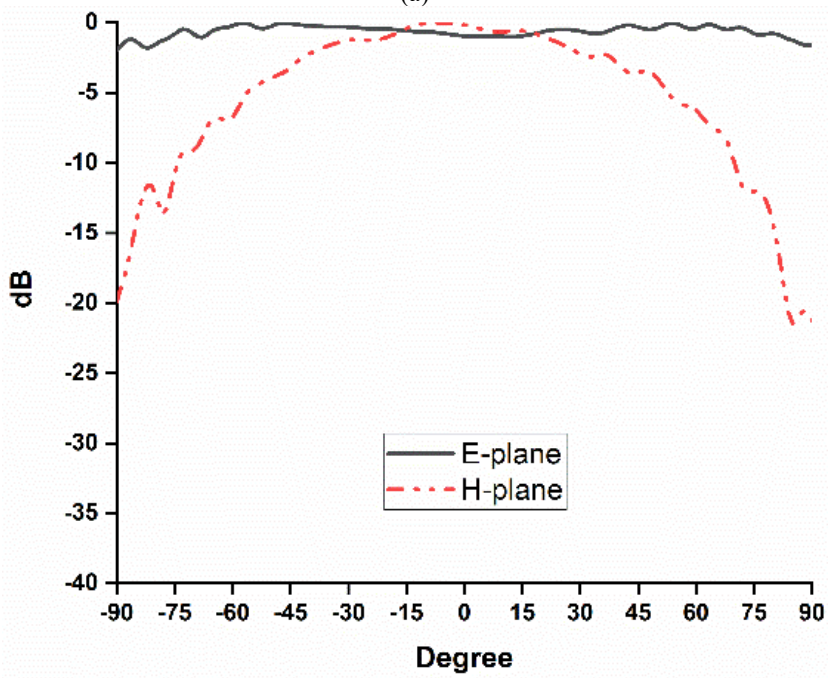

(b)

Figure 6.11 Simulated and measured radiation patterns at 2.2 GHz (a) Simulated (b) Measured

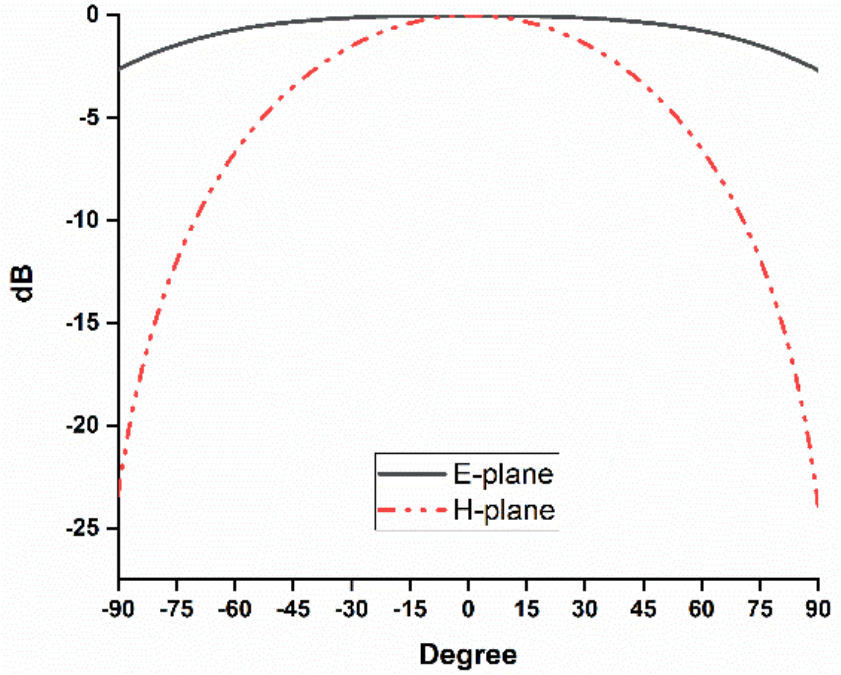

(a)

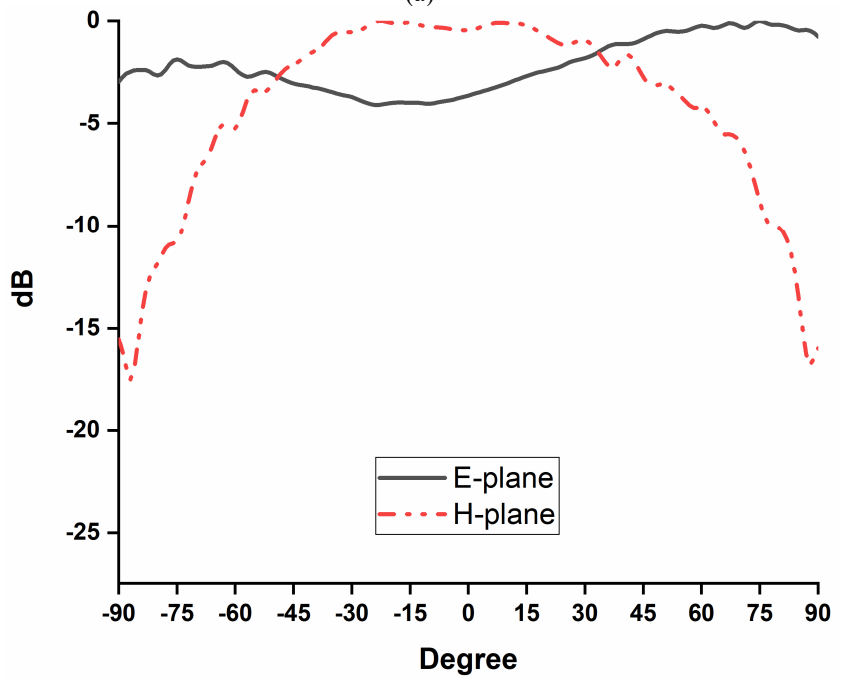

(b)

Figure 6.12 Radiation patterns at 2.5 GHz (a) Simulated (b) Measured

The simulated and measured radiation patterns of the proposed antenna have been presented in Figure 6.10-Figure 6.12 at 1.7 GHz, 2.2 GHz, and 2.5 GHz respectively. The simulated and measured patterns corelate very well. In Figure 6.13, the simulated and measured realized gain have been presented. The simulated peak realized gain of 5.7 dBi

achieved at 1.95 GHz. In the measurement, the peak measured gain of 5.45 dBi has been achieved at 1.85 GHz.

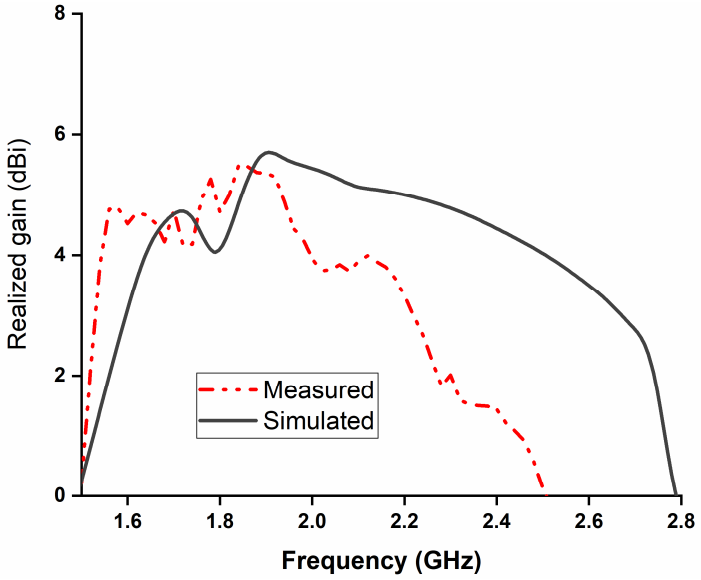

Figure 6.12 Simulated and measured realized gain of the proposed antenna over the frequency

Table 6.2 presents a comparison between the antenna introduced in this work and other planar log-periodic antennas that have been previously published. The proposed pixelated log periodic antenna design methodology is able to achieve antenna designs with enhanced bandwidth within significantly compact size.

Table 6.2: Comparison of several log-periodic antenna topology with the proposed antenna technique

Refs.	Design Methodology	% Bandwidth	Overall Size (λ)
[369]	Monopole based printed log periodic antenna	53.9	2.88 λ×0.98λ× 0.03λ
[370]	Monopole based log periodic antenna loaded with top hats	108	5.81 λ×3.32λ× 0.13λ
[371]	CPW-fed printed log periodic dipole	66.7	1.76 λ×1.08λ×0.02λ
[363]	Dielectric loaded log periodic dipole	120	0.96λ×0.7λ×0.05λ
Conventional	Conventional printed log periodic dipole illustrated in this study	31.9	0.48λ×0.44λ×0.012λ
This work	Pixelated log periodic dipole	Up to 54.1% (With flexibility to increase or decrease according to design requirements)	0.46λ×0.37λ×0.012λ
λ is the free-space wavelength of the centre frequency			

6.4 Summary

This chapter presents a novel approach to enhancing the bandwidth of log periodic antennas (LPAs) through the utilization of an enhanced binary particle swarm optimization technique. The proposed pixelated log periodic antenna (PLPA) design showcases remarkable improvements in bandwidth compared to traditional printed log periodic antennas of similar dimensions. Notably, the PLPAs in design case 1 achieved a bandwidth of 940 MHz, indicating a 13% increment in fractional bandwidth, and the antenna in design case 2 reached an even more impressive bandwidth of 1240 MHz, featuring a 22.2% increment in fractional bandwidth. These outcomes collectively highlight the potential of the presented LPDA antenna design methodology. It demonstrates the ability to create pixelated antennas with significantly enhanced bandwidth within compact dimensions compared to their conventional counterparts.

The goals of optimization can change based on what a particular application need. In this study, the focus is on exploring and suggesting a structured method for creating a wideband printed log periodic antenna. The purpose of the study is to develop a systematic approach, likely involving computer simulations and optimization algorithms, to design such an antenna with the desired wideband characteristics. This systematic approach ensures that the antenna meets the specified performance requirements and can be reliably manufactured for practical use.

Chapter 7

Conclusion and Recommendations for Future Work

7.1 Conclusion

Antenna technology has become more demanding due to the evolution of wireless mobile communication systems and the rapid surge in data traffic. New antenna design strategies and technologies to meet wireless communication system requirements are expected to develop with further miniaturization and integration.

A comprehensive survey of literature is conducted to explore various antenna designs, as well as existing solutions and significant challenges in the development of multifunctional receiving antennas for wireless systems are included in Chapter 1 and Chapter 2. In this thesis, four antenna design methods have been examined. This thesis presents four systematic approaches to design and optimize antenna to achieve desired performance.

Chapter 3 investigates a novel dual-band pixelated defected ground antenna (PDGA) design that utilizes a flexible design guide for achieving single-band and dual-band antenna configurations. The unique pixelated defected ground is designed using the binary particle swarm optimization (BPSO) algorithm, which provides enhanced searchability of pixel positions for efficient antenna design. The proposed PDG configuration allows for achieving different antenna characteristics, including single or multi-band antenna design, gain or efficiency enhancement, etc., with a great degree of freedom. The final PDGA operates at 3.5 GHz and 5.8 GHz bands, exhibiting almost omnidirectional radiation performance with nearly 90% efficiency. The proposed antenna is suitable for different applications in the Internet of Things (IoT) platform, including device to device communication and wireless power transfer in low power IoT devices. The simulated and measured results of the antenna are closely correlated, validating its

performance. The proposed antenna can be a potential candidate for future multidimensional antenna design capability using VBPSO.

Chapter 4 presents a new design methodology for multi-service pixelated stacked antennas, which can be optimized for various design goals with reduced computational time. The proposed antenna topology consists of two different pixel shapes, triangular and square, implemented on two radiating patches of the antenna to achieve low-profile single or multi-band antennas for wireless systems. The design methodology utilizes an enhanced V-shaped binary particle swarm optimization (VBPSO) algorithm to optimize the pixel positions of the radiating patches. The antenna is simulated using CST Microwave Studio and fabricated on Rogers 4003 substrate, and the measurement and simulation results are in good agreement. The proposed design methodology offers great potentials to be aligned with specific design requirements of wireless low-profile IoT devices and is a potential candidate for communication modules in portable IoT devices and other wireless communication systems.

Chapter 5 presents a pixelated cubic antenna design with enhanced isolation and diverse radiation patterns for vehicular applications. The antenna system consists of four radiating patches, pixelated and optimized simultaneously to achieve desired performance and high isolation at 5.4 GHz band. The antenna achieved measured isolation of more than -34 dB between antenna elements, and an overall isolation improvement of about 18 dB compared to a configuration using standard patch antennas. The antenna achieved up to 6.9 dB realized gain in each direction and is equipped with an E-shaped GPS antenna. The antenna prototype has been fabricated on Rogers substrate and measured to verify the simulation results, showing good correlation. The proposed antenna features low-profile, simple design for ease of manufacture, good radiation characteristics with

multidirectional property and high isolation, which are well-suited to vehicular applications in different environments.

Chapter 6 introduces a new method for enhancing log periodic antenna (LPA) bandwidth using an enhanced binary particle swarm optimization technique. The design, called pixelated log periodic antenna (PLPA), surpasses traditional printed LPAs in bandwidth. In design case 1, PLPAs achieved a 940 MHz bandwidth, marking a 13% increase in fractional bandwidth. In design case 2, the bandwidth expanded to 1240 MHz, with a 22.2% fractional bandwidth improvement. This innovative approach showcases the potential to create compact pixelated antennas with significantly enhanced bandwidth compared to conventional designs.

7.2 Recommendations for Future Work

Antenna module is often one of the most critical limiting factors for the widespread development of smart technology, WSNs, wearable electronics, wireless systems, portable electronic devices and IoT sensors. Looking into the future, making the receiving antennas efficient, compact, cheaper, and practically feasible are some of the viable solutions to achieve the optimum performance. The methods for designing antennas that are presented in the thesis could potentially be extended to accommodate multiple standards and a variety of applications. The following are some potential unexplored areas for future research:

- In this thesis, the antennas are optimized using two square and triangular shaped pixels. Other pixel shapes can be considered for better exploration of design configurations.

- New fabrication methods hold great potential for efficient and effective manufacturing of optimized pixelated antenna designs. Antenna can be an outer casing of portable device. Exploration of advanced pixelated antenna design considering 3D shapes could be advantageous. Moreover, efficient use of volume can be achieved with 3D printing technology that can facilitate low frequency of operation with a small antenna volume. Investigation of antenna performance using new substrates based on novel efficient materials has a great research scope. However, exploration of new fabrication techniques should be cost-effective.
- Although a wide range of binary optimization algorithms are available, many of them have not yet been utilized for antenna designs. Nature-Inspired Algorithms, for example Particle Swarm Algorithm (PSO), Differential Evolution (DE), Ant Colony Optimization (ACO) etc. are gaining prominence in the antenna designers' community as examples of computational intelligence approaches. Also, there are many variants and hybrid version of these mainstream algorithms that perform better than their original version. They can be used to achieve innovative antenna structures that are not possible to design using the built-in optimizers of conventional electromagnetic simulators.

BIBLIOGRAPHY

[1] W. Guo, S. Zhou, Y. Chen, S. Wang, X. Chu, and Z. Niu, "Simultaneous information and energy flow for IoT relay systems with crowd harvesting," *IEEE Communications Magazine,* vol. 54, no. 11, pp. 143-149, 2016.

[2] I. Zhou *et al.*, "Internet of Things 2.0: Concepts, Applications, and Future Directions," *IEEE Access,* vol. 9, pp. 70961-71012, 2021.

[3] L. S. Vailshery, "Internet of things (iot) and non-iot active device connections worldwide from 2010 to 2025," *Online, https://bit. ly/2SwKVuB,* 2021.

[4] F. Akhtar and M. H. Rehmani, "Energy replenishment using renewable and traditional energy resources for sustainable wireless sensor networks: A review," *Renewable and Sustainable Energy Reviews,* vol. 45, pp. 769-784, 2015.

[5] A. Cama, F. G. Montoya, J. Gómez, J. L. De La Cruz, and F. Manzano-Agugliaro, "Integration of communication technologies in sensor networks to monitor the Amazon environment," *Journal of Cleaner Production,* vol. 59, pp. 32-42, 2013.

[6] J. Heidemann, M. Stojanovic, and M. Zorzi, "Underwater sensor networks: applications, advances and challenges," *Philosophical Transactions of the Royal Society A: Mathematical, Physical and Engineering Sciences,* vol. 370, no. 1958, pp. 158-175, 2012.

[7] I. F. Akyildiz and E. P. Stuntebeck, "Wireless underground sensor networks: Research challenges," *Ad Hoc Networks,* vol. 4, no. 6, pp. 669-686, 2006.

[8] S. Kim *et al.*, "Ambient RF energy-harvesting technologies for self-sustainable standalone wireless sensor platforms," *Proceedings of the IEEE,* vol. 102, no. 11, pp. 1649-1666, 2014.

[9] J. Bito, R. Bahr, J. G. Hester, S. A. Nauroze, A. Georgiadis, and M. M. Tentzeris, "A novel solar and electromagnetic energy harvesting system with a 3-D printed package for energy efficient Internet-of-Things wireless sensors," *IEEE Transactions on Microwave Theory and Techniques,* vol. 65, no. 5, pp. 1831-1842, 2017.

[10] J. A. Stankovic, "Research directions for the internet of things," *IEEE Internet of Things Journal,* vol. 1, no. 1, pp. 3-9, 2014.

[11] M. M. Mansour and H. Kanaya, "High-Efficient Broadband CPW RF Rectifier for Wireless Energy Harvesting," *IEEE Microwave and Wireless Components Letters,* vol. 29, no. 4, pp. 288-290, 2019.

[12] R. Keshavarz and N. Shariati, "High-Sensitivity and Compact Time-domain Soil Moisture Sensor Using Dispersive Phase Shifter for Complex Permittivity Measurement," *IEEE Transactions on Instrumentation and Measurement,* 2021, doi: doi: 10.1109/TIM.2021.3132367.

[13] R. Keshavarz, J. Lipman, D. Schreurs, and N. Shariati, "Highly Sensitive Differential Microwave Sensor for Soil Moisture Measurement," *IEEE Sensors Journal,* 2021, doi: 10.1109/JSEN.2021.3125718.

[14] T. J. Kazmierski and S. Beeby, *Energy harvesting systems*. Springer, 2014.

[15] N. Shariati, W. S. Rowe, and K. Ghorbani, "Highly sensitive FM frequency scavenger integrated in building materials," in *2015 European Microwave Conference (EuMC)*, 2015: IEEE, pp. 68-71.

[16] N. Shariati, W. S. Rowe, and K. Ghorbani, "Highly sensitive rectifier for efficient RF energy harvesting," in *2014 44th European Microwave Conference*, 2014: IEEE, pp. 1190-1193.

[17] X. Lu, P. Wang, D. Niyato, D. I. Kim, and Z. Han, "Wireless networks with RF energy harvesting: A contemporary survey," *IEEE Communications Surveys & Tutorials,* vol. 17, no. 2, pp. 757-789, 2014.

[18] M. A. Green *et al.*, "Solar cell efficiency tables (Version 55)," *Progress in Photovoltaics,* vol. 28, no. NREL/JA-5900-75827, 2019.
[19] F. Akhtar and M. H. Rehmani, "Energy harvesting for self-sustainable wireless body area networks," *IT Professional,* vol. 19, no. 2, pp. 32-40, 2017.
[20] T.-C. Cheng, C.-H. Cheng, Z.-Z. Huang, and G.-C. J. E. Liao, "Development of an energy-saving module via combination of solar cells and thermoelectric coolers for green building applications," *Energy,* vol. 36, no. 1, pp. 133-140, 2011.
[21] D. Enescu, "Thermoelectric Energy Harvesting: Basic Principles and Applications," in *Green Energy Advances*: IntechOpen, 2019.
[22] S. Cao and J. J. A. i. M. E. Li, "A survey on ambient energy sources and harvesting methods for structural health monitoring applications," *Advances in Mechanical Engineering,* vol. 9, no. 4, p. 1687814017696210, 2017.
[23] M. R. Sarker, S. Julai, M. F. M. Sabri, S. M. Said, M. M. Islam, and M. Tahir, "Review of piezoelectric energy harvesting system and application of optimization techniques to enhance the performance of the harvesting system," *Sensors and Actuators A: Physical,* vol. 300, p. 111634, 2019.
[24] S. Roundy, P. K. Wright, and J. Rabaey, "A study of low level vibrations as a power source for wireless sensor nodes," *Computer communications,* vol. 26, no. 11, pp. 1131-1144, 2003.
[25] C. Mikeka, H. J. S. E. H. T.-P. Arai, Present, and Future, "Design issues in radio frequency energy harvesting system," *Sustainable Energy Harvesting Technologies - Past, Present and Future,* pp. 235-256, 2011.
[26] A. Ghazanfari, H. Tabassum, and E. Hossain, "Ambient RF energy harvesting in ultra-dense small cell networks: Performance and trade-offs," *IEEE Wireless Communications,* vol. 23, no. 2, pp. 38-45, 2016.
[27] W. Y. Toh, Y. K. Tan, W. S. Koh, and L. Siek, "Autonomous wearable sensor nodes with flexible energy harvesting," *IEEE sensors journal,* vol. 14, no. 7, pp. 2299-2306, 2014.
[28] N. Barroca *et al.*, "Antennas and circuits for ambient RF energy harvesting in wireless body area networks," in *2013 IEEE 24th annual international symposium on personal, indoor, and mobile radio communications (PIMRC)*, 2013: IEEE, pp. 532-537.
[29] N. Shariati, W. S. Rowe, J. R. Scott, and K. Ghorbani, "Multi-service highly sensitive rectifier for enhanced RF energy scavenging," *Scientific reports,* vol. 5, p. 9655, 2015.
[30] N. Shariati, J. R. Scott, D. Schreurs, and K. Ghorbani, "Multitone excitation analysis in RF energy harvesters—Considerations and limitations," *IEEE Internet of Things Journal,* vol. 5, no. 4, pp. 2804-2816, 2018.
[31] N. Shariati, "Sensitive ambient RF energy harvesting," PhD, Dept. Elect. Comput. Eng., RMIT Univ.,Melbourne, VIC, Australia.
[32] M. Danesh and J. R. Long, "Photovoltaic antennas for autonomous wireless systems," *IEEE Transactions on Circuits and Systems II: Express Briefs,* vol. 58, no. 12, pp. 807-811, 2011.
[33] A. Collado and A. Georgiadis, "Conformal hybrid solar and electromagnetic (EM) energy harvesting rectenna," *IEEE Transactions on Circuits and Systems I: Regular Papers,* vol. 60, no. 8, pp. 2225-2234, 2013.
[34] R. Dickinson, "Evaluation of a microwave high-power reception-conversion array for wireless power transmission," *NTRS - NASA Technical Reports Server,* 1975.
[35] Powercastco. "Power over distance: RF Energy Harvesting & Wireless Power." https://www.powercastco.com/ (accessed.
[36] M. Ettorre, W. A. Alomar, A. J. I. T. o. A. Grbic, and Propagation, "Radiative wireless power-transfer system using wideband, wide-angle slot arrays," vol. 65, no. 6, pp. 2975-2982, 2017.
[37] D. C. K. Wu, and H. Matsumoto, "Wireless power transmission, technology, and applications," *Proc. IEEE,* vol. 101, pp. 1271-1275, 2013.

[38] L. Xie, Y. Shi, Y. T. Hou, and A. J. I. W. C. Lou, "Wireless power transfer and applications to sensor networks," *IEEE Wireless Communications,* vol. 20, no. 4, pp. 140-145, 2013.

[39] H.-f. Huang, T. J. I. A. Li, and W. P. Letters, "A spiral electrically small magnetic antenna with high radiation efficiency for wireless power transfer," *IEEE Antennas and Wireless Propagation Letters,* vol. 15, pp. 1495-1498, 2016.

[40] Z. Chen, S. Kawasaki, and N. B. J. I. M. M. Carvalho, "Wireless Power Transmission-The Last Cut of Wires...[From the Guest Editors' Desk]," *IEEE Microwave Magazine* vol. 14, no. 2, pp. 22-24, 2013.

[41] H. J. P. o. t. I. Shoki, "Issues and initiatives for practical deployment of wireless power transfer technologies in Japan," *Proceedings of the IEEE,* vol. 101, no. 6, pp. 1312-1320, 2013.

[42] J.-H. Kim, Y. Lim, S. J. I. T. o. A. Nam, and Propagation, "Efficiency Bound of Radiative Wireless Power Transmission Using Practical Antennas," *IEEE Transactions on Antennas and Propagation,* vol. 67, no. 8, pp. 5750-5755, 2019.

[43] R. Keshavarz and N. Shariati, "Low Profile Metamaterial Band-Pass Filter Loaded with 4-Turn Complementary Spiral Resonator for WPT Applications," in *ICECS 2020*, Glasgow, Scotland, 2020.

[44] R. Keshavarz and N. Shariati, "Highly Sensitive and Compact Quad-Band Ambient RF Energy Harvester," *IEEE Transactions on Industrial Electronics,* 2021, doi: 10.1109/TIE.2021.3075888.

[45] F. Akhtar and M. H. J. I. P. Rehmani, "Energy harvesting for self-sustainable wireless body area networks," *IT Professional,* vol. 19, no. 2, pp. 32-40, 2017.

[46] P. Lu, X.-S. Yang, J.-L. Li, and B.-Z. Wang, "A compact frequency reconfigurable rectenna for 5.2-and 5.8-GHz wireless power transmission," *IEEE Transactions on Power Electronics,* vol. 30, no. 11, pp. 6006-6010, 2014.

[47] S. C. Wang, M. J. Li, and M. S. Tong, "A High-Performance Rectenna for Wireless Power Transfer in CubeSats," *IEEE Antennas and Wireless Propagation Letters,* vol. 19, no. 12, pp. 2197-2200, 2020.

[48] P. Lu, C. Song, and K. M. Huang, "A compact rectenna design with wide input power range for wireless power transfer," *IEEE Transactions on Power Electronics,* vol. 35, no. 7, pp. 6705-6710, 2020.

[49] P. Lu, X.-S. Yang, J.-L. Li, and B.-Z. Wang, "Polarization reconfigurable broadband rectenna with tunable matching network for microwave power transmission," *IEEE Transactions on Antennas and Propagation,* vol. 64, no. 3, pp. 1136-1141, 2016.

[50] K. Bhatt, S. Kumar, P. Kumar, and C. C. Tripathi, "Highly efficient 2.4 and 5.8 GHz dual-band rectenna for energy harvesting applications," *IEEE Antennas and Wireless Propagation Letters,* vol. 18, no. 12, pp. 2637-2641, 2019.

[51] A. Raza, R. Keshavarz, and N. Shariati, "Miniaturized Patch Rectenna Using 3-Turn Complementary Spiral Resonator for Wireless Power Transfer," in *2021 IEEE Asia-Pacific Microwave Conference (APMC)*, 2021: IEEE, pp. 455-457.

[52] S. Chandravanshi, S. S. Sarma, and M. J. Akhtar, "Design of triple band differential rectenna for RF energy harvesting," *IEEE Transactions on Antennas and Propagation,* vol. 66, no. 6, pp. 2716-2726, 2018.

[53] S. Shen, C.-Y. Chiu, and R. D. Murch, "A dual-port triple-band L-probe microstrip patch rectenna for ambient RF energy harvesting," *IEEE Antennas and Wireless Propagation Letters,* vol. 16, pp. 3071-3074, 2017.

[54] M. Wang, Y. Fan, L. Yang, Y. Li, J. Feng, and Y. Shi, "Compact dual-band rectenna for RF energy harvest based on a tree-like antenna," *IET Microwaves, Antennas & Propagation,* vol. 13, no. 9, pp. 1350-1357, 2019.

[55] C. Song, Y. Huang, J. Zhou, J. Zhang, S. Yuan, and P. Carter, "A high-efficiency broadband rectenna for ambient wireless energy harvesting," *IEEE Transactions on Antennas and Propagation,* vol. 63, no. 8, pp. 3486-3495, 2015.

[56] S. K. Goudos, D. E. Anagnostou, Z. Bayraktar, S. D. Campbell, P. Rocca, and D. H. Werner, "Guest Editorial: Special Section on Computational Intelligence in Antennas and Propagation: Emerging Trends and Applications," *IEEE Open Journal of Antennas and Propagation,* vol. 2, pp. 224-229, 2021.

[57] X. Yu and M. Gen, *Introduction to evolutionary algorithms*. Springer Science & Business Media, 2010.

[58] Y. Tenne and C.-K. Goh, *Computational intelligence in expensive optimization problems*. Springer Science & Business Media, 2010.

[59] A. E. Eiben and J. Smith, "From evolutionary computation to the evolution of things," *Nature,* vol. 521, no. 7553, pp. 476-482, 2015.

[60] G. Hornby, A. Globus, D. Linden, and J. Lohn, "Automated antenna design with evolutionary algorithms," in *Space 2006*, 2006, p. 7242.

[61] M. John and M. J. Ammann, "Antenna optimization with a computationally efficient multiobjective evolutionary algorithm," *IEEE Transactions on Antennas and Propagation,* vol. 57, no. 1, pp. 260-263, 2009.

[62] S. K. Goudos, C. Kalialakis, and R. Mittra, "Evolutionary algorithms applied to antennas and propagation: A review of state of the art," *International Journal of Antennas and Propagation,* vol. 2016, 2016.

[63] X. Jia and G. Lu, "A hybrid Taguchi binary particle swarm optimization for antenna designs," *IEEE Antennas and Wireless Propagation Letters,* vol. 18, no. 8, pp. 1581-1585, 2019.

[64] A. A. Minasian and T. S. Bird, "Particle swarm optimization of microstrip antennas for wireless communication systems," *IEEE Transactions on Antennas and Propagation,* vol. 61, no. 12, pp. 6214-6217, 2013.

[65] J. Robinson and Y. Rahmat-Samii, "Particle swarm optimization in electromagnetics," *IEEE transactions on antennas and propagation,* vol. 52, no. 2, pp. 397-407, 2004.

[66] N. Jin and Y. Rahmat-Samii, "Particle swarm optimization for antenna designs in engineering electromagnetics," *Journal of Artificial evolution and applications,* vol. 2008, 2008.

[67] D. W. Boeringer and D. H. Werner, "Particle swarm optimization versus genetic algorithms for phased array synthesis," *IEEE Transactions on antennas and propagation,* vol. 52, no. 3, pp. 771-779, 2004.

[68] Y.-L. Li, W. Shao, L. You, and B.-Z. Wang, "An improved PSO algorithm and its application to UWB antenna design," *IEEE Antennas and wireless propagation letters,* vol. 12, pp. 1236-1239, 2013.

[69] A. Lalbakhsh, M. U. Afzal, and K. P. Esselle, "Multiobjective particle swarm optimization to design a time-delay equalizer metasurface for an electromagnetic band-gap resonator antenna," *IEEE Antennas and Wireless Propagation Letters,* vol. 16, pp. 912-915, 2016.

[70] M.-C. Tang, X. Chen, M. Li, and R. W. Ziolkowski, "Particle swarm optimized, 3-D-printed, wideband, compact hemispherical antenna," *IEEE Antennas and Wireless Propagation Letters,* vol. 17, no. 11, pp. 2031-2035, 2018.

[71] S. Mirjalili and A. Lewis, "S-shaped versus V-shaped transfer functions for binary particle swarm optimization," *Swarm and Evolutionary Computation,* vol. 9, pp. 1-14, 2013.

[72] W. Serdijn, A. Mansano, and M. Stoopman, "Introduction to RF energy harvesting," in *Wearable Sensors*: Elsevier, 2014, pp. 299-322.

[73] C. Liu, Y. Zhang, and X. Liu, "Circularly polarized implantable antenna for 915 MHz ISM-band far-field wireless power transmission," *IEEE Antennas and Wireless Propagation Letters,* vol. 17, no. 3, pp. 373-376, 2018.

[74] "FCC Rules for Unlicensed Wireless Equipment operating in the ISM bands." AFAR Communications. https://afar.net/tutorials/fcc-rules/ (accessed 03/12/21, 2021).

[75] L.-G. Tran, H.-K. Cha, W.-T. J. M. Park, and N. S. Letters, "RF power harvesting: a review on designing methodologies and applications," *Micro and Nano Systems Letters,* vol. 5, no. 1, p. 14, 2017.

[76] N. Shariati, W. Rowe, and K. Ghorbani, "RF field investigation and maximum available power analysis for enhanced RF energy scavenging," in *2012 42nd European Microwave Conference*, 2012: IEEE, pp. 329-332.

[77] X. Gu, L. Grauwin, D. Dousset, S. Hemour, and K. Wu, "Dynamic Ambient RF Energy Density Measurements of Montreal for Battery-Free IoT Sensor Network Planning," *IEEE Internet of Things Journal,* 2021.

[78] T. Soyata, L. Copeland, W. J. I. C. Heinzelman, and S. Magazine, "RF energy harvesting for embedded systems: A survey of tradeoffs and methodology," *IEEE Circuits and Systems Magazine,* vol. 16, no. 1, pp. 22-57, 2016.

[79] G. De Vita and G. Iannaccone, "Design criteria for the RF section of UHF and microwave passive RFID transponders," *IEEE Transactions on microwave theory and techniques,* vol. 53, no. 9, pp. 2978-2990, 2005.

[80] S. Hemour and K. Wu, "Radio-frequency rectifier for electromagnetic energy harvesting: Development path and future outlook," *Proceedings of the IEEE,* vol. 102, no. 11, pp. 1667-1691, 2014.

[81] H. Ostaffe. "RF-based Wireless Charging and Energy Harvesting Enables New Applications and Improves Product Design." https://au.mouser.com/applications/rf_energy_harvesting/ (accessed 05/08/2020, 2020).

[82] P. Baronti, P. Pillai, V. W. Chook, S. Chessa, A. Gotta, and Y. F. Hu, "Wireless sensor networks: A survey on the state of the art and the 802.15. 4 and ZigBee standards," *Computer communications,* vol. 30, no. 7, pp. 1655-1695, 2007.

[83] S. Nikolidakis, D. Kandris, D. Vergados, and C. Douligeris, "Energy efficient routing in wireless sensor networks through balanced clustering," *Algorithms,* vol. 6, no. 1, pp. 29-42, 2013.

[84] F. K. Shaikh and S. Zeadally, "Energy harvesting in wireless sensor networks: A comprehensive review," *Renewable and Sustainable Energy Reviews,* vol. 55, pp. 1041-1054, 2016.

[85] B. Kusy *et al.*, "Radio diversity for reliable communication in sensor networks," *ACM Transactions on Sensor Networks (TOSN),* vol. 10, no. 2, pp. 1-29, 2014.

[86] T. D. P. Perera, D. N. K. Jayakody, S. K. Sharma, S. Chatzinotas, and J. Li, "Simultaneous wireless information and power transfer (SWIPT): Recent advances and future challenges," *IEEE Communications Surveys & Tutorials,* vol. 20, no. 1, pp. 264-302, 2017.

[87] L. Liu, J. Xu, and R. Zhang, "Transmit beamforming for simultaneous wireless information and power transfer," in *Academic Press Library in Signal Processing, Volume 7*: Elsevier, 2018, pp. 479-506.

[88] F. Engmann, F. A. Katsriku, J.-D. Abdulai, K. S. Adu-Manu, and F. K. Banaseka, "Prolonging the lifetime of wireless sensor networks: a review of current techniques," *Wireless Communications and Mobile Computing,* vol. 2018, 2018.

[89] P. Nintanavongsa, M. Y. Naderi, and K. R. Chowdhury, "A dual-band wireless energy transfer protocol for heterogeneous sensor networks powered by RF energy harvesting," in *2013 International Computer Science and Engineering Conference (ICSEC)*, 2013: IEEE, pp. 387-392.

[90] D. Dondi, S. Scorcioni, A. Bertacchini, L. Larcher, and P. Pavan, "An autonomous wireless sensor network device powered by a RF energy harvesting system," in *IECON 2012-38th Annual Conference on IEEE Industrial Electronics Society*, 2012: IEEE, pp. 2557-2562.

[91] A. N. Parks, A. P. Sample, Y. Zhao, and J. R. Smith, "A wireless sensing platform utilizing ambient RF energy," in *2013 IEEE Topical Conference on Biomedical Wireless Technologies, Networks, and Sensing Systems*, 2013: IEEE, pp. 154-156.

[92] C. Merz, G. Kupris, and M. Niedernhuber, "A low power design for radio frequency energy harvesting applications," in *2014 2nd International Symposium on Wireless Systems within the Conferences on Intelligent Data Acquisition and Advanced Computing Systems*, 2014: IEEE, pp. 74-78.

[93] N. Tung, "Multi-band ambient RF energy harvesting rectifier for autonomous Wireless Sensor networks," in *2016 IEEE Region 10 Conference (TENCON)*, 2016: IEEE, pp. 3736-3739.

[94] A. M. Baranov, A. Somov, D. Spirjakin, A. Bragar, and A. Karelin, "RF Powered Gas Wireless Sensor Node for Smart Applications," in *Multidisciplinary Digital Publishing Institute Proceedings*, 2017, vol. 1, no. 4, p. 575.

[95] L. Yang, Y. J. Zhou, C. Zhang, X. M. Yang, X.-X. Yang, and C. Tan, "Compact multiband wireless energy harvesting based battery-free body area networks sensor for mobile healthcare," *IEEE Journal of Electromagnetics, RF and Microwaves in Medicine and Biology,* vol. 2, no. 2, pp. 109-115, 2018.

[96] N. Bradai, L. Chaari, and L. Kamoun, "A comprehensive overview of wireless body area networks (WBAn)," *International Journal of E-Health and Medical Communications (IJEHMC),* vol. 2, no. 3, pp. 1-30, 2011.

[97] R. GK and K. Baskaran, "A survey on futuristic health care system: WBANs," *Procedia Engineering,* vol. 30, pp. 889-896, 2012.

[98] T. Wu, F. Wu, J.-M. Redouté, and M. R. Yuce, "An autonomous wireless body area network implementation towards IoT connected healthcare applications," *IEEE Access,* vol. 5, pp. 11413-11422, 2017.

[99] M. Ghamari, B. Janko, R. S. Sherratt, W. Harwin, R. Piechockic, and C. Soltanpur, "A survey on wireless body area networks for ehealthcare systems in residential environments," *Sensors,* vol. 16, no. 6, p. 831, 2016.

[100] A. Stapeleton. "Scientists Have Made Implantable Batteries That Run on Body-Friendly Fluids." https://www.sciencealert.com/new-flexible-batteries-run-on-body-friendly-fluids (accessed 2020).

[101] B. J. DeLong, A. Kiourti, and J. L. Volakis, "A radiating near-field patch rectenna for wireless power transfer to medical implants at 2.4 GHz," *IEEE Journal of Electromagnetics, RF and Microwaves in Medicine and Biology,* vol. 2, no. 1, pp. 64-69, 2018.

[102] S.-E. Adami *et al.*, "A flexible 2.45-GHz power harvesting wristband with net system output from− 24.3 dBm of RF power," *IEEE Transactions on Microwave Theory and Techniques,* vol. 66, no. 1, pp. 380-395, 2017.

[103] S. J. Chen, C. Fumeaux, D. C. Ranasinghe, and T. Kaufmann, "Paired snap-on buttons connections for balanced antennas in wearable systems," *IEEE Antennas and Wireless Propagation Letters,* vol. 14, pp. 1498-1501, 2014.

[104] H. J. Visser, S. Keyrouz, A. Kihshen, and I. Paraschiv, "Optimizing RF energy transport: Channel modelling and transmit antenna and rectenna design," in *2012 Loughborough Antennas & Propagation Conference (LAPC)*, 2012: IEEE, pp. 1-8.

[105] P. Kamalinejad, C. Mahapatra, Z. Sheng, S. Mirabbasi, V. C. Leung, and Y. L. J. I. C. M. Guan, "Wireless energy harvesting for the Internet of Things," *IEEE Communications Magazine,* vol. 53, no. 6, pp. 102-108, 2015.

[106] U. Raza, P. Kulkarni, and M. J. Sooriyabandara, "Low power wide area networks: An overview," *IEEE Communications Surveys Tutorials,* vol. 19, no. 2, pp. 855-873, 2017.

[107] F. Botman, J. De Vos, S. Bernard, F. Stas, J.-D. Legat, and D. Bol, "Bellevue: A 50MHz variable-width SIMD 32bit microcontroller at 0.37 V for processing-intensive wireless sensor nodes," in *2014 IEEE International Symposium on Circuits and Systems (ISCAS)*, 2014: IEEE, pp. 1207-1210.

[108] O. Elijah, T. A. Rahman, I. Orikumhi, C. Y. Leow, and M. N. J. I. I. o. T. J. Hindia, "An overview of Internet of Things (IoT) and data analytics in agriculture: Benefits and challenges," *IEEE Internet of Things Journal,* vol. 5, no. 5, pp. 3758-3773, 2018.
[109] S. Ivanov, K. Bhargava, and W. J. I. I. s. Donnelly, "Precision farming: Sensor analytics," *IEEE Intelligent Systems,* vol. 30, no. 4, pp. 76-80, 2015.
[110] A. Z. Abbasi, N. Islam, Z. A. J. C. S. Shaikh, and Interfaces, "A review of wireless sensors and networks' applications in agriculture," *Computer Standards & Interfaces,* vol. 36, no. 2, pp. 263-270, 2014.
[111] I. Mohanraj, K. Ashokumar, and J. J. P. C. S. Naren, "Field monitoring and automation using IOT in agriculture domain," *Procedia Computer Science,* vol. 93, pp. 931-939, 2016.
[112] "Wireless Leaf & Soil Moisture/Temperature Station." https://www.davisinstruments.com/product/wireless-leaf-soil-moisture-temperature-station/ (accessed 30/06/2020.
[113] "List of wireless sensor nodes." https://en.wikipedia.org/wiki/List_of_wireless_sensor_nodes (accessed 30/06/2020.
[114] M. M. Fakharian, "A Wideband Rectenna Using High Gain Fractal Planar Monopole Antenna Array for RF Energy Scavenging," *International Journal of Antennas and Propagation,* vol. 2020, 2020.
[115] H. Sun and W. Geyi, "A new rectenna with all-polarization-receiving capability for wireless power transmission," *IEEE Antennas and Wireless Propagation Letters,* vol. 15, pp. 814-817, 2015.
[116] S. Shen, Y. Zhang, C.-Y. Chiu, and R. Murch, "An ambient RF energy harvesting system where the number of antenna ports is dependent on frequency," *IEEE Transactions on Microwave Theory and Techniques,* vol. 67, no. 9, pp. 3821-3832, 2019.
[117] A. Bakkali, J. Pelegrí-Sebastiá, T. Sogorb, V. Llario, and A. Bou-Escriva, "A dual-band antenna for RF energy harvesting systems in wireless sensor networks," *Journal of Sensors,* vol. 2016, 2016.
[118] C. A. Balanis, *Antenna theory: analysis and design*. John wiley & sons, 2016.
[119] G. Charalampidis, A. Papadakis, and M. Samarakou, "Power estimation of RF energy harvesters," *Energy Procedia,* vol. 157, pp. 892-900, 2019.
[120] D. M. Pozar, *Microwave engineering*. John wiley & sons, 2011.
[121] P. S. Hall *et al.*, "Reconfigurable antenna challenges for future radio systems," in *2009 3rd European Conference on Antennas and Propagation*, 2009: IEEE, pp. 949-955.
[122] S.-Y. Suh and S. Ooi, "Challenges on multi-radio antenna system for mobile devices," in *2007 IEEE Antennas and Propagation Society International Symposium*, 2007: IEEE, pp. 1221-1224.
[123] H. L. Thal, "Radiation efficiency limits for elementary antenna shapes," *IEEE Transactions on Antennas and Propagation,* vol. 66, no. 5, pp. 2179-2187, 2018.
[124] S. D. Assimonis, V. Fusco, A. Georgiadis, and T. Samaras, "Efficient and sensitive electrically small rectenna for ultra-low power RF energy harvesting," *Scientific reports,* vol. 8, no. 1, pp. 1-13, 2018.
[125] A. Georgiadis, G. V. Andia, and A. Collado, "Rectenna design and optimization using reciprocity theory and harmonic balance analysis for electromagnetic (EM) energy harvesting," *IEEE Antennas and Wireless Propagation Letters,* vol. 9, pp. 444-446, 2010.
[126] U. Olgun, C.-C. Chen, and J. L. Volakis, "Design of an efficient ambient WiFi energy harvesting system," *IET Microwaves, Antennas & Propagation,* vol. 6, no. 11, pp. 1200-1206, 2012.
[127] G. Monti, F. Congedo, D. De Donno, and L. Tarricone, "Monopole-based rectenna for microwave energy harvesting of UHF RFID systems," *Progress In Electromagnetics Research,* vol. 31, pp. 109-121, 2012.

[128] S. Ladan, N. Ghassemi, A. Ghiotto, and K. Wu, "Highly efficient compact rectenna for wireless energy harvesting application," *IEEE microwave magazine,* vol. 14, no. 1, pp. 117-122, 2013.
[129] F. Zhang *et al.*, "Design of a compact planar rectenna for wireless power transfer in the ISM band," *International Journal of Antennas and Propagation,* vol. 2014, 2014.
[130] M. K. Hosain, A. Z. Kouzani, M. F. Samad, and S. J. Tye, "A miniature energy harvesting rectenna for operating a head-mountable deep brain stimulation device," *IEEE access,* vol. 3, pp. 223-234, 2015.
[131] S.-T. Khang, J. W. Yu, and W.-S. Lee, "Compact folded dipole rectenna with RF-based energy harvesting for IoT smart sensors," *Electronics Letters,* vol. 51, no. 12, pp. 926-928, 2015.
[132] Y. Shi, J. Jing, Y. Fan, L. Yang, Y. Li, and M. Wang, "A novel compact broadband rectenna for ambient RF energy harvesting," *AEU-International Journal of Electronics and Communications,* vol. 95, pp. 264-270, 2018.
[133] Q. Awais, Y. Jin, H. T. Chattha, M. Jamil, H. Qiang, and B. A. Khawaja, "A compact rectenna system with high conversion efficiency for wireless energy harvesting," *IEEE access,* vol. 6, pp. 35857-35866, 2018.
[134] Y. Shi, J. Jing, Y. Fan, L. Yang, and M. Wang, "Design of a novel compact and efficient rectenna for WiFi energy harvesting," *Progress in Electromagnetics Research,* vol. 83, pp. 57-70, 2018.
[135] V. Palazzi *et al.*, "A novel ultra-lightweight multiband rectenna on paper for RF energy harvesting in the next generation LTE bands," *IEEE Transactions on Microwave Theory and Techniques,* vol. 66, no. 1, pp. 366-379, 2017.
[136] M. A. M. Said, Z. Zakaria, M. N. Husain, M. H. Misran, and F. S. M. Noor, "2.45 GHz rectenna with high gain for RF energy harvesting," *Telkomnika,* vol. 17, no. 1, pp. 384-391, 2019.
[137] A. Okba, A. Takacs, and H. Aubert, "Compact rectennas for ultra-low-power wireless transmission applications," *IEEE Transactions on Microwave Theory and Techniques,* vol. 67, no. 5, pp. 1697-1707, 2019.
[138] N. Singh *et al.*, "Low profile multiband rectenna for efficient energy harvesting at microwave frequencies," *International Journal of Electronics,* vol. 106, no. 12, pp. 2057-2071, 2019.
[139] S. Kuzu and N. Akcam, "Array antenna using defected ground structure shaped with fractal form generated by Apollonius circle," *IEEE Antennas and Wireless Propagation Letters,* vol. 16, pp. 1020-1023, 2016.
[140] B. S. Dhaliwal and S. S. Pattnaik, "BFO–ANN ensemble hybrid algorithm to design compact fractal antenna for rectenna system," *Neural Computing and Applications,* vol. 28, no. 1, pp. 917-928, 2017.
[141] Y. K. Choukiker, S. K. Sharma, and S. K. Behera, "Hybrid fractal shape planar monopole antenna covering multiband wireless communications with MIMO implementation for handheld mobile devices," *IEEE Transactions on Antennas and Propagation,* vol. 62, no. 3, pp. 1483-1488, 2013.
[142] U. Olgun, C.-C. Chen, and J. L. Volakis, "Low-profile planar rectenna for batteryless RFID sensors," in *2010 IEEE Antennas and Propagation Society International Symposium*, 2010: IEEE, pp. 1-4.
[143] V. Palazzi, M. Del Prete, and M. Fantuzzi, "Scavenging for energy: A rectenna design for wireless energy harvesting in UHF mobile telephony bands," *IEEE Microwave Magazine,* vol. 18, no. 1, pp. 91-99, 2016.
[144] W. Liu, L. Xu, and H. Zhan, "Design of 2.4 GHz/5 GHz planar dual-band electrically small slot antenna based on impedance matching circuit," *AEU-International Journal of Electronics and Communications,* vol. 83, pp. 322-328, 2018.

[145] P. Nintanavongsa, U. Muncuk, D. R. Lewis, and K. R. Chowdhury, "Design optimization and implementation for RF energy harvesting circuits," *IEEE Journal on emerging and selected topics in circuits and systems,* vol. 2, no. 1, pp. 24-33, 2012.
[146] V. Marian, B. Allard, C. Vollaire, and J. Verdier, "Strategy for microwave energy harvesting from ambient field or a feeding source," *IEEE Transactions on Power Electronics,* vol. 27, no. 11, pp. 4481-4491, 2012.
[147] K.-L. Wong, *Compact and broadband microstrip antennas*. John Wiley & Sons, 2004.
[148] L. J. Chu, "Physical limitations of omni-directional antennas," *Journal of applied physics,* vol. 19, no. 12, pp. 1163-1175, 1948.
[149] H. A. Wheeler, "Fundamental limitations of small antennas," *Proceedings of the IRE,* vol. 35, no. 12, pp. 1479-1484, 1947.
[150] M. Fallahpour and R. Zoughi, "Antenna miniaturization techniques: A review of topology-and material-based methods," *IEEE Antennas and Propagation Magazine,* vol. 60, no. 1, pp. 38-50, 2017.
[151] M. A. Ullah, T. Alam, and M. T. Islam, "A UHF CPW-fed patch antenna for nanosatellite store and forward mission," *Microsystem Technologies,* pp. 1-7, 2020.
[152] P. Lande, D. Davis, N. Mascarenhas, F. Fernandes, and A. Kotrashetti, "Design and development of printed Sierpinski Carpet, Sierpinski Gasket and Koch Snowflake fractal antennas for GSM and WLAN applications," in *2015 International Conference on Technologies for Sustainable Development (ICTSD)*, 2015: IEEE, pp. 1-5.
[153] K. C. J. I. a. Hwang and w. p. letters, "A modified Sierpinski fractal antenna for multiband application," vol. 6, pp. 357-360, 2007.
[154] F. Wang, F. Bin, Q. Sun, J. Fan, and H. J. I. A. Ye, "A compact UHF antenna based on complementary fractal technique," *IEEE Access,* vol. 5, pp. 21118-21125, 2017.
[155] J. L. Volakis, *Antenna engineering handbook*. McGraw-Hill Education, 2007.
[156] R. Bancroft and H. A. Wheeler, "Fundamental dimension limits of antennas ensuring proper antenna dimensions in mobile device designs," 2004.
[157] D. Mair, M. Renzler, A. Pfeifhofer, and T. Ußmüller, "Evolutionary Optimization of Asymmetrical Pixelated Antennas Employing Shifted Cross Shaped Elements for UHF RFID," *Electronics,* vol. 9, no. 11, p. 1856, 2020.
[158] J. L. Ethier and D. A. McNamara, "Antenna shape synthesis without prior specification of the feedpoint locations," *IEEE Transactions on Antennas and Propagation,* vol. 62, no. 10, pp. 4919-4934, 2014.
[159] F. M. Caimi, "Meander Line Antennas," *SkyCross. Inc., August,* 2002.
[160] G. Khanna and N. Sharma, "Fractal antenna geometries: A review," *International Journal of Computer Applications,* vol. 153, no. 7, 2016.
[161] I. S. Bangi and J. S. Sivia, "Minkowski and Hilbert curves based hybrid fractal antenna for wireless applications," *AEU-International Journal of Electronics and Communications,* vol. 85, pp. 159-168, 2018.
[162] M. K. Khandelwal, B. K. Kanaujia, and S. Kumar, "Defected ground structure: fundamentals, analysis, and applications in modern wireless trends," *International Journal of Antennas and Propagation,* vol. 2017, 2017.
[163] M. S. Islam, M. T. Islam, M. A. Ullah, G. K. Beng, N. Amin, and N. Misran, "A modified meander line microstrip patch antenna with enhanced bandwidth for 2.4 GHz ISM-band Internet of Things (IoT) applications," *IEEE Access,* vol. 7, pp. 127850-127861, 2019.
[164] O. Calla, A. Singh, A. K. Singh, S. Kumar, and T. Kumar, "Empirical relation for designing the meander line antenna," in *2008 International Conference on Recent Advances in Microwave Theory and Applications*, 2008: IEEE, pp. 695-697.
[165] M. Elayachi, P. Brachat, and J.-M. Ribero, "Novel EBG structure for antenna miniaturization," 2007.

[166] S. M. Haque and K. M. Parvez, "Slot antenna miniaturization using slit, strip, and loop loading techniques," *IEEE Transactions on Antennas and Propagation,* vol. 65, no. 5, pp. 2215-2221, 2017.

[167] W. Hu, Y.-Z. Yin, P. Fei, and X. Yang, "Compact triband square-slot antenna with symmetrical L-strips for WLAN/WiMAX applications," *IEEE Antennas and Wireless Propagation Letters,* vol. 10, pp. 462-465, 2011.

[168] F. C. Commission, "Guidelines for Determining the Effective Radiated Power (ERP) and Equivalent Isotropically Radiated Power (EIRP) of a RF Transmitting System," ed: Oct, 2010.

[169] V. Rizzoli, A. Costanzo, D. Masotti, and F. Donzelli, "Integration of numerical and field-theoretical techniques in the design of single-and multi-band rectennas for micro-power generation," *International Journal of Microwave and Wireless Technologies,* vol. 2, no. 3-4, pp. 293-303, 2010.

[170] C. Song *et al.*, "A novel six-band dual CP rectenna using improved impedance matching technique for ambient RF energy harvesting," *IEEE Transactions on Antennas and Propagation,* vol. 64, no. 7, pp. 3160-3171, 2016.

[171] S. K. Divakaran and D. D. Krishna, "RF energy harvesting systems: An overview and design issues," *International Journal of RF and Microwave Computer-Aided Engineering,* vol. 29, no. 1, p. e21633, 2019.

[172] F.-J. Huang, C.-M. Lee, C.-L. Chang, L.-K. Chen, T.-C. Yo, and C.-H. Luo, "Rectenna application of miniaturized implantable antenna design for triple-band biotelemetry communication," *IEEE Transactions on Antennas and Propagation,* vol. 59, no. 7, pp. 2646-2653, 2011.

[173] A. Nimo, D. Grgić, and L. M. Reindl, "Ambient electromagnetic wireless energy harvesting using multiband planar antenna," in *International Multi-Conference on Systems, Signals & Devices*, 2012: IEEE, pp. 1-6.

[174] K. Niotaki, S. Kim, S. Jeong, A. Collado, A. Georgiadis, and M. M. Tentzeris, "A compact dual-band rectenna using slot-loaded dual band folded dipole antenna," *IEEE Antennas and Wireless Propagation Letters,* vol. 12, pp. 1634-1637, 2013.

[175] D.-K. Ho, I. Kharrat, V.-D. Ngo, T.-P. Vuong, Q.-C. Nguyen, and M.-T. Le, "Dual-band rectenna for ambient RF energy harvesting at GSM 900 MHz and 1800 MHz," in *2016 IEEE International Conference on Sustainable Energy Technologies (ICSET)*, 2016: IEEE, pp. 306-310.

[176] S. Agrawal, M. S. Parihar, and P. N. Kondekar, "A quad-band antenna for multi-band radio frequency energy harvesting circuit," *AEU-International Journal of Electronics and Communications,* vol. 85, pp. 99-107, 2018.

[177] A. Khemar, A. Kacha, H. Takhedmit, and G. Abib, "Design and experiments of a dual-band rectenna for ambient RF energy harvesting in urban environments," *IET Microwaves, Antennas & Propagation,* vol. 12, no. 1, pp. 49-55, 2017.

[178] M. Zeng, Z. Li, A. S. Andrenko, Y. Zeng, and H.-Z. Tan, "A compact dual-band rectenna for GSM900 and GSM1800 energy harvesting," *International Journal of Antennas and Propagation,* vol. 2018, 2018.

[179] N. Singh, B. K. Kanaujia, M. T. Beg, T. Khan, and S. Kumar, "A dual polarized multiband rectenna for RF energy harvesting," *AEU-International Journal of Electronics and Communications,* vol. 93, pp. 123-131, 2018.

[180] A. Bakytbekov, T. Q. Nguyen, C. Huynh, K. N. Salama, and A. Shamim, "Fully printed 3D cube-shaped multiband fractal rectenna for ambient RF energy harvesting," *Nano energy,* vol. 53, pp. 587-595, 2018.

[181] A. M. Jie, N. Nasimuddin, M. F. Karim, and K. T. Chandrasekaran, "A dual-band efficient circularly polarized rectenna for RF energy harvesting systems," *International Journal of RF and Microwave Computer-Aided Engineering,* vol. 29, no. 1, p. e21665, 2019.

[182] C. M. Lee, T. C. Yo, F. J. Huang, and C. H. Luo, "Bandwidth enhancement of planar inverted-F antenna for implantable biotelemetry," *Microwave and Optical Technology Letters,* vol. 51, no. 3, pp. 749-752, 2009.
[183] C.-M. Lee, T.-C. Yo, F.-J. Huang, and C.-H. Luo, "Dual-resonant π-shape with double L-strips PIFA for implantable biotelemetry," *Electronics Letters,* vol. 44, no. 14, pp. 837-839, 2008.
[184] H. Sun, Y.-x. Guo, M. He, and Z. Zhong, "A dual-band rectenna using broadband Yagi antenna array for ambient RF power harvesting," *IEEE Antennas and Wireless Propagation Letters,* vol. 12, pp. 918-921, 2013.
[185] H. Wong, K.-L. Lau, and K.-M. Luk, "Design of dual-polarized L-probe patch antenna arrays with high isolation," *IEEE Transactions on Antennas and Propagation,* vol. 52, no. 1, pp. 45-52, 2004.
[186] N. H. Nguyen *et al.*, "A novel wideband circularly polarized antenna for RF energy harvesting in wireless sensor nodes," *International Journal of Antennas and Propagation,* vol. 2018, 2018.
[187] Y.-J. Ren and K. Chang, "5.8-GHz circularly polarized dual-diode rectenna and rectenna array for microwave power transmission," *IEEE Transactions on Microwave Theory and Techniques,* vol. 54, no. 4, pp. 1495-1502, 2006.
[188] T.-C. Yo, C.-M. Lee, C.-M. Hsu, and C.-H. Luo, "Compact circularly polarized rectenna with unbalanced circular slots," *IEEE Transactions on Antennas and Propagation,* vol. 56, no. 3, pp. 882-886, 2008.
[189] H. Mei, X. Yang, B. Han, and G. Tan, "High-efficiency microstrip rectenna for microwave power transmission at Ka band with low cost," *IET Microwaves, Antennas & Propagation,* vol. 10, no. 15, pp. 1648-1655, 2016.
[190] H. Takhedmit, L. Cirio, S. Bellal, D. Delcroix, and O. Picon, "Compact and efficient 2.45 GHz circularly polarised shorted ring-slot rectenna," *Electronics letters,* vol. 48, no. 5, pp. 253-254, 2012.
[191] A. M. Jie, M. F. Karim, and K. T. Chandrasekaran, "A Wide-Angle Circularly Polarized Tapered-Slit-Patch Antenna With a Compact Rectifier for Energy-Harvesting Systems [Antenna Applications Corner]," *IEEE Antennas and Propagation Magazine,* vol. 61, no. 2, pp. 94-111, 2019.
[192] S. S. Gao, Q. Luo, and F. Zhu, *Circularly polarized antennas*. John Wiley & Sons, 2013.
[193] C. C. Counselman, "Multipath-rejecting GPS antennas," *Proceedings of the IEEE,* vol. 87, no. 1, pp. 86-91, 1999.
[194] M. Braasch and M.-p. Effects, "Global Positioning System: theory and applications," *Chapter,* vol. 14, pp. 547-568, 1996.
[195] E. Brookner, W. M. Hall, and R. H. Westlake, "Faraday loss for L-band radar and communications systems," *IEEE transactions on aerospace and electronic systems,* no. 4, pp. 459-469, 1985.
[196] K. Davies, *Ionospheric radio propagation*. US Department of Commerce, National Bureau of Standards, 1965.
[197] L. Bian, Y.-X. Guo, L. Ong, and X.-Q. Shi, "Wideband circularly-polarized patch antenna," *IEEE Transactions on Antennas and Propagation,* vol. 54, no. 9, pp. 2682-2686, 2006.
[198] B. Y. Toh, R. Cahill, and V. F. Fusco, "Understanding and measuring circular polarization," *IEEE Transactions on Education,* vol. 46, no. 3, pp. 313-318, 2003.
[199] W. L. Stutzman and G. A. Thiele, *Antenna theory and design*. John Wiley & Sons, 2012.
[200] G. Li, H. Zhai, L. Li, and C. Liang, "A nesting-L slot antenna with enhanced circularly polarized bandwidth and radiation," *IEEE Antennas and Wireless Propagation Letters,* vol. 13, pp. 225-228, 2014.
[201] K. Shafique *et al.*, "Energy harvesting using a low-cost rectenna for Internet of Things (IoT) applications," *IEEE Access,* vol. 6, pp. 30932-30941, 2018.

[202] Y. Shi, Y. Fan, Y. Li, L. Yang, and M. Wang, "An efficient broadband slotted rectenna for wireless power transfer at LTE band," *IEEE Transactions on Antennas and Propagation,* vol. 67, no. 2, pp. 814-822, 2018.

[203] J. Kimionis, M. Isakov, B. S. Koh, A. Georgiadis, and M. M. Tentzeris, "3D-printed origami packaging with inkjet-printed antennas for RF harvesting sensors," *IEEE Transactions on Microwave Theory and Techniques,* vol. 63, no. 12, pp. 4521-4532, 2015.

[204] S. Shen, C.-Y. Chiu, and R. D. Murch, "Multiport pixel rectenna for ambient RF energy harvesting," *IEEE Transactions on Antennas and Propagation,* vol. 66, no. 2, pp. 644-656, 2017.

[205] Z.-Y. Zhang, N.-W. Liu, J.-Y. Zhao, and G. Fu, "Wideband circularly polarized antenna with gain improvement," *IEEE antennas and wireless propagation letters,* vol. 12, pp. 456-459, 2013.

[206] R. Xu, J.-Y. Li, and W. Kun, "A broadband circularly polarized crossed-dipole antenna," *IEEE Transactions on Antennas and Propagation,* vol. 64, no. 10, pp. 4509-4513, 2016.

[207] T. K. Nguyen, H. H. Tran, and N. Nguyen-Trong, "A wideband dual-cavity-backed circularly polarized crossed dipole antenna," *IEEE Antennas and Wireless Propagation Letters,* vol. 16, pp. 3135-3138, 2017.

[208] G. Feng, L. Chen, X. Xue, and X. Shi, "Broadband circularly polarized crossed-dipole antenna with a single asymmetrical cross-loop," *IEEE Antennas and Wireless Propagation Letters,* vol. 16, pp. 3184-3187, 2017.

[209] Z.-H. Tu, K.-G. Jia, and Y.-Y. Liu, "A differentially fed wideband circularly polarized antenna," *IEEE Antennas and Wireless Propagation Letters,* vol. 17, no. 5, pp. 861-864, 2018.

[210] W.-J. Yang, Y.-M. Pan, and S.-Y. Zheng, "A Compact Broadband Circularly Polarized Crossed-Dipole Antenna With a Very Low Profile," *IEEE Antennas and Wireless Propagation Letters,* vol. 18, no. 10, pp. 2130-2134, 2019.

[211] Y.-M. Cai, K. Li, Y.-Z. Yin, and W. Hu, "Broadband circularly polarized printed antenna with branched microstrip feed," *IEEE Antennas and Wireless Propagation Letters,* vol. 13, pp. 674-677, 2014.

[212] Y. M. Pan, S. Y. Zheng, and W. Li, "Dual-band and dual-sense omnidirectional circularly polarized antenna," *IEEE Antennas and Wireless Propagation Letters,* vol. 13, pp. 706-709, 2014.

[213] W. Liang, Y.-C. Jiao, Y. Luan, and C. Tian, "A dual-band circularly polarized complementary antenna," *IEEE Antennas and Wireless Propagation Letters,* vol. 14, pp. 1153-1156, 2015.

[214] K. Li, L. Li, Y.-M. Cai, C. Zhu, and C.-H. Liang, "A novel design of low-profile dual-band circularly polarized antenna with meta-surface," *IEEE Antennas and Wireless Propagation Letters,* vol. 14, pp. 1650-1653, 2015.

[215] X. Chen, L. Yang, J.-y. Zhao, and G. Fu, "High-efficiency compact circularly polarized microstrip antenna with wide beamwidth for airborne communication," *IEEE Antennas and Wireless Propagation Letters,* vol. 15, pp. 1518-1521, 2016.

[216] T. V. Hoang, T. T. Le, Q. Y. Li, and H. C. Park, "Quad-band circularly polarized antenna for 2.4/5.3/5.8-GHz WLAN and 3.5-GHz WiMAX applications," *IEEE Antennas and Wireless Propagation Letters,* vol. 15, pp. 1032-1035, 2015.

[217] L. Lu, Y.-C. Jiao, H. Zhang, R. Wang, and T. Li, "Wideband circularly polarized antenna with stair-shaped dielectric resonator and open-ended slot ground," *IEEE Antennas and Wireless Propagation Letters,* vol. 15, pp. 1755-1758, 2016.

[218] M. S. Ellis, Z. Zhao, J. Wu, X. Ding, Z. Nie, and Q.-H. Liu, "A novel simple and compact microstrip-fed circularly polarized wide slot antenna with wide axial ratio bandwidth for C-band applications," *IEEE Transactions on Antennas and Propagation,* vol. 64, no. 4, pp. 1552-1555, 2016.

[219] J. Wei, X. Jiang, and L. Peng, "Ultrawideband and high-gain circularly polarized antenna with double-Y-shape slot," *IEEE Antennas and Wireless Propagation Letters,* vol. 16, pp. 1508-1511, 2017.
[220] M. F. Farooqui and A. Kishk, "3-D-Printed tunable circularly polarized microstrip patch antenna," *IEEE Antennas and Wireless Propagation Letters,* vol. 18, no. 7, pp. 1429-1432, 2019.
[221] U. Ullah and S. Koziel, "A geometrically simple compact wideband circularly polarized antenna," *IEEE Antennas and Wireless Propagation Letters,* vol. 18, no. 6, pp. 1179-1183, 2019.
[222] Y. Yang *et al.*, "A 5.8 GHz circularly polarized rectenna with harmonic suppression and rectenna array for wireless power transfer," *IEEE Antennas and Wireless propagation letters,* vol. 17, no. 7, pp. 1276-1280, 2018.
[223] S. Shrestha, S.-K. Noh, and D.-Y. Choi, "Comparative study of antenna designs for RF energy harvesting," *International Journal of Antennas and Propagation,* vol. 2013, 2013.
[224] A. M. Jie, M. F. Karim, L. Bin, F. Chin, and M. Ong, "A proximity-coupled circularly polarized slotted-circular patch antenna for RF energy harvesting applications," in *2016 IEEE Region 10 Conference (TENCON)*, 2016: IEEE, pp. 2027-2030.
[225] L. B. Bernard and A. Alphones, "AN e-shaped slotted-circular-patch antenna for circularly polarized radiation and radiofrequency energy harvesting," *Microwave and Optical Technology Letters,* vol. 58, no. 4, pp. 868-875, 2016.
[226] J.-H. Chou, D.-B. Lin, K.-L. Weng, and H.-J. Li, "All polarization receiving rectenna with harmonic rejection property for wireless power transmission," *IEEE Transactions on Antennas and Propagation,* vol. 62, no. 10, pp. 5242-5249, 2014.
[227] J. F. Kuhling, M. Feenaghty, and R. Dahle, "A Wideband Cascaded Skew Planar Wheel Antenna for RF Energy Harvesting," in *2018 IEEE Wireless Power Transfer Conference (WPTC)*, 2018: IEEE, pp. 1-4.
[228] X. Lou and G.-M. Yang, "A dual linearly polarized rectenna using defected ground structure for wireless power transmission," *IEEE Microwave and Wireless Components Letters,* vol. 28, no. 9, pp. 828-830, 2018.
[229] H. Sun, H. He, and J. Huang, "Polarization-insensitive rectenna arrays with different power combining strategies," *IEEE Antennas and Wireless Propagation Letters,* vol. 19, no. 3, pp. 492-496, 2020.
[230] Z.-X. Du, S. F. Bo, Y. F. Cao, J.-H. Ou, and X. Y. Zhang, "Broadband Circularly Polarized Rectenna with Wide Dynamic-Power-Range for Efficient Wireless Power Transfer," *IEEE Access,* 2020.
[231] G.-R. Duncan. "Nokia developing phone that recharges itself without mains electricity." https://www.theguardian.com/environment/2009/jun/10/nokia-mobile-phone (accessed 27/5/2020.
[232] C. E. Greene, D. W. Harrist, and M. T. McElhinny, "Powering cell phones and similar devices using RF energy harvesting," ed: Google Patents, 2009.
[233] R. Metz. "Self-Charging Phones Are on the Way, Finally." https://www.technologyreview.com/2015/07/15/167148/self-charging-phones-are-on-the-way-finally/ (accessed 27/5/2020.
[234] M. Johnston. "Mid-air wireless charging could keep drones aloft indefinitely." https://www.itnews.com.au/news/mid-air-wireless-charging-could-keep-drones-aloft-indefinitely-532697 (accessed 27/05/2020.
[235] T. W. J. I. t. o. a. East and propagation, "A self-steering array for the SHARP microwave-powered aircraft," *IEEE Transactions on Antennas and Propagation,* vol. 40, no. 12, pp. 1565-1567, 1992.
[236] A. Oida, H. Nakashima, J. Miyasaka, K. Ohdoi, H. Matsumoto, and N. J. J. o. T. Shinohara, "Development of a new type of electric off-road vehicle powered by microwaves transmitted through air," *Journal of Terramechanics,* vol. 44, no. 5, pp. 329-338, 2007.

[237] R. L. Haupt, *Antenna arrays: a computational approach*. John Wiley & Sons, 2010.
[238] P. J. Bevelacqua, *Antenna arrays: Performance limits and geometry optimization*. Arizona state university, 2008.
[239] U. Olgun, C.-C. Chen, J. L. J. I. a. Volakis, and w. p. letters, "Investigation of rectenna array configurations for enhanced RF power harvesting," *IEEE Antennas and Wireless Propagation Letters,* vol. 10, pp. 262-265, 2011.
[240] H. Sun, Y.-x. Guo, M. He, and Z. J. Zhong, "A dual-band rectenna using broadband Yagi antenna array for ambient RF power harvesting," *IEEE Antennas Wireless Propagation Letters,* vol. 12, pp. 918-921, 2013.
[241] F. Xie, G.-M. Yang, and W. J. Geyi, "Optimal design of an antenna array for energy harvesting," *IEEE Antennas Wireless Propagation Letters,* vol. 12, pp. 155-158, 2013.
[242] A. Z. Ashoor and O. M. J. P. I. E. R. Ramahi, "Dielectric resonator antenna arrays for microwave energy harvesting and far-field wireless power transfer," *Progress In Electromagnetics Research C,* vol. 59, pp. 89-99, 2015.
[243] D. Kumar and K. J. I. J. o. R. Chaudhary, "Design of an Improved Differentially Fed Antenna Array for RF Energy Harvesting," *IETE Journal of Research,* pp. 1-6, 2018.
[244] E. V. V. Cambero *et al.*, "A 2.4 GHz Rectenna Based on a Solar Cell Antenna Array," *IEEE Antennas Wireless Propagation Letters,* vol. 18, no. 12, pp. 2716-2720, 2019.
[245] H. Sun and W. J. Geyi, "A new rectenna using beamwidth-enhanced antenna array for RF power harvesting applications," *IEEE Antennas Wireless Propagation Letters,* vol. 16, pp. 1451-1454, 2016.
[246] A. C. Mak, C. R. Rowell, and R. D. J. Murch, "Isolation enhancement between two closely packed antennas," *IEEE Transactions on Antennas Propagation,* vol. 56, no. 11, pp. 3411-3419, 2008.
[247] J. W. Zhang, K. Y. See, and T. J. Svimonishvili, "Printed decoupled dual-antenna array on-package for small wirelessly powered battery-less device," *IEEE Antennas Wireless Propagation Letters,* vol. 13, pp. 923-926, 2014.
[248] E. V. V. Cambero *et al.*, "A 2.4 GHz Rectenna Based on a Solar Cell Antenna Array," vol. 18, no. 12, pp. 2716-2720, 2019.
[249] Y. Tawk, J. Costantine, F. Ayoub, and C. G. J. Christodoulou, "A communicating antenna array with a dual-energy harvesting functionality [wireless corner]," *IEEE Antennas Propagation Magazine,* vol. 60, no. 2, pp. 132-144, 2018.
[250] S. Jam and M. J. Simruni, "Performance enhancement of a compact wideband patch antenna array using EBG structures," *AEU-International Journal of Electronics Communications,* vol. 89, pp. 42-55, 2018.
[251] S. X. Ta and I. J. Park, "Compact wideband circularly polarized patch antenna array using metasurface," *IEEE Antennas Wireless Propagation Letters,* vol. 16, pp. 1932-1936, 2017.
[252] W. Lin and H. J. Wong, "Polarization reconfigurable aperture-fed patch antenna and array," *IEEE Access,* vol. 4, pp. 1510-1517, 2016.
[253] J. Hu, Z.-C. Hao, and W. J. Hong, "Design of a wideband quad-polarization reconfigurable patch antenna array using a stacked structure," *IEEE Transactions on Antennas Propagation,* vol. 65, no. 6, pp. 3014-3023, 2017.
[254] A. Massa, G. Oliveri, F. Viani, and P. Rocca, "Array designs for long-distance wireless power transmission: State-of-the-art and innovative solutions," *Proceedings of the IEEE,* vol. 101, no. 6, pp. 1464-1481, 2013.
[255] F. Xie, G.-M. Yang, W. J. I. A. Geyi, and W. P. Letters, "Optimal design of an antenna array for energy harvesting," vol. 12, pp. 155-158, 2013.
[256] W. Geyi, *Foundations of applied electrodynamics*. John Wiley & Sons, 2011.
[257] X. Li, L. Yang, and L. Huang, "Novel design of 2.45-GHz rectenna element and array for wireless power transmission," *IEEE Access,* vol. 7, pp. 28356-28362, 2019.

[258] M. Ridwan, M. Abdo, and E. Jorswieck, "Design of non-uniform antenna arrays using genetic algorithm," in *13th International Conference on Advanced Communication Technology (ICACT2011)*, 2011: IEEE, pp. 422-427.

[259] H. Sun, Y.-x. Guo, M. He, and Z. J. Zhong, "A dual-band rectenna using broadband Yagi antenna array for ambient RF power harvesting," *IEEE Antennas Wireless Propagation Letters,* vol. 12, pp. 918-921, 2013.

[260] J. W. Zhang, K. Y. See, and T. J. I. A. Svimonishvili, "Printed decoupled dual-antenna array on-package for small wirelessly powered battery-less device," *IEEE Antennas Wireless Propagation Letters,* vol. 13, pp. 923-926, 2014.

[261] K. Lee, J. Kim, and C. Cha, "Microwave-based wireless power transfer using beam scanning for wireless sensors," in *IEEE EUROCON 2019-18th International Conference on Smart Technologies*, 2019: IEEE, pp. 1-5.

[262] D. Subramaniam *et al.*, "High Gain Beam-Steerable Reconfigurable Antenna using Combined Pixel and Parasitic Arrays," in *European Microwave Conference (EuMC)*, 2020: IEEE.

[263] K. J. Nicholson, T. C. Baum, J. E. Patniotis, and K. Ghorbani, "Discrete Holographic Antenna Embedded in a Structural Composite Laminate," *IEEE Antennas and Wireless Propagation Letters,* vol. 19, no. 2, pp. 358-362, 2019.

[264] M. Ansari, H. Zhu, N. Shariati, and Y. J. Guo, "Compact planar beamforming array with endfire radiating elements for 5G applications," *IEEE Transactions on Antennas and Propagation,* vol. 67, no. 11, pp. 6859-6869, 2019.

[265] M. Nikfalazar *et al.*, "Two-dimensional beam-steering phased-array antenna with compact tunable phase shifter based on BST thick films," *IEEE Antennas and Wireless Propagation Letters,* vol. 16, pp. 585-588, 2016.

[266] D. Belo and N. B. Carvalho, "Far field WPT—Main challenges," in *2017 11th European Conference on Antennas and Propagation (EUCAP)*, 2017: IEEE, pp. 331-335.

[267] M. Poveda-García, J. Oliva-Sánchez, R. Sanchez-Iborra, D. Cañete-Rebenaque, and J. L. Gomez-Tornero, "Dynamic wireless power transfer for cost-effective wireless sensor networks using frequency-scanned beaming," *IEEE Access,* vol. 7, pp. 8081-8094, 2019.

[268] L. Minz and S. O. Park, "Beam scanning annular slot-ring antenna array with via-fence for wireless power transfer," *International Journal of RF and Microwave Computer-Aided Engineering,* vol. 30, no. 6, p. e22178, 2020.

[269] R. Hussain, "Shared Aperture Slot-Based Sub-6 GHz and mm-Wave IoT Antenna for 5G Applications," *IEEE Internet of Things Journal,* 2021.

[270] S. Li, L. Da Xu, and S. Zhao, "5G Internet of Things: A survey," *Journal of Industrial Information Integration,* vol. 10, pp. 1-9, 2018.

[271] I. Zhou, J. Lipman, M. Abolhasan, N. Shariati, and D. W. Lamb, "Frost Monitoring Cyber–Physical System: A Survey on Prediction and Active Protection Methods," *IEEE Internet of Things Journal,* vol. 7, no. 7, pp. 6514-6527, 2020.

[272] M. Amiri, F. Tofigh, N. Shariati, J. Lipman, and M. Abolhasan, "Review on Metamaterial Perfect Absorbers and Their Applications to IoT," *IEEE Internet of Things Journal,* vol. 8, no. 6, pp. 4105-4131, 2020.

[273] P. Dhull, A. P. Guevara Toledo, M. Ansari, S. Pollin, N. Shariati, and D. Schreurs, "Enabling Simultaneous Wireless Information and Power Transfer in IoT Networks," *Ieee Microwave Magazine,* 2021.

[274] A. Ali, H. Wang, J. Lee, Y. H. Ahn, and I. Park, "Ultra-low profile solar-cell-integrated antenna with a high form factor," *Scientific Reports,* vol. 11, no. 1, pp. 1-9, 2021.

[275] A. Ahmad, D.-y. Choi, and S. Ullah, "A compact two elements MIMO antenna for 5G communication," *Scientific Reports,* vol. 12, no. 1, pp. 1-8, 2022.

[276] R. Azim, T. Alam, M. S. Mia, A. F. Almutairi, and M. T. Islam, "An octa-band planar monopole antenna for portable communication devices," *Scientific reports,* vol. 11, no. 1, pp. 1-13, 2021.

[277] A. Whitmore, A. Agarwal, and L. Da Xu, "The Internet of Things—A survey of topics and trends," *Information systems frontiers,* vol. 17, no. 2, pp. 261-274, 2015.
[278] M. Ullah, R. Keshavarz, M. Abolhasan, J. Lipman, K. P. Esselle, and N. Shariati, "A Review on Antenna Technologies for Ambient RF Energy Harvesting and Wireless Power Transfer: Designs, Challenges and Applications," *IEEE Access,* 2022.
[279] L. Kannappan *et al.*, "3-D twelve-port multi-service diversity antenna for automotive communications," *Scientific reports,* vol. 12, no. 1, pp. 1-22, 2022.
[280] Y. Wang *et al.*, "Perfect control of diffraction patterns with phase-gradient metasurfaces," *ACS Applied Materials & Interfaces,* vol. 14, no. 14, pp. 16856-16865, 2022.
[281] K. Zhang, Y. Wang, S. N. Burokur, and Q. Wu, "Generating dual-polarized vortex beam by detour phase: From phase gradient metasurfaces to metagratings," *IEEE Transactions on Microwave Theory and Techniques,* vol. 70, no. 1, pp. 200-209, 2021.
[282] L. Li, H. Zhao, C. Liu, L. Li, and T. J. Cui, "Intelligent metasurfaces: control, communication and computing," *eLight,* vol. 2, no. 1, pp. 1-24, 2022.
[283] M. Hasan, M. R. I. Faruque, and M. T. Islam, "Dual band metamaterial antenna for LTE/bluetooth/WiMAX system," *Scientific reports,* vol. 8, no. 1, pp. 1-17, 2018.
[284] N. Shariati, W. S. Rowe, J. R. Scott, and K. Ghorbani, "Multi-service highly sensitive rectifier for enhanced RF energy scavenging," *Scientific reports,* vol. 5, no. 1, pp. 1-9, 2015.
[285] R. Keshavarz and N. Shariati, "Highly Sensitive and Compact Quad-Band Ambient RF Energy Harvester," *IEEE Transactions on Industrial Electronics,* vol. 69, no. 4, pp. 3609-3621, 2021.
[286] D. Guha, S. Biswas, and Y. M. Antar, "Defected ground structure for microstrip antennas," *Microstrip and Printed antennas,* 2011.
[287] A. A. Salih and M. S. Sharawi, "A dual-band highly miniaturized patch antenna," *IEEE Antennas and Wireless Propagation Letters,* vol. 15, pp. 1783-1786, 2016.
[288] C. Kumar and D. Guha, "Asymmetric and compact DGS configuration for circular patch with improved radiations," *IEEE Antennas and Wireless Propagation Letters,* vol. 19, no. 2, pp. 355-357, 2019.
[289] J. Kennedy and R. Eberhart, "Particle swarm optimization," in *Proceedings of ICNN'95-international conference on neural networks*, 1995, vol. 4: IEEE, pp. 1942-1948.
[290] J. Kennedy and R. C. Eberhart, "A discrete binary version of the particle swarm algorithm," in *1997 IEEE International conference on systems, man, and cybernetics. Computational cybernetics and simulation*, 1997, vol. 5: IEEE, pp. 4104-4108.
[291] R. Waterhouse, "Small Microstrip Patch Antennas," in *Microstrip Patch Antennas: A Designer's Guide*: Springer, 2003, pp. 197-276.
[292] M. Matinmikko-Blue, S. Yrjölä, V. Seppänen, P. Ahokangas, H. Hämmäinen, and M. Latva-Aho, "Analysis of spectrum valuation elements for local 5G networks: Case study of 3.5-GHz band," *IEEE Transactions on Cognitive Communications and Networking,* vol. 5, no. 3, pp. 741-753, 2019.
[293] "Auction Summary - 3.6 GHz band (2018)." Australian Communications and Media Authority. https://www.acma.gov.au/auction-summary-36-ghz-band-2018#spectrum-details (accessed 07/07/21, 2021).
[294] "CST Studio Suite Electromagnetic Field Simulation Software." https://www.3ds.com/products-services/simulia/products/cst-studio-suite/ (accessed 24/06/2022, 2022).
[295] N. Jin and Y. Rahmat-Samii, "Advances in particle swarm optimization for antenna designs: real-number, binary, single-objective and multiobjective implementations," *IEEE transactions on antennas and propagation,* vol. 55, no. 3, pp. 556-567, 2007.

[296] L. Dang, Z. Y. Lei, Y. J. Xie, G. L. Ning, and J. Fan, "A compact microstrip slot triple-band antenna for WLAN/WiMAX applications," *IEEE Antennas and Wireless Propagation Letters,* vol. 9, pp. 1178-1181, 2010.

[297] Y. Cao, S. Cheung, and T. Yuk, "A multiband slot antenna for GPS/WiMAX/WLAN systems," *IEEE Transactions on Antennas and Propagation,* vol. 63, no. 3, pp. 952-958, 2015.

[298] A. Bekasiewicz and S. Koziel, "Compact UWB monopole antenna for internet of things applications," *Electronics Letters,* vol. 52, no. 7, pp. 492-494, 2016.

[299] Z. Su, K. Klionovski, R. M. Bilal, and A. Shamim, "A dual band additively manufactured 3-D antenna on package with near-isotropic radiation pattern," *IEEE Transactions on Antennas and Propagation,* vol. 66, no. 7, pp. 3295-3305, 2018.

[300] A. Romputtal and C. Phongcharoenpanich, "IoT-linked integrated NFC and dual band UHF/2.45 GHz RFID reader antenna scheme," *IEEE Access,* vol. 7, pp. 177832-177843, 2019.

[301] J.-I. Oh, H.-W. Jo, K.-S. Kim, H. Cho, and J.-W. Yu, "A compact cavity-backed slot antenna using dual mode for IoT applications," *IEEE Antennas and Wireless Propagation Letters,* vol. 20, no. 3, pp. 317-321, 2021.

[302] Y. Dong, J. Choi, and T. Itoh, "Folded strip/slot antenna with extended bandwidth for WLAN application," *IEEE Antennas and Wireless Propagation Letters,* vol. 16, pp. 673-676, 2016.

[303] O. Björkqvist, O. Dahlberg, G. Silver, C. Kolitsidas, O. Quevedo-Teruel, and B. L. G. Jonsson, "Wireless sensor network utilizing radio-frequency energy harvesting for smart building applications," *IEEE Antennas & Propagation Magazine,* vol. 60, no. 5, pp. 124-136, 2018.

[304] A. Costanzo and D. Masotti, "Energizing 5G: Near-and far-field wireless energy and data trantransfer as an enabling technology for the 5G IoT," *IEEE Microwave Magazine,* vol. 18, no. 3, pp. 125-136, 2017.

[305] G. Li, Y. Huang, G. Gao, X. Wei, Z. Tian, and L.-A. Bian, "A handbag zipper antenna for the applications of body-centric wireless communications and Internet of Things," *IEEE Transactions on Antennas and Propagation,* vol. 65, no. 10, pp. 5137-5146, 2017.

[306] M. Ullah, R. Keshavarz, M. Abolhasan, J. Lipman, and N. Shariati, "Low-profile dual-band pixelated defected ground antenna for multistandard IoT devices," *Scientific Reports,* vol. 12, no. 1, pp. 1-19, 2022.

[307] P. Dhull, A. P. Guevara, M. Ansari, S. Pollin, N. Shariati, and D. Schreurs, "Internet of Things Networks," *IEEE Microwave Magazine,* vol. 23, no. 3, pp. 39-54, 2022.

[308] R. Hussain, "Shared-aperture slot-based sub-6-GHz and mm-wave IoT antenna for 5G applications," *IEEE Internet of Things Journal,* vol. 8, no. 13, pp. 10807-10814, 2021.

[309] Y. Koga and M. Kai, "A transparent double folded loop antenna for IoT applications," in *2018 IEEE-APS Topical Conference on Antennas and Propagation in Wireless Communications (APWC)*, 2018: IEEE, pp. 762-765.

[310] T. Houret, L. Lizzi, F. Ferrero, C. Danchesi, and S. Boudaud, "DTC-enabled frequency-tunable inverted-F antenna for IoT applications," *IEEE antennas and wireless propagation letters,* vol. 19, no. 2, pp. 307-311, 2019.

[311] H. F. Abutarboush and A. Shamim, "A reconfigurable inkjet-printed antenna on paper substrate for wireless applications," *IEEE Antennas and Wireless Propagation Letters,* vol. 17, no. 9, pp. 1648-1651, 2018.

[312] K. R. Jha, B. Bukhari, C. Singh, G. Mishra, and S. K. Sharma, "Compact planar multistandard MIMO antenna for IoT applications," *IEEE Transactions on Antennas and Propagation,* vol. 66, no. 7, pp. 3327-3336, 2018.

[313] J. Tak, S. Woo, J. Kwon, and J. Choi, "Dual-band dual-mode patch antenna for on-/off-body WBAN communications," *IEEE Antennas and Wireless Propagation Letters,* vol. 15, pp. 348-351, 2015.

[314] X.-Q. Zhu, Y.-X. Guo, and W. Wu, "A novel dual-band antenna for wireless communication applications," *IEEE Antennas and Wireless Propagation Letters,* vol. 15, pp. 516-519, 2015.
[315] N. L. Nhlengethwa and P. Kumar, "Fractal microstrip patch antennas for dual-band and triple-band wireless applications," *International Journal on Smart Sensing and Intelligent Systems,* vol. 14, no. 1, pp. 1-9, 2021.
[316] S. Ahmad, A. Ghaffar, N. Hussain, and N. Kim, "Compact dual-band antenna with paired L-shape slots for on-and off-body wireless communication," *Sensors,* vol. 21, no. 23, p. 7953, 2021.
[317] M. A. Haque *et al.*, "Dual Band Antenna Design and Prediction of Resonance Frequency Using Machine Learning Approaches," *Applied Sciences,* vol. 12, no. 20, p. 10505, 2022.
[318] "RLAN use in the 5 GHz and 6 GHz bands - consultation 12/2021." Australian Communication and Media Authority. https://www.acma.gov.au/consultations/2021-04/rlan-use-5-ghz-and-6-ghz-bands-consultation-122021#consultation-documents (accessed 27/11/21, 2021).
[319] "Point-to-point (5.8 GHz band)." Australian Communication and Media Authority. https://www.acma.gov.au/point-point-58-ghz-band (accessed 27/11/2021, 2021).
[320] D. H. Wolpert and W. G. Macready, "No free lunch theorems for optimization," *IEEE transactions on evolutionary computation,* vol. 1, no. 1, pp. 67-82, 1997.
[321] S. Goudos, "Antenna design using binary differential evolution: Application to discrete-valued design problems," *IEEE antennas and propagation magazine,* vol. 59, no. 1, pp. 74-93, 2017.
[322] S. P. Adam, S.-A. N. Alexandropoulos, P. M. Pardalos, and M. N. Vrahatis, "No free lunch theorem: A review," *Approximation and optimization,* pp. 57-82, 2019.
[323] C. A. Balanis, *Antenna theory: analysis and design*. John wiley & sons, 2015.
[324] T. Olawoye and P. Kumar, "A high gain antenna with DGS for sub-6 GHz 5G communications," *Advanced Electromagnetics,* vol. 11, no. 1, pp. 41-50, 2022.
[325] J.-M. Chen and J.-S. Row, "Wideband circularly polarized slotted-patch antenna with a reflector," *IEEE Antennas and Wireless Propagation Letters,* vol. 14, pp. 575-578, 2014.
[326] R. Q. Lee and K.-F. Lee, "Experimental study of the two-layer electromagnetically coupled rectangular patch antenna," *IEEE Transactions on Antennas and Propagation,* vol. 38, no. 8, pp. 1298-1302, 1990.
[327] N. Jin and Y. Rahmat-Samii, "Parallel particle swarm optimization and finite-difference time-domain (PSO/FDTD) algorithm for multiband and wide-band patch antenna designs," *IEEE Transactions on Antennas and Propagation,* vol. 53, no. 11, pp. 3459-3468, 2005.
[328] X.-X. Yang, C. Jiang, A. Z. Elsherbeni, F. Yang, and Y.-Q. Wang, "A novel compact printed rectenna for data communication systems," *IEEE transactions on antennas and propagation,* vol. 61, no. 5, pp. 2532-2539, 2013.
[329] L. Yang, L. Yang, Y. Zhu, K. Yoshitomi, and H. Kanaya, "Polarization reconfigurable slot antenna for 5.8 GHz wireless applications," *AEU-International Journal of Electronics and Communications,* vol. 101, pp. 27-32, 2019.
[330] L. Ge, S. Gao, Y. Li, W. Qin, and J. Wang, "A low-profile dual-band antenna with different polarization and radiation properties over two bands for vehicular communications," *IEEE Transactions on Vehicular Technology,* vol. 68, no. 1, pp. 1004-1008, 2018.
[331] L. Liang, H. Peng, G. Y. Li, and X. Shen, "Vehicular communications: A physical layer perspective," *IEEE Transactions on Vehicular Technology,* vol. 66, no. 12, pp. 10647-10659, 2017.
[332] M. Bilgic and K. Yegin, "Modified annular ring antenna for GPS and SDARS automotive applications," *IEEE Antennas and Wireless Propagation Letters,* vol. 15, pp. 1442-1445, 2015.

[333] Q. Wu, Y. Zhou, and S. Guo, "An L-sleeve L-monopole antenna fitting a shark-fin module for vehicular LTE, WLAN, and car-to-car communications," *IEEE Transactions on Vehicular Technology,* vol. 67, no. 8, pp. 7170-7180, 2018.

[334] J.-K. Che, C.-C. Chen, and J. F. Locke, "A compact four-channel MIMO 5G sub-6 GHz/LTE/WLAN/V2X antenna design for modern vehicles," *IEEE Transactions on Antennas and Propagation,* vol. 69, no. 11, pp. 7290-7297, 2021.

[335] M. A. Ullah, R. Keshavarz, M. Abolhasan, J. Lipman, K. P. Esselle, and N. Shariati, "A Review on Antenna Technologies for Ambient RF Energy Harvesting and Wireless Power Transfer: Designs, Challenges and Applications," *IEEE Access,* 2022.

[336] B. R. Jackson, S. Rajan, B. J. Liao, and S. Wang, "Direction of arrival estimation using directive antennas in uniform circular arrays," *IEEE Transactions on Antennas and propagation,* vol. 63, no. 2, pp. 736-747, 2014.

[337] C.-H. Ou, B.-Y. Wu, and L. Cai, "GPS-free vehicular localization system using roadside units with directional antennas," *Journal of Communications and Networks,* vol. 21, no. 1, pp. 12-24, 2019.

[338] T. Mondal, S. Maity, R. Ghatak, and S. R. B. Chaudhuri, "Compact circularly polarized wide-beamwidth fern-fractal-shaped microstrip antenna for vehicular communication," *IEEE Transactions on Vehicular Technology,* vol. 67, no. 6, pp. 5126-5134, 2018.

[339] C.-Y. Chiu, C.-H. Cheng, R. D. Murch, and C. R. Rowell, "Reduction of mutual coupling between closely-packed antenna elements," *IEEE transactions on antennas and propagation,* vol. 55, no. 6, pp. 1732-1738, 2007.

[340] M. G. N. Alsath *et al.*, "An integrated tri-band/UWB polarization diversity antenna for vehicular networks," *IEEE Transactions on Vehicular Technology,* vol. 67, no. 7, pp. 5613-5620, 2018.

[341] S. Xiao, M.-C. Tang, Y.-Y. Bai, S. Gao, and B.-Z. Wang, "Mutual coupling suppression in microstrip array using defected ground structure," *IET microwaves, antennas & propagation,* vol. 5, no. 12, pp. 1488-1494, 2011.

[342] Y. Liu, X. Yang, Y. Jia, and Y. J. Guo, "A low correlation and mutual coupling MIMO antenna," *IEEE Access,* vol. 7, pp. 127384-127392, 2019.

[343] A. Habashi, J. Nourinia, and C. Ghobadi, "Mutual coupling reduction between very closely spaced patch antennas using low-profile folded split-ring resonators (FSRRs)," *IEEE antennas and wireless propagation letters,* vol. 10, pp. 862-865, 2011.

[344] J. Mu'Ath, T. A. Denidni, and A. R. Sebak, "Millimeter-wave compact EBG structure for mutual coupling reduction applications," *IEEE Transactions on Antennas and Propagation,* vol. 63, no. 2, pp. 823-828, 2014.

[345] B. L. Dhevi, K. S. Vishvaksenan, and K. Rajakani, "Isolation enhancement in dual-band microstrip antenna array using asymmetric loop resonator," *IEEE Antennas and Wireless Propagation Letters,* vol. 17, no. 2, pp. 238-241, 2017.

[346] M. G. N. Alsath, M. Kanagasabai, and B. Balasubramanian, "Implementation of slotted meander-line resonators for isolation enhancement in microstrip patch antenna arrays," *IEEE Antennas and Wireless Propagation Letters,* vol. 12, pp. 15-18, 2012.

[347] M. Alibakhshikenari *et al.*, "Study on isolation improvement between closely-packed patch antenna arrays based on fractal metamaterial electromagnetic bandgap structures," *IET Microwaves, Antennas & Propagation,* vol. 12, no. 14, pp. 2241-2247, 2018.

[348] A. Ghadimi, V. Nayyeri, M. Khanjarian, M. Soleimani, and O. M. Ramahi, "A systematic approach for mutual coupling reduction between microstrip antennas using pixelization and binary optimization," *IEEE Antennas and Wireless Propagation Letters,* vol. 19, no. 12, pp. 2048-2052, 2020.

[349] A. Kwoczek, Z. Raida, J. Láčík, M. Pokorny, J. Puskelý, and P. Vágner, "Influence of car panorama glass roofs on Car2Car communication (poster)," in *2011 IEEE Vehicular Networking Conference (VNC)*, 2011: IEEE, pp. 246-251.

[350] N. Herscovici, "New considerations in the design of microstrip antennas," *IEEE Transactions on Antennas and Propagation,* vol. 46, no. 6, pp. 807-812, 1998.
[351] S. Haykin, D. J. Thomson, and J. H. Reed, "Spectrum sensing for cognitive radio," *Proceedings of the IEEE,* vol. 97, no. 5, pp. 849-877, 2009.
[352] L.-y. Chen, J.-s. Hong, and M. Amin, "A Twelve-Ports Dual-Polarized MIMO Log-Periodic Dipole Array Antenna for UWB Applications," *Radioengineering,* vol. 28, no. 1, 2019.
[353] J.-J. Liang, J.-S. Hong, J.-B. Zhao, and W. Wu, "Dual-band dual-polarized compact log-periodic dipole array for MIMO WLAN applications," *IEEE Antennas and Wireless Propagation Letters,* vol. 14, pp. 751-754, 2014.
[354] J. L. Volakis and J. L. Volakis, *Antenna engineering handbook*. McGraw-hill New York, 2007.
[355] Q. Chen, H. Zhang, Y.-J. Shao, and T. Zhong, "Bandwidth and gain improvement of an L-shaped slot antenna with metamaterial loading," *IEEE Antennas and Wireless Propagation Letters,* vol. 17, no. 8, pp. 1411-1415, 2018.
[356] Z. M. Razi, P. Rezaei, and A. Valizade, "A novel design of Fabry-Perot antenna using metamaterial superstrate for gain and bandwidth enhancement," *AEU-International Journal of Electronics and Communications,* vol. 69, no. 10, pp. 1525-1532, 2015.
[357] G. Muntoni *et al.*, "A curved 3-D printed microstrip patch antenna layout for bandwidth enhancement and size reduction," *IEEE Antennas and Wireless Propagation Letters,* vol. 19, no. 7, pp. 1118-1122, 2020.
[358] Y. Chen, S. Yang, and Z. Nie, "Bandwidth enhancement method for low profile E-shaped microstrip patch antennas," *IEEE transactions on antennas and propagation,* vol. 58, no. 7, pp. 2442-2447, 2010.
[359] S. Weigand, G. H. Huff, K. H. Pan, and J. T. Bernhard, "Analysis and design of broad-band single-layer rectangular U-slot microstrip patch antennas," *IEEE transactions on antennas and propagation,* vol. 51, no. 3, pp. 457-468, 2003.
[360] H. Malekpoor and S. Jam, "Enhanced bandwidth of shorted patch antennas using folded-patch techniques," *IEEE antennas and wireless propagation letters,* vol. 12, pp. 198-201, 2013.
[361] R. Kubacki, M. Czyżewski, and D. Laskowski, "Enlarged frequency bandwidth of truncated log-periodic dipole array antenna," *Electronics,* vol. 9, no. 8, p. 1300, 2020.
[362] S. Trinh-Van *et al.*, "A low-profile high-gain and wideband log-periodic meandered dipole array antenna with a cascaded multi-section artificial magnetic conductor structure," *Sensors,* vol. 19, no. 20, p. 4404, 2019.
[363] L. Chang, S. He, J. Q. Zhang, and D. Li, "A compact dielectric-loaded log-periodic dipole array (LPDA) antenna," *IEEE Antennas and Wireless Propagation Letters,* vol. 16, pp. 2759-2762, 2017.
[364] D. E. Anagnostou, J. Papapolymerou, M. M. Tentzeris, and C. G. Christodoulou, "A printed log-periodic Koch-dipole array (LPKDA)," *IEEE Antennas and Wireless Propagation Letters,* vol. 7, pp. 456-460, 2008.
[365] Q.-X. Chu, X.-R. Li, and M. Ye, "High-gain printed log-periodic dipole array antenna with parasitic cell for 5G communication," *IEEE Transactions on Antennas and Propagation,* vol. 65, no. 12, pp. 6338-6344, 2017.
[366] C. Yu *et al.*, "Ultrawideband printed log-periodic dipole antenna with multiple notched bands," *IEEE Transactions on Antennas and Propagation,* vol. 59, no. 3, pp. 725-732, 2010.
[367] M. A. Ullah, R. Keshavarz, M. Abolhasan, J. Lipman, and N. Shariati, "Low-profile dual-band pixelated defected ground antenna for multistandard IoT devices," *Scientific Reports,* vol. 12, no. 1, p. 11479, 2022.
[368] M. Ullah, R. Keshavarz, M. Abolhasan, J. Lipman, and N. Shariati, "Multi-Service Compact Pixelated Stacked Antenna with Different Pixel Shapes for IoT Applications," *IEEE Internet of Things Journal,* 2023.

[369] X. Wei, J. Liu, and Y. Long, "Printed log-periodic monopole array antenna with a simple feeding structure," *IEEE Antennas and Wireless Propagation Letters,* vol. 17, no. 1, pp. 58-61, 2017.

[370] Z. Hu, Z. Shen, W. Wu, and J. Lu, "Low-profile log-periodic monopole array," *IEEE transactions on Antennas and propagation,* vol. 63, no. 12, pp. 5484-5491, 2015.

[371] G. A. Casula, P. Maxia, G. Montisci, G. Mazzarella, and F. Gaudiomonte, "A printed LPDA fed by a coplanar waveguide for broadband applications," *IEEE Antennas and Wireless Propagation Letters,* vol. 12, pp. 1232-1235, 2013.